Sven Michael Revfi

An optimization method for the design of beads in long fiber reinforced polymer structures including the manufacturing process as an approach to realize methodically identified lightweight potentials

Eine Optimierungsmethode zur Gestaltung von Sicken in langfaserverstärkten Kunststoffstrukturen unter Berücksichtigung des Herstellungsprozesses als Ansatz zur Realisierung methodisch identifizierter Leichtbaupotentiale

Band 146

Systeme ▪ Methoden ▪ Prozesse

IPEK
Institut für Produktentwicklung
am Karlsruher Institut für Technologie

Sven Michael Revfi

An optimization method for the design of beads in long fiber reinforced polymer structures including the manufacturing process as an approach to realize methodically identified lightweight potentials

Eine Optimierungsmethode zur Gestaltung von Sicken in langfaserverstärkten Kunststoffstrukturen unter Berücksichtigung des Herstellungsprozesses als Ansatz zur Realisierung methodisch identifizierter Leichtbaupotentiale

An optimization method for the design of beads in long fiber reinforced polymer structures including the manufacturing process as an approach to realize methodically identified lightweight potentials

Zur Erlangung des akademischen Grades eines

DOKTORS DER INGENIEURWISSENSCHAFTEN (Dr.-Ing.)

von der KIT-Fakultät für Maschinenbau des

Karlsruher Instituts für Technologie (KIT)

angenommene

DISSERTATION

von

Sven Michael Revfi, M.Sc.

Tag der mündlichen Prüfung: 20.12.2021

Hauptreferent: Univ.-Prof. Dr.-Ing. Dr. h. c. Albert Albers

Korreferent: Prof. Dr. Kamran Behdinan

Vorwort der Herausgeber (Stand: Juli 2017)

Wissen ist einer der entscheidenden Faktoren in den Volkswirtschaften unserer Zeit. Der Unternehmenserfolg wird mehr denn je davon abhängen, wie schnell ein Unternehmen neues Wissen aufnehmen, zugänglich machen und verwerten kann. Die Aufgabe eines Universitätsinstitutes ist es, hier einen wesentlichen Beitrag zu leisten. In den Forschungsarbeiten wird ständig Wissen generiert. Dieses kann aber nur wirksam und für die Gemeinschaft nutzbar werden, wenn es in geeigneter Form kommuniziert wird. Diese Schriftenreihe dient seit mehr als 20 Jahren als eine Plattform zum Transfer und macht damit das Wissenspotenzial aus aktuellen Forschungsarbeiten am IPEK - Institut für Produktentwicklung Karlsruhe* am Karlsruher Institut für Technologie (KIT) verfügbar. Die Forschung des IPEK ist dabei strukturiert in die Kategorien Systeme, Methoden und Prozesse, um so der Komplexität heutiger Produktentwicklung ganzheitlich gerecht zu werden. Erst die Verknüpfung dieser drei Kategorien ermöglicht die Synthese innovativer Systeme durch Nutzung neuester Methoden und Prozesse. Gleichzeitig werden durch die Systemsynthese die erforschten neuen Methoden und Prozesse validiert und deren Mehrwert für die Praxis abgesichert. Dieses Forschungskonzept prägt nicht nur das IPEK-Leitbild, sondern auch den Charakter dieser Schriftenreihe, da immer alle drei Kategorien und deren Wechselwirkungen berücksichtigt werden. Jeder Band setzt hier individuelle Schwerpunkte und adressiert dabei folgende Forschungsgebiete des IPEK:

- das Entwicklungs- und Innovationsmanagement,
- die Entwicklungs- und Konstruktionsmethodik,
- der Leichtbau von der Ebene des ganzen Systems bis hinunter zur Optimierung des Bauteils,
- die Validierung technischer Systeme auch unter Berücksichtigung der NVH Aspekte (Noise, Vibration, Harshness) mit dem Fokus auf Schwingungen und Akustik an Komponenten und in den Gesamtsystemen sowie deren subjektiver Beurteilung durch den Menschen,
- die Antriebssystemtechnik mit den Schwerpunkten komplette Antriebslösungen für Fahrzeuge und Maschinen,
- das Design, die Tribologie und Erprobung von Kupplungen und Bremsen sowie
- die Gerätetechnik mit dem Schwerpunkt auf Power-Tools.

Die Forschungsberichte stellen Ergebnisse unserer Forschung sowohl anderen Wissenschaftlern als auch den Unternehmen zu Verfügung um damit die Produktentwicklung in allen ihren Facetten mit innovativen Impulsen zu optimieren

Albert Albers und Sven Matthiesen

* Eh.: Institut für Maschinenkonstruktionslehre und Kraftfahrzeugbau, Universität Karlsruhe (TH)

Vorwort zu Band 146

Bereits über viele Jahrzehnte gibt es im Maschinenbau sowie im Fahrzeugbau einen Megatrend zu einer immer weiteren Steigerung der Leistungsdichte, aber auch zu einer immer größeren Anreicherung der Produkte mit zusätzlichen Funktionen. Hier hat insbesondere auch die Mechatronisierung einen wichtigen Einfluss. Durch die Kombination von mechanischen Lösungen mit den Potentialen und Möglichkeiten einer elektronischen Ansteuerung und Regelung ergeben sich für die Gestalter der technischen Systeme ganz neue Möglichkeiten, um Kundennutzen zu stiften. Dieser generelle Trend zur Anreicherung der Funktionalitäten hat aber auch – ganz besonders im Fahrzeugbau – zu einem Trend der steigenden Gewichte der Fahrzeuge geführt. Mit jeder Generation hat sich das Gesamtfahrzeuggewicht gesteigert. Damit entsteht natürlich auch, wie bei allen dynamisch bewegten Systemen, durch die zu bewegende Masse ein zusätzlicher Energieaufwand zur Realisierung der Hauptfunktion „Transport von Personen und Gütern". Neben diesen technischen Randbedingungen und den Bedürfnissen, die sich aus den Märkten ergeben haben, wird in den letzten Jahren ein weiterer wichtiger Aspekt bei der Gestaltung von Fahrzeugen in den Fokus genommen. Es geht darum, im Angesicht der Erderwärmung, den Ausstoß von klimaschädlichen Gasen zu reduzieren oder gar vollständig zu vermeiden. Dies kann durch Wirkungsgrad- und Verbrauchsoptimierung im Bereich der konventionellen Antriebe erreicht werden oder aber auch durch den Wechsel der Antriebsart hin zu hybriden oder elektrischen Antrieben, bei denen dann zumindest im Betrieb Emissionen vermieden werden können. Sowohl die Wirkungsgradoptimierung des konventionell angetriebenen Fahrzeugs als auch die Gestaltung von elektrischen Antriebssträngen, insbesondere mit Batterien als Energiespeicher, führen dann aber zu einer weiteren Erhöhung der Gesamtgewichte. Um hier neue Lösungen zu erarbeiten und den Trend der steigenden Gewichte zu brechen, kommt dem Leichtbau in all seinen Ausprägungen eine besondere Rolle zu. Leichtbau kann dabei durch eine entsprechende Auswahl des Werkstoffes, die Gestaltung der Strukturbauteile oder aber auch durch den sogenannten Systemleichtbau als Optimierung des Gesamtsystems erreicht werden. Alle diese Möglichkeiten werden heute und müssen in Zukunft genutzt werden, um unter anderem die Treibhausgas-Thematik in den Griff zu bekommen und dabei gleichzeitig die individuelle Mobilität für die Menschen zu erhalten. Leichtbau als Strategie der Produktsynthese hat somit eine sehr hohe Bedeutung. Die Gruppe um ALBERS arbeitet auf dem Gebiet des Leichtbaus bereits seit vielen Jahren und hat hier durch eine kontinuierliche und strukturierte Grundlagenforschung Lösungsansätze und Methoden für die Praxis erarbeitet.

Im Kontext dieser Forschung ist auch die Arbeit von Herrn Dr.-Ing. Sven Michael Revfi angeordnet. Er hat im Rahmen seiner Forschung im Graduiertenkolleg (IRTG – International Research Training Group) *DFG GRK 2078/2* die Nutzung von faserverstärkten Kunststoffen bei gleichzeitiger Optimierung der Versickung als einen Forschungsschwerpunkt bearbeitet. Ergänzend zu dieser Forschung hat Herr Revfi in einem zweiten Teil seiner

Arbeit das Thema *Multi-Material Design* im Systemleichtbau über den sogenannten Erweiterten Target Weighing Ansatz (ETWA) erforscht. Die Arbeit bedient also zwei der großen Bereiche des Leichtbaus und liefert hierfür grundlagenbasierte Lösungen für die Praxis und gleichzeitig einen wichtigen wissenschaftlichen Beitrag für die Forschung auf dem Gebiet der Produktentwicklung mit Fokus auf den Leichtbau.

Dezember, 2021   Albert Albers

Kurzfassung

Mobilitätssysteme befinden sich in einer Zeit des Umbruchs, da sich die Randbedingungen aus Politik und Gesellschaft gerade stark verändern. Im Fokus steht dabei, den Energie- und Ressourcenverbrauch sowie die CO_2-Emissionen zu senken. Eine Möglichkeit diesen Herausforderungen zu begegnen, stellt der Leichtbau dar. Um die größtmögliche Gewichtsreduzierung erreichen zu können, ist eine konsequente Integration der Leichtbauaktivitäten in den gesamten Produktentstehungsprozess notwendig.

Die vorliegende Arbeit liefert einen Beitrag zur Unterstützung des Produktentwicklers in verschiedenen Aktivitäten des Produktentstehungsprozesses, indem sie sich mit den Fragen „*wie* können Bauteile aus langfaserverstärkten Kunststoffen fasergerecht gestaltet werden" und „*wo* sind diese in einem intelligenten Multi-Material Design (MMD) zielführend einzusetzen" beschäftigt. Zur Frage „*wie*" wird für die initiale Designfindung von versickten, langfaserverstärkten Bauteilen eine rechnergestützte, automatisierte Optimierungsmethode entwickelt. Bei diesem anisotropen Werkstoff ist es entscheidend, dass die aus dem Herstellungsprozess resultierenden Faserorientierungen im Bauteildesign berücksichtigt werden. Deshalb liegt der Optimierungsmethode eine iterative Kopplung von validierten Prozess- und Struktursimulationen zugrunde. Die Ergebnisse zeigen, dass die Berücksichtigung der lokal anisotropen Materialeigenschaften im Vergleich zu einer isotropen Materialmodellierung zu deutlich unterschiedlichen Designs führt.

Um diese last- und fasergerecht designten Bauteile in einem MMD zielführend einsetzen zu können, ist jedoch zusätzlich die Frage nach dem „*wo*" zu beantworten. Deshalb beschäftigt sich die Arbeit weiterhin mit der Entwicklung des funktionsbasierten Erweiterten Target Weighing Ansatzes (ETWA) zur komponentenübergreifenden Identifikation und Evaluation von Leichtbaupotentialen. Der ETWA unterstützt den Produktentwickler bei der Konzeptgenerierung in frühen Phasen des Produktentstehungsprozesses, in denen bereits ein Großteil des späteren Produktgewichts festgelegt wird. Dabei werden sowohl in der Analyse als auch in der Synthese die mit dem Gewicht und dessen Reduktion einhergehenden Kosten und CO_2-Emissionen gemeinschaftlich betrachtet. Die Ergebnisse der mithilfe des ETWA im Rahmen dieser Arbeit entwickelten MMD eines Automobil-Federbeindoms und -Längsträgers zeigen das Potential der Methode auf.

Die Kombination des ETWA und der fasergerechten Gestaltung versickter langfaserverstärkter Bauteile bietet eine methodische Unterstützung bei der Entwicklung von MMD insbesondere in frühen Phasen der Produktentstehung.

Abstract

Mobility systems are in times of upheaval, as the requirements from politics and society are currently undergoing major changes. The focus is on reducing energy and resource consumption as well as CO_2 emissions. One way to face these challenges is lightweight design. In order to achieve the greatest possible mass reduction, it is necessary to consistently integrate lightweight design into the entire product engineering process.

The present work contributes to various activities of the product engineering process. It supports the product developer by addressing the questions of "*how* parts made of long fiber reinforced polymers can be designed fiber-adapted" and "*where* they can be used purposefully in an intelligent multi-material design (MMD)". To answer the question of "*how*", a computer-aided, automated optimization method for the initial design of beaded long fiber reinforced parts is developed. For this anisotropic material, it is crucial that the fiber orientations resulting from the manufacturing process are taken into account in the part design. Therefore, the optimization method is based on an iterative coupling of validated process and structural simulations. The results show that the consideration of locally anisotropic material properties leads to significantly different designs compared to an isotropic material modeling.

To be able to use these load- and fiber-adapted designed components successfully in an MMD, it is necessary to answer additionally the question of "*where*". Therefore, this work further deals with the development of the function-based Extended Target Weighing Approach (ETWA) for the cross-component identification and evaluation of lightweight design potentials. The ETWA supports the product developer in concept generation in early phases of the product engineering process, where most of the later product mass is already determined. In the method, the costs and CO_2 emissions associated with the mass and its reduction are considered together in both the analysis and the synthesis. In this work, the results of applying the ETWA for the development of an MMD for an automotive strut tower and rail show the potential of the method.

The combination of the ETWA and the fiber-adapted design of beaded long fiber reinforced parts provides methodological support for the development of MMD, especially in early phases of product engineering.

Acknowledgment

This thesis was written as part of my work as a doctoral researcher at IPEK – Institute of Product Engineering at the Karlsruhe Institute of Technology (KIT).

I would like to express my special thanks to my supervisor, Univ.-Prof. Dr.-Ing. Dr. h. c. Albert Albers, for the scientific supervision of this thesis as well as the responsibility and the trust he placed in me. During the collaboration, in which he not only challenged and encouraged me, but also decisively shaped me, he had a great influence on the achieved research results by fruitful discussions and valuable suggestions. The environment he created at IPEK – Institute of Product Engineering significantly influenced my thinking as well as acting and therefore contributed a great deal to the success of this work.

For taking over the co-supervision and the productive collaboration, I would like to thank Prof. Dr. Kamran Behdinan. He mentored my work within the International Research Training Group GRK 2078/2 where he decisively broadened my perspective on the topics of simulation, optimization, and design readiness. I am grateful that he invited me to the University of Toronto for a three-month research stay. But even during the Corona pandemic, he was always available for online discussions of my research topics.

I also thank all the staff at IPEK – Institute of Product Engineering, both in the scientific and administrative areas. In particular, I would like to thank my colleagues in the CAE/Optimization research group for the many scientific discussions and impulses. The productive and friendly working atmosphere provided an essential basis for my research work. Furthermore, I thank my colleagues from the International Research Training Group GRK 2078/2. This unique research environment and the interdisciplinary discussions made a significant contribution to the success of this work. Moreover, I would like to thank my colleagues from the EU project ALLIANCE, through whom my research received direct feedback from industry. I also thank all my research assistants as well as bachelor and master students for their contributions. They provided a great support in my research work.

My biggest thanks go to my family, who have made me who I am today. I can't thank enough my parents Karin and Andreas and my stepparents Bernd and Nicole for their support and encouragement over the years. Thanks to my brother Maximilian, who helped me clear my head with welcome distractions especially in challenging phases. I would also like to extend my big thanks to Stephanie, who has tirelessly supported me through all phases of this work. Likewise, I would like to thank all my friends for the wonderful moments we spent together, which provided important breaks.

Sven Revfi   December, 2021

"Make things as simple as possible – but no simpler"

Albert Einstein, 1879-1955

Table of Contents

List of Figures

List of Tables

Acronyms

1D	One-dimensional
2D	Two-dimensional
3D	Three-dimensional
AHP	Analytical hierarchy process
AIL	Agile Innovation Lab
ALLIANCE	Affordable Lightweight Automobiles Alliance
ALLSE	Recoverable strain energy
ALLWK	External work
ARD	Anisotropic rotary diffusion
ASME	American Society of Mechanical Engineers
AV	Attribute variation
BMWi	Federal Ministry for Economic Affairs and Energy
BEV	Battery electric vehicle
C	Connector
CAD	Computer-aided design
CAE	Computer-aided engineering
CAO	Computer-aided optimization
C&C²-A	Contact, Channel and Connector Approach
CF	Carbon fiber
CoDiCoFRP	Continuous Discontinuous fiber reinforced polymers

CRF	Centro Ricerche Fiat
CSS	Channel and support structure
CT	Computed tomography
CTE	Coefficient of thermal expansion
CV	Carryover variation
DIC	Digital Image Correlation
DIN	German Institute for Standardization
DRL	Design Readiness Level
DFG	German Research Foundation
DRM	Design Research Methodology
EDA	Energy Distribution Analysis
ETS	Exponential smoothing
ETWA	Extended Target Weighing Approach
EU	European Union
EUCAR	European Council for Automotive R&D
EV	Embodiment variation
FAS4M	Functional Architectures of Systems for Mechanical Engineers
FAST	Institute of Vehicle System Technology
FCA	Fiat-Chrysler Research Centre
FE	Finite element
FEM	Finite element method
FLD	Forming limit diagrams

FMA	Function Mass Analysis
FME	Function Mass Estimation
FRP	Fiber reinforced polymer
FTP-75	Federal Test Procedure
GA	Genetic algorithm
GFRP	Glass fiber reinforced polymer
GRK	International Research Training Group
GWP	Global warming potential
IAM-WK	Institute for Applied Materials – Materials Science and Engineering
IC	Information Check
ICEV	Internal combustion engine vehicle
ICT	Fraunhofer Institute for Chemical Technology
ika	Institute for Automotive Engineering – RWTH Aachen University
IP	Integrated Product Development
IPEK	Institute of Product Engineering
iPeM	Integrated Product engineering Model
IRL	Integration Readiness Level
IRTG	International Research Training Group
ISO	International Organization for Standardization
ITM	Institute of Engineering Mechanics
JP 10-15	Japanese test cycle: 10-15 mode

KaSPro	Karlsruhe School of Product Engineering
KIS	Continuous Idea Storage
KIT	Karlsruhe Institute of Technology
LCA	Life-cycle assessment
LCC	Life-cycle cost
LFT(-D)	Long Fiber Reinforced Thermoplastic (Direct Method)
LFT-G	Long Fiber Reinforced Thermoplastic Granulates
MBSE	Model-based systems engineering
MDO	Multidisciplinary design optimization
MMD	Multi-material design
MNEDC	Modified New European Driving Cycle
MP	Mathematical programming
NASA	National Aeronautics and Space Administration
OC	Optimality criteria
OEM	Original equipment manufacturer
PAN	Polyacrylonitrile
PBS	Principal bending stress
PBSD	Principal bending stress direction
PGE	Product Generation Engineering
PLT	Problem Solving Team
PP	Polypropylene
PV	Principle variation

R&D	Research and development
ROI	Return on investment
RSC	Reduced-strain closure
RTM	Resin Transfer Molding
SE	Systems engineering
SIMP	Solid Isotropic Material with Penalization
SLM	Selective laser melting
SM	Submodule
SMC	Sheet molding compound
SysML	Systems Modeling Language
SRL	System Readiness Level
TRB	Tailor Rolled Blanks
TRL	Technology Readiness Level
TWA	Target Weighing Approach
UD	Unidirectional
UPPH	Unsaturated polyester-polyurethane hybrid
VDI	The Association of German Engineers
VPA	Validation Prioritization Approach
WSP	Working Surface Pair

Symbols

Latin letters

α	Slip coefficient function
α_g	Data-fitted coefficient
α_F	Coefficient of thermal expansion of the fiber
α_M	Coefficient of thermal expansion of the matrix
α_R	Slope of a road
α_S	Flank angle
α_T	Trajectory angle
α_1	Coefficient of thermal expansion of the composite in longitudinal direction
α_2	Coefficient of thermal expansion of the composite in transverse direction
α^*	Degree of cure
β	Polymer expansivity
Γ_t	Traction part of the boundary of the domain
$\dot{\boldsymbol{\gamma}}$	Strain rate tensor
$\dot{\gamma}$	Shear rate
$\boldsymbol{\varepsilon}$	Strain tensor
$\boldsymbol{\varepsilon}^C$	Complicated strain
$\boldsymbol{\varepsilon}^T$	Transformation strain
ε_{g0}	Strains due to thermal shrinkage
η	Viscosity
η_0	Zero shear viscosity
κ	Scalar reduction factor
λ	Shape factor

λ_m	Mass factor
λ_{1-3}	Eigenvalues of the fiber orientation tensor $\boldsymbol{A}$
ν_F	Poisson's ratio of the fiber
ν_M	Poisson's ratio of the matrix
ν_{iso}^{LFT}	Isotropic Poisson's ration of LFT
ν_{iso}^{SMC}	Isotropic Poisson's ration of SMC
ν_{12}, ν_{xy}	Poisson's ratio of fiber and transverse directions
ν_{13}, ν_{xz}	Poisson's ratio of fiber and transverse material plane directions
ν_{23}, ν_{yz}	Poisson's ratio of transverse directions
ρ	Density
ρ_C	Composite density
ρ_F	Fiber density
ρ_M	Matrix density
$\rho(x)$	Local density
ρ_0	Initial density
ρ_{Air}	Air density
$\boldsymbol{\sigma}$	Cauchy stress tensor
σ	Force
σ_B	Bending stress
σ_M	Membrane stress
σ_O	Stresses on the top of the part
σ_P	Maximum principal stress
σ_U	Stresses on the bottom of the part
σ_g	Initial stresses
σ_{g0}	Pressure at freeze stresses
$\sigma_I, \sigma_{II}, \sigma_{III}$	Principal stresses
σ_1	Stress component in the material's principal axis 1

σ_2	Stress component in the material's principal axis 2
$\boldsymbol{\tau}$	Viscous stress tensor
τ_C	Critical shear stress above which slip occurs
τ_W	Wall shear stress
τ_{12}	Shear component in the material's principal axes 1,2
τ^*	Data-fitted coefficient
$\dot{\phi}$	Angular velocity of a fiber
φ	Fiber angle
ψ	Probability density function
Ω	Problem domain

Greek letters

$\boldsymbol{A}$	Fiber orientation tensor
A	Projected frontal area
A_{Bead}	Bead cross sectional area
a	Acceleration
B	Data-fitted coefficient
B^*	Pressure sensitivity of the material
$\boldsymbol{b}$	Body force density vector
b_O	Top chord width
b_P	Plate width
b_R	Rib width
b_S	Bead width
b_1-b_5	Scalar constants
b_{1m-4m}	Data-fitted coefficients
b_{5*}	Data-fitted coefficient
$\mathbb{C}$	Stiffness tensor

$\boldsymbol{C}_i$	Anisotropic rotary tensor
C	Constant
$CO2$	CO_2 emissions
C_I	Fiber-fiber interaction coefficient
C_p	Specific heat capacity of the melt
C_1	Data-fitted coefficient
C_2	Data-fitted coefficient
c_F	Fiber weight fraction
c_W	Drag coefficient
D	Fiber diameter
D_g	Stress-strain relationship matrix
$\boldsymbol{d}$	Global displacement vector
d_F	Fiber bundle width
$\mathbf{E}_E$	Eshelby tensor
$E(x)$	Local stiffness
E_F	Young's modulus of the fiber
E_M	Young's modulus of the matrix
E_{iso}^{LFT}	Isotropic Young's modulus of LFT
E_{iso}^{SMC}	Isotropic Young's modulus of SMC
E_0	Initial Young's modulus
E_1, E_{11}, E_x	Young's modulus of fiber direction
E_2, E_{22}, E_y	Young's modulus of transverse direction
E_3, E_z	Young's modulus of transverse material plane direction
€	Costs
e_i	Vector between element center of the source mesh and the target mesh
e_n	Average element edge length
e_{1-3}	Eigenvectors of the fiber orientation tensor $\boldsymbol{A}$

e^*_{1-3}	Centroidal distances
F	Force (scalar)
F_{total}	Total driving resistance
F_{Air}	Air resistance force
F_{Roll}	Rolling resistance force
F_{Grade}	Grade resistance force
$F_{Acceleration}$	Acceleration resistance force
$\boldsymbol{f}$	Global force vector
f	Fitness function
f_T	Trajectory fineness
$f(\boldsymbol{x})$	Objective function
f_r	Rolling resistance coefficient
G_F	Shear modulus of the fiber
G^{SMC}_{iso}	Isotropic shear modulus of SMC
G_{12}, G_{xy}	Shear modulus of fiber and transverse directions
G_{13}, G_{xz}	Shear modulus of fiber and transverse material plane directions
G_{23}, G_{yz}	Shear modulus of transverse directions
$\boldsymbol{g}$	Gravitational acceleration vector
$g_j(\boldsymbol{x})$	Inequality constraints
$h_k(\boldsymbol{x})$	Equality constraints
h_R	Rib height
h_S	Bead height
$\dot{h}$	Tool closing speed
I_y	Second moment of area
$\boldsymbol{K}$	Global stiffness matrix
k	Polymer thermal conductivity
$\boldsymbol{L}$	Fourth-order tensor

l_F	Fiber length
$\boldsymbol{M}$	Fourth-order tensor
m	Mass
m_K	Number of components
m_S	Slip exponent
m_V	Vehicle mass
$\boldsymbol{n}$	Unit normal vector
n	Data-fitted coefficient
n_i	Nodes of the target mesh
P	Probability
P_x	Parameter set
p	Pressure
p_{SIMP}	Penalty factor of the SIMP model
R^c	Compressive strength
R^t	Tensile strength
R_{shear}	Shear strength
$R_{\perp\parallel}$	Shear strength of fiber and transverse directions
$R_{\parallel}^c$	Compressive strength in fiber direction
$R_{\perp}^c$	Compressive strength in transverse direction
$R_{\parallel}^t$	Tensile strength in fiber direction
$R_{\perp}^t$	Tensile strength in transverse direction
r_e	Aspect ratio
s_{n-1}	Increment
T	Temperature
T_t	Volumetric transition temperature
T_b	Data-fitted coefficient
$\boldsymbol{t}$	Traction vector

t	Time
t_P	Plate thickness
V	Volume
$\mathbf{v}$	Velocity vector
v	Velocity
v	Specific volume
v_n	Cardinal coefficients
v_{rel}	Relative velocity
v_s	Slip velocity
v_t	Specific volume at the volumetric transition temperature T_t
v_0	Specific volume at zero gauge pressure
$\boldsymbol{w}$	Vorticity tensor
$\boldsymbol{w(x)}$	Weight function
w_{CO2}	Weighting factor for CO_2 emissions
w_{ϵ}	Weighting factor for costs
w_m	Weighting factor for mass
$\boldsymbol{x}$	Design variables
x_i^L	Lower bound of side constraint
x_i^U	Upper bound of side constraint
x_n	New trajectory point
x_{n-1}	Current trajectory point

1   Introduction

"Lightweight design is one of the game-changer technologies of the 21st century"[1] (German Federal Ministry for Economic Affairs and Energy, 2019, p. 1). With these words, the German Federal Minister of Economics Peter Altmaier opened the 2019 Lightweighting Summit at HANNOVER MESSE. The German Federal Ministry for Economic Affairs and Energy (BMWi) considers lightweight design to be one of the "key technologie[s]"[2] (German Federal Ministry for Economic Affairs and Energy, 2019, p. 1). (German Federal Ministry for Economic Affairs and Energy, 2019)

The fact that lightweight design plays such a major role in politics is due to the important contribution it can make to environmental and climate protection as well as to resource conservation. Combating the causes of climate change has been on the global political agenda for years and found expression in the signing of the Paris Agreement by 195 UN states in 2016.

The European Union (EU) is at the forefront in this combat. That is why, the European Council requested, in March 2018, a long-term strategy for reducing greenhouse gas emissions. The European Commission responded with a vision for climate neutrality by 2050 that affects all economic sectors. (European Commission, 2018)

A look at the greenhouse gas emissions per sector in Figure 1.1 shows that the transport sector accounts for almost a quarter of it. These emissions are related to fuel combustion for energy supply, which is needed to accelerate the mass. Accordingly, one possibility to decrease these emissions is to reduce the mass of the products through lightweight design (Heuss, Müller, van Sintern, Starke, & Tschiesner, 2012).

To illustrate the potential of lightweight design, the following examples can be given with regard to a mass reduction of 100 kilograms: In the aviation industry, 100 kilograms less mass of an Airbus A 320 corresponds to almost 10,000 liters less kerosene per aircraft and year. In the automotive industry, 100 kilograms less mass of

---

[1]   Translated by the author: „Der Leichtbau gehört zu den Game-Changer-Technologien des 21. Jahrhunderts" [German Federal Ministry for Economic Affairs and Energy (2019, p. 1)]

[2]   Translated by the author: „Schlüsseltechnologie[n]" [German Federal Ministry for Economic Affairs and Energy (2019, p. 1)]

an internal combustion engine vehicle (ICEV) corresponds to 0.5 liters less fuel consumption per 100 kilometers. (German Federal Ministry for Economic Affairs and Energy, 2021) For battery electric vehicles (BEV), a reduction of 100 kilograms in mass leads to a saving of about 4% of the drive energy (Hohmann, Hillebrecht, & Schäfer, 2018). This allows populist assertions (e.g., Ntv (2018)) to be refuted, according to which lightweight design no longer plays a significant role in heavier electric vehicles due to their recuperation capability. Consequently, lightweight design will continue to retain its relevance in the ongoing transformation of the transport sector toward battery solutions. Or to put it in the words of Peter Altmaier: "We are in a window of opportunity with an ideal momentum for lightweight design"[3] (Siebel, 2021, "Ein ideales Momentum für den Leichtbau").
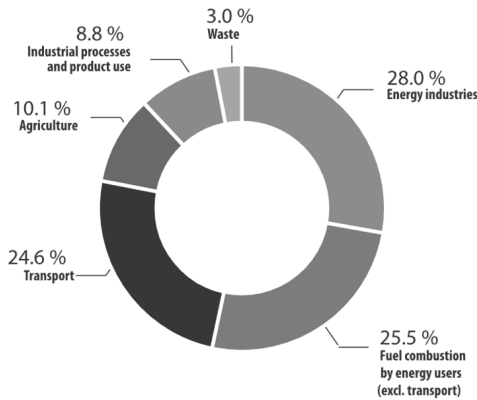
Figure 1.1: Shares of European greenhouse gas emissions in 2018 adapted from Eurostat (2021)

In order to perform lightweight design, there are various strategies available. However, the greatest possible lightweight potential can only be exploited if lightweight design is consistently integrated throughout the entire product engineering process

---

[3] Translated by the author: „Wir befinden uns in einem Window of Oportunity [*sic*] mit einem idealen Momentum für den Leichtbau" [Siebel (2021, "Ein ideales Momentum für den Leichtbau")]

(Albers, Holoch, Revfi, & Spadinger, 2021). This represents a complex development challenge to which the author's research work makes a contribution.

1.1 Focus of the Thesis

The present work focuses on the lightweight design strategies of material, form and system lightweight design (see Section 2.2).

In the context of material and form lightweight design, the fiber-adapted design of parts made of long fiber reinforced polymers is considered (see Chapter 4). Long fiber reinforced polymers offer great potential in the field of material lightweight design as they combine high mass-specific stiffnesses and strengths. In addition, they give the product developer a superior design freedom. Nevertheless, they are still rarely used for load-bearing components. This is partly due to the fact that the fiber-adapted design is not yet sufficiently understood. To exploit the full potential of this class of materials, it is necessary to take into account the anisotropic material properties resulting from the manufacturing process in the design process. At the same time, this must already be done in the early phases of product development, before the molds required for the manufacturing of the part are commissioned, since their iterative adjustments entail high costs in the further course of product development. This thesis uses the example of bead designs to answer the question of "*how*" to deal with the anisotropic material in the design process. In this context, the focus is on the interactions between design, manufacturing and material, which are modeled with the aid of numerical simulation methods.

Considering system lightweight design, which closely interacts with material and form lightweight design and aims to optimize the overall mass of the system, the question of "*where*" to use fiber reinforced polymers purposefully in a multi-material design (MMD) is addressed (see Chapter 5). However, the developed method of the Extended Target Weighing Approach (ETWA) is not limited to fiber reinforced polymers, but is open for the use of all material classes.

The model-theoretical context of the work, which is shown in Figure 1.2, is based on the elements of the KaSPro – Karlsruhe School of Product Engineering. In particular, the understanding of product development as defined by the model of PGE – Product Generation Engineering according to Albers (see Subsection 2.1.2) forms the basis for the developed lightweight design methods. Further fundamentals are the Contact, Channel and Connector Approach (C&C²-A) (see Subsection 2.1.3), the Target Weighing Approach (TWA) (see Subsection 2.2.6) as well as the numerous preliminary works at IPEK – Institute of Product Engineering in the context of the

coupling of simulation methods for structural optimization (see Section 2.6) and especially bead optimization (see Section 2.7).
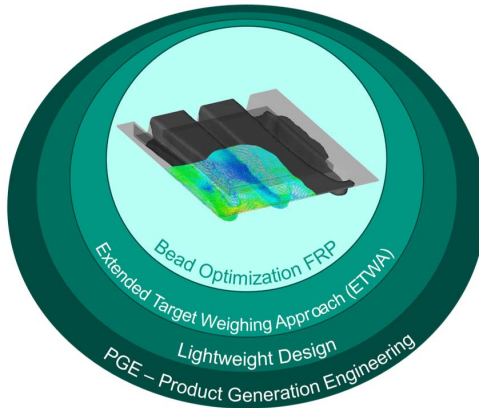
Figure 1.2: Context of the present research work. The framework is set by the PGE – Product Generation Engineering and in particular by lightweight design. In the context of lightweight design, a method for the process-based bead optimization of fiber reinforced parts and the Extended Target Weighing Approach (ETWA) are being researched.

1.2   Thesis Organization

This thesis is divided into six chapters, whose organizational structure is shown in Figure 1.3. The individual chapters are described subsequently.
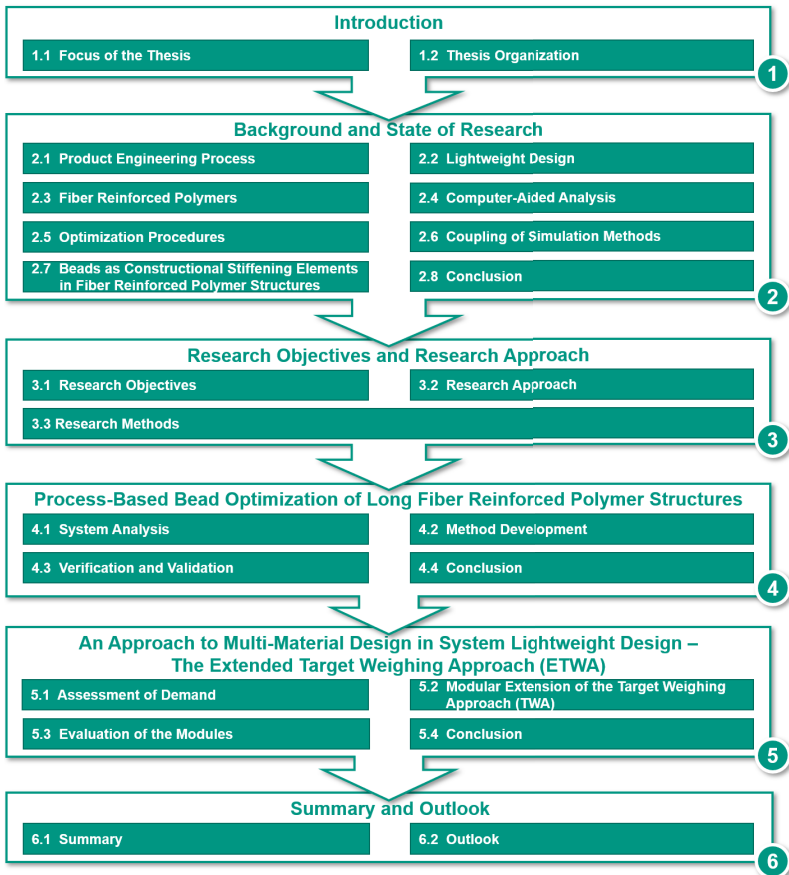
Figure 1.3: Organization of the thesis

Following the introduction, the necessary background for the understanding of the present work and the state of research are presented in Chapter 2. This includes the pillars of the KaSPro – Karlsruhe School of Product Engineering, such as the iPeM – Integrated Product Engineering Model (see Subsection 2.1.1), the model of PGE – Product Generation Engineering (see Subsection 2.1.2) and the Contact,

Channel and Connector Approach (C&C²-A) (see Subsection 2.1.3), which have decisively determined the mindset underlying the work. Subsequently, the lightweight research fields relevant for the work are introduced. The focus is set on function-based methods as a methodical support of lightweight design activities in system lightweight design as well as the combination of material and form lightweight design for the use of beads in fiber reinforced polymer structures. In addition, the necessary simulative background and related state of research to investigate the fiber-adapted design of beaded parts will be presented.

Based on the findings from the state of research, the research objective and the research approach are described in Chapter 3. The research hypotheses derived from the research gap are operationalized by research questions and arranged in a structured research approach, which is based on the *Design Research Methodology (DRM)* according to Blessing and Chakrabarti (2009). Additionally, the research methods used are presented.

Chapter 4 is devoted to the computer-aided, process-based bead optimization of long fiber reinforced polymers. Based on a system analysis, the demands for a methodical support of the product developer in the fiber-adapted design of beaded parts are first derived, for which a *simulative optimization method* is subsequently developed. Finally, the individual methods of the optimization method are validated in order to verify the overall method. Thus, Chapter 4 deals with the question of "*how*" to design fiber-adapted parts.

In Chapter 5, the question of "*where*" fiber reinforced polymers are suitable for the application in system lightweight design is posed in order to be able to achieve lightweight design targets while taking into account costs and emissions. For this purpose, the function-based lightweight design method *Extended Target Weighing Approach (ETWA)* is developed on the basis of identified demands, and its individual methods are ultimately evaluated.

Finally, in Chapter 6, the results of the present work are summarized and an outlook on future research topics linked to this thesis is given.

2 Background and State of Research

The present research work deals with lightweight design optimization at both system and component level. For this purpose, on the one hand, development methods and, on the other hand, computer-aided analyses and optimizations are used.

The aim of this chapter is to provide the necessary background for the understanding of the thesis and to summarize the relevant state of research.

2.1 Product Engineering Process – Process, Product and Description Models

Lightweight design activities have their specific potential at different phases in the development process, but can only reach their full potential if they are applied consistently and in an integrated way (Albers, Holoch, et al., 2021). Therefore, for the later classification of the developed methods in the product engineering process, the models and methods of the KaSPro – Karlsruhe School of Product Engineering, which are central elements of this thesis, are presented and discussed. These include the iPeM – Integrated Product Engineering Model (see Subsection 2.1.1), the PGE – Product Generation Engineering model (see Subsection 2.1.2), the Contact, Channel and Connector Approach (C&C²-A) (see Subsection 2.1.3), the function-based product development (see Subsection 2.1.4), and the Validation Prioritization Approach (VPA) (see Subsection 2.1.5).

2.1.1 iPeM – Integrated Product Engineering Model

In order to be economically successful, companies must launch new products on the market. A mere technical finding, an invention, can only become a successful product on the market, an innovation, if it is of benefit to the customer (Schumpeter, 1912). To achieve this, the necessary process of product engineering ranges from the identification of needs over the development of technical solutions to commercial sales (Whitney, 1990). Therefore, product engineering comprises product planning, product development, and production system development (Albers & Gausemeier, 2012; VDI 2221 Part 1, 2018). In this context, product development describes all activities required to develop a product from the initial idea to market maturity (Al-

bers, Braun, Heimicke, & Richter, 2020). Although different product engineering processes have common characteristics, each of them is "unique and individual"[4] (Albers, 2010, p. 4) according to Albers. In addition, the complexity of the technical solutions themselves, but also of their development processes, continues to increase due to various influences (e.g., globalization, market saturation, etc.) (Albers, 2008). Therefore, in the past, various description models have been developed in order to structure the product development process and to be able to manage it proactively. In this context, for example, the stage-gate process (Cooper, 1990), the V-model (VDI 2206, 2004) or the revised VDI guideline 2221 (VDI 2221 Part 1, 2018) can be mentioned. For further process models, it is referred to Wynn and Clarkson (2018).
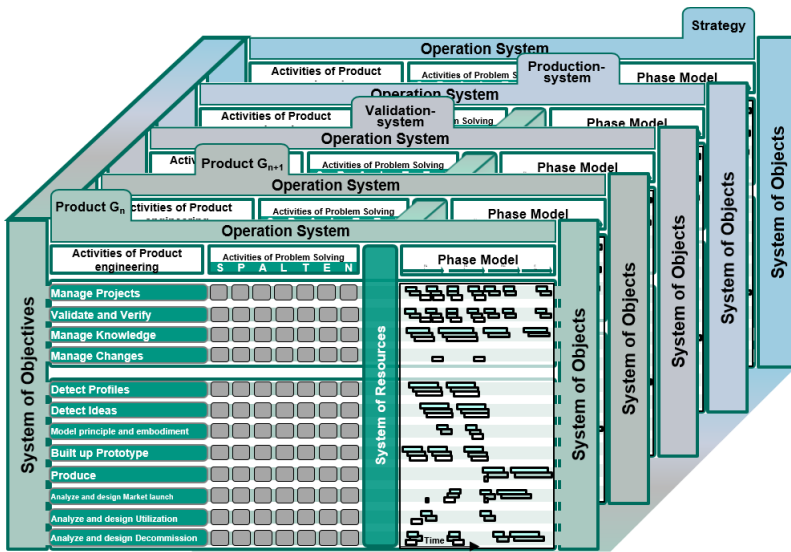
Figure 2.1:   iPeM – Integrated Product Engineering Model adapted from Albers, Reiß, Bursac, and Richter (2016)

---

4   Translated by the author: „einzigartig und individuell" [Albers (2010, p. 4)]

However, most of these models are not able to capture the individuality of projects because they are too formalized, have a specific perspective (product developer vs. management) on the process or different granularities. Moreover, these models reach their limits when dealing with the described complexity, which is additionally increased by highly interconnected processes with many interactions, because they are sequential and therefore cannot describe recursions and parallelisms of processes. Therefore, Albers developed the iPeM – Integrated Product Engineering Model (Albers & Meboldt, 2007), which was continuously extended in the following years (Albers, Reiß, Bursac, & Richter, 2016). iPeM is a meta-model that allows the derivation of specific, problem-oriented models for individual product engineering processes (Albers & Meboldt, 2007). It is based on the five basic hypotheses about engineering processes according to Albers (2010) and aims to bridge the gap between product developers and management through its integrative approach. Figure 2.1 shows the schematic graphical representation of the iPeM.

In the following, the central components of iPeM are introduced in more detail.

System of Objectives, Operation System, System of Objects – The ZHO-Model[5]

The iPeM is based on the elements *system of objectives*, *operation system* and *system of objects* of the ZHO-Model. This ZHO-Model can be traced back to the systems theory according to Ropohl (1975), who models product engineering with the help of systems engineering (SE). Accordingly, product engineering describes the transfer of a system of objectives into a system of objects by an operation system. The system of objectives contains the objectives of the product to be developed, their interactions and justifications, as well as associated requirements, restrictions and boundary conditions. The solutions as well as partial solutions are elements of the system of objects. (Albers & Meboldt, 2007) In the course of product engineering, the system of objectives is continuously expanded and concretized, for example, through the validation of intermediate results (Albers & Braun, 2011). The system of objectives and the system of objects are only indirectly connected via the socio-technical operation system. This includes besides structuring activities, methods and processes also, in the system of resources, the resources required for the development (Albers & Braun, 2011). The system of resources comprises, among others, the work capacity of the product developer, workplaces, budget, etc. The

---

[5] The German abbreviation ZHO means "Zielsystem" (engl.: system of objectives), "Handlungssystem" (engl.: operation system), and "Objektsystem" (engl.: system of objects)

connection of the system of resources with the system of objectives can be supported by knowledge management approaches (Richter, Wong, & Albers, 2020). In order to define appropriate next steps in the product engineering process based on the ZHO model, a description model (Richter, Troester, Felber, Albers, & Behdinan, 2020), a visualization model (Richter, Felber, Troester, Albers, & Behdinan, 2020), and a process model (Richter, Schmidt, Hahlweg, Behdinan, & Albers, 2020) can be used.

The transformation of elements of the system of objectives into elements of the system of objects by the operation system is understood as an activity of problem solving. To approach this problem solving systematically, Albers developed the problem solving method SPALTEN.

Activities of Problem Solving – SPALTEN

Product engineering can generally be understood as problem solving (Albers, Saak, Burkardt, & Schweinberger, 2002). A problem is characterized by an unwanted initial state that cannot be transformed, due to the existence of a barrier, into a desired final state (Dörner, 1979). In contrast to this, in tasks, both the initial and the final state are known and there is no barrier (VDI 2221 Part 1, 2018). Therefore, in problem solving, something new has to be generated (knowledge work), whereas in task solving, only reproductive thinking is necessary (process work) (Dörner, 1979).

To support a purposeful and systematic solution of problems, Albers (Albers et al., 2002) developed the problem solving method SPALTEN, which has been continuously developed since then (Albers, Burkardt, Meboldt, & Saak, 2005; Albers, Reiß, Bursac, & Breitschuh, 2016). SPALTEN is an acronym composed of the first letters (in German) of the problem solving activities that have to be performed to solve the problem. Figure 2.2 shows the individual steps and the workflow of the method. The SPALTEN method has a fractal character, as it can be used again within the individual problem solving activities (see Figure 2.2). Three further important elements are the Problem Solving Team (PLT), the Information Check (IC), and the Continuous Idea Storage (KIS). Prior to each application of the method, the PLT has to be initially compiled. Afterwards, it needs to be monitored and adapted in the course of the process, since different activities of problem solving require different competencies. In the IC, it has to be checked before each activity whether all relevant information is available. The KIS is used to collect all generated ideas. In this way, ideas that are not to be pursued immediately can be reused in the further process or are available for future problem solving processes.
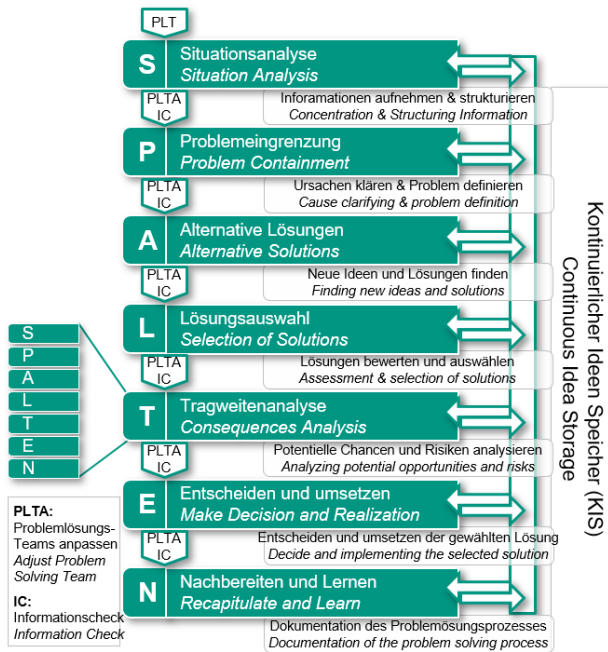
Figure 2.2: Workflow of the problem solving method SPALTEN (Albers, Reiß, Bursac, & Breitschuh, 2016)

SPALTEN can be applied individually to each activity in the product engineering process in order to solve arising problems in a structured way.

Activities of Product Engineering

The activities of product engineering comprise activities of different product life cycle phases. However, they are generic, i.e. they can be specifically adapted to the respective use cases, and have no logical or temporal correlation (Albers & Braun, 2011). It can be further distinguished between four basic activities (Manage Projects, Validate and Verify, Manage Knowledge, Manage Changes) and eight core activities (Detect Profiles, Detect Ideas, Model principle and embodiment, Built up Prototype,

11

Produce, Analyze and design Market launch, Analyze and design Utilization, Analyze and design Decommission) of product engineering (Albers, Reiß, Bursac, & Richter, 2016).

For the orientation in the process, being aware of the own situation with regard to the activities of product engineering as well as problem solving is helpful. For this, the activity matrix provides support.

Activity Matrix

The activities of product engineering and the activities of problem solving span the activity matrix, which in iPeM consists of 84 fields. The classification of the own situation offers an orientation in the product engineering process. (Albers, Braun, et al., 2020) In addition, with the help of the situation determination, supporting methods can be derived. Albers, Reiß, Bursac, Walter, and Gladysz (2015) developed an interactive tool for situation- and demand-oriented method recommendation under the name *InnoFox*. A detailed description of this developed application for end-user devices can be found in the work of Reiß (2018). A material-specific enhancement of this work, which proposes methods for the situation-specific use of continuous-discontinuous fiber reinforced polymers based on the classification in the activity matrix, was researched by the work of Butenko (2020) and published under the name *CoDico-FiberFox* (Butenko & Albers, 2019).

Different Layers in iPeM and Their Interactions

The increasing interconnectedness and complexity of products require an integrated view of the product engineering process. A good example to show this is the connection between product and production system, because every product development always includes a production system development or adaptation. Only if the development is closely coordinated the highest possible user benefit can be achieved. Particularly in the field of the development of lightweight solutions made of fiber reinforced polymers (FRP), the consideration of the interdependence of product and production is crucial, as the full potential of FRP can only be exploited through a manufacturing process-based design (May, 2020).

In order to be able to model these observations with the iPeM, it was expanded to include other relevant company sectors (Albers, Reiß, Bursac, & Richter, 2016). The introduced layers *Product G$_{n+1}$*, *Strategy*, *Production System* and *Validation System* give the iPeM a three-dimensional (3D) structure (see Figure 2.1). In the context of the description of the product engineering by means of the systems theory, each layer contains its own system of objects. However, there is an interdependence between them, which allows an interaction of the objects. In contrast, the system of

resources and the system of objectives are modeled continuously in order to create only one consistent system of objectives and to be able to clearly control the overall resources in the company or in a specific development process. (Albers, Reiß, Bursac, & Richter, 2016)

The layer *Product G_n* describes the product that will be launched on the market next. However, since products are developed in generations, it makes sense from a strategic and planning perspective to already consider the next product generation G_{n+1} in a separate layer. This planning activity should not be limited to products under development, but can be applied analogously to the other layers. The observation that products are developed in generations is described with the description model of the PGE – Product Generation Engineering according to Albers which is discussed in the next subsection.

2.1.2 Description Model of the PGE – Product Generation Engineering

To describe product development processes, the theories known, for example, in innovation management (Henderson & Clark, 1990) or the classifications of design types widely used in design methodology (Ehrlenspiel, 2009; Feldhusen, Pahl, & Beitz, 2013) are not sufficient (Albers, Braun, et al., 2020). Rather, product development processes have a large amount of transferred knowledge from other products, which is adapted or extended in a product-specific way. Based on this insight, Albers developed the description model of PGE – Product Generation Engineering (Albers, Bursac, & Wintergerst, 2015). The PGE is based on two central basic hypotheses:

- New product generations are always developed on the basis of a reference system. The reference system and its elements are the basis and starting point of every development. The reference system elements can, for example, originate from preceding products within the company, from competitor products, but also from external (i.e. new to the respective industry) products. (Albers, Rapp, et al., 2019)
- New product generations are developed by the systematic combination of carryover variation (CV), attribute variation (AV) and principle variation (PV) of reference system elements. A variation of the product embodiment is described as embodiment variation (EV), which is a special case of attribute variation. (Albers, Rapp, et al., 2020)

The validity and applicability of the model have already been demonstrated in a wide variety of practical examples. For example, the research group led by Albers successfully investigated six generations of a dual-mass flywheel (Albers, Bursac, &

Rapp, 2017). With the PGE model, it is also possible to describe the special case of a new development, a so-called "product generation 1", where no preceding product generation exists in the reference system (Albers, Ebertz, et al., 2020).

By determining the types of variation used for the product generation under development and the type or origin of the reference system elements, a development risk can be estimated (Albers, Rapp, Birk, & Bursac, 2017). Figure 2.3 shows a graphical representation of this developmental risk. The graphic shows that external reference system elements in combination with high shares of AV and PV tend to lead to an increased development risk. The assumption behind this is that there mostly is only limited knowledge available about external reference system elements compared to internal reference system elements. This results in an increased need for validation. Similarly, the increased risk can be explained by high AV and PV shares, as these cause an increased development effort and, for example, require new manufacturing tools. (Albers, Rapp, et al., 2017)
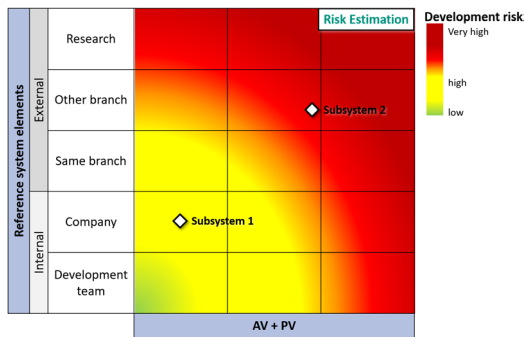
Figure 2.3:   Risk portfolio based on the origin of the reference system elements and the types of variation adapted from Albers, Rapp, et al. (2017) considering Albers, Rapp, et al. (2019) and Albers, Rapp, et al. (2020)

The determination of used variation types can be methodically supported by indicators (Albers, Bursac, & Rapp, 2017). For this purpose, the product model of the Contact, Channel and Connector Approach (C&C²-A), which is presented in the next subsection, is a suitable support.

2.1.3 Contact, Channel and Connector Approach (C&C²-A)

Product models play an important role in product generation engineering because they contain information about the reference system and also contribute to the design process. For the design process, the important activities of analyzing and synthesizing products are supported by the Contact, Channel and Connector Approach (C&C²-A). This is a meta-model used to describe the relation between product embodiment and function (Matthiesen, 2021). The approach traces back to Albers and Matthiesen (Albers & Matthiesen, 2002; Matthiesen, 2002) and already has a successful history of more than 20 years (Grauberger et al., 2019).

The C&C²-Approach is based on the three key elements *Working Surface Pair (WSP)*, *Channel and Support Structure (CSS)* and *Connector (C)* as well as on three basic hypotheses (see Figure 2.4).
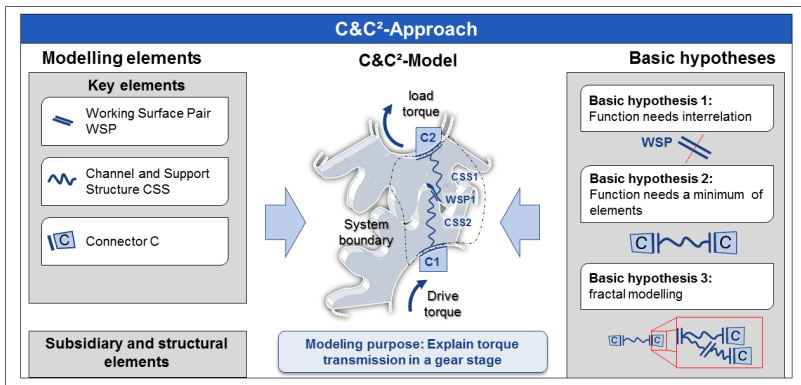
Figure 2.4: The C&C²-Approach – Modeling elements and basic hypotheses adapted from Matthiesen et al. (2018)

A working surface pair describes the interface at which component surfaces are in contact during function fulfillment. A channel and support structure is defined as a physical structure that connects two WSP. The connector is used to describe the system boundaries. It represents a model of the system environment. (Albers & Wintergerst, 2014) These elements again comprise embodiment parameters that are

mandatory to fulfill the functions. For example, the stiffness of a subsystem or component is a parameter of the CSS, while a friction coefficient is a parameter of the WSP (Albers, Matthiesen, et al., 2019).

The set of all CSS that is required in all states during function fulfillment is called *support structure*. Such volumes that do not become support structure at any time are called *residual structure*. (Albers & Matthiesen, 2002)

The basic hypotheses are to be understood as rules for modeling. They state that an interaction with at least one other element is required to fulfill a function (first basic hypothesis) and that a function requires at least two WSP, which are integrated into the environment by a connector, and an intermediate CSS (second basic hypothesis). Furthermore, the third basic hypothesis describes that modeling can be done at different levels of detail and abstraction, depending on the purpose of modeling. (Albers & Wintergerst, 2014; Matthiesen, 2021)

Lightweight design activities, which are in the focus of this thesis, therefore are aimed, in the context of the C&C²-Approach, at designing components with the highest possible share of support structure while simultaneously reducing the residual structure, thereby taking into account the system of objectives. Both approaches are usually not trivial, which motivates the use of numerical optimization methods (see Section 2.5). In the context of simulative analyses, it has already been shown several times that the C&C²-Approach decisively supports the necessary modeling (Matthiesen et al., 2018; Reichert, 2019).

In addition, the function definition which is central to the C&C²-Approach can be used to connect solution-open product attributes with concrete subsystems or components. This approach to function-based product development is presented in the next subsection.

2.1.4 Function-Based Product Development

The aim of product development is to translate customer and user needs into concrete product solutions in order to achieve an economic profit (Bender & Gericke, 2016). Therefore, successful product development requires the early involvement of the customer or user in the product development process. This can be achieved by the help of functions that represent a solution-open formulation of the intended use of a technical system. (Ehrlenspiel & Meerkamm, 2017)

A function can have different meanings in product development. For this reason, a distinction must be made here between product functions and technical functions.

Product functions can immediately be perceived by the customer or user by means of a directly perceptible value or benefit of the overall product. Product functions that describe a cause-effect relationship between an initiating event and a resulting outcome are realized with the help of technical functions. From the point of view of the product developer, technical functions are described by material, energy and/or information flows. (Albers, Fahl, Hirschter, Endl, et al., 2020) In the context of this thesis, the technical function is defined as the intended purpose of a technical product (Matthiesen, 2021). Consequently, technical functions link product functions to individual physical subsystems (Albers, Fahl, Hirschter, Endl, et al., 2020). Figure 2.5 graphically depicts the underlying product model with the relationship between solution-open product attributes over solution-open product functions to solution-specific subsystem solutions and the technical functions realized with them.
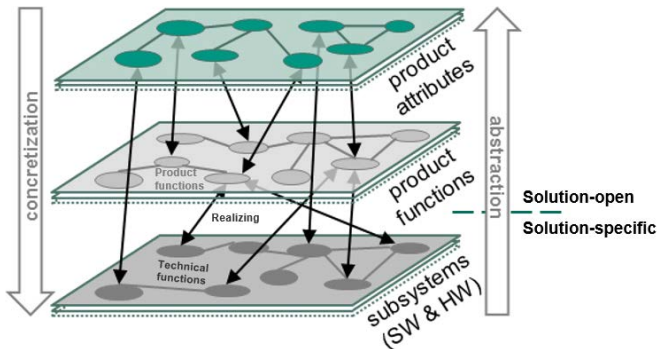
Figure 2.5: Product model: Relationship between product attributes, product functions, and subsystems in function-based product development adapted from Albers, Heitger, et al. (2018) considering Albers, Fahl, Hirschter, Endl, et al. (2020)

Based on this understanding, which was developed by the research group led by Albers, it is possible to support the systematic concretization of customer requirements (solution-open) to the subsystem level (solution-specific) (Albers, Heitger, et al., 2018). This allows to overcome existing component-based patterns of thought and to conceive new solutions. Together with the enabling of customer orientation, this significantly contributes to the development of potential innovations.

For modeling the interrelationships of the product model and especially the functions, Model-Based Systems Engineering (MBSE) can be used (Albers, Fahl, Hirschter, Haag, et al., 2020). MBSE is an approach to support systems engineering (SE) based on formalized modeling to migrate from document-based to model-based development (International Council on Systems Engineering [INCOSE], 2007). SE is an interdisciplinary, methodical approach for the development of products or systems (Walden, Roedler, Forsberg, Hamelin, & Shortell, 2015).

Generally, modeling in the sense of MBSE requires an integrated view of the three pillars of MBSE: language, tool, and method (Delligatti, 2014). In this context, the Systems Modeling Language (SysML)[6] is the most widely used modeling language (Delligatti, 2014), which can be implemented using many different tools[7].

For the development of mechanical system components, the *Functional Architectures of Systems for Mechanical Engineers (FAS4M)* approach was developed by the research group led by Albers (Moeser et al., 2016). It uses the MechML language as a SysML profile. In the FAS4M approach, a system is described by the four system views function view, principle view, conceptual view and component view.

In the function view, a functional architecture is modeled on the basis of the functions to be fulfilled by the system components. The principle view comprises the possible principles for the realization of the functions. The conceptual view defines the logical architecture of the system, while the component view describes the individual components and assemblies analogously to a CAD structure tree. The FAS4M approach additionally provides the integration of sketches, which play an important role in product development, in the conceptual and the component view. (Moeser et al., 2016)

Since the four system views are all linked, function to component correlations are implicitly defined in a model developed using the FAS4M approach.

In addition to the previously described models and methods, which represent central elements of the KaSPro – Karlsruhe School of Product Engineering and thus determine the mindset underlying this work, further models and methods of product engineering relevant for the understanding of this thesis are introduced in the next subsection.

---

[6] https://www.omgsysml.org/ (accessed January 20, 2021)
[7] https://www.omg.org/sysml-directory/vendor/list.htm (accessed January 20, 2021)

2.1.5   Further Models and Methods in Product Engineering

In the following, further models and methods are presented that can be used in the product engineering process and are applied in the context of this work.

Benchmarking

In order to make external knowledge accessible to the own company, benchmarking can be used as an effective method. In literature, numerous definitions of benchmarking can be found. A widely used and cited definition is given by Camp (1989), who describes benchmarking as the search for best industry practices, the introduction of which leads to a superior performance. For their implementation, the best industry practices have to be individually adapted (Fahrni, Völker, & Bodmer, 2002).

There are several ways to classify benchmarking (Anand & Kodali, 2008). One possibility is to subdivide by content and type of benchmarking (Wah Fong, Cheng, & Ho, 1998). According to Sabisch and Tintelnot (1997), with regard to content, a distinction can be made between product, organization, process and strategy benchmarking. Depending on the benchmarking object, different quantitative or qualitative evaluation criteria such as function, quality, customer benefit, costs or time can be used. Concerning the type of benchmarking, on the one hand the origin of the benchmarking partner has to be defined (see Figure 2.6) and on the other hand the choice of the right reference product has to be made.
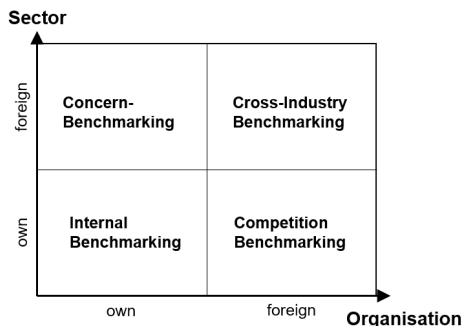
Figure 2.6:   Types of benchmarking adapted from Fahrni et al. (2002)

With internal benchmarking, there is good accessibility to the required data. This makes it easy to compare the benchmarking content. But, the potential for gaining new knowledge is rather low. For concern benchmarking, the required data is also easily obtainable. However, the transfer of knowledge between different departments is rather limited. This type of benchmarking offers great potential on the one hand, but on the other hand is characterized by limited access to required data. Cross-industry benchmarking offers the greatest innovation potential, but it is very time-consuming and has to consider transferability and data collection. (Fahrni et al., 2002)

Validation Prioritization Approach (VPA)

In particular, major changes in late phases of the product engineering process lead to high costs (Weber, 2009). To reduce these late changes, validation activities should be included as early as possible in the product engineering process. The Validation Prioritization Approach (VPA), which was developed in the research group led by Albers and is part of the KaSPro – Karlsruhe School of Product Engineering, helps to prioritize validation activities (Albers, Klingler, & Wagner, 2014). The idea underlying the VPA is that the subsystems most critical to the function fulfillment of the product are validated first with the highest priority (Albers et al., 2014). This criticality is composed of the three factors *impact*, *application scenario* and *technology* (see Figure 2.7).
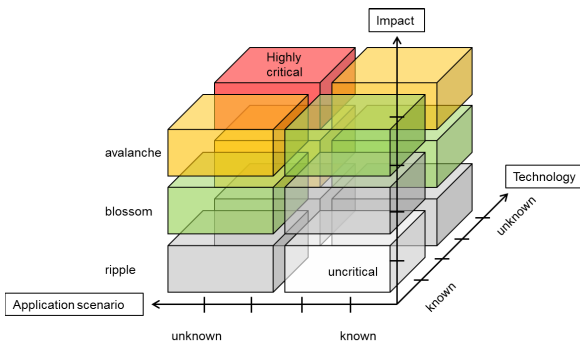
Figure 2.7:   Criticality matrix for the prioritization of validation activities based on the factors impact, application scenario and technology (Albers et al., 2014)

The impact describes the dependencies of a subsystem and its connectivity. The factors application scenario and technology assess their degree of familiarity, for example from previous developments or competitor products. The factor technology covers the used materials, the active principles and the manufacturing process, while the factor application scenario comprises the functions that a component has to fulfill under the given boundary conditions. (Albers et al., 2014)

System Readiness Level (SRL)

In order to assess the maturity of technologies, the National Aeronautics and Space Administration (NASA) developed the Technology Readiness Level (TRL). NASA's TRL distinguishes nine technology maturity levels according to Table 1.

Table 1: TRL and corresponding definition (Mankins, 1995)

TRL	Definition
1	Basic principles observed and reported
2	Technology concept and/or application formulated
3	Analytical and experimental critical function and/or characteristic proof of concept
4	Component and/or breadboard validation in laboratory environment
5	Component and/or breadboard validation in relevant environment
6	System/subsystem model or prototype demonstration in a relevant environment (ground or space)
7	System prototype demonstration in operational environment
8	Actual system completed and qualified through test and demonstration (ground or space)
9	Actual system proven through successful mission operations

However, the assessment of the maturity level of a technology with the TRL is also only possible to a limited extent, since the influence of interactions with other technologies in the overall system is not taken into account (Sauser, Ramirez-Marquez, Magnaye, & Weiping, 2009). To assess the interaction of individual subsystems Sauser, Gove, Forbes, and Ramirez-Marquez (2010) developed the Integration Readiness Level (IRL) according to Table 2.

Table 2: IRL and corresponding definition (Sauser et al., 2010)

IRL	Definition
1	An Interface between technologies has been identified with sufficient detail to allow characterization of the relationship
2	Some level of specification to characterize an interaction between technologies has been achieved
3	There is compatibility between technologies to orderly and efficiently integrate and interact
4	There is enough detail in the quality and assurance of the integration between technologies
5	There is enough control between technologies necessary to establish, manage and terminate the integration
6	The integration technologies can accept, translate and structure information for its intended application
7	The integration of technologies has been verified and validated with enough detail to be actionable
8	Actual integration completed and mission qualified through test and demonstration in the system environment
9	Integration is mission proven through successful mission operations

From the combined consideration of the individual technology maturity as well as their interoperability, Sauser et al. (2009) developed the System Readiness Level (SRL). The SRL is calculated by multiplying the IRL values, which are collected in a matrix, by the TRL values, which are subsumed in a vector (see Equation 1). Here, m denotes the number of components in the system under consideration.

$$SRL_{m \times 1} = [IRL]_{m \times m} * [TRL]_{m \times 1}$$ **1**

The scalar SRL value for the maturity level of the system is calculated as the average of the normalized SRL vector entries according to Equation 2 (Sauser et al., 2009).

$$SRL = \frac{\frac{SRL_1}{I_1} + \frac{SRL_2}{I_2} + \cdots + \frac{SRL_m}{I_m}}{m}$$ **2**

$with\ I_i = Number\ of\ interactions\ on\ subsystem\ i\ and\ with\ itself$

This approach is based on the underlying assumption that the TRL and IRL values can be applied in mathematical calculations. However, the TRL and IRL values are ordinal numbers. They indicate a certain stage in the product engineering process, but do not provide a relative degree of maturity. Consequently, they could be replaced, for example, by letters at any time without loss of information. So, due to their ordinal nature, the values cannot be used for mathematical calculations. (Fahimian & Behdinan, 2017)

As a consequence, Fahimian and Behdinan (2017) developed an approach for TRL calculation based on cardinal coefficients using quantitative data. The quantitative criterion applied to calculate the cardinal numbers is the development time it takes to reach the respective TRL. They defined this time as maturity time. To implement the criterion time for the calculation of the TRL, they use the Analytical Hierarchy Process (AHP) (Saaty, 1990) according to Equation 3, where the index m^* represents for the number of defined TRL levels (NASA scale: $m^* = 9$)

$$A_{ij} = \begin{bmatrix} \dfrac{t_{TRL\,1}}{t_{TRL\,1}} & \cdots & \dfrac{t_{TRL\,1}}{t_{TRL\,m^*}} \\ \vdots & \ddots & \vdots \\ \dfrac{t_{TRL\,m^*}}{t_{TRL\,1}} & \cdots & \dfrac{t_{TRL\,m^*}}{t_{TRL\,m^*}} \end{bmatrix}, m^* \in \mathbb{N} \qquad\qquad \textbf{3}$$

Since the mere discovery of a technology, i.e. the achievement of TRL 1, cannot be described by a time period, zero could be chosen as a value. However, this leads to a division by zero in the first column of the matrix. Therefore, Fahimian and Behdinan (2017) propose to use the value of one year for all TRL 1 to eliminate any influence of the discovery.

The cardinal coefficients v_n can be calculated from the eigenvectors of $\mathbf{A}$ according to Equation 4 (Fahimian & Behdinan, 2017).

$$v_n = \frac{1}{m^*} \sum_{j=1}^{m^*} \frac{a_{nj}}{\left(\sum_{i=1}^{m^*} a_{in}\right)} \qquad\qquad \textbf{4}$$

One central characteristic of the cardinal coefficients is that their sum always equals 1, irrespective of the selected TRL scale. Retrospectively, this characteristic is unproblematic for technologies that are ready for the market, as these technologies have passed all TRLs. Therefore, their cardinal coefficients are directly comparable with each other. However, the situation is different for technologies under development. For example, for a technology that is in TRL 4 out of 9, the sum of the cardinal

coefficients equals 1. Therefore, when comparing it to another technology that has reached TRL 7 out of 9, no conclusions can be drawn because the sum of their cardinal coefficients is also 1.

To assess a design maturity level, Behdinan, Fahimian, and Pop-Iliev (2017) propose a nine-level Design Readiness Level (DRL) analogous to the previously presented TRL and IRL scales. However, this remains at the level of verbal description.

After introducing the process, product and description models for modeling the product engineering process, the next section introduces lightweight design strategies and construction methods that need to be used in a systematic way in the basic and core activities of product engineering.

2.2 Lightweight Design – Strategies and Construction Methods

Lightweight design should not be used as an end in itself. The objective of lightweight solutions should always be increased energy efficiency with accelerated masses. (Klein, 2013) To make systems lighter, product developers can choose from a variety of lightweight design strategies, construction methods and principles (Ellenrieder, Gänsicke, Goede, & Herrmann, 2013), that can be combined individually. In literature, there are countless different lightweight design strategies (see e.g., Kopp, Burkardt, and Majic (2011), Klein (2013), Krause, Schwenke, Gumpinger, and Plaumann (2018)) that are not used consistently. In the context of this work, a distinction is made between the lightweight design strategies of *system lightweight design*, *form lightweight design*, *material lightweight design*, *conditional lightweight design* and *manufacturing lightweight design*. Although the various strategies have different potentials during the product engineering process, the greatest possible lightweight design potential can only be achieved if the lightweight design strategies are consistently incorporated in the entire product engineering process, i.e. in the basic and core activities of product engineering (see Subsection 2.1.1) (Albers, Holoch, et al., 2021). Against this background, the assignment of different lightweight design strategies to construction phases, as proposed, for example, by Schmidt and Puri (2000) or Lüdeke (2016), does not appear to be expedient.

Central to this work are the lightweight design strategies of system, form and material lightweight design, which are discussed in more detail in the Subsections 2.2.1, 2.2.2 and 2.2.3. Lightweight design strategies are used for the systematic application of the construction methods, materials and manufacturing technologies availa-

ble in lightweight design (Kopp et al., 2011). Subsection 2.2.4 deals with multi-material design, a special construction method that is relevant in the context of this thesis. Besides, there are also integral, differential and modular construction methods (Kopp et al., 2011), which will not be discussed in detail here. Section 2.3 addresses the lightweight design material of fiber reinforced polymers separately and explains their interdependencies with the manufacturing process.

Subsection 2.2.5 discusses the use of lightweight design between the conflicting priorities of costs and CO_2 emissions, which define relevant boundary conditions particularly for the transport sector. Finally, Subsection 2.2.6 presents function-based lightweight design methods to support the product developer in the generation of lightweight design solutions.

2.2.1 System Lightweight Design

System lightweight design focuses on the purpose of the system. In contrast to classical, component-based approaches, system lightweight design opens up the possibility of fulfilling the same purpose with a completely different embodiment and/or principle. (Albers & Burkardt, 2011) In the understanding of Albers (Albers & Burkardt, 2011), system lightweight design therefore describes the holistic optimization of mass and/or second moment of area at the subsystem or overall system level, taking into account all interactions. In order to identify the necessary interactions and to develop an understanding of the system, the C&C²-Approach (see Subsection 2.1.3) can be used as an analysis support tool. In synthesis, the design principles of *integration of functions* and *separation of functions* are closely related to system lightweight design. The integration of functions aims at integrating additional functions into a part, while the separation of functions strives to realize one function per component. (Albers & Burkardt, 2011)

Using system lightweight design as a lightweight design strategy can also cause individual components to have an increased mass if this allows an integration of functions. However, in terms of system lightweight design, this does not pose a problem as long as the mass can be reduced at the overall system level. (Albers & Burkardt, 2011)

System lightweight design should not be considered in isolation. It rather interrelates directly with the other lightweight design strategies, particularly with form lightweight design and material lightweight design. For example, the possible design of a component may depend on the available space, or the position of the component in the overall system may require a certain choice of material due to environmental influences. (Albers & Burkardt, 2011)

2.2.2 Form Lightweight Design

The objective of the lightweight design strategy form lightweight design is to optimize the material distribution in the part so that there only is material in those areas where it is needed (Ellenrieder et al., 2013). This strategy is used to generate an optimized structure with respect to the force distribution under given requirements that has a minimum mass (Kopp et al., 2011). Based on this objective, there is a direct correlation with the lightweight design strategies system lightweight design (see Subsection 2.2.1), since, for example, the design space limits the possible geometries, and material lightweight design (see Subsection 2.2.3), since, for example, possible part geometries depend on the selected material. The design process in form lightweight design can be supported by computer-aided structural optimization (see Subsection 2.5.2).

In the context of the present work, form lightweight design using beads as constructional stiffening elements is particularly relevant. Therefore, this specific case is discussed separately and in detail in Section 2.7.

2.2.3 Material Lightweight Design

In material lightweight design, a material is substituted by another material with higher specific material properties. The change of material entails a necessary modification of the design in order to be able to still fulfill the same boundary conditions and to achieve the maximum lightweight design potential. Simply substituting the material is not expedient. (Kopp et al., 2011)

When using fiber reinforced polymers, and in particular compression molded, long fiber reinforced polymers, the dependence of the material selection on the defined design is particularly relevant. The part geometry determines the fiber orientations in the manufacturing process, which are responsible for the resulting material properties (Kärger, 2019). Therefore, for these materials in particular, it is imperative to consider material and form lightweight design in combination. This issue will be discussed in more detail in Subsection 2.3.3.

Figure 2.8 shows exemplarily the lightweight design potential possible by material lightweight design for a bending beam, which is adapted in its cross section based on the chosen material, in order to satisfy the same bending stiffness as a steel beam.
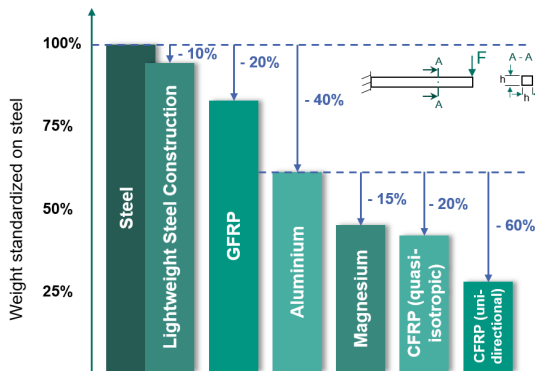
Figure 2.8: Lightweight design potential using material lightweight design adapted from Ellenrieder et al. (2013)

At this point, it should be noted that material lightweight design is mostly limited by economic and ecological constraints (Ellenrieder et al., 2013). A detailed discussion of lightweight design between the conflicting priorities of benefit, costs, and emissions is provided in Subsection 2.2.5.

Material selection can also be supported by the selection method according to Ashby (2005). In this established method, performance indices are calculated depending on the present function or loading, the objective (e.g., minimum mass) and the boundary condition (e.g., stiffness). These performance indices can be used to select a material in an Ashby chart.

The combination of different materials leads to multi-material design, which is discussed next.

2.2.4   Multi-Material Design (MMD)

The philosophy of multi-material design is: "The right material for the right application"[8] (Klein, 2013, p. 38). Multi-material design is a special construction method that

---

[8]   Translated by the author: „De[r] richtige Werkstoff für den richtigen Anwendungsfall" [Klein (2013, p. 38)]

represents a promising lightweight design trend (Friedrich & Krishnamoorthy, 2013) towards achieving the full lightweight design potential (Kopp et al., 2011). In contrast to hybrid design, which combines different materials in one component, MMD describes the combination of different materials at the component level (Kopp et al., 2011). The aim of MMD is to make a requirement-specific material selection for each component (Kopp et al., 2011). This results in a material mix in the product, which is conceivable in various ways – from the combination of different material types to the combination of different material major classes (Nestler, 2014). Figure 2.9 shows the three levels of multi-material design.
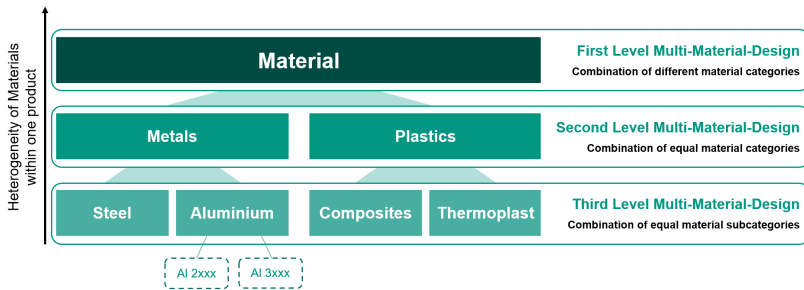
Figure 2.9:   Multi-material design: Level Model adapted from Kleemann, Inkermann, Bader, Türck, and Vietor (2017)

The level with the least mass reduction potential is the third level, where materials within a material type of different compositions are combined (e.g., different aluminum compositions Al 2xxx, Al 3xxx, etc.). At level 2, different materials within a material class (e.g., metals) are combined. This results in combinations such as steel and aluminum. The first level, which has the greatest mass reduction potential but is also the most challenging in terms of design, combines materials from different material major classes. (Nestler, 2014)

In addition to the design challenges, MMD products on the first and second level also pose joining challenges. Different melting temperatures, durability, temperature and corrosion resistance or different coefficients of thermal expansion reduce the selection of potentially suitable joining processes. Therefore, mechanical or chemical joining processes are often used. (Kopp et al., 2011) Moreover, the decision for

a joining process directly affects recycling, which is another challenge for products in multi-material design.

Closely related to the question of the lightest material combination is always the economic aspect. Therefore, Schöll, Friedrich, Kopp, and Kopp (2009) add to their definition that MMD represents "an economic lightweight design optimum depending on production volumes"[9] (Schöll et al., 2009, p. 54). Hence, in the next subsection lightweight design will be discussed under ecological and economic boundary conditions.

2.2.5 Lightweight Design Between the Conflicting Priorities of Benefit, Costs, and Emissions

Lightweight design activities should always be in an economic cost-benefit ratio (Klein, 2013), otherwise there will be no market demand. The additional expenses that are always necessary for lightweight design projects can be listed on the cost side. The benefit side is manifold, depends on the particular industry, and offers, through secondary effects, more than pure mass reduction. For example, the benefits of lightweight design solutions in the automotive industry range from improved driving dynamics and acceleration to lower emissions over the possibility of increased vehicle load capacities to the utilization as a marketing tool. In the following, mainly the reduction of CO_2 emissions will be considered on the benefit side, which will be compared to the additional costs.

Since lightweight design does not always lead to a directly tangible product function (see Subsection 2.1.4), customers' willingness to pay per kilogram saved is rather low, especially in large-volume automotive manufacture. Affordable lightweight design for large-volume passenger cars is therefore considered the "supreme discipline"[10] (Ellenrieder et al., 2013, p. 100). However, this is not the case for all industries. The accepted additional costs in aerospace are three orders of magnitude higher than those in the automotive industry (Ellenrieder et al., 2013; Klein, 2013; Klein & Gänsicke, 2019). This can be explained by cost reduction potentials in operations or an increased load capacity for very expensive flights into space. Consequently, the accepted additional costs per kilogram saved depend on the respective industry (see Table 3).

---

[9] Translated by the author: „in Abhängigkeit der Produktionsvolumina ein betriebswirtschaftliches Leichtbau-Optimum" [Schöll et al. (2009, p. 54)]

[10] Translated by the author: „Königsdisziplin" [Ellenrieder et al. (2013, p. 100)]

Table 3: Accepted additional costs for lightweight design depending on the respective industry adapted from Ellenrieder et al. (2013), Klein (2013) as well as Klein and Gänsicke (2019)

Industry	Additional costs [€/kg]
Aerospace	< 5000
Aviation	< 500
Sports / Medical engineering	< 100
Automotive industry	2-10
Trucks / Rail vehicles	1-3
Architecture	0

The accepted additional costs per kilogram saved influence the choice of lightweight design technologies and strategies that can be applied to the product. Figure 2.10 shows a schematic diagram of the relationship between the expected costs, the achievable lightweight design potential and based on that, the available approaches.
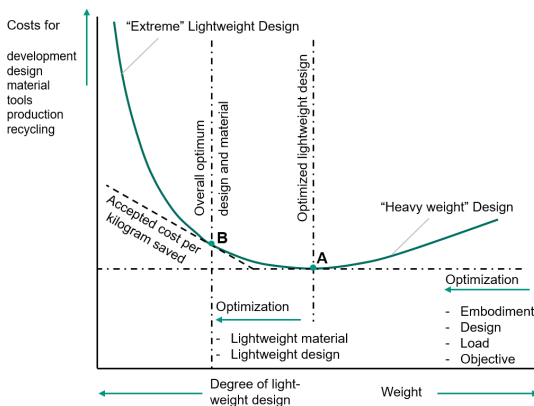
Figure 2.10: Schematic diagram of the relationship between costs and weight in lightweight design adapted from Klein (2013)

It can be seen that a distinction has to be made between a cost optimum and an overall optimum. The overall optimum results as the optimal combination between accepted additional costs and minimum weight. Accordingly, the location of point B in Figure 2.10 is variable and depends on the considered industry (see Table 3).

In the automotive industry, which this thesis focuses on, additional costs for lightweight design are accepted. This is, among other things, due to the direct impact of mass on three of the four summands in the driving resistance equation (see Equation 5) (Gänsicke & Goede, 2013).

$$F_{total} = \quad F_{Air} \quad + \quad F_{Roll} \quad + \quad F_{Grade} \quad + F_{Acceleration}$$
$$= \frac{\rho_{Air}}{2} v_{rel}^2 c_W A + f_r m_V g \cos \alpha_R + m_V g \sin \alpha_R + \lambda_m m_V a \qquad \textbf{5}$$

F_{total} describes the total driving resistance, which is composed of the air resistance force F_{Air} (with air density ρ_{Air}, relative velocity v_{rel}, drag coefficient c_W and projected frontal area A), the rolling resistance force F_{Roll} (with rolling resistance coefficient f_r, vehicle mass m_V, acceleration of gravity g and slope of the road α_R), the grade resistance force F_{Grade} (with vehicle mass m_V, acceleration of gravity g and slope of the road α_R) and the acceleration resistance force $F_{Acceleration}$ (with mass factor λ_m, vehicle mass m_V and acceleration of the vehicle a). Depending on the driving situation, the individual summands contribute differently to the total resistance. The mass-related shares are 92% for a city drive, 55% for a state road drive and approximately 30% for a highway drive (Gänsicke & Goede, 2013). This is due to the increasing influence of the air resistance at high speeds. With respect to the different driving cycles (MNEDC, FTP-75, JP 10-15), mass also is the most important influencing factor in the driving resistance. These physical relationships remain intact even if the drive system is changed. With respect to an E-Golf, the greatest increase in range results from a reduction in mass. (Gänsicke & Goede, 2013) Henning, Gauterin, Dollinger, and Burgert (2019) have shown that only a small part of the additional energy which is needed due to the higher overall weight can be recovered through recuperation. This means that the influence of lightweight design is definitely not negligible in electric vehicles, even if it is lower than in vehicles with combustion engines (Ellenrieder et al., 2013).

In the recent past, increasing environmental awareness in politics and society has led to an additional ecological component in the evaluation of lightweight structures (Ellenrieder et al., 2013; Kopp et al., 2011). For emission assessments, the holistic consideration of the energy balance over the entire product life cycle is particularly crucial. This includes, in addition to the consideration of material and process emissions, the previously discussed definition of the driving cycles and, above all, the

analysis of the recycling process. (ISO 14040, 2006) The holistic view is becoming more and more important precisely as the increasing reduction of emissions in the use phase means that the previous production phase and the subsequent recycling phase account for a larger percentage share of the overall balance. In particular, this is relevant for lightweight materials, which often have higher CO_2 emissions in production and recycling due to their energy-intensive raw material extraction and further processing. As a measure of the climate impact of greenhouse gases, the Global Warming Potential (GWP) or CO_2 equivalent[11] can be analyzed in all product life phases using a Life-cycle Assessment (LCA). The procedure for conducting an LCA is prescribed in ISO 14040:2006 (ISO 14040, 2006). In the *cradle-to-grave* approach, all environmental impacts are considered from raw material extraction, through manufacturing and use, to end-of-life. This is particularly important for evaluating the emissions generated by vehicles with internal combustion engines compared to battery electric vehicles. As a result, for example, the electricity mixes during the BEV use phase and the increased production emissions are also taken into account, enabling a more reflective comparison of the two drive systems (Del Pero, Delogu, & Pierini, 2018).

From the discussions in this subsection, a complex lightweight design challenge arises between the conflicting priorities of mass, costs and CO_2 emissions. The perfect lightweight design solution is as light as possible, cheap and causes few CO_2 emissions. However, this solution will not exist for the previously described reasons. As a consequence, the product developer's task in lightweight design is always to identify the optimum between low mass, low costs and low CO_2 emissions for a specific application.

2.2.6 Function-Based Lightweight Design Methods

As shown in the previous subsections, the design of lightweight solutions is a complex problem in which many interactions have to be handled. Additionally, the propagation of changes can become apparent via secondary effects. Therefore, the mere application of single lightweight design strategies (such as e.g., form lightweight design (see Subsection 2.2.2) or material lightweight design (see Subsection 2.2.3)) is mostly not sufficient, as they only focus on product design at the component level (Ponn & Lindemann, 2011). Rather, lightweight design must be incorporated in all phases of product engineering (see Subsection 2.1.1) (Ponn

---

[11] In the context of this work, the terms GWP, CO_2 equivalent and CO_2 emissions are used analogously. For reasons of better readability, only the term *CO_2 emissions* will be used in the following.

& Lindemann, 2011). Especially in early phases of the product engineering process, the greatest lightweight design potential can be realized (Ponn & Lindemann, 2011; Schmidt & Puri, 2001), since the product concept already defines up to 80 percent of the mass or energy and resource consumption (Leichtbau BW GmbH, 2015).

Due to the complexity of the problem, numerous authors have already addressed the development of lightweight design methods to support the product developer. Lüdeke (2016) summarizes and classifies some of them in his work. Also Laufer, Roth, and Binz (2019) examined a large number of lightweight design methods and categorized them in terms of the economic, ecological, and technical dimensions which need to be addressed with lightweight design solutions (see Subsection 2.2.5). In the context of the present thesis, not all of these methods will be discussed. For more information, the author refers to the relevant literature. Instead, the findings obtained so far in the state of the art will be taken into account, whereby the greatest lightweight design potential can be achieved in early phases using system lightweight design approaches. For this purpose, solution-open approaches based on functional formulations are particularly suitable. Therefore, the *function-based lightweight design methods* identified in literature will be discussed in the following.

Value Analysis Weight (Feyerabend, 1991)

The standard value analysis (DIN EN 1325, 2014) aims at cost optimization by assigning a value to a function, which subsequently has to be increased without additional costs. In the early 1990s, Feyerabend (1991) developed the method *Value Analysis Weight*. Feyerabend's method is based on the idea of value analysis and abstracts its basic principle into the context of lightweight design. A weight is assigned to the technical functions of a product, which then has to be optimized. The procedure of the method is inspired by the procedure of DIN EN 1325 (2014). Feyerabend's work has laid the foundation and starting point for further methods.

Functional Weight Analysis (Ponn & Lindemann, 2008)

The *Functional Weight Analysis* developed by Ponn and Lindemann (2008) is also based on the assignment of mass to functions. The method transfers the idea of target costing (Kato, 1993) to the lightweight design context. The components of the reference product are assigned in a matrix proportionally, by percentage to their functions. This assignment is made with the aid of expert knowledge. Functional weights are obtained by multiplying the component weights by the percentages and by subsequent summation across all components. Subsequently, these functional weights can be evaluated using further methods such as ABC analysis. Further-

more, an additional evaluation of the functional weights with regard to the importance of the functions is proposed in order to derive the target weight of the functions. From the comparison of the target and actual state, lightweight design potentials can be identified.

Function Mass Analysis (FMA) (Posner, Binz, & Roth, 2013)

Based on the Value Analysis Weight (Feyerabend, 1991) and the Functional Weight Analysis (Ponn & Lindemann, 2008), Posner et al. (2013) developed the *Function Mass Analysis (FMA)*. To this end, they previously published a framework that formulated the requirements for a holistic lightweight design method based on existing approaches (Posner, Keller, Binz, & Roth, 2012). From this, they deduced that such a method should include not only the mass but also the mass moment of inertia and the mass distribution. However, the FMA does not yet include the mass moment of inertia and the mass distribution (Posner et al., 2013). Using the FMA, the customer-oriented functions are first weighted against each other. Then, the technical functions of a reference product from the reference system are determined and a correlation between customer-oriented and technical functions is made. From this, the authors conclude their function mass aim, which specifies the target state. This means that the target values are determined by analysis activities and not during the synthesis. In the next step, the reference system is analyzed: The mass of the individual components is assigned percentagewise to the functions according to their contribution to the fulfillment of the function. The procedure is analogous to the approach proposed by Ponn and Lindemann (2008). From this, the function masses are calculated. By comparing the function mass aims with the actual function masses, deviations between the target and actual state are determined, which serve as an indicator for lightweight design potential. Based on this, new lightweight solutions are subsequently developed. Furthermore, the FMA approach was extended to include a Function Mass Estimation (FME) (Posner, Binz, & Roth, 2014) in order to be able to evaluate solution principles from the reference system that have not already been used in a preceding product generation but are being adapted by competitors, for example

Continuing work by the research group led by Binz addresses the additional possibility of considering mass moment of inertia and mass distribution in the search for lightweight design potential, thus extending the FMA, as envisioned in the 2012 concept paper (Posner et al., 2012). For this purpose, Laufer, Roth, and Binz (2018) developed the *Energy Distribution Analysis (EDA)*. In addition, the research group is pursuing the idea of a generally applicable, use-case-independent lightweight design method in which user-specific influencing variables on lightweight design potential can be defined. Therefore, Laufer, Roth, and Binz (2020) developed a method

for the individual prioritization of lightweight design activities. However, the advantage of prioritization is opposed by the disadvantage that the procedure is bound to the existing subsystem structure and cannot eliminate the existing component boundaries.

Target Weighing Approach (TWA) (Albers et al., 2013)

To support the identification and evaluation of lightweight design potentials, the research group led by Albers developed the *Target Weighing Approach (TWA)*. The TWA is based on the approaches of value engineering and target costing and abstracts their basic principles in the context of lightweight design. (Albers et al., 2013) Thus, on the one hand, the value of a function originating from value engineering is defined as the mass of a function and, on the other hand, the target value from target costing is understood as the synthesis-based target weight on the basis of the user-specific knowledge base.

Function and embodiment are directly related via analysis and synthesis, respectively. By analysis activities, the functions of a product can be identified from an existing product embodiment, while by synthesis activities, functions can be translated into a concrete embodiment. (Matthiesen, 2011) Through the abstraction of the product to the solution-open level of its functions, which can be fulfilled by several subsystems, the TWA supports the identification of cross-subsystem lightweight design potentials. Therefore, the TWA can be classified as a method in system lightweight design (see Subsection 2.2.1). However, when applying the TWA, it is crucial to make use of all lightweight design strategies and construction methods (see Subsections 2.2.2 - 2.2.4) in order to realize the greatest possible mass reductions in concept generation. Figure 2.11 shows the workflow of the TWA, which is described in more detail in the following.

The TWA itself can be seen as a problem solving process (Albers, Revfi, & Spadinger, 2018). Therefore, it can be divided into the individual steps of SPALTEN (see Subsection 2.1.1) as shown in Figure 2.11. The starting point for the application of the TWA is ideally a preceding product (Albers et al., 2013) from the reference system in the sense of the PGE – Product Generation Engineering according to Albers (see Subsection 2.1.2), since usually a large knowledge base is available for this product. This may also be only a subsystem of the preceding product. Regardless, it is important that the design space is made transparent to all members of the development team. In the context of the *Situation Analysis* (S), the first step is to identify the subsystems in the design space and determine their masses. This can be done, for example, on the basis of existing CAD data or by weighing real components. In the following description of the procedure, only the masses are considered

for simplification reasons. For the consideration of the costs, the procedure is analogous. The determination of the masses is followed by the analysis of the technical functions of the examined (sub)system (Albers et al., 2013). This functional analysis is very important for the success of the method. Only if all functions are identified, it can be ensured that the product to be developed again contains all function scopes. For complex and comprehensive systems, functions can be clustered into function groups as well as subsystems can be grouped appropriately (Wagner, 2015).
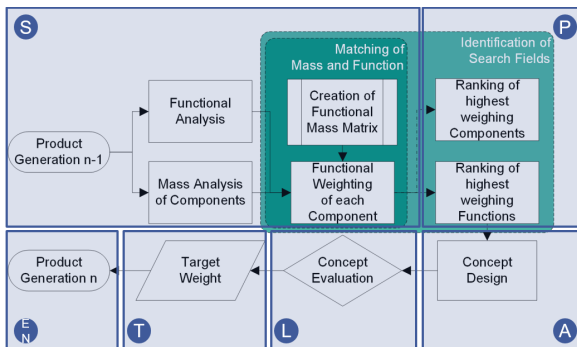
Figure 2.11: Workflow of the Target Weighing Approach (TWA) adapted from Albers et al. (2013) and Wagner (2015) considering Albers, Revfi, and Spadinger (2018). The TWA is a problem solving process and can therefore be divided according to SPALTEN.

Subsequently, the Function-Mass-Matrix is created (analogous for the cost analysis: Function-Cost-Matrix) (see Figure 2.12). For this purpose, the identified subsystems are listed in the rows of a matrix, while the functions are listed in the columns of this matrix (Albers et al., 2013). Following this, with the help of expert knowledge, each subsystem is assigned its percentage share in the fulfillment of the function – analogous to the Functional Weight Analysis of Ponn and Lindemann (2008). Here, it has to be noted that the row sum needs to be 100%, since a subsystem always carries out 100% of function. Finally, the functional masses are calculated via the column-wise addition of the percentage masses. (Albers et al., 2013) The percentage allocation of the subsystems to the functions is done independently (= general function fulfillment) and explicitly not according to the mass or cost share. Thus, the assignment can also be used for other values besides mass and costs (Albers et al., 2013; Wagner, 2015).
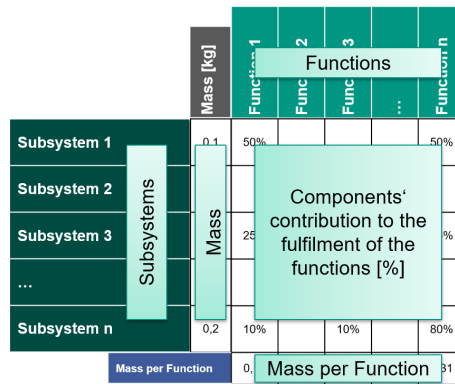
Figure 2.12: Function-Mass-Matrix adapted from Revfi, Albers, and Stegmiller (2018). Percentagewise assignment of the components' contribution to the fulfillment of the functions.

The next step is the *Problem Containment* (P), i.e. the generation of search fields for lightweight design. This can be supported by an ABC analysis of the functional masses (see Figure 2.13 (b)) (Albers, Revfi, & Spadinger, 2017; Wagner, 2015). Heavy functions are found in area A. Due to their mass, they should be analyzed in more detail. In area B, the most interesting functions are those that are less important for the product. Functions in area C have a low mass anyway, so the search for lightweight design potential should not focus on this. Another possibility to identify lightweight search fields is a function portfolio (Albers et al., 2013). For this purpose, firstly, the relative importance of the functions among each other is determined. Here, for example, the method of paired comparison or the AHP can be used (Albers et al., 2013). Subsequently, the function portfolio can be generated by plotting the (relative) functional mass over the relative importance (see Figure 2.13 (a)). By drawing the regression line in the function portfolio, those functions can be identified which are "too heavy" in relation to their relative importance. They indicate lightweight search fields that should be addressed by new lightweight design concepts.
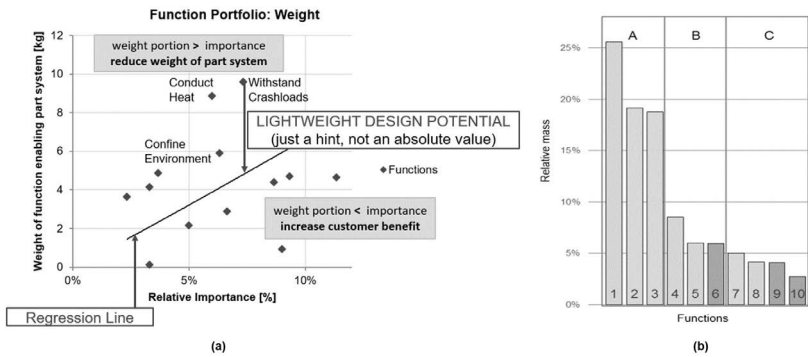
Figure 2.13: Identification of search fields: (a) Function portfolio adapted from Albers et al. (2013) and (b) ABC-Analysis (Albers, Revfi, & Spadinger, 2017)

Since the actual feasible lightweight design potential depends on the developed concepts, the amount of mass reduction can only be estimated after the synthesis and is here explicitly not substantiated with theoretical values. Based on the identified functions, further evaluations can be carried out using the Function-Mass-Matrix to analyze the components' contributions. If only one component contributes 100% to a function identified as too heavy, a separation of the function into several components could be a possibility for mass reduction. If the high functional mass comes from the contributions of many subsystems, it should be examined whether an integration of functions is a better solution. (Albers et al., 2013)

Based on the identified functions with lightweight design potential, new lightweight design solutions are generated in the problem solving step *Alternative Solutions* (A). Intuitive as well as discursive creativity techniques or a combination of them can be used for this purpose. Examples of such techniques include TRIZ, brainwriting, brainstorming and the World Café (Albers et al., 2013; Albers, Revfi, & Spadinger, 2017).

In the subsequent step of the *Selection of Solutions* (L), the generated concepts are evaluated. Albers et al. (2013) propose a three-step procedure, which suggests a rough preselection in the first step. This involves examining the concepts in terms of physical conflicts and technical feasibility and comparing them with the project tar-

gets. In this step, about two thirds of the generated concepts can already be excluded. In the second step, a qualitative evaluation of the achievable mass, costs, functionalities and technical feasibility is carried out. (Albers et al., 2013) During this process, a utility analysis can be used as a support tool (Wagner, 2015). In the last step of the selection process, a quantitative evaluation of the remaining concepts is performed (Albers et al., 2013).

This evaluation step is additionally supported by the impact analysis to be performed as part of the *Consequences Analysis* (T). Figure 2.14 shows the workflow of the impact analysis. The Function-Mass-Matrix is used in reverse: The remaining concepts are evaluated in terms of new subsystems and the functions they affect. Thus, the theoretical maximum mass reduction potential for the respective concept idea can be determined. However, this maximum potential can only be realized in the rarest of cases (Wagner, 2015). Therefore, a correction factor is necessary to reduce the maximum potential to a realistic level. These correction factors are part of the user-specific knowledge base. They can be estimated by experts or can be derived from previous projects that had a similar focus. Multiplying these factors by the maximum mass reduction potential results in the Target Weight as the development target value, which is also used for the final concept selection – *Make Decision and Realization* (E) – in the third step. (Albers et al., 2013) In the last problem solving step – *Recapitulate and Learn* (N) – it can be checked to what extent the mass estimates were correct.
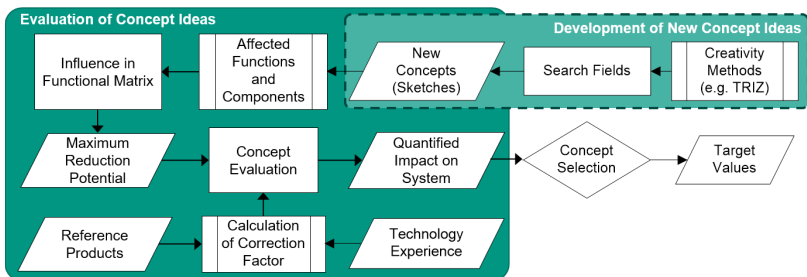
Figure 2.14: Impact analysis for the evaluation of developed concepts adapted from Albers et al. (2013) and Wagner (2015)

In summary, the TWA represents a cross-subsystem lightweight design method based on PGE – Product Generation Engineering according to Albers, which supports the product developer with its function-based, solution-open approach in the identification and evaluation of lightweight design potentials. The TWA integrates the approach of Functional Weight Analysis according to Ponn and Lindemann and extends their idea by the additional evaluation of costs. This is also the advantage of the TWA over the Function Mass Analysis of Binz's research group. Another decisive advantage of the TWA over the FMA is, in the author's point of view, the synthesis-driven determination of the target weight. In the FMA, this target value is already determined in the analysis phase on the basis of a defined weight reduction, whose validity cannot yet be estimated at that time.

In addition, due to the mass- and cost-independent, purely function-based assignment of components to functions, the TWA allows an extension of the considered lightweight design influencing variables. This appears to be particularly relevant because none of the presented methods addresses the conflicting priorities of mass, costs and CO_2 emissions, in which today's lightweight design solutions must be able to prove themselves (see Subsection 2.2.5). Against the background of these findings, the following work focuses on the TWA as a starting point for the development or extension to holistically evaluate multi-material designs (see Chapter 5).

One possibility for generating multi-material designs to realize the identified lightweight design potentials in the TWA is the use of fiber reinforced polymers, which will be discussed in the following section.

2.3 Fiber Reinforced Polymers

In the previous subsections, the importance of lightweight design for society and the environment as well as the application of lightweight design strategies, construction methods and lightweight design methods in the product engineering process have already been elaborated. Fiber reinforced polymers – as a subclass of composites – are characterized by outstanding mass-specific stiffnesses and strengths (May, 2020). They allow extraordinary mass reduction to be achieved. However, mere material substitution does not make sense from a technical, economic or ecological point of view, as not every load case is suitable for the use of FRPs and they often have increased costs and a poor carbon footprint. As a consequence, multi-material design has proven to be a promising approach in lightweight design (see Subsection 2.2.4). In MMD, mass reductions can be achieved through the intelligent use of FRP in appropriate parts of the product, also taking into account additional costs and emission requirements.

This thesis focuses on the stiffness-optimized design of long fiber reinforced polymer components for their use in multi-material design. Therefore, this section provides a review of the types of fiber reinforced polymers (see Subsection 2.3.1), their manufacturing and processing (see Subsection 2.3.2), as well as the fundamentals for understanding fiber-adapted design (see Subsection 2.3.3).

2.3.1 Types of Fiber Reinforced Polymers – Fiber, Matrix, Composite

Polymers without fiber reinforcement are rarely used in load-bearing structures (Klein, 2013). This is due to, among other things, their brittleness (thermosets) or their tendency to creep (thermoplastics) (Schürmann, 2007). However, the addition of fibers, which are used to carry the mechanical loads, creates properties that the individual components *fiber* and *matrix* cannot achieve (Henning, Drechsler, & Chatzigeorgiou, 2011; Schürmann, 2007). The properties of the FRP can be adjusted by the choice of fibers and matrix as well as by the selected manufacturing process. In the following, the fibers and matrix materials relevant for the present work as well as their composite are presented.

Fiber

The choice of the reinforcing fibers determines, in addition to stiffness and strength, impact strength, heat resistance and creep behavior (Henning et al., 2011).

Glass fibers are predominantly produced by a direct melt process, in which the melted raw materials flow through nozzles to form the filaments (Gries, 2013). Depending on the choice of raw materials, different types of glass fibers can be distinguished (e.g., E-glass fiber, S-glass fiber, etc.). The material properties of glass fibers are isotropic, which means they are identical in fiber direction and transverse to fiber direction. Glass fibers are often processed as roving, yarn or as flat or three-dimensional semi-finished products. Rovings are bundles of fibers combined into one strand. (Henning et al., 2011)

Carbon fibers are predominantly produced with the aid of structurally preformed precursors made of polyacrylonitrile (PAN), which are further processed in a multi-stage process (Gries, 2013; Karger-Kocsis, 2014). Depending on the chosen temperature in the final treatment, different fiber stiffnesses and strengths can be set (Henning et al., 2011). In contrast to glass fibers, carbon fibers have a strongly anisotropic material behavior (Henning et al., 2011).

Matrix

The matrix embedding the fibers has the function of introducing the forces into the fibers and transferring these forces between the fibers. In addition, it determines the possible part geometry and protects the fibers from environmental influences. (Ehrenstein, 2006) The selection of the suitable matrix is crucial, as it defines important properties such as the operating temperature limits or the thermal conductivity (Schürmann, 2007). To each matrix material, additives are added to obtain certain properties during processing or subsequent use (Henning et al., 2011). For the present work, thermoset and thermoplastic matrix materials are relevant.

Thermoset matrix systems are characterized by a high Young's modulus and good thermal resistance. They are obtained by an irreversible chemical reaction of a reactive resin with the addition of a hardener. (Karger-Kocsis, 2014) After curing, they cannot be reshaped by heating.

Thermoplastic matrix systems have, i. a., the advantage of shorter processing cycles or increased impact strength (Henning et al., 2011). During the processing of thermoplastics, there is no chemical reaction, but a melting and solidification of the matrix (Ehrenstein, 2006). This process is reversible and can be repeated as often as desired. This means that thermoplastics are recyclable. (Schürmann, 2007)

Fiber-Matrix Composite

The extraordinary specific material properties of the FRP result from the combination of fibers and matrix. According to Puck (1996), in order to achieve any increase in stiffness and strength at all, the conditions must be met that the fibers have a higher strength and stiffness than the matrix and fracture before the matrix. To make optimal use of the maximum strength of the fiber, a minimum fiber length can be determined (Ehrenstein, 2006; Rösler, Harders, & Bäker, 2019). External forces are introduced into the composite via the matrix. In the interface between matrix and fiber, shear stresses transfer the forces to the fiber (Rösler et al., 2019).

This embodiment function relation can be illustrated using the C&C²-Approach (see Figure 2.15) and creates an understanding of the way the fiber-matrix composite works. At the highest level, the fiber-matrix composite initially represents a homogeneous material, which can be used, for example, to transmit forces. If this view is taken one level deeper, which is possible through the fractal character of the C&C²-Approach, the conditions described can be identified. While fiber and matrix represent two CSS, the WSP at the interface is decisive for the behavior of the fiber-matrix composite. It determines the adhesion between fiber and matrix and is responsible for the load transfer (May, 2020).
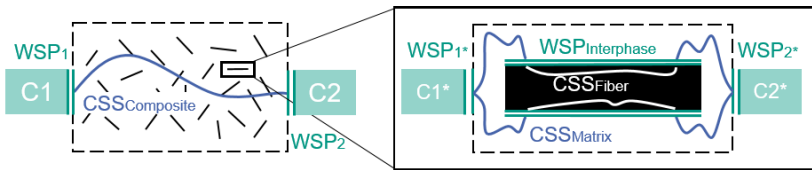
Figure 2.15: C&C²-Model for modeling interactions between fiber and matrix in fiber reinforced polymers

Optimally, the force σ is applied parallel to the fiber orientation (fiber angle $\varphi=0$), as this is the only way to achieve the best possible material properties (see Figure 2.16).
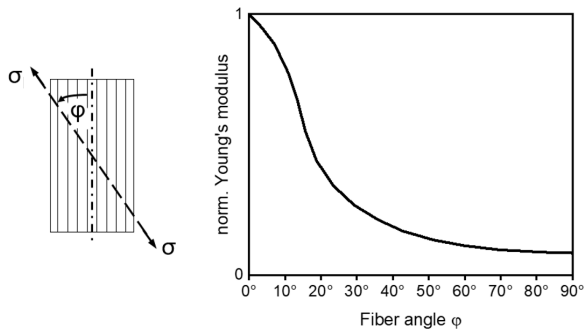
Figure 2.16: Correlation between fiber angle and Young's modulus adapted from Roos, Maile, and Seidenfuß (2017)

Fiber-matrix composites are often classified according to the processed fiber length. A distinction is made between *discontinuous* and *continuous* fibers. In general, it can be said: the longer the fibers, the better the reinforcing effect (Schürmann, 2007).

Discontinuous fibers include short and long fibers. Short fibers have a length of up to 1 mm (Rösler et al., 2019; Schürmann, 2007). They are randomly distributed in

the matrix. This results in quasi-isotropic material properties. Consequently, the reinforcing effect of short fibers is low, which is why they are usually used for parts subjected to low loads (Schürmann, 2007). The term "long fiber" is used when the fiber length is between 1 mm and 50 mm (Rösler et al., 2019; Schürmann, 2007). They provide significantly increased strength and impact resistance in the composite (Wilhelm, 2013b). Long fibers can align themselves during the manufacturing process and are thus responsible for a macroscopically anisotropic material behavior.

Continuous fibers are often also referred to as endless fibers. They have a length of more than 50 mm and are used to reinforce highly loaded parts. In such parts, the chosen fiber length often corresponds to the size of the part to be reinforced. (Rösler et al., 2019; Schürmann, 2007) The use of continuous fibers as unidirectional (UD) tapes, which should be oriented along the highest principal stress in a fiber-adapted design, results in the mechanically advantageous material properties This allows load case-specific reinforcements to be introduced into the part in a targeted manner. However, this also results in preferential directions in the part, as significantly lower stiffness and strength properties are obtained transverse to the uniaxial orientation (see Figure 2.16) (Rösler et al., 2019). In order to avoid this strong directionality, different fiber directions are often combined in woven or non-crimp fabrics (Schürmann, 2007).

In the context of this thesis, discontinuous fibers (in the form of long fibers) as well as the combination of long fibers and continuous fibers (as UD-tapes) are considered.

2.3.2 Manufacturing and Processing of SMC, LFT and UD-Tapes

There are various technologies for the manufacturing and processing of fiber-matrix composites. Henning (2020) gives an overview of the possible technologies for thermosets and thermoplastics. Figure 2.17 shows the manufacturing and processing methods relevant for the investigations in the present work. An understanding of the manufacturing and processing methods is essential for correct modeling (see Subsection 2.4.1). The focus of the investigations is on the sheet molding compound (SMC). The thermoplastic UD-tapes are only presented for completeness, but are not relevant for this work.
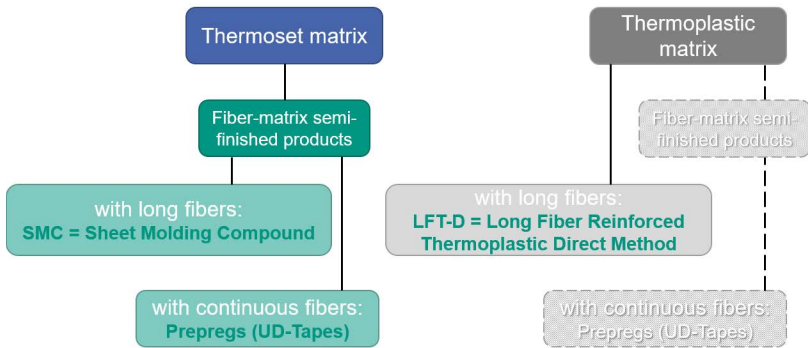
Figure 2.17: Overview of manufacturing and processing methods considered in this work

Sheet Molding Compound (SMC)

SMC are thin sheets of flowable semi-finished composites that are processed into the final part shape by compression molding (Stachel, 2013).

In the manufacturing of SMC semi-finished composites, the thermoset resin (see Subsection 2.3.1) is mixed with further additives to a paste and spread to a carrier film (see Figure 2.18) (Gandhi, Goris, Osswald, & Song, 2020; Stachel, 2013). The glass fiber rovings used in SMC (see Subsection 2.3.1) are cut into a defined length with the aid of cutting tools. The chopped glass fibers randomly fall onto the paste spread on the carrier film. In order to create a symmetrical structure of the SMC, a second carrier film containing matrix is applied as a top layer (Medina, Mack, & Christmann, 2014). Afterwards, the semi-finished composite passes an impregnation/compaction belt, where the components are mixed and the semi-finished product is compacted. Finally, the semi-finished product is rolled up and stored for a defined maturing time for thickening before it can be further processed. (Diestel & Hausding, 2016) Figure 2.18 illustrates a schematic representation of the SMC manufacturing process.
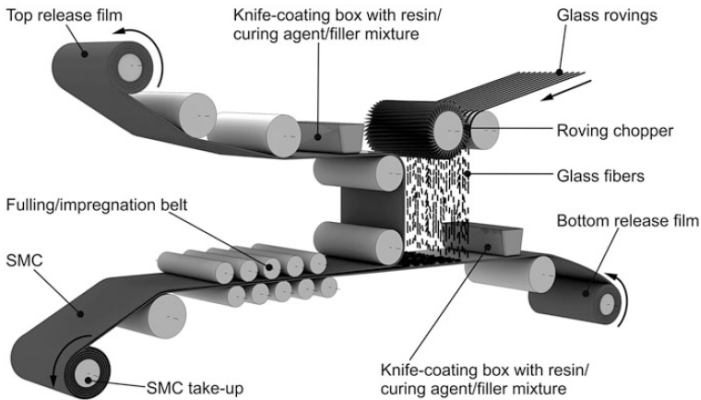
Figure 2.18: Schematic representation of the manufacturing of SMC semi-finished products (Diestel & Hausding, 2016)

SMC is usually processed in compression molding (see Figure 2.19) (Gandhi et al., 2020). For this purpose, the matured SMC semi-finished product is cut into the desired shape (usually rectangular pieces), the carrier films are removed and the individual pieces are stacked to a pre-defined initial charge (Gandhi et al., 2020; Henning, 2011). This initial charge is then weighed to check whether it has sufficient volume to fill the mold. Afterwards, it is placed in the heated (between 140°C and 160°C) mold at a defined position (Henning, 2011; Sommer et al., 2014). Under controlled velocity and force control, the initial charge is molded into the final part. Due to the mold temperature and the pressure that builds up, the viscosity of the matrix system decreases and the semi-finished product becomes flowable (Diestel & Hausding, 2016; Henning et al., 2011; Henning, 2011; Sommer et al., 2014). To be able to manufacture complex geometries, a larger flow distance is required. During processing, the SMC shows a characteristic flow behavior of a plug flow (see Figure 2.24), due to the incipient heating of the initial charge from the surface to the core, which is caused by the hot mold (Gandhi et al., 2020; Sommer et al., 2014). This flow behavior results in fiber alignment and anisotropic material properties (Gandhi et al., 2020; Sommer et al., 2014). When simulating the processing, this behavior needs to be represented by models for compression molding. These models will be discussed in detail in Subsection 2.4.1.
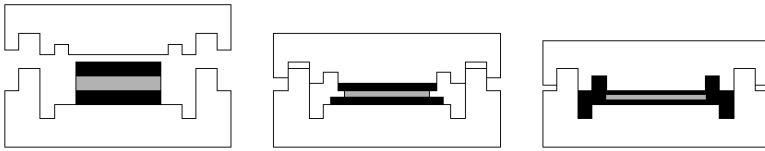
Figure 2.19: Schematic flow behavior during compression molding of SMC (Sommer et al., 2014)

Due to the described processing, which involves heating and cooling of the SMC semi-finished product, process-induced residual stresses have to be discussed. Residual stresses are stresses in the part that are present without external forces or temperature gradients. They cause warpage of the part and, depending on their orientation (residual tensile or compressive stresses), can increase or decrease the strength. In SMC materials, in addition to chemical shrinkage that occurs during the crosslinking reaction of the matrix, the different coefficients of thermal expansion of the fiber and matrix during the cooling of the part are particularly responsible for the development of residual stresses (Metehri, Serier, Bachir bouiadjra, Belhouari, & Mecirdi, 2009). However, with SMC, it is possible to practically avoid warpage of the part due to the possibility of adjusting the filler content (Kornas, 2013; Schürmann, 2007; Stachel, 2013).

Long Fiber Reinforced Thermoplastics in the Direct Process (LFT-D)

Long fiber reinforced thermoplastics can be processed either via semi-finished products in the form of granulates (LFT-G) or via direct processes (LFT-D), which do not require semi-finished products (Henning, 2020). In the LFT-D process, the matrix is compounded in-line and plasticized in a twin screw extruder. The fiber rovings are added directly to the melt via a feeding system. As a result, a composite strand is formed, which is transported to the press on a hot conveyor belt. On its way, the strand is divided into suitable pieces by a cutting unit. (Henning, 2011) Figure 2.20 shows a schematic representation of the LFT-D process.
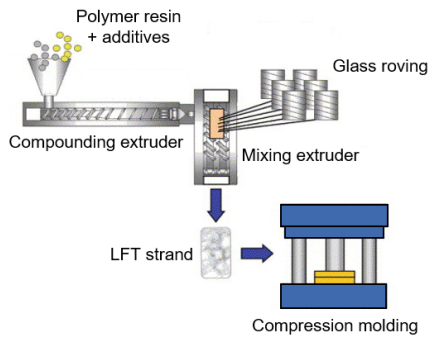
Figure 2.20: Schematic representation of the LFT-D process adapted from Geiger, Henning, Eyerer, Brüssel, and Ernst (2006)

The major advantage of the LFT-D process over the LFT-G process, which requires a semi-finished product like the thermoset SMC, primarily is a greater achievable fiber length. During the processing of the granulates into a moldable compound, the fiber length decreases significantly. (Kunc, Frame, Nguyen, Tucker, & Velez-Garcia, 2007) In addition, a further advantage of LFT-D is a great flexibility with regard to the choice of matrix material. Therefore, the LFT-D process will be considered in the context of this thesis.

As with SMC, compression molding is used for processing in LFT-D (see Figure 2.21). The cut-to-size, hot plastic compound is taken from the conveyor belt by a gripper unit and placed in the mold. The mold temperatures range between 25°C and 80°C (Sommer et al., 2014). Therefore, in contrast to processing SMC, the mold can be said to be "cold". Accordingly, the flow behavior also changes and is characterized as a fountain flow (see Figure 2.25), since the melt first solidifies at the mold surface (Davis, Gramann, Osswald, & Rios, 2003). Again, the fibers align during the mold filling and cause an anisotropic material behavior (Sommer et al., 2014). This flow behavior should be taken into account for process simulations in appropriate models for compression molding (see Subsection 2.4.1).
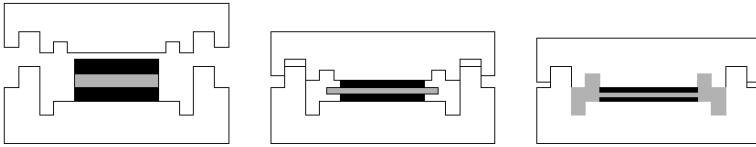
Figure 2.21: Schematic flow behavior during compression molding of LFT (Sommer et al., 2014)

For LFT parts, the residual stresses induced by the manufacturing process cannot be neglected. The arising residual stresses have two main reasons, which are related to the mold filling and the cooling process. On the one hand, residual stresses are induced during mold filling due to the uneven solidification process. The reason for this is that the immediate layer of the charge starts to solidify first when it comes into contact with the mold surface, while the inner core still remains hot. As a result, the adhesion to the mold surface prevents the solidified layer from moving on the surface, while the recently solidified layers experience forces from the flowing melt. (Gandhi et al., 2020) The prevailing melt pressure prevents shrinkage and longitudinal forces stretch the recently solidified layers (Fan, Yu, Zuo, & Speight, 2017). This creates residual compressive stresses at the part surface, while the slowly cooling core causes residual tensile stresses (Sunderland, Yu, & Månson, 2001). On the other hand, temperature-induced residual stresses build up during the cooling process (Gandhi et al., 2020). These depend on the thermal expansion of the used LFT and the prevailing temperature difference. As a consequence of these two phenomena, shrinkage and warpage occur after ejection of the part, which affect the stiffness and strength of the part and have to be considered in the part design (Balaji Thattaiparthasarathy, Pillay, Ning, & Vaidya, 2008).

Unidirectional Tapes (UD-Tapes)

Unidirectional tapes are aligned fibers that undergo an impregnation process and are subsequently available as semi-finished products (Henning, 2011). The matrix material can be thermoset or thermoplastic, and the fibers can be, for example, glass or carbon fibers. In the context of this thesis, only thermoset UD-tapes made of carbon fibers (CF) are considered. The advantage of UD-tapes in combination with the two previously described fiber composites is the possibility of hybridization by using the UD-tapes as inlays in compression molding. In order to systematically reinforce

components using UD-tapes, it is essential to ensure that the fibers have a higher strength than the base material.

In the manufacturing of thermoset UD-tapes, rovings or fiber mats are placed on a carrier film with resin and covered with a protection film. Then, the composite is pressed for better impregnation and finally rolled up. (Ehrenstein, 2006) Figure 2.22 schematically shows the manufacturing process.

Release film

Prepreg

Impregnation

Release film
with resin
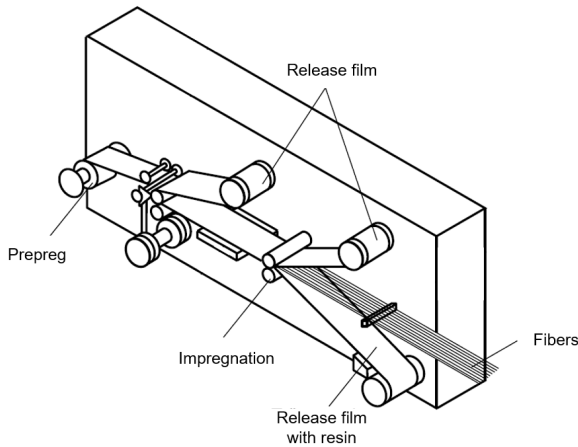
Fibers

Figure 2.22: Schematic manufacturing of thermoset UD-tape adapted from Ehrenstein (2006)

The tapes can be processed in many different ways, either manually (e.g., hand lay-up) or automatically (e.g., fiber patch placement). An overview of automated processes can be found in the work of Majic (2014). The focus of the present work is the further processing of the UD-tapes in compression molding in combination with the thermoset SMC semi-finished composite. For this processing, the carrier films are removed and the UD-tapes are placed in the mold. During compression molding, the tapes are co-molded with the flowable SMC and thus firmly bonded into the part. However, since strong shear forces act on the UD-tapes during mold filling, they must be fixed in the mold (Henning, Weidenmann, & Bader, 2020).

2.3.3 Fiber-Adapted Product Development and Fiber-Adapted Design

The lightweight design potential of products can be addressed by different strategies and construction methods (see Section 2.2). The integration of these strategies into the product engineering process (see Section 2.1) already is a challenge and needs to be planned individually. An additional challenge is posed by the use of FRP, for which the final material properties – as described in the previous subsection – result from the manufacturing process of the part. This is a decisive difference compared to product development with materials that are produced in a standardized mass process (e.g., metals such as steel) after which the part is manufactured separately (May, 2020). Therefore, it is insufficient to adapt methods and processes known e.g. from the use of steel. As an example of the potential of fiber-adapted design, which means fibers are oriented along the load path, it can be stated that in the ideal case, seven times the specific stiffness as well as nine times the specific strength can be achieved compared to steel (May, 2020). However, the previously mentioned advantages are also opposed by disadvantages such as increased development costs and "incomplete simulation abilities"[12] (May, 2020, p. 10).

Therefore, the use of FRP parts poses special challenges along the entire product life cycle, which require specific methods and processes as well as integrated product development approaches. This makes interdisciplinary collaboration "between the disciplines of design, material, manufacturing, simulation and economics indispensable"[13] (May, 2020, p. 17).

In terms of profitability, FRP components are often more expensive than designs with metallic materials. However, a cost advantage can be achieved through the integration of functions. The possibility to form complex geometries – especially for parts processed by compression molding – offers potential for reducing the number of parts compared with steel constructions. This is accompanied by a reduction in the number of tools required for part manufacturing. However, in order to be able to realize these cost potentials, it is necessary to carefully choose semi-finished products and processes that are tailored to the specific application. (May, 2020) With this in mind, the use of FRP in MMD is very promising. Supported by the lightweight design strategy of system lightweight design, load-adapted, function-integrated

---

[12] Translated by the author: „lückenhafte Simulationsfähigkeiten" [May (2020, p. 10)]
[13] Translated by the author: „zwischen den Fachdisziplinen Konstruktion, Werkstoffe, Fertigung, Berechnung und Wirtschaftlichkeit unumgänglich" [May (2020, p. 17)]

parts can be designed that dissolve existing component structures and can achieve an advantage in the overall economic assessment.

In the context of this thesis, costs are to be considered as a side constraint. Therefore, from the point of view of fiber-adapted design, interdependencies with the subdisciplines material and manufacturing remain. The integrated consideration of the three subdisciplines can be supported by simulation methods (see Figure 2.23).
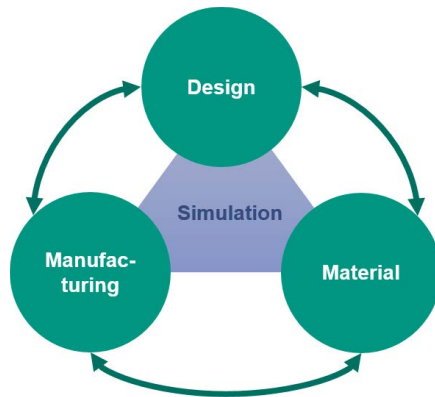
Figure 2.23: Interdependencies between design, manufacturing and material using simulation as a support tool to make the interdependencies manageable

A fiber-adapted design can be realized by continuous fibers (UD-tapes) oriented in load direction along the load paths. However, continuous fibers limit the design freedom and result in increased costs (Böhlke et al., 2019). For this reason, discontinuous fibers are used as an alternative, which increase design freedom due to their flowability and also allow complex geometries (Böhlke et al., 2019). In order to achieve comparable stiffnesses and strengths as with continuous fibers, only long fibers are promising. These are manufactured as described in Subsection 2.3.2 and processed in compression molding. However, the designed geometry influences the flow of the material during manufacturing and thus the resulting fiber orientations. The fiber orientations, along with other influencing parameters, are ultimately responsible for the resulting material properties. Therefore, it is inevitable to consider the direct interactions between design, manufacturing, and material during product development in order to obtain load-adapted part designs (Kärger, 2019). However,

these interdependencies lead to a complex design process that needs to be made manageable. As a consequence, it is possible to design the cost-intensive molds in advance and to avoid – according to the rule of ten (Clark & Fujimoto, 1991; Reinhart, Lindemann, & Heinzl, 1996) – high follow-up costs.

By combining long fiber reinforced parts and UD-tapes, the long fiber reinforced parts can be additionally reinforced in a load-adapted design. This results in the material class of continuous-discontinuous fiber reinforced polymers (CoDiCoFRP). (Böhlke et al., 2019) However, the UD-tapes bring additional design parameters.

The decisive factor for fiber-adapted design mainly is the knowledge of the orientation of the fibers after the manufacturing process in order to be able to take the resulting material properties into account in the synthesis. In the determination of the fiber orientations in the part as well as the resulting structural behavior, the product developer can be supported by simulation methods. These will be explained in more detail in the next section.

2.4   Computer-Aided Analysis

Product developers are confronted with a high level of complexity when developing new product generations (Albers, Spadinger, et al., 2017). At the same time, the number of variants and the quality requirements of the products are increasing. The demand to reduce development costs also contributes to the fact that the product developer faces great challenges. In order to successfully meet these challenges, the integration of virtual product development into the product engineering process as well as the use of innovative simulation methods helps. (Albers & Nowicki, 2003) The use of simulation methods requires models that describe the physical correlations of the reality. According to Stachowiak (1973), models have three main features:

- Depiction feature
- Reduction feature
- Pragmatic feature

The depiction feature states that models are always depictions of something. The reduction feature implies that models do not capture all properties of the original, but only those that seem relevant to the modeler or user. The pragmatic feature refers to the characteristic of models that they are built for a specific purpose. This means that models only contain the information relevant to an intended purpose. (Stachowiak, 1973) These main features are not only valid for models applied in computer-

aided analysis, but also for the previously presented models in the context of the product engineering process (see Sections 2.1 - 2.3). For the following investigations in this thesis, the main features are central and have to be considered when generalizing the findings.

Subsequently, models for describing the processing of long fiber reinforced polymers in compression molding are presented (see Subsection 2.4.1). The fiber orientations identified as being important in the previous section can only be determined by appropriate modeling of the manufacturing process. In particular, the special flow behavior of SMC will be addressed. The flow behavior of LFT is completely different (see Subsection 2.3.2) and therefore needs to be modeled separately.

Then, in Subsection 2.4.2, models are presented that serve to macroscopically describe the microscopically present fiber orientations. These models allow the prediction of macroscopic, structural mechanical part behavior. Only by understanding the component behavior already in early development phases, in which the costs for a change of the concept or design according to the rule of ten (Clark & Fujimoto, 1991; Reinhart et al., 1996) are still acceptable, it is possible to design load-adapted components that contribute decisively to lightweight design.

Numerical methods are commonly used to calculate and simulate compression molding and structural mechanics, and they have become an essential part of the product engineering process. The finite element method (FEM) is one of the most popular methods and nowadays considered a standard tool in product development for predicting the behavior of complex structures. Also, in the context of this work, the FEM is used to solve the equations underlying the models, which is why it is introduced in Subsection 2.4.3.

2.4.1   Compression Molding: Models

Correct modeling of mold filling in FRP processing is crucial for determining the fiber orientations. Hence, the velocity fields occurring during mold filling have to be calculated in order to use fiber orientation models to predict the orientation of the fibers.

Modeling of the Mold Filling

In the following, it is assumed for all modeling approaches of SMC compression molding that there is no curing during mold filling. This assumption corresponds to the current state of research (see e.g., Barone and Caulk (1979)). Also for new, fast-curing SMC formulations, this assumption is still valid (Bücheler, 2018).

There are numerous approaches for the modeling of FRP flows. Three types of models can be distinguished with respect to their level of detail:

- Models that can resolve fiber and matrix separately (e.g., Kuhn, Walter, Täger, and Osswald (2018))
- Models that combine multiple fibers into fiber bundles and then resolve the fiber bundles and the matrix separately (Meyer, Schöttl, Bretz, Hrymak, and Kärger (2020))
- Models that treat fibers and the matrix as one macroscopic phase (one phase models)

The advantage of separate modeling of fiber/fiber bundle and matrix is the possibility to resolve fiber-matrix separation, as it can occur, for example, in the filling of ribs. A decisive disadvantage is the high computation time required to solve the equations on which the models are based. For this reason, one phase models are more widely used nowadays, also in the context of the present work. One phase model means that fiber and matrix have the same velocity and thus no fiber-matrix separation can occur. In these models, the fiber orientations are calculated in a subsequent step via fiber orientation models (see next paragraph), which are based on the velocity field. In the past, models describing a flow in a small gap (gap length >> gap height) were applied (e.g., Silva-Nieto, Fisher, and Birley (1980)). These generalized Hele-Shaw models describe a two-dimensional (2D) flow, assuming that the flow velocity at the mold surface is zero (Silva-Nieto et al., 1980). Thus, they model a fountain flow of the material from the center of the initial charge (see Subsection 2.3.2). The advantage of these models is that the effort required to solve the underlying equations is relatively low compared to fully developed 3D flows.

However, Barone and Caulk (1986) showed with their experiments that these assumptions do not sufficiently reflect the real flow conditions during compression molding of SMC and developed a model with lubrication layers on the mold surface and a central plug flow (see Figure 2.24). This approach has been pursued by many authors and represents the state of research (e.g., Dumont, Orgéas, Favier, Pizette, and Venet (2007), Hohberg, Kärger, Henning, and Hrymak (2017)). Therefore, it is also employed in the context of this thesis. The underlying observation of these models is that the flow velocity at the mold surface is not zero. Wall slip takes place at the mold surface (Osswald & Menges, 2012), which needs to be captured in the model.
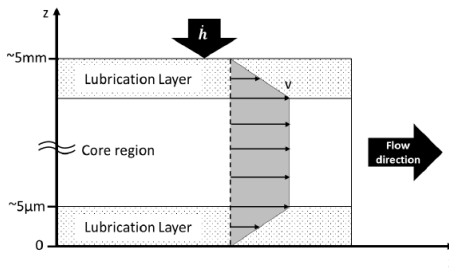
Figure 2.24: Flow conditions during compression molding (with tool closing speed $\dot{h}$) of SMC: plug flow (Hohberg, 2019)

In contrast, the flow conditions during compression molding of LFT differ significantly. Here, the molten material solidifies as soon as it comes into contact with the cold mold surface (see Subsection 2.3.2). Hence, one way to model the flow in the mold is to set the velocity boundary condition at the mold surface such that the material is no longer flowable (v = 0 m/s), i.e., no wall slip occurs (Gandhi et al., 2020). Accordingly, other flow conditions result, which can be described as a fountain flow (see Figure 2.25). During processing, the warm material flows from in between the two solidification layers to the outside, where it also solidifies. (Davis et al., 2003)
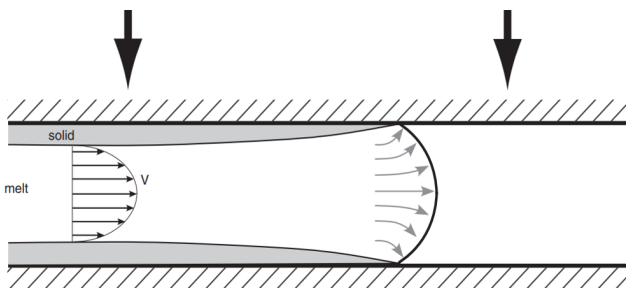
Figure 2.25: Flow conditions and solidification during compression molding of LFT: fountain flow (Davis et al., 2003)

These phenomenological observations are now to be described mathematically. The balance equations for mass, momentum and energy serve as the basis for a generally valid, *material-independent* description of the one phase flow as a continuum fluid during compression molding. These equations are known as continuity equation (see Equation 6), conservation of momentum (see Equation 7) and conservation of energy (see Equation 9).

To derive the *continuity equation*, the change in mass over time in a volume element is balanced by considering the sum of the inflowing minus the outflowing masses. This results in the conservation of mass from Equation 6 with the density ρ, the time t and the velocity vector $\mathbf{v}$.

$$\frac{\delta \rho}{\delta t} + \nabla \cdot (\rho \mathbf{v}) = 0 \qquad \textbf{6}$$

Conservation of momentum balances the change in momentum over time in the volume element, which is equal to the sum of the momentum fluxes, the shear and normal forces acting on the volume element, and the volume forces acting on the volume element. With the pressure p, the viscous stress tensor $\boldsymbol{\tau}$ and the gravitational acceleration vector $\boldsymbol{g}$, the conservation of momentum equation is obtained according to Equation 7.

$$\rho \frac{D\mathbf{v}}{Dt} = \nabla \cdot \boldsymbol{\tau} - \nabla p + \rho \boldsymbol{g} \qquad \textbf{7}$$

In addition to the already introduced equations, the conservation of energy is needed, which is not given in its general form here, but in the following in Equation 9 in a specified, reduced form.

While for the mold filling simulation of LFT a relative motion between material and mold surface can be neglected, this has to be taken into account for SMC due to the previously described findings. Consequently, a suitable friction model is necessary, which in the context of the present work is given by Equation 8 (Rosenbaum & Hatzikiriakos, 1997) and serves as a boundary condition for the solution of the differential equations in the simulation.

$$v_s = \frac{\alpha}{1 + \left(\frac{\tau_C}{\tau_W}\right)^{10}} \tau_W^{m_S} \qquad \qquad \textbf{8}$$

v_s is the slip velocity defined by the slip coefficient function α, the critical shear stress τ_C at which slip sets in, the wall shear stress τ_W, and the slip exponent m_S. This model is based on the assumption that slip occurs at the mold surface as soon as a critical shear stress τ_C is exceeded.

The balance equations can only be solved by the introduction of *material-dependent* constitutive equations and material characteristics. On the one hand, the constitutive equations establish the connection between the viscous stress tensor in momentum conservation and the velocity field (see Equation 11) and, on the other hand, the material characteristics describe the material behavior as a function of pressure and temperature (Herwig & Schmandt, 2015). Therefore, in the following, the material-dependent energy conservation equation, the modeling of the stress tensor, the viscosity model and the model for the compressibility of the material, that form the basis of this thesis, are presented.

The energy conservation equation shown in Equation 9 results from the application of Fourier's heat conduction law and is valid for thermoplastic (e.g., LFT) as well as thermoset materials (e.g., SMC) under the assumption of neglecting curing, which is allowed for SMC as explained at the beginning of this subsection.

$$\rho C_p \frac{DT}{Dt} = \nabla \cdot (k\nabla T) + \boldsymbol{\tau} : \nabla\mathbf{v} + \beta T \frac{Dp}{Dt} \qquad \qquad \textbf{9}$$

Here C_p denotes the specific heat capacity of the melt, T the temperature, k the polymer thermal conductivity and β the polymer expansivity. The polymer expansivity β is further defined according to Equation 10.

$$\beta = -\frac{1}{\rho}\frac{\delta p}{\delta T} \qquad \qquad \textbf{10}$$

In order to solve the conservation of momentum equation (see Equation 7), the viscous stress tensor $\boldsymbol{\tau}$ has to be modeled. For a generalized Newtonian fluid, which is assumed as a simplification in the present work because it can still represent the essential characteristics of the anisotropic material, the viscous stress tensor $\boldsymbol{\tau}$ is

assumed to be proportional to the symmetric strain rate tensor $\dot{\gamma}$ via the viscosity η (see Equation 11).

$$\tau = \eta\dot{\gamma} \qquad\qquad \textbf{11}$$

The viscosity model used in the present work is the Cross Castro Macosko model (Tamil et al., 2012) shown in Equation 12.

$$\eta(\alpha^*, T, \dot{\gamma}) = \frac{\eta_0(T)}{1 + \left(\frac{\eta_0(T)\dot{\gamma}}{\tau^*}\right)^{1-n}} \left(\frac{\alpha_g}{\alpha_g - \alpha^*}\right)^{(C_1 + C_2\alpha^*)} \qquad\qquad \textbf{12}$$

η is the viscosity, $\dot{\gamma}$ the shear rate, α^* the degree of cure, and n, τ^*, α_g, C_1, C_2 data-fitted coefficients. The zero shear viscosity $\eta_0(T)$ is specified via Equation 13 (Tamil et al., 2012). Here, B and T_b are also data-fitted coefficients.

$$\eta_0(T) = B \exp\left(\frac{T_b}{T}\right) \qquad\qquad \textbf{13}$$

For glass fiber SMC, a compressible material behavior is reported in literature (Guiraud, Dumont, Orgéas, & Favier, 2012; Hohberg, Kärger, Bücheler, & Henning, 2017). For compressible materials, the density is to be modeled as a function of pressure and temperature. For this purpose, Equation 14 shows the two-domain Tait pvT model (Chiang, Hieber, & Wang, 1991) employed in this thesis.

$$v(T, p) = v_0(T)\left[1 - C \ln\left(1 + \frac{p}{B^*(T)}\right)\right] + v_t(T, p) \qquad\qquad \textbf{14}$$

Here, $v(T, p)$ describes the specific volume at a given temperature T and a given pressure p, $v_0(T)$ the specific volume at zero gauge pressure, C a constant and $v_t(T, p)$ the specific volume at the volumetric transition temperature T_t. $B^*(T)$ is the pressure sensitivity of the material, which itself can be expressed by Equation 15. b_{3m}, b_{4m} and b_{5*} represent data-fitted coefficients.

$$B^*(T) = b_{3m}e^{(-b_{4m}(T - b_{5*}))} \qquad\qquad \textbf{15}$$

The specific volume at zero gauge pressure $v_0(T)$ is characterized more precisely by Equation 16. Again, b_{1m} and b_{2m} are data-fitted coefficients.

$$v_0(T) = b_{1m} + b_{2m}(T - b_{5*})$$

<div align="right">**16**</div>

To calculate the equations underlying the presented models of mold filling, material data are required, which have to be determined experimentally.

Models for the Determination of the Fiber Orientation

To calculate the fiber orientation in one phase models, the fibers and their orientation are described as a function of the flow. For modeling the fiber orientation, many approaches can be found in literature (Kugler, Kech, Cruz, & Osswald, 2020).

Mathematically, the position of a fiber in a three-dimensional space at a certain point in time t can be described by the angle pair θ and ϕ (see Figure 2.26). The angles θ and ϕ change with time during mold filling. For compression molding processes of long fiber reinforced polymers (SMC and LFT), where the fibers can only align in the plane (here: xy-plane), it is even sufficient to describe the orientation by only one angle ϕ. (Osswald & Menges, 2012)
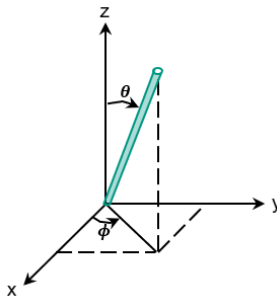
Figure 2.26: Mathematical description of the position of a fiber in the three-dimensional space adapted from Gandhi et al. (2020)

Based on these assumptions, a probability density function $\psi(\phi, x, y, t)$ can be defined, which mathematically describes the probability P of the orientation of the fiber

in space. The probability that a fiber is oriented at time t at position (x,y) between angles ϕ_1 and ϕ_2 can be calculated using Equation 17. (Osswald & Menges, 2012)

$$P(\phi_1 < \phi < \phi_2) = \int_{\phi_1}^{\phi_2} \psi(\phi, x, y, t)d\phi \qquad \textbf{17}$$

To calculate the probability density function, the angular velocity $\dot{\phi}$ of the fibers is needed. Jeffery (1922) presented one of the first models to describe the motion of an ellipsoidal single fiber in a viscous fluid (see Equation 18).

$$\dot{\phi} = \frac{r_e{}^2}{r_e{}^2 + 1}\left(-sin\phi cos\phi \frac{\partial v_x}{\partial x} - \sin^2\phi \frac{\partial v_x}{\partial y} + \cos^2\phi \frac{\partial v_y}{\partial x}\right.$$
$$\left. + sin\phi cos\phi \frac{\partial v_y}{\partial y}\right) - \frac{1}{(l_F/D)^2 + 1} \qquad \textbf{18}$$
$$\left(-sin\phi cos\phi \frac{\partial v_x}{\partial x} - \cos^2\phi \frac{\partial v_x}{\partial y} + \sin^2\phi \frac{\partial v_y}{\partial x} + sin\phi cos\phi \frac{\partial v_y}{\partial y}\right)$$

In this equation, r_e represents the aspect ratio of the fiber, which relates the fiber length l_F to the fiber diameter D ($r_e = l_F/D$). v_i indicates the components of the velocity vector $\mathbf{v}$ of the fiber in the respective spatial direction.

Based on this work, Folgar and Tucker III (1984) developed a model that allowed consideration of fiber interactions in concentrated suspensions by introducing a phenomenological, scalar fiber-fiber interaction coefficient C_I. Consideration of fiber-fiber interactions is particularly important for industrially relevant fiber volume contents in compression molding of 20-50%. Advani and Tucker (1987) introduced the fiber orientation tensor A for numerical computation of three-dimensional fiber orientations because it is more efficient to determine the components of A over multiple time steps and spatially distributed nodes than the distribution function ψ (Phelps & Tucker, 2009). However, this leads to the problem that computing the temporal change of A ($\dot{A} = DA/Dt$) requires a fourth-order tensor. To solve this problem, various closure approximations have been developed, for which the author refers to literature (e.g., Kugler et al. (2020)). Graphically, the second-order fiber orientation tensor can be illustrated by an orientation ellipsoid (see Figure 2.27), where the eigenvectors e_1, e_2, e_3 of the fiber orientation tensor A indicate the principal directions of fiber orientation and the eigenvalues $\lambda_1, \lambda_2, \lambda_3$ provide a measure of the statistical proportions of orientation in each direction (Willems, Reitinger, & Bonten, 2020).
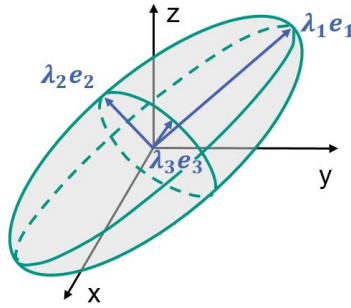
Figure 2.27: Orientation ellipsoid for the visualization of the second-order fiber orientation tensor adapted from Willems et al. (2020)

To further minimize the differences between the fiber orientations calculated by these models and the fiber orientations observed in experiments, Phelps and Tucker (2009) developed the Anisotropic Rotary Diffusion (ARD) model. In the ARD model, the scalar phenomenological interaction coefficient C_I is replaced by a second-order tensor $\boldsymbol{C_i}$ to describe the anisotropic orientation behavior due to spatially non-uniform rotational diffusion. Also based on experimental observations that show that the rate of change of the orientation tensor in concentrated suspensions is overestimated by the Folgar and Tucker III model, Wang, O'Gara, and Tucker (2008) developed the Reduced-Strain Closure (RSC) model. The RSC model contains a parameter κ that slows down the orientation kinetics in order to achieve better agreement between calculation and experiment for long fiber reinforced polymers. The parameter κ is a scalar determined by data-fitting with experimental results.

As the ARD and RSC models capture different effects which should both be considered independently for modeling fiber orientation in long fiber reinforced polymers, Phelps and Tucker (2009) developed the ARD-RSC model for long fibers (see Equation 19).

$$
\begin{aligned}
\frac{Da_{ij}}{Dt} = &-\frac{1}{2}\big(w_{ik}a_{kj} - a_{ik}w_{kj}\big) \\
&+\frac{1}{2}\lambda\Big[\dot{\gamma}_{ik}a_{kj} + a_{ik}\dot{\gamma}_{kj} \\
&-2\dot{\gamma}_{kl}\Big(a_{ijkl} + (1-\kappa)\big(L_{ijkl} - M_{ijmn}a_{mnkl}\big)\Big)\Big] \\
&+\dot{\gamma}\Big[2\big(c_{ij} - (1-\kappa)c_{kl}M_{ijkl}\big) - 2\kappa c_{kk}a_{ij} \\
&-5\big(c_{ik}a_{kj} + a_{ik}c_{kj}\big) \\
&+10c_{kl}\Big(a_{ijkl} + (1-\kappa)\big(L_{ijkl} - M_{ijmn}a_{mnkl}\big)\Big)\Big]
\end{aligned}
\qquad \textbf{19}
$$

Here, a_{ij} denotes the components of the fiber orientation tensor $\boldsymbol{A}$, w_{ij} the components of the vorticity tensor $\boldsymbol{w}$, $\dot{\gamma}_{ij}$ the components of the symmetric strain rate tensor $\dot{\boldsymbol{\gamma}}$, L_{ijkl} and M_{ijkl} the components of the fourth-order tensors $\boldsymbol{L}$ and $\boldsymbol{M}$, λ the shape factor (see Equation 20) with the aspect ratio r_e

$$
\lambda = \frac{r_e^2 - 1}{r_e^2 + 1}
\qquad \textbf{20}
$$

and c_{ij} (see Equation 21) the components of the rotary diffusion tensor $\boldsymbol{C}_i$ from the ARD model

$$
c_{ij} = b_1\delta_{ij} + b_2 a_{ij} + b_3 a_{ik}a_{kj} + b_4\frac{\dot{\gamma}_{ij}}{\dot{\gamma}} + b_5\frac{\dot{\gamma}_{ik}\dot{\gamma}_{kj}}{\dot{\gamma}^2}
\qquad \textbf{21}
$$

where b_1-b_5 are scalar constants that have to be chosen in alignment with experiments.

The ARD-RSC model is able to describe the slower alignment of long fibers resulting from their interaction. Therefore, this model represents the state of research for the calculation of long fiber reinforced polymers and is also used in the context of the investigations of this thesis.

2.4.2   Structural Mechanics: Models

In order to calculate the stiffnesses of structures made of SMC or LFT, following the mold filling simulations (see Subsection 2.4.1), it is necessary to transfer the material

properties resulting from the fiber orientations into a structural model. For this purpose, it is first introduced how structural mechanical stiffnesses can be calculated. Based on this, the calculation of the material properties resulting from the fiber orientations is described in more detail. Finally, the strength evaluation of long fiber reinforced polymers is discussed.

Models for the Calculation of Structural Mechanical Stiffnesses

For the mathematical description of solids on a macroscopic level, as with fluids, continuum mechanical modeling is used. For this purpose, analogous to Subsection 2.4.1, the balance equations are considered, which describe the cause of the kinematics of solids. The balancing of the mass at an infinitesimal volume element yields Equation 22, analogous to the consideration for flows.

$$\frac{\delta \rho}{\delta t} + \nabla \cdot (\rho \mathbf{v}) = 0 \qquad \textbf{22}$$

The momentum balance is obtained by taking into account the mass balance analogously to Equation 7 without separating the stress tensor into a hydrostatic and a deviatoric part. This results in Equation 23 with the second-order Cauchy stress tensor $\boldsymbol{\sigma}$ and the body force density vector $\boldsymbol{b}$.

$$\rho \frac{D\mathbf{v}}{Dt} = \nabla \cdot \boldsymbol{\sigma} + \rho \boldsymbol{b} \qquad \textbf{23}$$

In the quasi-static case, where the inertia effects are neglected, the momentum balance simplifies to Equation 24. This simplification is underlying the results of the present work. $\boldsymbol{g}$ again is the gravitational acceleration vector.

$$0 = \nabla \cdot \boldsymbol{\sigma} + \rho \boldsymbol{g} \qquad \textbf{24}$$

The significant difference between continuum mechanics modeling of solids and flows is in the description of the stress tensor. While in fluid mechanics the viscous stresses depend on the shear rates, in linear elastic solid mechanics the stresses are linear in the strain tensor (Hooke's law). This relationship is given in Equation 25.

$$\boldsymbol{\sigma} = \mathbb{C}[\boldsymbol{\varepsilon}] \qquad \textbf{25}$$

Here, ε represents the strain tensor and $\mathbb{C}$ the fourth-order stiffness tensor. Consequently, $\mathbb{C}$ has 81 independent material coefficients in the most general case. For the anisotropic elastic case, due to symmetries, there are 21 unknowns, which can be reduced to nine elastic coefficients assuming orthotropic symmetry. These nine coefficients ($E_1, E_2, E_3, G_{12}, G_{13}, G_{23}, \nu_{12}, \nu_{13}, \nu_{23}$) are also called engineering constants. They are sufficient for the description of long fiber reinforced polymers. On this assumption Equation 25 can be simplified as shown in Equation 26.

$$
\begin{Bmatrix} \varepsilon_{11} \\ \varepsilon_{22} \\ \varepsilon_{33} \\ \gamma_{12} \\ \gamma_{13} \\ \gamma_{23} \end{Bmatrix} = \begin{Bmatrix} \begin{matrix} 1/E_1 & -\nu_{21}/E_2 & -\nu_{31}/E_3 \\ -\nu_{12}/E_1 & 1/E_2 & -\nu_{32}/E_3 \\ -\nu_{13}/E_1 & -\nu_{23}/E_2 & 1/E_3 \end{matrix} & & 0 & \\ & & 1/G_{23} & 0 & 0 \\ & 0 & 0 & 1/G_{13} & 0 \\ & & 0 & 0 & 1/G_{12} \end{Bmatrix} \begin{Bmatrix} \sigma_{11} \\ \sigma_{22} \\ \sigma_{33} \\ \tau_{23} \\ \tau_{31} \\ \tau_{21} \end{Bmatrix} \qquad \textbf{26}
$$

Due to the symmetry of the compliance tensor, which results from the inversion of the stiffness tensor, Equation 27 additionally applies.

$$
\nu_{21} = \frac{E_2}{E_1}\nu_{12}, \nu_{31} = \frac{E_3}{E_1}\nu_{13}, \nu_{32} = \frac{E_3}{E_2}\nu_{23} \qquad \textbf{27}
$$

As a consequence, the macromechanical structural behavior of parts made of long fiber reinforced polymers can be described by transferring the results of the fiber orientation analysis (see Subsection 2.4.1) into the engineering constants. This is achieved with the help of a two-stage process, which is presented in the following.

The first stage is the application of micromechanical models that allow the determination of the elastic parameters of the composite through homogenization. Micromechanics models widely used in literature are, i. a., Halpin-Tsai (Halpin & Kardos, 1976), Mori-Tanaka (Mori & Tanaka, 1973) and Tandon-Weng (Tandon & Weng, 1984). According to the pragmatic feature of Stachowiak (1973), the selection and application of a model is based on a specific purpose. The Tandon-Weng model is most suitable for two-phase materials consisting of isotropic constituents (Tandon & Weng, 1984). If the constituents have anisotropic material properties, more advanced models such as that of Kehrer (2019) should be applied. Since the materials to be homogenized in this work are glass fiber reinforced polymers (GFRP), the Tandon-Weng model is employed, which is explained in the following. This model has already been successfully used by Foss (2004) for the prediction of the structural mechanical behavior based on a coupling with a mold filling simulation.

The Tandon-Weng model is characterized by the model assumption of a composite with unidirectionally aligned spheroidal inclusions (see Figure 2.28).
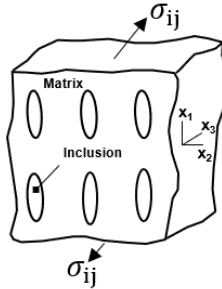
Figure 2.28: Model of a composite with unidirectionally aligned spheroidal inclusions in an infinite, elastic matrix (Tandon & Weng, 1984)

It was developed from Eshelby's solution for elliptical inclusions (Eshelby, 1957) and the model of Mori-Tanaka, which are discussed in more detail in the following. Figure 2.29 shows Eshelby's inclusion problem.
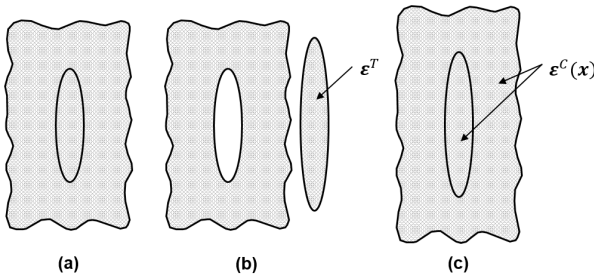
Figure 2.29: Eshelby's inclusion problem: (a) stress free state (b) inclusion undergoes a stress free transformation (c) inclusion causes a complicated strain field adapted from Tucker III and Liang (1999)

Initially, an infinite, homogeneous matrix with an ellipsoidal inclusion is assumed (see Figure 2.29 (a)). This ellipsoidal inclusion is notionally removed from the matrix in Figure 2.29 (b) and subjected to a uniform strain $\boldsymbol{\varepsilon}^T$. After reinserting the inclusion into the matrix (see Figure 2.29 (c)) the inclusion and the matrix experience the complicated strain field $\boldsymbol{\varepsilon}^C(\boldsymbol{x})$. The result of Eshelby's assumptions is that the strain $\boldsymbol{\varepsilon}^C$ is uniform within the inclusion and depends on the previously applied strain $\boldsymbol{\varepsilon}^T$ via the Eshelby tensor $\mathbf{E}_E$ (see Equation 28). The Eshelby tensor itself only depends on the aspect ratio of the inclusion and the matrix elastic constants. (Tucker III & Liang, 1999)

$$\boldsymbol{\varepsilon}^C = \mathbf{E}_E \boldsymbol{\varepsilon}^T \qquad\qquad \textbf{28}$$

Based on Eshelby's results, Mori and Tanaka (1973) developed their model for multiple identical inclusions by approximating the strain and stress field at a sufficiently large distance from the inclusion with a mean value (Gross & Seelig, 2016). This means that each inclusion sees a far-field strain equal to the average strain in the matrix (Tucker III & Liang, 1999). An interaction between the fibers is not taken into account.

Following the homogenization, in the second stage the homogenized material properties are adjusted to the calculated fiber orientations (see Subsection 2.4.1) by orientation averaging to determine the engineering constants. Orientation averaging means that the stiffness tensor of a composite consisting of differently oriented fibers can be calculated by averaging the unidirectional stiffness tensors over all directions weighted by the orientation distribution function (Advani & Tucker, 1987). The necessary mathematical relationships can be found in the work of Advani and Tucker (1987) or Lin, Jin, Zheng, Costa, and Fan (2004).

Another approach to determine macroscopic material properties which does not rely on a prior mold filling simulation but provides a faster initial estimate of the macroscopic material properties, can be found in the work of the research group led by Albers (Troll, 2015; Troll, Marston, & Albers, 2013, 2014). In their work, they describe a phenomenological, mathematical approach to account for the influence of the processing on the fiber orientations and use this to calculate the elastic material properties. Additionally, they are able to model local variations of the composite properties.

If the fibers are unidirectionally aligned like in UD-tapes (see Subsection 2.3.2), the modeling is simpler. UD-tapes can be modeled transversely isotropic (see Fig-

ure 2.30). Although this assumption is only valid for an ideal UD layer with homogeneous fiber distribution, it simplifies the modeling because only five material properties (E_1, E_2, G_{12}, v_{12}, v_{23}) have to be determined. (Schürmann, 2007) Since the investigation of the tapes is not the focus of this work, this simplified modeling is used.
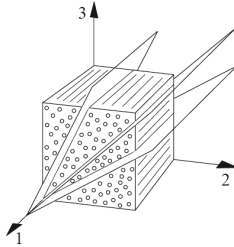
Figure 2.30: Illustration of transverse isotropy. Isotropic plane normal to the fiber. Perpendicular to it, all sections have the same material properties. (Schürmann, 2007)

Strength Evaluation of Long Fiber Reinforced Polymers

In literature, there are numerous criteria for modeling damage in laminates. They are classified as general (e.g., Tsai and Wu (1971)) or differentiating criteria that describe the type of failure in more detail. These include fiber breakage, inter-fiber failure (e.g., Puck (1996)), or delamination criteria. However, the advantage of laminates is that they can be subdivided into unidirectional individual layers. This is not the case with long fiber reinforced polymers, since the fibers align themselves during the processing (see Subsection 2.3.2). Long fiber reinforced polymers mainly fail by interface damage (primary damage mechanism) and matrix damage (secondary damage mechanism) (Fitoussi, Bocquet, & Meraghni, 2013; Larbi, Sai, Sidhom, & Baptiste, 2006). Accordingly, the micro-scale condition is crucial for failure evaluation. But there are only a few models that consider micro-scale damage and are still efficiently applicable for industrially relevant part sizes. Schemmann, Görthofer, Seelig, Hrymak, and Böhlke (2018) and Schemmann (2018) developed such an approach. However, this approach is still very costly for the use in early phases of product development, where a first (conservative) indication of the linear elastic stresses is of interest. For this purpose, a conservative but easily applicable maxi-

mum stress criterion for a plane stress state in the material principal coordinate system is suitable (see Equation 29). $R_\parallel^c$ describes the compressive strength parallel and $R_\perp^c$ transverse to the fiber direction, $R_\parallel^t$ the tensile strength parallel and $R_\perp^t$ transverse to the fiber direction, and $R_{\perp\parallel}$ the shear strength. σ_1, σ_2 and τ_{12} describe the stress components related to the material principal axes.

$$F = max\left\{\frac{\sigma_1}{-R_\parallel^c}, \frac{\sigma_1}{R_\parallel^t}, \frac{\sigma_2}{-R_\perp^c}, \frac{\sigma_2}{R_\perp^t}, \left|\frac{\tau_{12}}{R_{\perp\parallel}}\right|\right\} \qquad\qquad \textbf{29}$$

This general criterion evaluates the direction-dependent stresses with respect to a defined critical value. If this limit is exceeded, failure is expected. After an initial part design has been generated on the basis of this criterion, more detailed failure investigations can still be undertaken in subsequent development phases.

2.4.3 Finite Element Method (FEM)

Having discussed the models describing the mold filling (see Subsection 2.4.1) and the structural mechanics (see Subsection 2.4.2), the underlying, presented equations have to be solved. However, the systems of equations can usually only be calculated analytically for a number of selected special cases. Therefore, the solution of the differential equations must be supported by numerical approximation methods. In the context of this thesis, all previously presented equations are solved with the FEM, which is why its basic procedure is presented in the following. For more detailed information, the author for example refers to the publications of Bathe and Zimmermann (2002) as well as Fish and Belytschko (2007).

General Procedure

The idea of FEM is the decomposition of a complex problem into a *finite* number of subproblems. Having solved the individual subproblems, the partial solutions are assembled to the overall solution. The general procedure can be divided into five steps (Fish & Belytschko, 2007):

    1.   Preprocessing: Meshing

First, within the meshing, the geometry to be analyzed is divided into finite elements which consist of different nodes (see Figure 2.31). This causes geometric discretization errors (see Figure 2.31), but the complexity of the continuous domain can be

reduced to a finite number of evaluation points (nodes). As a result of this procedure, the problem becomes numerically (or analytically) solvable.
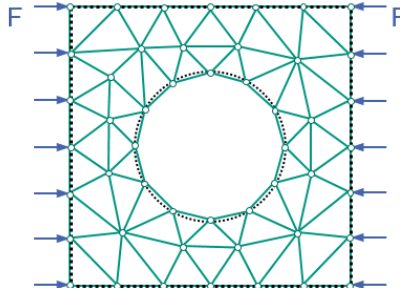
Figure 2.31: Spatial subdivision of the geometry: CAD geometry (black dashed) and discretization with finite elements (green) adapted from Fish and Belytschko (2007)

For meshing, different element types (1D, 2D or 3D) are available. In addition, the boundary conditions, material properties and, if necessary, constraints such as contacts are defined in this first step.

2. Element formulation: establishing the weak form of the equations for each finite element

Within the element-wise consideration, the strong form of the differential equation (see e.g., Equations 6, 7, 9, 22, 23, 24) is converted into the equivalent weak form via multiplying the equations by a weighting function $w(x)$ and integrating over the entire problem domain Ω. This results in the weak form, here as an example the momentum balance for quasi-static structure problems, in Equation 30, using Cauchy's stress theorem ($t = \sigma n$) and Hooke's law (see Equation 25). Γ_t describes the traction part of the boundary of the discretized geometry.

$$0 = \int_{\Gamma_t} \bar{t} \cdot w \, \mathrm{dA} + \int_{\Omega} \left(\rho b \cdot w - \mathbb{C}[\varepsilon(u)] \cdot \varepsilon(w) \right) \mathrm{dV} \qquad \textbf{30}$$

In addition, based on the discretization in the preprocessing, local shape functions are defined. As a result, the solution of the equations only has to be determined at

the nodes and the values in between can be interpolated. Here, it is distinguished between different element types with the corresponding shape function (see Figure 2.32).
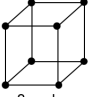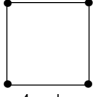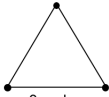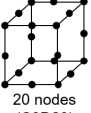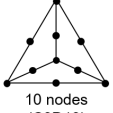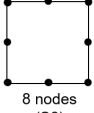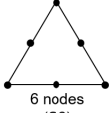
Linear shape function	8 nodes (C3D8)	4 nodes (C3D4)	4 nodes (S4)	3 nodes (S3)
Quadratic shape function	20 nodes (C3D20)	10 nodes (C3D10)	8 nodes (S8)	6 nodes (S6)
	Hexahedral element	Tetrahedral element	Quadrilateral element	Triangular element

Figure 2.32: Element types and number of nodes: hexahedral, tetrahedral, quadrilateral and triangular element with linear and quadratic shape function adapted from Steinbuch (1998)

Depending on the shape function, different result accuracies are obtained, with higher orders usually leading to better results. However, with higher orders, the computation times also increase, since the equations must be solved at a larger number of nodes. The integrations to be performed in the solution of the differential equations can be carried out, for example, by means of the Gauss quadrature.

3. Assembly: creation of the global problem formulation from the element equations

In the assembly step, the element-wise defined equations for the entire domain are combined and transformed from the element to the system level. This results in the global problem description, which for quasi-static problems can be formulated as shown in Equation 31. Here, K denotes the global stiffness matrix, d the global displacement vector, and f the global force vector.

$$Kd = f \qquad\qquad 31$$

4. Solving the global system of equations

The global system of equations from Equation 31 is subsequently solved numerically with either direct or indirect solvers. For the solution of nonlinear problems, the solution in time must also be determined. For this purpose, explicit or implicit solution methods can be used.

For more detailed information on the solution of the systems of equations, it is referred to the respective literature (e.g., Klein (2015)).

5. Postprocessing: evaluation of the results

After solving the equations by the solver, postprocessing is performed, i.e. the results are evaluated. For this purpose, the quantities of interest, such as stresses, strains or fiber orientations, are observed and visualized. On this basis, the product developer is able to interpret the mold filling or structural behavior and derive new design solutions through analytical and synthetic procedures. This design activity can be supported by optimization methods, which will be presented in the next section.

To solve the equations of the structural and flow models, customized or commercially available solvers can be used. For the flow models, specialized solutions or, for example, the commercial software Autodesk Moldflow[14], which is used in this thesis, are suitable. For the structural models, the commercial software Abaqus[15], ANSYS[16] or LS-Dyna[17] can be mentioned as examples. In the context of the present work, Abaqus is employed.

Based on the presented models, the mold filling and structural behavior can be adjusted to each other in an optimized design. For this purpose, mathematical optimization procedures can be applied, which will be presented in the next section.

---

[14] https://www.autodesk.com/products/moldflow/overview (accessed May 18, 2021)
[15] https://www.3ds.com/products-services/simulia/products/abaqus/ (accessed May 18, 2021)
[16] https://www.ansys.com/products/structures/ansys-mechanical (accessed May 18, 2021)
[17] https://www.ansys.com/products/structures/ansys-ls-dyna (accessed May 18, 2021)

2.5 Optimization Procedures

Optimization is generally understood as the strategy for finding the optimal solution to a given problem (Harzheim, 2014). For the development of products, this means improving their design so that they best meet the requirements from the system of objectives with the available resources (Kirsch, 1993). This strategy can be carried out manually by the product developer who, based on his experience, varies certain design parameters, such as wall thickness, within permissible ranges to obtain the best result. However, such an approach is usually time-consuming, hence mathematical algorithms can be used to support it. Nevertheless, it does not mean that the product developer can be replaced. Unlike some software vendors propagate, an inexperienced user cannot solve a complex optimization task at the push of a button. (Harzheim, 2014) Supporting this argument, Vanderplaats (1999) points out that it is important to be aware of the limitations of optimization. Expecting to obtain the absolute best design with numerical optimization approaches will result in "maximum disappointment" (Vanderplaats, 1999, p. 24). He states that the term "design optimization" should better be replaced by "design improvement" (Vanderplaats, 1999, p. 24) in order to reflect the possibilities of the approaches. (Vanderplaats, 1999)

Optimization in this thesis only refers to simulation-based optimization in the context of structural optimization (see Subsection 2.5.2). Therefore, first of all, the general formulation of optimization problems is introduced and solution procedures are presented (see Subsection 2.5.1). Here, only those solution procedures are discussed which can be used in the context of structural optimization and which are relevant for the present work.

2.5.1 General Formulation and Solution Procedures

A general optimization problem can be described mathematically as in Equation 32 (Harzheim, 2014; Schumacher, 2020).

$$
\begin{aligned}
&\min f(\boldsymbol{x}) \\
&so\ that \\
&g_j(\boldsymbol{x}) \leq 0; \quad j = 1, m \\
&h_k(\boldsymbol{x}) = 0; \quad k = 1, q \\
&x_i^L \leq x_i \leq x_i^U; \quad i = 1, n
\end{aligned}
\tag{32}
$$

Here, $f(x)$ describes the objective function, which has to be minimized under consideration of inequality constraints $g_j(x)$ and/or equality constraints $h_k(x)$. The design variables x are combined in a vector (see Equation 33)

$$x = \begin{pmatrix} x_1 \\ \vdots \\ x_n \end{pmatrix}$$

33

and can be constrained by side constraints x_i^L (lower) and x_i^U (upper). The design variables are those model parameters which can be varied during the optimization.

In general, objective functions have several minima, but only one of them is the global minimum. However, when solving optimization problems, the solution space defined by the design variables is only evaluated at specific points, thus the continuous course of the objective function is not available. As a result, it is not possible to ensure the identification of the global optimum. By starting the optimization from different initial values, the probability of finding the global optimum can be increased. However, this procedure does not provide any certainty either. (Schumacher, 2020)

In the following, different procedures for solving optimization problems are presented.

Mathematical Programming (MP)

The methods of mathematical programming differ in several approaches (see e.g., Schumacher (2020)). They often have in common that they are sensitivity-based or gradient-based. This means that the partial derivative of the objective function with respect to the design variables has to be calculated (Enkler, 2010). Thus, these methods have the advantage of universal applicability (Kirsch, 1993), but mostly lead to high computation times for complex problems, since the computation of the gradients is time-consuming.

Optimality Criteria (OC)

OC methods have their origins in the late 1960s, where Prager and Shield (1968) presented analytical and Venkayya, Khot, and Reddy (1968) numerical approaches.

In contrast to mathematical programming methods, condition-based (optimality criterion) methods do not need to calculate the gradients of the objective function. This represents a major advantage in terms of efficiency and robustness with respect to their convergence. However, the description of the optimal state (optimality criterion)

has to be known a priori, which mostly limits OC methods to very specific problems or objective functions. A very popular optimality criterion is the Fully Stressed Design. In addition to the definition of the optimality criterion, a redesign formula has to be determined. The redesign formula is an iterative procedure that modifies the design variables depending on the calculated structural response. (Harzheim, 2014; Kirsch, 1993)

Stochastic Optimization Procedures

Other procedures that do not require the calculation of gradients are stochastic methods (Schumacher, 2020). In these methods, the design variables are varied randomly, but still strategically, to produce an optimized design. They are particularly suitable for problems where little is known about the system behavior, but the objective function can be evaluated at individual points with moderate effort. (Enkler, 2010) Examples of this group are evolutionary algorithms or swarm algorithms. In the context of this thesis, adapted genetic algorithms (GA) are used, which belong to the group of evolutionary algorithms (Talbi, 2009).

The inspiration for the GA comes from nature. They work on the principle of the *survival of the fittest* from Darwin's theory of evolution. GA were first proposed by Holland (1992). Often, the design variables in GA are encoded in binary numbers. However, there are also many GA that do not use this encoding (Talbi, 2009). At this point, it should be noted that GA are very efficient global optimization algorithms, but they cannot guarantee, like other optimization methods, that a global optimum will be found (Harzheim, 2014). For searching the optimum, GA use the operators selection, crossover, and mutation (Harzheim, 2014; Rao & Savsani, 2012; Talbi, 2009). The principle workflow of a GA is shown in Figure 2.33.

First, in the initialization, it is specified how many individuals are part of a generation. Individuals are potential combinations of the design variables, i.e. solutions of the optimization problem. Furthermore, the termination criterion, the crossover and mutation probabilities, the design variables and the range in which they may be varied are defined in the initialization. Based on this, an initial population of random individuals is generated. For this initial population, the fitness values of the individuals are calculated. The fitness values represent a measure for the fulfillment of the defined objective function. They are used for selection, where the best individuals are extracted from the population and the worst individuals are eliminated. On the one hand, for the creation of the next generation, the best individuals (*elite members*) are kept unchanged until a better solution is identified and on the other hand they are used as parents for reproduction. In reproduction, recombination (also called crossover) and mutation are used to generate new offspring that replace individuals

from the last evaluated population, thus ensuring a constant population size. In re-
combination, parts of two or more individuals are exchanged with a defined proba-
bility and combined to generate a new individual. Mutation replaces parts of a single
individual with a random value. Reproduction creates a new variety in the succeed-
ing generation, for which new fitness values are calculated. These steps are itera-
tively run through, starting with selection, until a defined termination criterion is
reached. (Rao & Savsani, 2012)
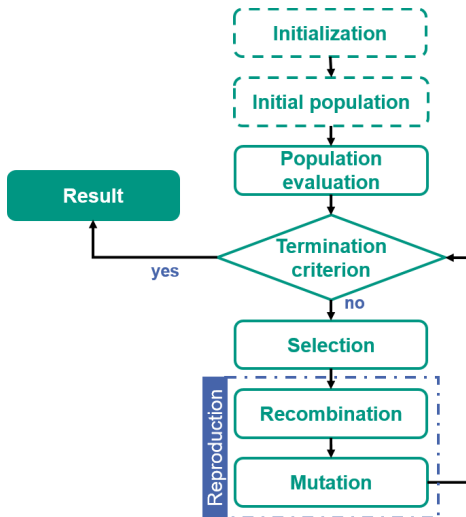
Figure 2.33: Workflow of a genetic algorithm

Genetic algorithms have already successfully demonstrated their suitability for de-
sign optimization (Ali, Behdinan, & Fawaz, 2003; Perez, Chung, & Behdinan, 2000).
Design optimization, which is referred to as structural optimization, can be distin-
guished into three classes, which will be discussed in more detail in the following
subsection.

2.5.2 Structural Optimization

The focus of this thesis is on the optimization of the design as a support tool for the product developer in the design process. Therefore, the optimization methods introduced in Subsection 2.5.1 are considered in the context of structural optimization. Structural optimization can be distinguished into three classes (see Figure 2.34): topology optimization, shape optimization and parameter or sizing optimization (Bendsøe & Sigmund, 2004; Harzheim, 2014).

Topology optimization:
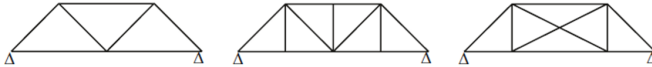
Shape optimization:
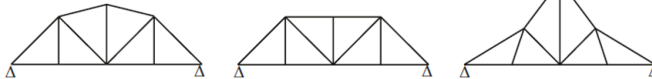
Sizing optimization:
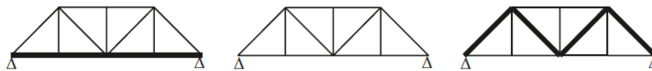
Figure 2.34: Visualization of the three classes of structural optimization adapted from Schumacher (2020)

These can support various activities of the product engineering process (see Subsection 2.1.1). Particularly topology optimization can be used in early phases to support the iPeM activity *Detect ideas* based on simplified model assumptions. Thus, it can provide valuable hints for the rough design of suitable support structures. All three classes can support the activity *Model principle and embodiment*. For this, an iterative application should be considered, e.g. in order to further adapt the design initially derived with a topology optimization by means of shape and parameter optimization. In the following, the individual classes are presented in detail.

Topology Optimization

Topology optimization varies and determines the number and position of holes and the connectivity of the structure in the design space. Accordingly, the objective of

topology optimization is to determine the optimal material distribution for prescribed loads and boundary conditions in a predefined design space. (Bendsøe & Sigmund, 2004) A commonly used approach especially in commercial software is the variation of the local density $\rho(x)$. This is used to define the design variable x in topology optimization (see Equation 34). ρ_0 describes the initial density.

$$x = \frac{\rho(x)}{\rho_0} \qquad \qquad \textbf{34}$$

To calculate the local stiffness $E(x)$ based on the design variable (see Equation 35), a power law is applied in the widely used SIMP[18] method (Bendsøe, 1989). E_0 represents the initial Young's modulus. p_{SIMP} indicates the penalty factor, which causes the design variable to converge towards 0 or 1 by penalizing intermediate values.

$$E(x) = \left(\frac{\rho(x)}{\rho_0}\right)^{p_{SIMP}} E_0 \qquad \qquad \textbf{35}$$

Topology optimization can be performed by both MP and OC methods. For a more detailed description of topology optimization, it is referred to literature (e.g., Bendsøe and Sigmund (2004) or Harzheim (2014)).

At IPEK – Institute of Product Engineering, applications and extensions of topology optimization to support an application-oriented design process have been successfully researched in the research group led by Albers (Albers et al., 2009; Albers & Ottnad, 2010; Pedersen, Hessenauer, Sigmund, & Albers, 2009; Sander, Petrich, & Albers, 2012). In this context, the beginnings of research on topology optimization at IPEK date back to Sauter, Mulfinger, and Müller (1992), from which the commercial software TOSCA evolved. In the area of topology optimization for FRP, the works of Troll et al. (2014) and Troll (2015) represent the basis for research at IPEK. However, the consideration of FRP manufacturing and processing influences in topology optimization still did not involve additional mold filling simulations. Spadinger and Albers (2019) reduced the model assumptions of this optimization approach to increase its maturity by integrating process simulations. This coupling approach will be explained in more detail in Section 2.6.

---

[18] SIMP = Solid Isotropic Material with Penalization

Shape Optimization

In shape optimization, the surface of the geometry is varied. This can be done either locally, for example to minimize stress peaks by varying the shape of notches (Schumacher, 2020), or globally, for example by introducing beads. The special case of numerical bead design and optimization is discussed in more detail in Subsection 2.7.2, hence only the general definition is given here.

In shape optimization, a distinction is made between parametric and nonparametric methods (see Figure 2.35) (Albers, Majic, & Schmid, 2011).
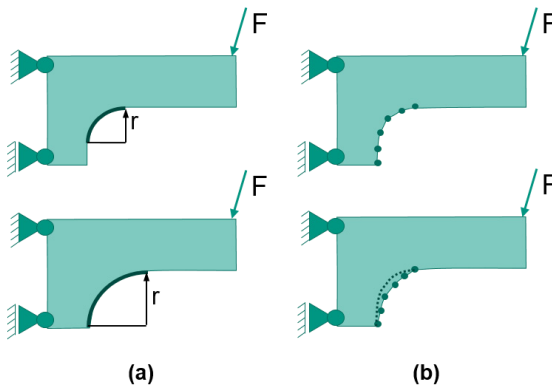
Figure 2.35: Different types of shape optimization: (a) parametric and (b) nonparametric optimization adapted from Troll (2015)

In the simplest case, in parametric shape optimization, geometric dimensions such as radii, angles, lengths, widths, etc. are used as design variables. These are often directly specified in CAD models, but can also be described in finite element (FE) models. The advantage of parametric methods lies in the simple constructive application of the optimization results. In nonparametric shape optimization, the surface nodes of an FE model serve as design variables (Harzheim, 2014). These nodes are manipulated by the optimization algorithm to generate the shape variation. A disadvantage of nonparametric methods is that mesh distortions can occur, leading to poor FEM results. (Harzheim, 2014). For further literature, it is referred, for example, to Schumacher (2020) or Harzheim (2014).

Shape optimization can be performed with MP or OC methods, but also with probabilistic methods. A shape optimization approach based on genetic algorithms was presented by the research group led by Albers, in which the outer contour of counterweights of an engine crankshaft was optimized (Albers, Noel Rovira, Aguayo Tellez, & Maier, 2008).

Sizing Optimization

Sizing or parameter optimization describes the variation of discrete part parameters such as wall thicknesses or fiber orientations of a laminate. At IPEK – Institute of Product Engineering, Heldmaier, Reichert, Li, and Albers (2018) successfully applied parameter optimization to the dimensioning of Tailor Rolled Blanks (TRB) subjected to thermomechanical loads. For further information, reference is made to literature (e.g., Harzheim (2014)).

In order to further increase the significance of optimization methods, they can be coupled with additional simulation models. Therefore, the next section discusses the coupling of simulation methods.

2.6   Coupling of Simulation Methods

Nowadays, the increasing complexity in the development of new products poses major challenges to the product developer. As described previously, simulations provide support in problem solving. For this, a variety of approaches is available for the simulation of different physical phenomena (see Section 2.4). With the optimization methods (see Section 2.5), additional approaches have been developed in order to raise further potentials in the design of products. But these approaches are limited, because they do not necessarily consider the results of previous simulations or simulations from other domains. However, in a connected environment or in functionally integrated components, it is crucial to take into account the interactions of different domains. (Albers, Spadinger, et al., 2017)

One way to overcome these limitations is through Multidisciplinary Design Optimization (MDO) approaches, which have been applied, for example, by the research group led by Behdinan to develop conceptual designs for aircraft (Perez, Liu, & Behdinan, 2004). These MDO approaches allow many different disciplines to be considered and optimized simultaneously, but require the parallel consideration of myriad design variables.

In the product development of components made of long fiber reinforced polymers, where a direct product-production dependency exists, the MDO approach for the simulation can be reduced to a coupled consideration of the manufacturing process (with the resulting material properties) and the design (see Subsection 2.3.3). In this context, it is important to couple the fiber orientations from the manufacturing process that determine the material properties into structural simulations in order to be able to derive a fiber-adapted initial design in early phases of product development.

For the simulation-based dimensioning of components made of CF fabrics, Kärger et al. (2018) developed a CAE chain in order to take into account the effects of the draping process on the structural behavior. Kärger et al. (2015) also used a CAE chain to consistently evaluate resin transfer molding (RTM) structures. In both CAE chains, specialized models and methods that are customized to the problem are used.

A more general, strategic approach for coupling simulation methods was developed by the research group led by Albers at IPEK – Institute of Product Engineering (Albers, Spadinger, et al., 2017), which can also be used to describe MDO approaches. Figure 2.36 shows a generic, graphical representation of the developed coupling framework.
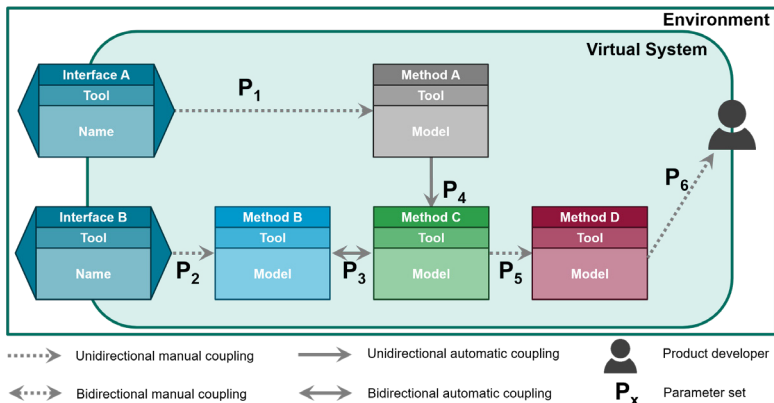
Figure 2.36: Generic coupling framework adapted from Albers, Reichert, Serf, Thorén, and Bursac (2017)

In the framework, a distinction is made between the environment and the virtual system. Via defined interfaces, it is possible to transfer boundary conditions from the environment to the virtual system. Boundary conditions can be, for example, material data or measurements from real systems. Based on the maturity of the system, the product developer can determine the right level of detail. Individual methods are represented by three-level blocks whose color indicates the used method (e.g., light blue corresponds to FEM). These methods are coupled either unidirectionally or bidirectionally in an automated or manual way. The type of coupling is distinguished by the different arrow styles. The coupling involves the transfer of defined parameter sets P_x. The product developer who sets up the coupling framework is at the center of the product development process. Therefore, he or she embodies the interface between the virtual system back to the environment by transferring the insights gained with the virtual coupling into a new product generation. (Albers, Reichert, et al., 2017)

The aim of the approach is to make complex problems manageable by coupling established, commercial methods and to enable applicability in real product development processes. With the help of the approach, the product developer can be supported in analysis and synthesis and continuous validation can be accelerated in early phases of product development. The advantage of commercial methods is their availability and robustness. (Albers, Reichert, et al., 2017)

Further potential can be raised by integrating the model of the PGE into the coupling framework. This enables the targeted controlling of the development direction, which can be done on the basis of a risk assessment during the further development of simulation generations (Albers, Schulz, et al., 2021).

With the coupling framework it is possible to create better initial designs for components made of long fiber reinforced polymers. Spadinger and Albers (2019) were able to show that the fiber orientations resulting from the processing have a decisive effect on the optimized part embodiment, which is generated by a topology optimization. Through the developed, iterative coupling of mold filling simulations in Moldflow with a homogenization and a topology optimization in Abaqus, process-based initial designs could be successfully generated.

However, the success of this approach is not limited to fiber reinforced polymers, but has already been demonstrated in other fields at IPEK – Institute of Product Engineering. For example, Majic, Albers, Kalmbach, and Clausen (2013) developed a method for the bead optimization in sheet metal components in which a deep-drawing simulation was coupled with the bead optimization in order to evaluate the

manufacturability of the optimization results. Furthermore, the influences of the additive manufacturing process Selective Laser Melting (SLM) on stiffness optimized structures were investigated (Albers, Holoch, Dietrich, & Spadinger, 2018; Holoch et al., 2020). The outer contour with altered material properties that arise due to the printing process causes changes in structures optimized based on the manufacturing process (Holoch et al., 2020). The added value of coupling has also been successfully demonstrated over many years in tribological studies (Joerger, Lin, Bause, Spadinger, & Albers, 2020; Reichert, Lorentz, & Albers, 2016). Here, the focus is primarily on the coupling of real, engineered surfaces measured with a white light interferometer and FE simulations.

For the transfer of results from one simulation environment to another (for example, the transfer of fiber orientations and material properties from the mold filling simulation to the structural simulation), additional tools are needed that enable the so-called *mapping*, which will be presented in more detail in the following.

Mapping

In order to consider the material properties resulting from the fiber orientations, which develop during mold filling, in the structural mechanical behavior, it is necessary to transfer this information to a structural mesh. This is achieved by the help of mapping techniques, which can translate information from a source mesh to a deviating target mesh. In the context of this thesis, this is particularly relevant, since flow-optimized meshes are required for the mold filling simulations, which are not necessarily suitable for structural simulations. There are several commercial tools available for mapping, for instance MSC Digimat[19]. In the context of the present work, the MpCCI MapLib of the Fraunhofer Institute for Algorithms and Scientific Computing (SCAI) (Spiess, Oeckerath, & Landvogt, 2018) is used. As important input variables for the mapping, it has to be specified whether the information to be transferred is contained in the elements or on the nodes, in which radius nodes of the target mesh should be searched and which mapping algorithm should be used. For the analyses in this thesis, the fiber orientation tensors, the engineering constants and, in the case of the LFT simulations, additionally the residual stresses are mapped. To this end, the mapping algorithm weightedElement is used (see Figure 2.37). This algorithm identifies for each node n_i of the target mesh in which element of the source mesh it is located. Afterwards, the length of the vector e_i between the element centers of the source mesh and the target mesh is calculated, which is used reciprocally as

---

weight to determine the value in the target mesh. For more detailed information, it is referred to the MapLib documentation (Spiess et al., 2018).
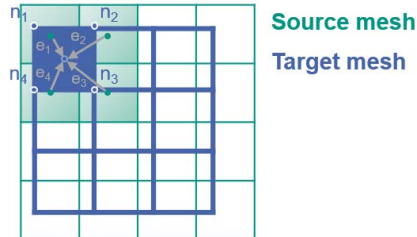
Figure 2.37: Representation of the working principle of the mapping algorithm weightedElement

The previously presented state of research has shown the relevance of lightweight design (see Section 2.2), fiber reinforced polymers (see Section 2.3), as well as computer-aided product development (see Section 2.4), optimization (see Section 2.5) and coupling. The next section is dedicated to beads as constructional stiffening elements in fiber reinforced polymer structures and thus represents a special cross-sectional topic from the previously discussed aspects.

2.7   Beads as Constructional Stiffening Elements in Fiber Reinforced Polymer Structures

In general, flat, thin-walled structures only provide low geometric bending stiffness. However, stiffness requirements are a necessary boundary condition in most developments and are an important aspect of the system of objectives.

Obvious constructional design solutions for improving stiffness are to increase the wall thickness or to add ribs, but this introduces additional mass into the structure. This is in conflict with the requirements for lightweight design solutions. One possibility for stiffening a structure without the use of additional mass can be the systematic generation of residual stresses. Furthermore, beads can be introduced as geometric stiffening elements into the support structures of lightweight designs in order

to increase the stiffness of the construction with a non-significant adding of additional material. (Bilik, Pahr, & Rammerstorfer, 2012). Figure 2.38 gives an overview of the possible measures to increase the stiffness of a part.
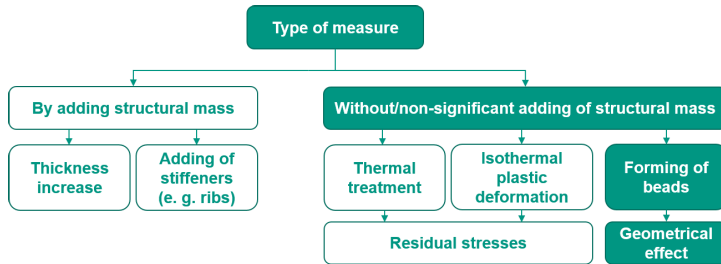
Figure 2.38: Measures to increase part stiffness adapted from Bilik et al. (2012)

When using beads in fiber reinforced polymers, material lightweight design (see Subsection 2.2.3) is combined with form lightweight design (see Subsection 2.2.2). Therefore, general aspects and the working principle of beads as well as their effect on a fiber-adapted design are first introduced in Subsection 2.7.1. In Subsection 2.7.2, the state of research on numerical bead design is discussed.

2.7.1   General Aspects

Beads are stiffening elements introduced by channel-like pits or elevations perpendicular to the surface in shell-shaped parts. The depth/height of the beads is small compared to their length. (Klein, 2013; Widmann, 1983)

The stiffening effect of beads is decisively determined by the two factors

- position and course of the bead[20] in the part
- bead cross section.

---

[20] The bead position defines the location of the beads in the part, while the bead course describes the spatial development and thus also includes, for example, the radius of curvature. In the following, the combination of bead position and bead course is referred to as bead pattern.

From the 1950s onwards, the design of beads was investigated – mainly in experimental research (see e.g., Oehler (1951), Kienzle (1955), Oehler and Draeger (1971), Oehler and Weber (1972)). This resulted in empirically determined design rules and design catalogs giving recommendations for *positions and courses* of the beads. Their aim was to provide generally applicable design guidelines. For stiffening against the load case "pressure normal to the part surface", Figure 2.39 shows examples of positions and courses. The stiffness increases from left to right, since unfavorable design elements, such as beads crossing in one point, are avoided.
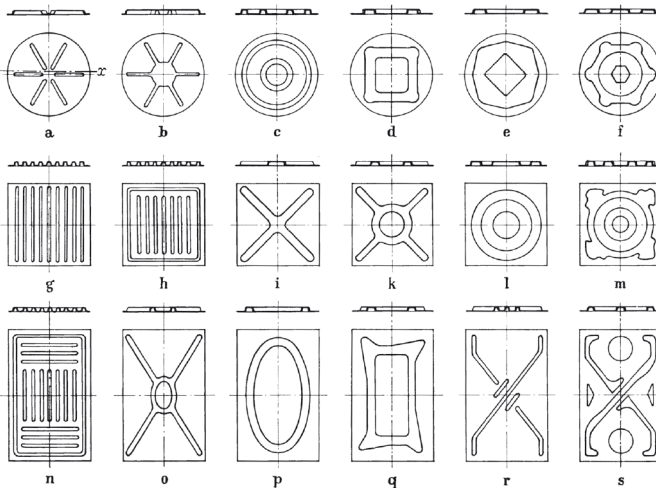
Figure 2.39: Different bead positions and courses for stiffening against the load case pressure normal to the part surface adapted from Oehler and Weber (1972): stiffening effect increasing from left to right

Beads can end at the edge (open beads) (see Figure 2.40) or have a defined end inside the part (closed beads) (see Figure 2.39). The type of end and the choice of the *bead cross section* usually depend on boundary conditions such as design space, stiffness requirements, connection to surrounding components or manufacturability. Typical bead cross sections are shown in Figure 2.40. The stiffening effect decreases from left to right. The reason for this is explained in more detail in the following.
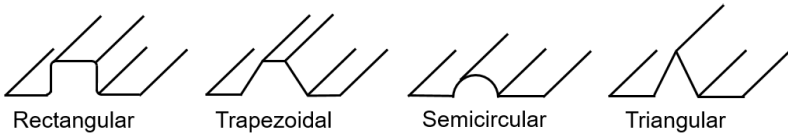
Figure 2.40: Typical bead cross sections adapted from Oehler and Draeger (1971)

Using the trapezoidal bead as an example, a bead cross section can be defined geometrically as shown in Figure 2.41. Thus, the bead parameters are bead height, bead width, flank angle, head radius, base radius and top chord width. Depending on the bead cross section, these parameters vary. As previously described, the bead parameters are limited by boundary conditions. For example, only certain head and base radii can be achieved due to manufacturing restrictions from deep drawing, casting or compression molding, or only defined maximum flank angles can be achieved due to part ejection.
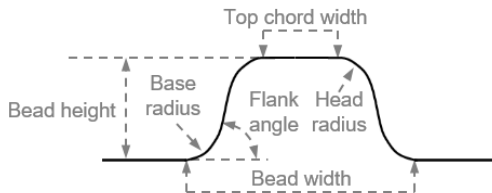
Figure 2.41: Bead cross section and bead parameters adapted from Emmrich (2004)

Beads cause a direction-dependent bending stiffness (geometric anisotropy), since they only have a stiffening effect in the longitudinal direction of the bead. The bending stiffness of the structure is reduced when a load is applied transversely to the bead. (Albers, Weiler, Emmrich, & Lauber, 2005) This is due to the working principle of the beads, which can be explained by the increase of the second moment of area (see Figure 2.42). The second moment of area is a merely geometric quantity of a cross section.
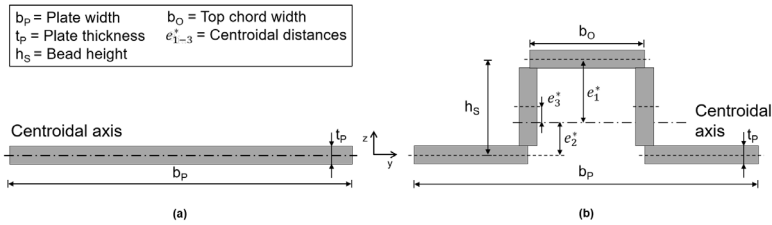
Figure 2.42: Working principle of beads by shifting the centroidal axis on the example of a rectangular bead: (a) flat plate (b) simplified fragmentation of the rectangular bead adapted from Emmrich (2004)

For the flat plate (see Figure 2.42 (a)), the bending stress is linear across the cross section. Due to the low height and the central position of the neutral axis, where the material does not contribute to the bending stiffness, this part is soft in bending. The associated second moment of area I_y is calculated according to Equation 36. Accordingly, the second moment of area can be increased by changing the wall thickness t_P or the geometry of the cross section.

$$I_y = \frac{b_P\, t_P{}^3}{12}$$

<div align="right">36</div>

By including beads in the plate, the material is moved from the neutral axis. This also shifts the centroidal axis (see Figure 2.42 (b)). As a result, bending stress components are transformed into membrane stress components, resulting in more efficient and homogeneous material stresses (Emmrich, 2004). Considering the parallel axis theorem, the second moment of area increases disproportionately (Klein, 2013). It can be calculated based on the notations from Figure 2.42 (b) according to Equation 37.

$$I_y = \frac{b_o t_P^3}{12} + e_1^{*2} b_o t_P + \frac{(b_p - b_o)t_P^3}{12} + e_2^{*2}(b_p - b_o)t_P$$
$$+ 2\left(\frac{t_P(h_S - t_P)^3}{12} + e_3^{*2}(h_S - t_P)t_P\right)$$

<div align="right">37</div>

Accordingly, the second moment of area can be increased more efficiently by increasing the bead height h_S than by increasing the wall thickness t_P. In addition, it is immediately apparent why the rectangular bead represents the stiffest cross section in Figure 2.40.

All these findings have been elaborated for the application of beads in metallic sheets. Here, the beads are mostly brought into the sheet metal part by forming processes (see DIN 8580, 2003) such as deep drawing. Consequently, the maximum bead course and cross section are influenced by manufacturing restrictions such as the residual forming capacity of the metal sheet or occurring material thinning (Maiwald, 1992). Assessments of the manufacturability of the designed bead geometry can be made, for example, using Forming Limit Diagrams (FLD) (Majic et al., 2013).

However, the use of beads for stiffening thin-walled, fiber reinforced parts, especially those made of long fiber reinforced SMC, has also been proposed in literature (European Alliance for SMC/BMC, 2016; Schürmann, 2007; Specker, Osswald, & Michaeli, 1990; Wilhelm, 2013a). But the decisive difference in the manufacturing process of beads for this class of materials compared to metallic materials is that the product developer almost has complete design freedom. There is no restriction due to residual forming capacity as in the case of metal, since the beads in SMC are formed in a primary forming process with the aid of a mold (see Subsection 2.3.2). Only the demoldability, minimum radii as well as minimum and ideally constant wall thicknesses have to be considered (Davis et al., 2003; Ehrenstein, 2006; European Alliance for SMC/BMC, 2016). However, this design freedom is not only an advantage over classical manufacturing processes. It also results in a huge variety of possible bead parameter combinations (see Figure 2.41), which can be selected independently of each other and whose interrelated complexity is difficult to oversee for the product developer. A change in the bead cross section or the bead position and course leads to a different geometry, which in turn influences the flow behavior in the mold filling and thus the fiber orientations and finally the resulting material properties (see Subsection 2.3.3) (Sanwald et al., 2013). This leads to a superposition of the geometric anisotropy introduced into the part by the beads with the material anisotropy caused by the used material. Thus, a complex design process for beaded, long fiber reinforced parts results, which inevitably requires the integration of the manufacturing process. But apart from general design guidelines (e.g., European Alliance for SMC/BMC (2016) or Schürmann (2007)) no further support tools for the product developer could be found in literature concerning the design of beads in long fiber reinforced polymer parts. In this context, the problem can no longer be solved analytically, which is why numerical methods for bead design have to be used.

2.7.2   Numerical Bead Design

The design of beaded parts can be determined for simple sheet metal geometries and load cases with the help of design catalogs and guidelines or the experience of the product developer. However, if the complexity of the load case and the geometry increase, these available support tools are no longer sufficient (Maiwald, 1992). The generally applicable catalogs and guidelines only represent a compromise solution in terms of a load case specific design for complex load cases (Maiwald, 1992).

The use of numerical optimization methods allows to overcome the challenge of load case specific design of beads and at the same time to achieve higher stiffnesses compared to the design catalogs (Schwarz, 2002). In numerical bead optimization, a distinction is made between direct and indirect methods (Emmrich, 2004). Indirect methods support the identification of optimal bead patterns. During the optimization process, however, no bead cross sections are generated in the part. Examples of methods in this category include topology optimization (see Subsection 2.5.2) (Harzheim, 2014), optimization of the orientation of orthotropic materials (Luo & Gea, 1998) or the introduction of substitute inertias in beam elements (Fusano, Priarone, Avalle, & Filippi, 2011). A decisive disadvantage of the indirect methods is that the question of the optimum bead cross section remains unresolved and has to be answered additionally by the product developer following the pattern optimization. Since the indirect methods are not considered in this work, it is referred to the work of Emmrich (2004) for more detailed information. Direct methods generate bead-like geometric changes to the simulation model as the optimization result. Thus, they offer the possibility to directly influence the bead cross section by the implementation of parameters. Therefore, the direct methods are suitable for the integrated evaluation of the manufacturability of the calculated bead geometries.

The direct methods can be further distinguished into sensitivity-based and condition-based approaches (cf. Subsection 2.5.1).

Sensitivity-Based Bead Optimization

In sensitivity-based bead optimization, the beads are generated using shape basis vectors that cause a local displacement of shell elements normal to the plane of the plate (Harzheim, 2014; Leiva, 2003; Thomas, Zhou, & Schramm, 2002). This results in a large number of design variables, which allow the variation of the shape to minimize the predefined objective function (Thomas et al., 2002). As boundary conditions, the minimum bead height, the minimum bead width, and the flank angle can be specified (Harzheim, 2014; Thomas et al., 2002). A disadvantage of these methods is that the optimization results, i.e. the generated bead cross sections, cannot

be manufactured directly, but have to be interpreted and constructively implemented by the product developer with the help of his experience (Schwarz, 2002; Thomas et al., 2002). In contrast, the advantage is that a wide variety of objective functions, such as displacements or natural frequencies, can be defined. Figure 2.43 shows a sensitivity-based bead optimization result generated with the software OptiStruct[21] from the company Altair and the constructive implementations interpreted from it.
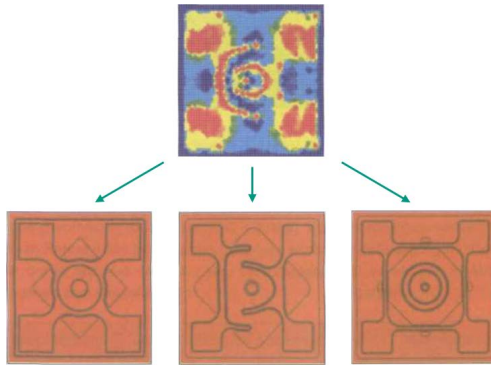
Figure 2.43: Different constructive implementations derived from a numerical, sensitivity-based bead optimization result (contour plot of the alteration of shape due to nodal displacement) (Schwarz, 2002)

Due to the necessary interpretation of the results, a significant part of the calculated stiffness increase is not realized (Schwarz, 2002). Although there is a function in OptiStruct that carries out the automatic interpretation of the optimization result, there is no integrated evaluation of the manufacturability of the bead geometries. In addition to Altair, there are other software vendors that allow sensitivity-based bead optimization. Examples of these are Dassault Systèmes with its Abaqus and TOSCA software and INTES with its PERMAS[22] software.

---

[21] https://www.altair.com/optistruct/ (accessed March 09, 2021)
[22] https://www.intes.de/kategorie_permas/einfuehrung (accessed March 09, 2021)

Condition-Based Bead Optimization

One of the first condition-based approaches for bead optimization was developed by Klein and Freitag (1995). Based on Michell's statement on the optimization of force paths (Michell, 1904), they developed the optimality criterion according to which constructive stiffening elements such as beads and ribs should be oriented along the trajectories of the first principal stress direction. The trajectory starting points are defined by the user. The principal stresses are calculated using the eigenvalues of the stress tensor, and the principal stress directions are obtained from the corresponding eigenvectors. The nodal displacement and thus the generation of the beads or ribs is applied following the calculation of the trajectories by means of a temperature strain displacement, which is based on the basic idea of the CAO[23] approach (Mattheck & Moldenhauer, 1990).

Teschner and Mattheck (1997) extended the CAO method by the *Höckerblechoptimierung* (see Figure 2.44). As an optimality criterion, they formulated that the stresses in shell parts introduced by a given load can be reduced by introducing beads. A displacement factor is determined for each node in the design space as a function of the present stress, and thus a nodal displacement is applied in normal direction based on a redesign rule. This means that each node in the design space is a design variable. The application of the method results in wave-like structures (see Figure 2.44), which do not give any information about the specific bead cross section to be used. The authors limit the method to certain loads and geometries, since it does not distinguish between bending and membrane stresses.
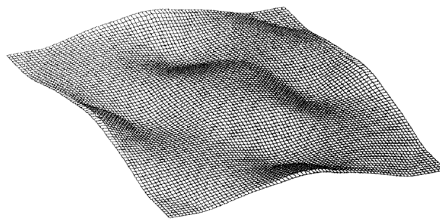
Figure 2.44: Höckerblechoptimierung: Optimized beads for a plate under pressure (Teschner & Mattheck, 1997)

---

[23] CAO = Computer-aided optimization

The research group led by Albers developed another optimality criterion, which states that beads should be formed along the highest principal bending stresses (PBS). An advantage of the approach is the easier interpretability compared to the sensitivity-based results and the focus on the bending stresses on which beads have a stiffening effect. (Albers, Weiler, et al., 2005) The bending stresses can be calculated by a decomposition of the linear elastic stress state according to Figure 2.45.
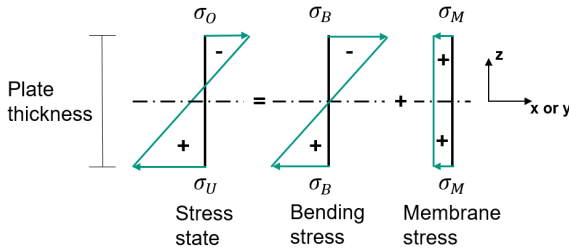
Figure 2.45: Decomposition of the linear elastic total stress into bending and membrane stress adapted from Emmrich (2004) and Majic (2014)

Mathematically, the decomposition of a linear elastic stress state into the bending stress σ_B can be calculated by the difference of the stresses at the top σ_O and the bottom σ_U of the part according to Equation 38 (Emmrich, 2004).

$$\begin{pmatrix} \sigma_{B,x} \\ \sigma_{B,y} \\ \tau_{B,xy} \end{pmatrix} = \frac{1}{2} \cdot \begin{pmatrix} \sigma_{O,x} - \sigma_{U,x} \\ \sigma_{O,y} - \sigma_{U,y} \\ \tau_{O,xy} - \tau_{U,xy} \end{pmatrix} \qquad \textbf{38}$$

The membrane stress σ_M is the mean value of the stresses at the top σ_O and the bottom σ_U of the part and can be calculated using Equation 39 (Emmrich, 2004).

$$\begin{pmatrix} \sigma_{M,x} \\ \sigma_{M,y} \\ \tau_{M,xy} \end{pmatrix} = \frac{1}{2} \cdot \begin{pmatrix} \sigma_{O,x} + \sigma_{U,x} \\ \sigma_{O,y} + \sigma_{U,y} \\ \tau_{O,xy} + \tau_{U,xy} \end{pmatrix} \qquad \textbf{39}$$

The principal bending stresses and principal bending stress directions (PBSD) required for the optimality criterion result from the eigenvalue eigenvector problem belonging to the bending stress state. For the computer-aided, FEM-based implementation of this optimality criterion, Albers and Emmrich developed a circular filter method (Albers, Weiler, et al., 2005; Emmrich, 2004; Emmrich & Albers, 2003), whose principal functionality is shown in Figure 2.46.

Top chord   Bottom chord

~Bead width

Principal bending stress direction
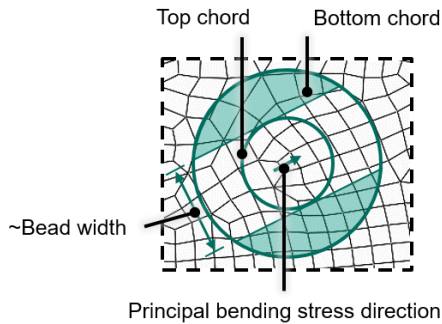
Figure 2.46: Bead generation with the circular filter method adapted from Albers, Weiler, et al. (2005) and Emmrich (2004)

The developed algorithm is also implemented in the commercial software TOSCA resp. Abaqus from Dassault Systèmes. The circular filter method is an empirical approach to generate as continuous as possible beads (Emmrich, 2004). For this purpose, the algorithm uses two circles to distinguish between nodes within the top chord, which roughly corresponds to the bead width, and the bottom chord. Initially, all nodes are moved to the specified bead height and the principal bending stresses occurring in the design space are sorted. The starting point of the method is the node with the highest principal bending stress and the corresponding direction. From there, the smaller circle is used to define a band describing the top chord (see Figure 2.46). The nodes determined in this way are frozen in position. The nodes assigned to the bottom chord, i.e. the remaining part of the large circle (see Figure 2.46), are moved back to their original position and cannot be raised again. For the nodes in the bead flank, an averaging is used. This procedure is repeated for descending principal bending stresses until all nodes in the design area are assigned to either the top chord or the bottom chord or until the algorithm runs into a

defined restriction (ratio between principal bending stress and principal membrane stress) (see Figure 2.47). (Albers, Weiler, et al., 2005; Emmrich, 2004)

This approach allows the product developer to define normalized bead cross sections, but it is not possible to specifically assign head and base radii. Consequently, directly manufacturable beads cannot be generated. The specified bead width is realized at the height of the centroidal axis, so that it differs from the bead width defined at the bead cross section (see Figure 2.41). Another disadvantage of the circular filter method is that it is not possible to generate continuous bead patterns and constant bead widths (see Figure 2.47) because the sorted principal bending stresses are not topographically connected. As a result, manual processing of the results is necessary to obtain a bead design suitable for manufacturing, despite the clearly defined bead patterns. Consequently, the manual processed designs have to be checked in another structural analysis and, if necessary, further optimized and adjusted iteratively. (Majic, 2014)
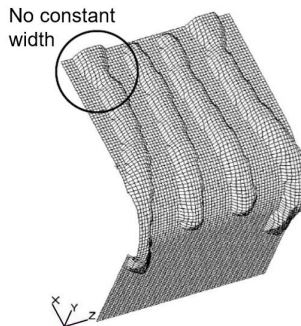
Figure 2.47: Result of a condition-based bead optimization with the circular filter method (Emmrich, 2004)

To raise the identified potentials of the circular filter method, Albers and Majic developed a trajectory-based approach (Majic, 2014). This approach is structured in two stages. First, the bead pattern is calculated by polygonal lines in the form of trajectories along the principal bending stress directions. Here, it is already possible to take into account manufacturing boundary conditions such as minimum radii in the bead curvature. As in the circular filter method, the starting point is the element-wise determined bending stress, which is calculated according to Equation 38. The

solution of the associated eigenvalue eigenvector problem leads to the PBS and PBSD of the element under consideration. (Majic, 2014) Sorted in a list, the algorithm starts with the highest principal bending stress, as in Albers, Weiler, et al. (2005). Afterwards, the trajectory is iteratively continued according to the principal bending stress direction $PBSD_{n-1}$ present in the respective element of the current trajectory point x_{n-1} with the increment s_{n-1} into the new trajectory point x_n based on the calculation rule in Equation 40.

$$x_n = x_{n-1} + PBSD_{n-1} \cdot s_{n-1} \qquad\qquad \textbf{40}$$

The increment s_{n-1} is calculated according to Equation 41. e_n denotes the average element edge length, f_T the trajectory fineness to be chosen by the product developer, which describes the distance of the trajectory points in relation to the element size, PBS_n the principal bending stress in element n of the trajectory point to be calculated, PBS_{n-1} the principal bending stress in the current element $n-1$ and $\Delta\alpha_T$ the trajectory angle between the principal bending stress direction of the current and the next element.

$$s_{n-1} = \frac{e_n \cdot f_T}{\dfrac{|PBS_n - PBS_{n-1}|}{0.5 \cdot |PBS_n + PBS_{n-1}|} + \cos(\Delta\alpha_T) + 0.5} \qquad\qquad \textbf{41}$$

This calculation method allows manufacturing aspects such as a minimum trajectory or bead length, a minimum distance between two beads, a minimum approximation of two trajectories or minimum radii of curvature in the bead course (by angle α_T) to be taken into account already in the computation of the bead pattern.

In the second stage, the bead cross section is generated along the principal bending trajectories with the help of piecewise defined functions. For this purpose, the nodes are moved perpendicular to the part surface (see Figure 2.48). Due to the exact geometric description of the bead cross section using mathematical functions, all bead parameters can be modeled and manufacturing restrictions such as minimum head and base radii, maximum flank angles or minimum bead widths can be included. (Majic, 2014)
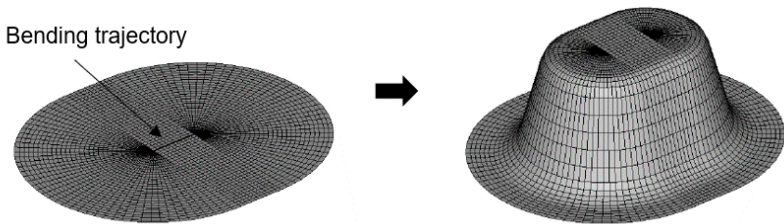
Figure 2.48: Bead generation via bending trajectories and perpendicular nodal displacement adapted from Majic (2014)

The trajectory-based approach has already been successfully applied to calculate bead patterns in a modified Nakajima experiment (Cha, Müller, Bursac, Albers, & Volk, 2017). Therefore, in the context of the present thesis, this approach is also used. For this purpose, it is adapted and extended at some functions for the investigation of long fiber reinforced polymer structures (see Chapter 4).

2.8 Conclusion

The use of FRP offers great potential for lightweight design. But very often only the lightweight design strategy of material lightweight design is applied in the context of FRP by substituting metal components with constructively unmodified FRP parts (May, 2020). In most cases, however, this is not expedient and leaves further lightweight design potential unexploited, since the excellent mass-specific material properties of FRP can only be achieved if the fibers are aligned in load direction. In order to realize this, a fiber-adapted design is necessary.

In the case of long fiber reinforced polymer structures, the part design directly influences the fiber orientations resulting from the primary forming process (such as compression molding) and thus the final material properties. Therefore, it is inevitable to consider design and manufacturing in combination. When beads are included in the support structures of parts as structural stiffening elements to increase bending stiffness, this coupled consideration plays an even more important role. The bending stiffness is calculated by the product of the second moment of area and the Young's modulus. For parts with isotropic material behavior, which have a constant, direction-independent Young's modulus, the bending stiffness can thus be adjusted

solely by changing the geometry. This is different for beads in long fiber reinforced parts, where, in addition to the geometric stiffness, a different bead geometry causing a different fiber orientation also affects the final material stiffness. Consequently, this results in a complex design process for beads in long fiber reinforced polymer parts, for which no sufficient support tools could be found in literature. A possible approach for the integrated consideration of design, manufacturing and material is provided by the presented simulation methods. Their potential lies in the automated coupling of process and structural simulations to support the product developer in the fiber-adapted, initial design process of beaded parts.

However, in the opinion of the author, even a consideration of manufacturing in the design, i.e. a combined consideration of material and form lightweight design, is not yet sufficient to fully exploit the lightweight design potential of FRP. Only the combined consideration of material, form and system lightweight design enables the product developer to design lightweight structures that meet the requirements between the conflicting priorities of mass, costs and CO_2 emissions. By applying the strategy of system lightweight design, it is questioned at which positions or places the use of FRP makes sense at all. Therefore, lightweight design methods that allow a detachment from metal-based designs and support requirement-specific constructions are necessary. This leads to the multi-material construction method, which aims for the right material in the right place. The resulting mix of materials allows to design lightweight design structures under economic and ecological constraints.

3 Research Objectives and Research Approach

In this chapter, the research objectives and research hypotheses of the work are derived from the state of research described in Chapter 2 (see Section 3.1). Based on that, research questions can be formulated, which are operationalized by the research approach (see Section 3.2). Finally, the used research methods are presented in Section 3.3.

3.1 Research Objectives

In the context of this work, the interaction between material, form and system lightweight design (see Subsections 2.2.1 - 2.2.3) is considered as a part of the multifaceted lightweight product engineering process. Constructional, geometric stiffening elements such as beads (see Section 2.7) can further reduce the wall thickness and thus the mass of thin-walled parts without reducing the resulting stiffness. In the case of beaded parts made of long fiber reinforced polymers, the bending stiffness is not only determined by the geometry but also by the anisotropic material behavior. The introduction of the beads changes the geometry, which influences the fiber orientations that develop during the processing and thus the final material properties of the part. This results in a complex interdependence of material, manufacturing and design, which can no longer be handled by the product developer using classic design methods such as design catalogs. In the state of research, numerical approaches have been shown that support the product developer in this challenging problem solving. However, the work is mainly focused on sheet metal parts, where the manufacturable bead geometry depends, among other things, on the residual forming capacity of the steel in the deep drawing process. Consequently, the manufacturable bead cross sections are constrained by the manufacturing process. However, none of these approaches addresses long fiber reinforced polymer (SMC or LFT) structures, although influences of beads on the fiber orientation and thus the resulting stiffness and strength are described. For fiber reinforced polymer structures, there are few manufacturing restrictions and the bead pattern and bead cross section can be largely individualized if the mold is properly designed. To address this identified research gap, a partial objective of this work is to develop a coupled method for the automated bead optimization of long fiber reinforced SMC and LFT parts. This method is intended to support the product developer during the initial

design phase and allow him or her to identify a proper bead design for the required stiffness behavior of long fiber reinforced SMC and LFT parts under load in early phases. For this purpose, an approach is needed that couples models for process simulation with models for structural simulation. The coupling of simulation models from different disciplines enables an improved quality of the model assumptions and thus increases the maturity of the simulation results.

Since commercial optimization tools cannot generate individually adaptable bead geometries, the approach for trajectory-based bead optimization developed at IPEK – Institute of Product Engineering is used (see Subsection 2.7.2). The iterative execution of the coupling between the beading tool for the generation of individual bead cross sections and a process simulation based on these cross sections in an optimization loop should enable the automated design of a stiffness optimized bead pattern as well as bead cross section that is adapted to the manufacturing process and the load case. Thus, the present work not only extends the extensive previous work at IPEK – Institute of Product Engineering, which focused on the design of ribs as structural stiffening elements in SMC structures (Spadinger & Albers, 2019; Troll, 2015), but also continues the long-term investigations in the field of bead optimization (Cha et al., 2017; Emmrich, 2004; Emmrich & Albers, 2003; Majic et al., 2013; Majic, 2014).

Based on the defined partial objective, the first relevant research hypothesis for this work can be formulated.

Research Hypothesis 1

The modeling of locally anisotropic linear elastic material properties resulting from the SMC/LFT manufacturing process and their consideration in the FE-based bead optimization lead to the process-based, stiffness-optimized synthesis of initial design proposals for beaded, thin-walled, long fiber reinforced parts.

To address this research hypothesis, research questions are formulated which help to structure and operationalize the problem. Answering these questions helps to achieve the stated partial objective.

   i.   Which demands exist with regard to methodical support for the product developer in the stiffness-optimized design of thin-walled, long fiber reinforced, beaded parts?

  ii.   Which requirements for the method to be developed result from the identified demands?

iii. Based on the SMC/LFT manufacturing process, how can an optimization method in the context of a product development process be structured to automatically provide a stiffness-optimized, load-adapted bead design for long fiber reinforced polymer structures?

iv. Which knowledge on the synthesis of bead designs is gained by applying the developed optimization method to SMC/LFT parts compared to isotropic, linear elastic material properties?

As criteria to evaluate the success of the developed method and the verification or falsification of the research hypothesis, comparisons between simulation results and experiments as well as between anisotropic and isotropic material modeling are used. To assess the validity of the optimization method, the individual submethods need to be verified and validated. The purpose of each model and the results that can be achieved with it will be discussed in the respective section in Chapter 4. The study of the first research hypothesis contributes to a better understanding of fiber-adapted design by considering the interdependencies between design, material and manufacturing. With regard to the modeling of the product engineering process in the iPeM (see Subsection 2.1.1), the bead optimization method can be used to generate A*lternative solutions* in the activity *Model principle and embodiment*.

Moreover, methods are needed to support the product engineering process in the iPeM activities *Detect ideas* and *Model principle and embodiment* (see Subsection 2.1.1) in early phases for the generation of the product concept, since the selection of a product concept already specifies up to 80% of the later product mass (Leichtbau BW GmbH, 2015). The impact of decisions in early phases is not only large in terms of lightweight design, but also influences, for example, the necessary production systems. At the same time, these decisions have to be made with a low maturity level of the system of objectives. This is precisely why it is necessary to support the product developer in this phase in order to exploit the lightweight design potential as good as possible. One possibility for support are function-based approaches (see Subsection 2.2.6), which address the cross-component potential of system lightweight design. From a cost and emission perspective (see Subsection 2.2.5), as well as for specific applications and batch sizes, the material classes relevant for lightweight design offer different levels of potential. In the case of single-material systems (e.g., FRP), CO_2 emissions can often be reduced during the use phase of the product life cycle, but production or recycling is usually associated with higher costs and CO_2 emissions. As a consequence, their overall balance over the entire product life cycle is not attractive anymore. Therefore, the trend in lightweight design is moving toward multi-material design (see Subsection 2.2.4), which aims for the right material in the right place. The advantages of the individual material

classes must be consciously implemented in the design. In parallel, costs and emission constraints have to be assessed in an integrated manner. Based on these considerations, the second partial objective of this work is to develop a method for the identification and evaluation of function-based lightweight design potentials, taking into account mass, costs and CO_2 emissions relevant for multi-material lightweight design. For this purpose, the method to be developed has to support the product developer as a human being in the center of the product engineering process in the targeted and situation specific development of multi-material designs, since these can only be achieved by an interdisciplinary consideration of design, material and manufacturing. The state of research shows some function-based lightweight design methods, but none of them allows a combined consideration of the conflicting priorities of mass, costs and CO_2 emissions relevant for lightweight design (see Subsection 2.2.6). However, the Target Weighing Approach (Albers et al., 2013) provides an appropriate basis for extension to be employed in multi-material problems. The systematic procedure and the solution-open description of the product on the functional level support the product developer in his or her creativity and synthesis of new principle and embodiment concepts. Based on these observations, the second research hypothesis for the present work can be specified.

Research Hypothesis 2

The Target Weighing Approach (TWA) is a suitable basis for the development of economic and ecological multi-material designs. With the extension of the TWA by appropriate method modules, the conflicting priorities of mass, costs, and CO_2 emissions can be addressed in the function-based analysis, synthesis, and consequences analysis of concept ideas.

This research hypothesis is also addressed by research questions that have to be answered in order to achieve the objective.

    i.   Which potentials does the TWA offer in the support of the product developer when developing lightweight design solutions in system lightweight design?

   ii.   Which demands exist with regard to an extension of the individual process steps of the TWA?

  iii.   How can the TWA be extended to systematically consider the conflicting priorities of mass, costs, and CO_2 emissions in the identification and evaluation of lightweight design potential?

  iv.   How can a method look like that supports the product developer in the Extended Target Weighing Approach (ETWA) within the function-based synthesis of new embodiment concepts based on a systematic analysis of the reference system?

v. For the concept ideas generated during the application of the ETWA, how can the consequences be assessed differentially in terms of technological uncertainties, maturity level and costs already in early phases?

vi. How can the PGE – Product Generation Engineering model and the FAS4M approach as further elements of the KaSPro – Karlsruhe School of Product Engineering be employed in the application of the ETWA in order to reduce the necessary expenditure of time?

The success evaluation of the developed method is carried out on the basis of the assessment of the developed method modules. This is discussed in detail in Section 5.3. The study of the second research hypothesis contributes to the methodical procedure in system lightweight design.

From the combination of the two defined partial objectives, the overall objective of the work can be defined.

> **Objective of the Work**
>
> Development of an optimization method for the design of beads in long fiber reinforced polymer structures including the manufacturing process as an approach to realize methodically identified lightweight potentials.

3.2 Research Approach

In this section, the research approach for answering the research questions and thus for achieving the research objective is presented. The research approach is based on the Design Research Methodology (DRM) of Blessing and Chakrabarti (2009). The DRM is divided into the four stages

- Research Clarification
- Descriptive Study I
- Prescriptive Study
- Descriptive Study II

and provides a framework for design research. Therefore, the DRM includes, among others, the following characteristics of design processes (Blessing & Chakrabarti, 2009):

- iterations within the stages but also between the stages to increase the quality

- analysis as well as synthesis stages
- the starting point of the work can be in each stage and not all stages have to be necessarily passed through.

These characteristics are also centrally included in the methods and tools of the KaSPro – Karlsruhe School of Product Engineering, which has been established over the last 30 years. This corroborates the choice of the DRM for structuring the present work. Figure 3.1 shows the research approach of this thesis based on the DRM.
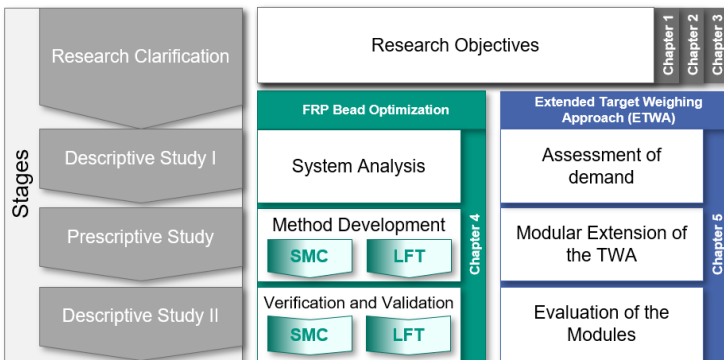
Figure 3.1:   Research approach of the present work based on the DRM

In Chapter 2, a literature review of the current state of research in the context of product engineering with a focus on lightweight design is presented. Based on this, the research objectives are condensed and operationalized into research hypotheses and questions in Chapter 3. In addition, the research approach and research methods are presented. Subsequently, the work elaborates the two partial objectives of bead optimization of long fiber reinforced SMC/LFT structures (see Chapter 4) and the extension of the Target Weighing Approach (see Chapter 5).

For the FRP bead optimization, analytical and numerical methods are used in the Descriptive Study I in order to further specify and substantiate the need for research (see Section 4.1). From the gained knowledge, requirements for the method to be developed are defined and included in the system of objectives. Subsequently, in

the Prescriptive Study, a numerical method is developed which, based on the coupling of submethods, provides support for the product developer in the design of process-based, load-adapted bead designs of SMC (see Subsection 4.2.1) and LFT (see Subsection 4.2.2) parts. Finally, the developed optimization methods are evaluated in the Descriptive Study II (see Section 4.3). For this purpose, the submethods are validated with experiments and the overall method is verified with the help of a comparative optimization based on isotropic material modeling.

For the extension of the Target Weighing Approach, empirical methods will be used in the Descriptive Study I to investigate the benefits of the existing TWA and to identify potential for optimization (see Section 5.1). Based on these findings, the TWA will be further developed into the Extended Target Weighing Approach (ETWA) in the Prescriptive Study (see Section 5.2). This will involve the development of method modules for function-based synthesis (see Subsection 5.2.2) and extended consequences analysis (see Subsection 5.2.3). In addition, synergy effects with further methods of the KaSPro – Karlsruhe School of Product Engineering are investigated (see Subsection 5.2.4). In the Descriptive Study II the developed method modules will be evaluated (see Section 5.3). The evaluation of the developed overall method is difficult, as two parallel development processes cannot be accompanied, one in which the method is applied and one in which it is not. However, due to the modular structure of the Extended Target Weighing Approach, it is possible to evaluate the individual method modules separately.

3.3   Research Methods

The generic framework of the DRM, as previously described, is used to structure and organize research in the field of design research. However, it does not provide researchers with concrete methods for conducting research. Therefore, the research methods used in the context of this work are outlined in this section.

The research environment for the development of the FRP bead optimization is the International Research Training Group (IRTG) "Integrated engineering of continuous-discontinuous long fiber reinforced polymer structures" (GRK 2078) of the German Research Foundation (DFG) which will be presented in more detail in Chapter 4. In the context of FRP bead optimization, in addition to an analytical rough calculation for potential analysis, numerical methods are used exclusively (see Section 4.1). This involves the use of the finite element method to solve the equations describing the compression molding and the structural mechanic behavior. Based on the identified demands, a process-based method for bead optimization is developed in Section 4.2 within the Descriptive Study. In order to validate the simulation

results, experiments are conducted for the individual models of compression molding and structural mechanics and compared to the simulations (see Section 4.3). The overall optimization method is verified based on an isotropic material modeling and evaluated on the basis of the validated submethods.

To achieve the partial objective of developing the ETWA, in the context of Descriptive Study I, a survey in the EU research and innovation project *Affordable Lightweight Automobiles Alliance (ALLIANCE)* and a case study in the Live-Lab *IP – Integrated Product Development* at IPEK – Institute of Product Engineering are employed. The EU project ALLIANCE is explained in more detail in Chapter 5. The Live-Lab IP as a part of the KaSPro – Karlsruhe School of Product Engineering is a course that, in addition to lectures and workshops, includes project work as a third pillar, in which problems from industrial partners are addressed (Albers, Bursac, Heimicke, Walter, & Reiß, 2018). A Live-Lab is a research environment for the investigation and evaluation of design methods, processes or tools, which is characterized by realistic but at the same time controllable boundary conditions. Live-Labs combine the advantages of field studies (high external validity) with those of laboratory studies (high internal validity). In IP, about 40 students chosen through a selection process with an interview go through a complete product engineering process from analysis to product profile definition to prototype development. (Albers, Bursac, et al., 2018) The findings obtained on the basis of Descriptive Study I, which lead to the more concrete derivation of the need for research, are addressed by the methods developed in the Prescriptive Study. In this way, a modular extension of the target weighing approach is carried out in Section 5.2. The evaluation of the developed methods is presented in Section 5.3. For this purpose, different research environments and methods are used. Some method modules are evaluated in industrial case studies or surveys to obtain dedicated feedback. Furthermore, Live-Labs are used. On the one hand, IP is used again and on the other hand, the Live-Lab *AIL – Agile Innovation Lab* is utilized. AIL is a course based on IP for six students who want to enhance their methodical competencies (Albers, Bursac, et al., 2018). Also in AIL, a real development problem is provided by an industrial partner, the solution of which, in contrast to IP, is elaborated by the students in an even more mature way. Thereby, students learn the targeted use of methods and processes. (Albers, Bursac, et al., 2018)

Based on previous works at IPEK – Institute of Product Engineering by Marxen (2014) and Albers, Walter, Wilmsen, and Bursac (2018), the empirical research methods of the survey, Live-Labs, and case study are summarized in Figure 3.2.

Survey

Field of application
- Empirical research: analysis of real-world design processes
- Experimental studies: evaluation in controlled environments
- Implementation studies: real-world deployment of design support

Advantages	Disadvantages
- Direct data acquisition - Easy access to large sample groups	- Researcher cannot intervene - Precise questions have to be formulated: misunderstandings can ruin the complete study

(a)

Live-Labs

Field of application
- Validation environments under realistic conditions and with a high controllability of the boundary conditions
- Evaluation of the suitability of new design methods concerning their intended use in companies to a certain degree

Advantages	Disadvantages
- Employment of control groups - Works even with very complex situations	- Deviating boundary conditions in Live-Labs and in companies - Take place only on an annual basis

(b)

Case Study

Field of application
- Investigation of complex situations
- Implementation studies: real-world deployment of design support
- Showing usability / value of a support tool

Advantages	Disadvantages
- Holistic approach - Works even with very complex situations	- Ongoing discussion whether or not it is a valid research method - Effort

(c)

Figure 3.2: Method profiles of the applied research methods: (a) survey adapted from Marxen (2014) (b) Live-Labs adapted from Albers, Walter, et al. (2018) (c) case study adapted from Marxen (2014)

4 Process-Based Bead Optimization of Long Fiber Reinforced Polymer Structures

In this chapter, the influence of the manufacturing process on the design of stiffness-optimized FRP bead geometries is investigated. To this end, the first step in Section 4.1 is to clarify the relevance of the topic in the product engineering process and to build up a comprehensive awareness of the system. Based on this, the system of objectives is derived, the elements of which must be taken into account in the method to be developed in order to improve the design process.

In the next step, in Section 4.2, the numerical optimization method (operation system of the simulation) is developed to support the product developer in the initial design of bead patterns and cross sections in long fiber reinforced SMC/LFT parts. For this purpose, an optimization workflow is developed based on the system of objectives derived from the system analysis in Section 4.1, which is supposed to reasonably balance effort (related to computation and data processing) and simulation depth. This is particularly important for the generation of initial designs in early phases of product development.

Finally, in Section 4.3, the validation and verification of the developed methods is presented. For this purpose, individual submethods are validated by experiments, while the overall method is verified with an optimization based on isotropic material modeling.

All data used in this chapter have been generated within the International Research Training Group (IRTG) "Integrated engineering of continuous-discontinuous long fiber reinforced polymer structures" (GRK 2078)[24] funded by the German Research Foundation (DFG) for a duration of nine years. The IRTG comprises a total of three generations of doctoral students within 14 subprojects. They are divided into four research areas: Characterization, Simulation, Technology and Design. The author of this thesis was part of the research area Design in the second generation. Generation-specific information is indicated by the indexing DFG GRK 2078/1 for the first generation and DFG GRK 2078/2 for the second generation.

---

[24] https://www.grk2078.kit.edu (accessed February 02, 2021)

4.1 System Analysis

The system analysis is divided into analytical and simulative considerations. From both areas, demands are identified with regard to methodical support for the product developer in the stiffness-optimized design of thin-walled, long fiber reinforced, beaded SMC/LFT parts. Based on this, requirements are derived for the method to be developed. In addition, further requirements resulting from the PGE – Product Generation Engineering are defined. Through the contents discussed in this section, the first two research questions of the first research hypothesis (see also Section 3.1) are answered.

Research Questions

---

    i.   Which demands exist with regard to methodical support for the product developer in the stiffness-optimized design of thin-walled, long fiber reinforced, beaded parts?

    ii. Which requirements for the method to be developed result from the identified demands?

4.1.1 Analytical Considerations

Structural stiffening elements can be distinguished (among others) between beads and ribs. For parts made of fiber reinforced polymers, UD-tapes can also be used as stiffening elements, so that the following considerations relate to these three stiffening options. The stiffness against bending deformation of beaded and ribbed parts is determined by two factors:

- material stiffness/Young's modulus
- second moment of area.

In the case of UD-tapes, the increase in part stiffness is mainly achieved by increasing the material stiffness through the introduction of fibers (with higher stiffness compared to the base part) in the load direction. For instance, glass fiber reinforced polymers are often reinforced by carbon fiber UD-tapes. The use of tapes is particularly suitable for parts where only limited design space is available and beads and ribs are therefore excluded due to their space requirements. For more extensive investigations and comparisons between the three stiffening variants, also including process simulations in the consideration, it is referred to the thesis of Reich-

mann (2019)[25], which was co-supervised by the author. In the following deliberations, only beads and ribs will be discussed and the effect of geometric stiffness will be considered.

For this purpose, the second moments of area of a bead cross section and a rib cross section are compared. Figure 4.1 shows simplified cross sections with the same height. The main stiffening effect of both cross sections is obtained by moving the centroidal axis away from the neutral axis. This effect is attributed to the parallel axis theorem (see Subsection 2.7.1 for beads). From Figure 4.1 it is directly evident that the area contributing to the parallel axis theorem is smaller for the rib. In contrast to the bead, no material is displaced from the base plate, but additional material is required to form the rib. Particularly with small rib heights or only few ribs on the geometry, this leads to a lower stiffness compared to the same number of beads.
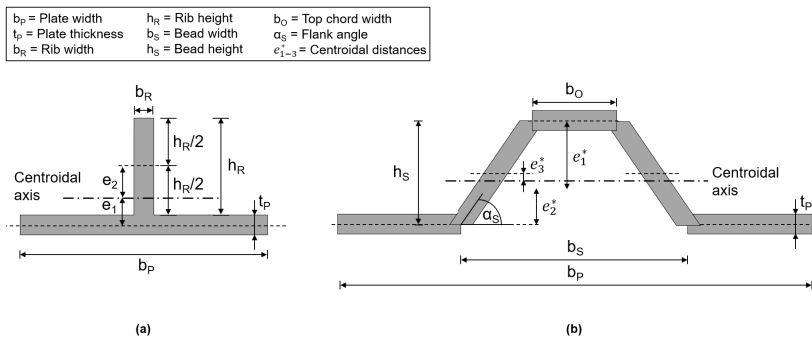
Figure 4.1: Comparison of the second moment of area: (a) simplified rib cross section (b) simplified bead cross section adapted from Revfi, Mikus, Behdinan, and Albers (2020)

Concomitantly, the fact that, in the case of the bead, the material is moved from the base plate also means that just slightly more material is required for the forming of beads compared to a flat geometry. Accordingly, there are further advantages if the achievable second moment of area is related to the required cross section, which can be seen as a comparative quantity for the required mass.

---

[25] Co-supervised thesis (unpublished)

From a manufacturing perspective, there is a decisive difference between beads and ribs. While in compression molding of beads the material is forced to flow through the beads because there is no alternative way, problems of rib filling (Butenko & Albers, 2019) can occur in the manufacturing of ribs. This results in the problem that parts of the rib are not filled with material at all or that only a few fibers can be found in the ribs. In both cases, the result is that the ribs no longer achieve their full effect. Furthermore, ribs may have sink marks on their opposite side, which pose cosmetic problems on visible surfaces (European Alliance for SMC/BMC, 2016).

The previous discussions show why it is relevant to consider beads as structural stiffening elements also in long fiber reinforced parts. Their basic principle of increasing the second moment of area remains the same in FRP structures. Up to this point, however, the influence of the anisotropic material stiffness on the bending stiffness of the part has not been included in the argumentation. This influence is definitely smaller than the geometric stiffness, which can be influenced to a large extent by the bead height. Compared to the bead height, the influence of the flank angle on the geometric stiffness is much smaller. Figure 4.2 shows the second moment of area relative to the bead cross sectional area over the flank angle for an analytical calculation using the simplified bead cross section from Figure 4.1 (b). From this graph, it can be observed that an isolated consideration of the increase in the flank angle on the cross-sectional second moment of area in the flank angle range between 70° and 86°, which is relevant for industrial applications, shows that the achievable stiffening effect decreases with increasing flank angle. This can be seen from the decreasing slope of the curve. As a result, it is possible that the material stiffness, which in the case of FRP depends on the processing, compensates for some of the geometric stiffness. Different bead cross sections cause different flow behaviors in the processing of the material, i.e. depending on the resulting fiber orientation, it could then even be possible that the lower geometric stiffness of smaller flank angles is overcompensated and thus bead cross sections with lower flank angles have a higher stiffness (Revfi, Mikus, et al., 2020). In order to be able to investigate this, the first requirement for a method to be developed arises: The bead cross section with the bead parameters bead height, bead width, head radius, root radius and flank angle (see Figure 2.41) has to be individually definable in the study environment.
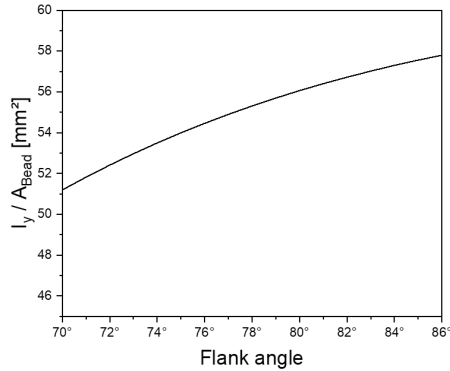
Figure 4.2: Second moment of area relative to the bead cross sectional area over flank angle (b_P=50 mm, b_S=25 mm, h_S=18 mm, t = 2 mm) adapted from Revfi, Mikus, et al. (2020)

These general analytical considerations justify a more detailed investigation of the stiffening effect of beads in FRP parts and substantiate the need for research. Superimposed on these considerations is the additional challenge of the great design freedom available to the product developer when designing beads in FRP structures. However, as shown in Subsection 2.7.1, this design process, which is part of the iPeM core activity of *Model principle and embodiment*, is not sufficiently supported methodically for FRP. Therefore, design freedom cannot only be seen as an advantage. As discussed in Subsection 2.3.2, primary molding processes such as compression molding are used to manufacture parts made of long fiber reinforced polymers (SMC/LFT). These processes require cost-intensive molds that have to be developed in early phases of product development. If design problems are identified during experiments or prototyping, or if it is determined that the design does not meet the requirements from the system of objectives, optimizations to the geometry can only be achieved through experimental trial-and-error and expensive mold modifications (Li et al., 2017; Rios, Davis, & Gramann, 2001).

4.1.2   Simulative Considerations

In order to reduce the number of mold modifications and prototypes, simulations are used to support the design process. A common practice in the design of FRP parts is to avoid modeling the anisotropic material behavior due to the fibers and instead use isotropic material properties (Davis, Gramann, & Rios, 2002). However, this leads to significant differences in the assessment of the structural behavior of the part, making it inevitable to combine process simulations with structural simulations (Davis et al., 2002). An influence of the simplified isotropic assumption on the optimized bead pattern and the resulting stiffness could also be shown in a simulation study conducted by the author, which will be discussed in more detail in Subsection 4.3.1.2. Concretizing this observation, the question arises which characteristics of the mold filling have to be modeled in the sense of the reduction feature according to Stachowiak (1973) and which type of modeling is suitable. In their development of a virtual process chain for SMC, Görthofer et al. (2019) identify the dependence of the mechanical part behavior on the resulting fiber orientation distribution. This fiber orientation distribution in turn depends on further material and process parameters. Figure 4.3 shows the material and process properties identified by the author as relevant for the fiber orientation distribution in the present work, which have to be considered and modeled in the method development in Section 4.2.
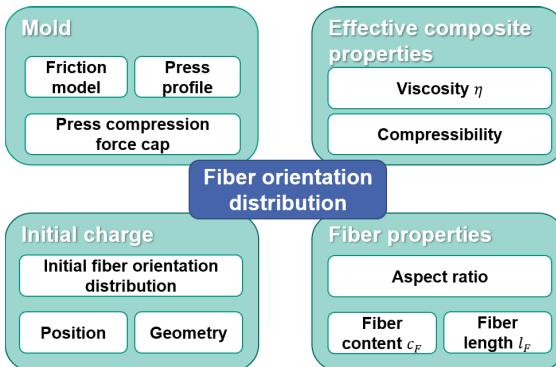
Figure 4.3:   Material and process properties identified as relevant to the fiber orientation distribution

The material properties resulting from the fiber orientation are dependent on the part design, since the flow directly depends on the designed geometry (see Subsection 2.3.3). Therefore, the local material properties are calculated from the predicted fiber orientations using orientation averaging (see Subsection 2.4.2). Figure 4.4 shows an overview of the necessary material data for the determination of the local material properties. From this it is already obvious that a complete material and flow behavior characterization is of crucial importance for the determination of the real part behavior.

Matrix properties

| Young's modulus E_M | Poisson's ratio v_M |
| CTE α_M | Density ρ_M |

Effective composite properties

| Young's modulus E_{11} | Young's modulus E_{22} | Poisson's ratio v_{12} | Poisson's ratio v_{23} |
| Density ρ_c | Shear modulus G_{12} | CTE α_{11} | CTE α_{22} |

Mechanical properties

Models

| Thermal expansion coefficient model |
| Homogenization method |

Fiber properties

| Young's modulus E_F | Poisson's ratio v_F | CTE α_F | Density ρ_F |
| Shear modulus G_F |

Figure 4.4: Necessary material data for the determination of the local material properties[26]

Especially in the context of bead design in compression molded parts, where a variation of bead parameters results in new geometries and thus flow behaviors, the coupling of mold filling and structural simulation for each geometry under investigation is a necessary requirement for the method to be developed. Troll (2015) distinguishes three modeling options for predicting fiber orientations: mathematical models, mold filling simulations, and measured data. At the same time, she points out that the effort increases in just this order. In her work, she chooses a simplified representation of mold filling by mathematical models. She justifies her choice by the insufficient maturity of models for predicting fiber orientations at that time and the resources required by the iterative integration of simulation. In the course of the

---

[26] CTE = Coefficient of thermal expansion; Index F indicates fiber properties; Index M indicates matrix properties

further development of the simulation software and the easier accessibility to larger computing capacities, a disregard of mold filling simulations seems no longer justifiable at the time of the present work. Therefore, an additional element of the system of objectives of this work is the sufficiently accurate modeling of the fiber orientations using mold filling simulations in order to be able to predict the mechanical part behavior.

Commercial simulation software already established in practice offer the possibility of simulating compression molding as well as bead optimization. Therefore, to estimate the need for research in FRP bead optimization, these commercially available methods will be used first. To this end, a mold filling simulation in Autodesk Moldflow 2019 is coupled with a bead optimization in Abaqus 2019 to assess the added value of the results in supporting the product developer in the initial design generation. The transfer of the resulting material properties from the mold filling simulation is done using a mapping (see Section 2.6). Abaqus offers both direct methods for bead optimization (sensitivity-based and condition-based) described in Subsection 2.7.2. The only condition is that the part has to be modeled as a shell model.

Both direct methods were used to generate stiffness-optimized bead designs based on a previous mold filling simulation in Moldflow. A maximum bead height of 18 mm and a maximum bead width of 25 mm were specified as boundary conditions. Further geometric restrictions such as a minimum radius or maximum flank angle could not be defined. The results generated by the direct coupling of the commercial software for a one-sided clamped plate under bending load are shown in Figure 4.5. It is directly evident that the two optimization results have highly varying bead cross sections and sharp edges. Consequently, both optimization approaches do not lead to directly manufacturable bead geometries (Revfi, Mikus, Behdinan, & Albers, 2021). This makes an additional interpretation of the results by the product developer unavoidable for the part design, which is very challenging since the specific values for the bead parameters (apart from the bead height) do not emerge from the optimization result. As a result, it requires experience in the translation of the optimization results and there is an increased risk that the interpreted design does not meet the requirements of the part. Therefore, mold modifications may become necessary despite simulation support. This observation emphasizes the need for a bead optimization method for long fiber reinforced FRP that provides load-adapted, manufacturable bead designs as a result. This is also defined as a further requirement for the method to be developed.
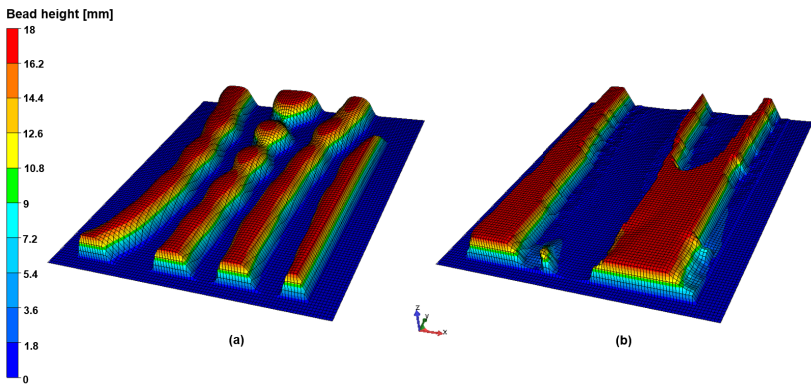
Figure 4.5: Bead optimization in Abaqus based on a mold filling simulation in Mold-flow: (a) controller-based and (b) sensitivity-based bead optimization result for a one-sided clamped plate under bending load adapted from Revfi, Mikus, et al. (2021)

4.1.3 Further Requirements Based on the Model of PGE – Product Generation Engineering

According to the model of PGE – Product Generation Engineering, products are developed in generations (see Subsection 2.1.2). From this, it can be derived that the method to be developed should not represent a niche solution for specific geometries or boundary conditions. Its transferability to new product generations has to be guaranteed as well as the possibility to transfer it to other development teams. From these considerations, the author deduces the use of commercial software as a further relevant requirement for the method to be developed, since this is updated and supported by the vendor and is likely to be available for years. In addition, commercial software is characterized by high robustness and good availability. From the point of view of knowledge transfer, it should be mentioned that the companies distributing commercial software offer training courses, which enable new employees to get used to the software quickly. This is usually not the case with non-commercial software, which means that the user is reliant on good documentation.

Supporting these requirements, the intended purpose of the simulative support is to be specified. The method is supposed to support the product developer in the industrial environment during the initial design process in early phases of the product engineering process. This purpose also argues in favor of the use of commercial software. Detailed dimensioning, which requires specialized software for context-specific questions, is to be carried out in subsequent development phases and is not part of the claim of the method to be developed in the context of this work. However, the example in Figure 4.5 shows that the mere coupling of commercially available software is not sufficient. Therefore, the parts assessed as insufficiently covered by the commercial software (e.g., the insufficient representation of the bead cross section in Figure 4.5) should, if possible, be varied by means of attribute variations.

Furthermore, the PGE – Product Generation Engineering as a description model for the development of simulation methods in generations sets the frame of this work and defines the development environment. For the development of new simulation generations, elements from the reference system are used. By CV, AV or PV of these reference system elements, new generations of simulations are developed (Albers, Schulz, et al., 2021). The type or origin of the reference system elements influences the risk (see Subsection 2.1.2) of the method to be developed. This risk may be higher for research projects compared to industrial projects, but should not endanger a successful development. (Albers, Schulz, et al., 2021) Since the realization of the previously elaborated requirements from a simulation point of view involves a high new development share (combination of AV and PV), it was decided that, when selecting the reference system elements, institute-internal preliminary work is preferred, if reasonably possible, in order to keep the development risk within an acceptable extent. Nevertheless, the possibility of transferring the developed method to a corporate environment has to be ensured at any time.

In conclusion, the needs for the development of an optimization method to support the product developer in the design of beads in SMC/LFT parts have been identified and the consequent requirements have been defined in the system of objectives of this thesis. Consequently, the first and second research question of the first research hypothesis formulated at the beginning of this section (see also Section 3.1) are considered to be answered. In the following, the development of the optimization method is described, which is a part of the operation system.

4.2 Method Development

The method development represents the Prescriptive Study of the process-based SMC/LFT bead optimization. According to the DRM, the development of the method is carried out incrementally and iteratively. The models and methods presented in the following are the result of an iterative procedure between method development as well as verification and validation (see Section 4.3). In order to keep it concise, the presentation of any development generations of the models is not included here.

First of all, the necessary models for the description of compression molding are discussed. Thereby, the focus is on SMC materials (see Subsection 4.2.1). The LFT materials are considered separately and are only to be regarded as a methodical extension by process-induced residual stresses (see Subsection 4.2.2). This is followed by a description of the structural mechanical models including the trajectory calculation. These trajectories are based on the results of the previous mold filling simulations. Finally, an iterative optimization scheme is added to the serially running method so that the design of SMC/LFT parts can be automated. The contents presented in this chapter answer the third research question of the first research hypothesis (see also Section 3.1).

Research Question

---

iii. Based on the SMC/LFT manufacturing process, how can an optimization method in the context of a product development process be structured to automatically provide a stiffness-optimized, load-adapted bead design for long fiber reinforced polymer structures?

The investigations of the stiffening effect and the optimal positioning of the UD-tapes are not in the primary focus of this work, as they have already been addressed within the DFG GRK2078/1 (Fengler, 2019; Fengler, Hrymak, & Kärger, 2019). In the context of the present work, UD-tapes are investigated with respect to the realization of further lightweight potential in beaded SMC parts. For this purpose, the beads will be used as a positioning support for the tapes during processing.

4.2.1 SMC

First, the SMC material system is considered and the automated method for the bead optimization of SMC parts is developed. For this purpose, the models for the compression molding process (see Subsection 4.2.1.1), the structural mechanics (see Subsection 4.2.1.2), and the optimization (see Subsection 4.2.1.3) are discussed separately.

4.2.1.1 Manufacturing and Processing

The overall purpose of modeling the SMC processing is to predict the material properties that are relevant for the structural mechanical behavior. As explained in Subsection 4.1.2, this requires correct modeling of the influencing parameters relevant for the fiber orientation distribution as well as the mechanical properties of fiber, matrix and fiber-matrix composite. Some of the content of this subsection has been published previously in the publication Revfi, Albers, et al. (2021).

The analyzed SMC manufacturing and processing for which the modeling is presented in the following is based on the SMC used in the DFG GRK 2078/2[27], which consists of a thermoset, unsaturated polyester-polyurethane hybrid (UPPH) matrix in a two component resin system and glass fibers. Subsequently, the individual manufacturing steps, which were generally introduced in Subsection 2.3.2, are presented in detail and the model assumptions valid for this thesis are derived from them.

The first step is the manufacturing of the SMC semi-finished product. For this purpose, the UPPH matrix is mixed and filled into the production line. The fibers are chopped to a length of 25 mm (see Figure 4.6 (b)) and randomly fall onto the bottom resin film (see Figure 4.6 (a)).

From this SMC manufacturing, the first relevant aspects for modeling arise: Material properties for the fiber and the matrix have to be determined, which serve as an input for the manufacturing and processing to be investigated.

---

[27] The same material system was also used in DFG GRK 2078/1.
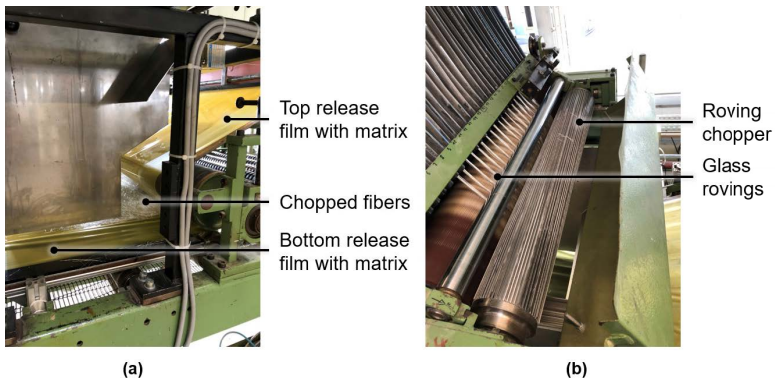
Figure 4.6: (a) SMC semi-finished product manufacturing (overview) (b) chopping of the fiber rovings

In the context of this work, Moldflow is used as simulation software, which computes the material properties for the matrix from the fiber as well as fiber-matrix material properties to be specified by the product developer. The major advantage of this procedure is that the product developer can characterize fiber-matrix samples and does not have to rely on the characterization of the pure matrix, which is usually not available since the finished semi-finished product is purchased. The matrix material properties are then calculated in combination using the characterized composite properties (Young's modulus (E_{11}, E_{22}), shear modulus G_{12}, Poisson's ratio (v_{12}, v_{23}), density ρ_C, CTE (α_1, α_2)) and the characterized fiber properties (Young's modulus E_F, shear modulus G_F, Poisson's ratio v_F, CTE α_F, density ρ_F). Since the SMC considered in this work includes glass fibers as reinforcing fibers, which show isotropic material behavior, the directionality of the fiber material properties can be neglected. However, this can be adapted to other fiber materials in Moldflow at any time and thus does not represent a limitation of the developed method or the subsequent optimization. Furthermore, due to the fact that the SMC consists of glass fiber bundles, rather than the individual fiber diameter, the fiber bundle width d_F is used to calculate the aspect ratio. This means that the homogenization models can be used to calculate the resulting composite properties, which assume ellipsoidal inclusions (see Subsection 2.4.2). Table 4 lists the material properties for the glass fibers, Table 5 shows the material properties used in this thesis for the SMC composite that relate to a perfectly aligned, unidirectional fiber orientation.

Table 4: Material properties: glass fiber

Parameter	Symbol	Value	Unit
Length	l_F	25	mm
Fiber weight fraction	c_F	0.4	-
Fiber bundle width	d_F	1	mm
Density	ρ_F	2.58	g/cm^3
Young's modulus	E_F	73 000	MPa
Poisson's ratio	ν_F	0.22	-
Shear modulus	G_F	29 918	MPa
CTE	α_F	0.000005	1/C

Table 5: Effective material properties: SMC composite (unidirectional fiber orientation)[28]

Parameter	Symbol	Value	Unit
Density	ρ_C	1.4766	g/cm^3
Young's modulus (1st principal direction)	E_{11}	17 109.6	MPa
Young's modulus (2nd principal direction)	E_{22}	5 539	MPa
Poisson's ratio	ν_{12}	0.34	-
Poisson's ratio	ν_{23}	0.52	-
Shear modulus	G_{12}	1 924	MPa
CTE (in longitudinal direction)	α_1	0.00001443	1/C
CTE (in transverse direction)	α_2	0.00007508	1/C

Following the manufacturing of the SMC semi-finished product, it is rolled onto a coil and exposed to a maturing process, which is not further considered in the modeling. In order to prepare the initial charge, the coil is unrolled (see Figure 4.7 (a)), the initial charge geometry is cut to size and single SMC layers are stacked on top of each other (see Figure 4.7 (b)).

Semi-finished SMC

Stacked initial charge

(a)   (b)
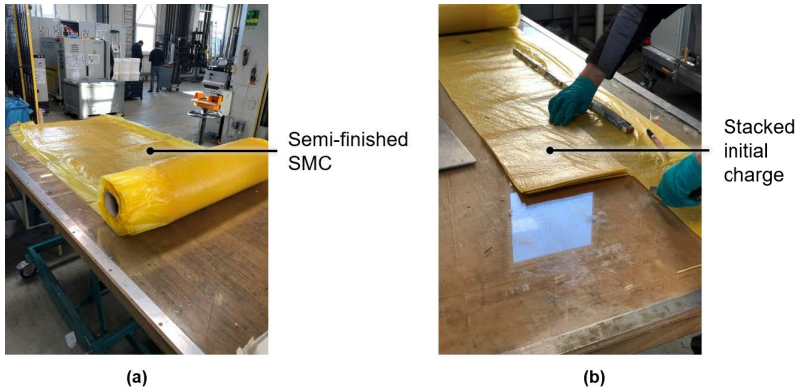
Figure 4.7:   (a) Semi-finished SMC coil (b) stacking of the initial charge

From the analysis of the SMC manufacturing process and the stacking of the initial charge, it can be seen that both the geometric shape of the initial charge can be freely varied within the part dimensions and the volume of the initial charge can be adjusted via the number of SMC layers. The volume needs to be chosen in such a way that the mold can be completely filled during compression molding. Due to the compressibility of the SMC, which will be discussed in more detail in the following, it is necessary to ensure that the initial charge has a larger volume than the part to be processed. For modeling, this means that the geometry and dimension of the initial charge used in the real manufacturing process must be virtually recreated.

Furthermore, for the modeling of the SMC semi-finished product, it can be deduced from the manufacturing that a homogeneous distribution of the fibers through the thickness with a planar isotropic orientation can be assumed (Revfi, Albers, et al., 2021). Since the fibers are randomly distributed in each single SMC layer (see Figure 4.6 (a)), stacking these does not change anything. Even if stacking is done manually in the research project, this assumption is also valid for automated stacking

processes. In Moldflow, this observation can be modeled via the fiber orientation components in flow and cross-flow direction (see Table 6). The orientation is assumed to be in-plane only since the fibers cannot protrude from the semi-finished product.

Table 6:   In-plane fiber orientation over normalized thickness

Normalized thickness	Component in flow direction	Component in cross-flow direction
0	0.5	0.5
0.5	0.5	0.5
1	0.5	0.5

Subsequently, the stacked initial charge is placed in the preheated mold (see Figure 4.8 (b)), which is mounted on a press (see Figure 4.8 (a)). The position of the initial charge in the hot mold influences the flow behavior during mold filling. Since the initial charge position is usually defined by experience of the experts in manufacturing, it represents a necessary boundary condition for the product developer. It is therefore of great importance to define the position of the initial charge in the mold in the simulation model according to the real situation (Revfi, Albers, et al., 2021).

(a)   (b)
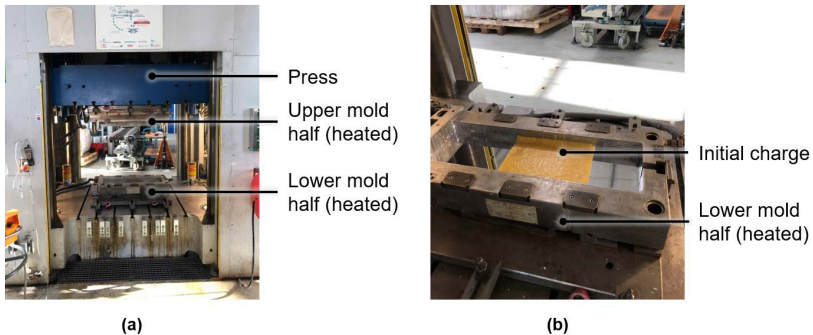
Figure 4.8:   (a) Heated mold halves mounted on the press (b) initial charge placed in the lower mold half

After that, the compression molding process begins. The press closes displacement-controlled until a defined maximum force is reached. Once this force is exceeded, the press switches to force control. From this behavior, a closing profile or press profile results, which has to be reproduced in the model because it influences the flow behavior in the mold. Moreover, this closing profile determines the duration of the compression molding process. The closing profiles are typically specified in the press via distance-speed diagrams. These specify how many millimeters the press is moved at which speed. The force for switching from displacement control to force control is set by the press operator and can be selected individually. This value is based on experience and is varied during the first press cycles in order to study the influence on the flow pattern. In Moldflow, the press compression time, the press compression force cap and a distance-speed profile, for which the real press profile has to be converted, are also specified. In addition, the compression direction and the initial press open distance have to be defined in Moldflow.

Up to this point, only boundary and initial conditions have been defined for the compression molding simulation model. During the actual processing, physical processes take place which have to be described by the model in order to be able to predict the resulting fiber orientations. To compute compression molding, the balance equations introduced in Subsection 2.4.1 are solved under the previously described boundary and initial conditions. For this purpose, the flow problem is modeled in Moldflow as a single-phase flow. To simulate compression molding in Moldflow, 3D models have to be built up. With this modeling, varying flow behavior over the thickness can be realized. Additionally, further model assumptions are necessary, which will be discussed in the following.

As shown in the state of research, the flow of the SMC in the mold can be described by lubrication layers at the mold surfaces and a plug-flow of the core region (see Subsection 2.4.1). Thereby, a constant temperature in the core region can be assumed. Only in the resin-rich lubrication layers, a deviating higher temperature is present (Barone & Caulk, 1979). This higher temperature arises due to the low thermal conductivity of the SMC and the direct contact of the initial charge, which is at room temperature, with the hot mold surfaces. However, the thickness of the lubrication layers, which is only a few micrometers, will not be modeled (Revfi, Albers, et al., 2021) in this thesis. Instead, the friction effects induced by the lubrication layers, which result in wall slip, are completely accounted for in the friction model (Revfi, Albers, et al., 2021). Therefore, when modeling SMC in this work, a *constant temperature distribution* is assumed and all temperature effects are subsumed in the friction model of the lubrication layers (Revfi, Albers, et al., 2021).

For modeling the previously described plug-flow (see Figure 2.24) the presence of a *wall slip* on the mold surface is necessary. This wall slip occurs due to the resin-rich lubrication layers in which a high velocity gradient occurs. As a consequence, this leads to a constant velocity over the thickness of the core region. The friction model which can be used to describe the wall slip on the mold surface is presented in Equation 8. The required values for the parameters are chosen according to Table 7. By specifying the value for the critical shear stress τ_C, the simplification made by neglecting the geometric resolution of the thin lubrication layers can be compensated. The value chosen here is the result of an iterative adjustment of the compression force behavior in the simulation to the experimentally determined compression force behavior obtained from several measurements in the press. This iterative adjustment will be discussed in more detail in Subsection 4.3.1.1.

Table 7:   Wall slip parameters (Revfi, Albers, et al., 2021)

Parameter	Symbol	Value	Unit
Critical shear stress	τ_C	0.2	MPa
Slip exponent	m	1.67	-
Slip coefficient	α	1E-08	m/Pa s

As presented in Subsection 2.4.1, the relationship between the viscous stress and the strain rate is described through the *viscosity*. This requires a viscosity model. In the context of this work, the SMC is modeled as a Newtonian fluid. This assumption is made because the non-Newtonian behavior described in literature cannot be reliably characterized for the UPPH, on which this thesis is based, at the macro scale (Hohberg, 2019). Therefore, the assumption of a Newtonian fluid is preferred, as this reduces the number of parameters to be characterized and shows high agreement with experimental results for the considered deformation rates. To model the viscosity as a Newtonian fluid, the Cross Castro Macosko Model from Equation 12 is simplified. With $n = 1$, $\tau^* = 1\ Pa$, $C_1 = 0$ and $C_2 = 0$, this results in Equation 42.

$$\eta(\alpha^*, T, \dot{\gamma}) = \frac{\eta_0(T)}{2} \qquad \textbf{42}$$

Since as previously described, a dependence on the temperature is neglected, a constant viscosity can be set. For the present studies, the viscosity is chosen to $\eta = 100\ 000\ Pa \cdot s$, which is in the order of magnitude known from literature for the viscosity of SMC (Revfi, Albers, et al., 2021).

As another part of the modeling, the *compressibility* of the SMC needs to be considered since it has an impact on the flow behavior. The compressible material behavior is a result of the manufacturing process, which, among other things, causes pores in the SMC (Guiraud et al., 2012). For the UPPH SMC considered in this work, compressibility has already been experimentally demonstrated by Hohberg (2019). To model the compressibility, the two-domain Tait pvT model presented in Equation 14 is applied, whose parameters are specified in such a way that an experimentally characterized pv behavior (Meyer, 2021) can be reproduced as precisely as possible. Due to the assumption of a constant temperature, no temperature influence is considered for the compressibility. Figure 4.9 shows the correlation between the pressure and the specific volume measured in the experiment, from which the compressibility can be clearly seen.
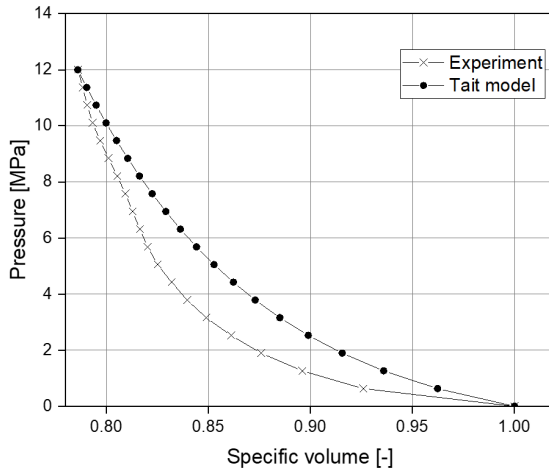
Figure 4.9: pV diagram: correlation between pressure and specific volume. Curve fitting of the parameters of the Tait model. (Revfi, Albers, et al., 2021)

In curve fitting it was ensured that the start and end points of the curves are identical and that the curves converge sufficiently in the pressure regions occurring in the press (> 6 MPa). Equation 14 shows direct dependencies on the temperature. To basically exclude them, the specific volume $v_t(T, p)$ at the volumetric transition temperature T_t is set to zero and the other parameters are chosen according to Table 8.

The volumetric transition temperature T_t is set so low that there is no transition from melt to solid in the uncured state and thus the melt state is present during the entire simulation.

Table 8:   Chosen values for the compressibility modeling with the two-domain Tait pvT model

Symbol	Value	Unit
$v_t(T, p)$	0	-
b_{1m}	0.0005118	m³/kg
b_{2m}	1.001E-09	m³/kg K
b_{3m}	1.205E+06	Pa
b_{4m}	1.001E-07	1/K
b_{5*}	0.01	K

As already indicated, a further aspect of modeling derived from the compressible material behavior is that the initial charge needs to have a larger volume than the final part volume. The additional volume to be defined directly depends on the specified compression force cap and can be estimated with the help of Figure 4.9.

The applied *fiber orientation model* is the ARD-RSC model, since it represents the state of research for the computation of long fiber reinforced polymers (see Subsection 2.4.1). The required parameters in the model are assigned as calculated by Moldflow according to Table 9.

Table 9:   Chosen values in the ARD-RSC model for SMC

Parameter	Symbol	Value	Unit
Reduced Strain Closure factor	κ	0.1	-
Parameters for long fiber ARD model	b_1	0.000572	-
	b_2	-0.009945	-
	b_3	0.050000	-
	b_4	0.000699	-
	b_5	0	-

Eventually, the part is removed from the mold and shows individual fiber orientations, which are decisively responsible for the mechanical part behavior. For the SMC used in the present thesis, no significant macroscopic warpage could be observed, which is why no process-induced residual stresses are modeled in all subsequent SMC studies. Figure 4.10 shows an example of a part removed from the mold. In this part, the fiber orientations can be easily detected visually. The objective of the previously described modeling is to predict this fiber orientation distribution with sufficient accuracy. Perfect agreement can never be the goal here, since the process is subject to many stochastic effects that are not captured by the previously presented models.
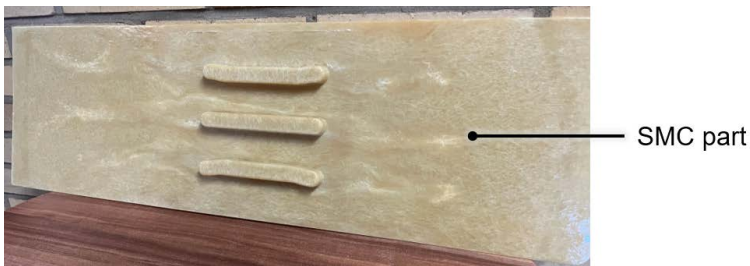
Figure 4.10: Exemplary SMC part after removal from the mold

The presented models and the discussed boundary and initial conditions are used to solve the balance equations. Moldflow uses a FE solver (see Subsection 2.4.3) for this purpose, which subdivides the overall problem into subproblems by meshing the model. As with all other numerical methods, this leads to a certain dependence of the results on the selected mesh. Moldflow recommends to choose 1-2 times the part thickness for the element size on the surface (Autodesk Support, 2020).

All models introduced in this subsection are used in this work to simulatively predict the fiber orientation that results from the manufacturing process. This simulative implementation represents a central element of the system of objectives and can be transferred into an element of the system of objects with the help of the presented models. In order to achieve a fiber orientation distribution on the macroscopic level that matches the real-world situation as closely as possible, in Figure 4.3, relevant material and process properties were identified, which are addressed by the presented models. Accordingly, this requirement for the method to be developed can

be considered fulfilled. Based on the calculated fiber orientation distribution, the resulting material properties of the part are determined (see Subsection 4.2.1.2). For this purpose, the material properties identified in Figure 4.4 have to be characterized and provided as an input for the simulation. Therefore, this requirement for the method to be developed is also fulfilled.

The assumptions made were justified by observations from manufacturing and processing. The validity of the developed models can only be evaluated for the comprehensively characterized SMC. For other material systems or SMC formulations, other model assumptions may be more appropriate. Nonetheless, from a methodical point of view, it is no problem to transfer the approaches to other materials. However, this requires the same comprehensive characterization of the alternative material system. The quality of the modeling is evaluated by validation in Section 4.3.

In addition, the use of carbon fiber reinforced UD-tapes is being studied to further stiffen the glass fiber reinforced SMC parts. This requires a slightly adapted modeling, which is presented in the following.

SMC in Combination with UD-Tapes

The manufacturing of the carbon fiber reinforced UD-tapes is not modeled and simulated separately. For modeling purposes, it is assumed that the fibers in the tape are perfectly aligned and distributed, which is why they are modeled to be transversely isotropic (see Subsection 2.4.2). The UD-tapes are only studied in combination with the SMC parts. This requires adjustments in the simulation of the manufacturing process of the SMC parts, which will be presented subsequently.

In the CoDiCo compression molding process, the UD-tapes (see Figure 4.11 (a)) are first inserted into the mold (see Figure 4.11 (b)), before the final part is formed by adding the initial charge and subsequent compression molding. The tapes are also impregnated with a thermoset matrix, so that a successful co-molding process results in a material bond between the part and the tape.

The CF UD-tapes[29] used in the project DFG GRK2078/2 measure 1.1-1.3 mm in thickness and are integrated into the part by co-molding with the semi-finished product. Due to the fact that the resulting part wall thickness does not change, the SMC wall thickness is reduced at the location of the UD-tapes. For this reason, the part geometries are adapted in the modeling by recessing the areas according to the

---

[29] Since only *CF UD-tapes* are considered in this work, simply the term "UD-tapes" is used in the following for better readability.

thickness of the tapes where the UD-tapes are located in the final part (see Figure 4.12). This means that new geometries and process simulations are required for each variation of the UD-tape form and position.
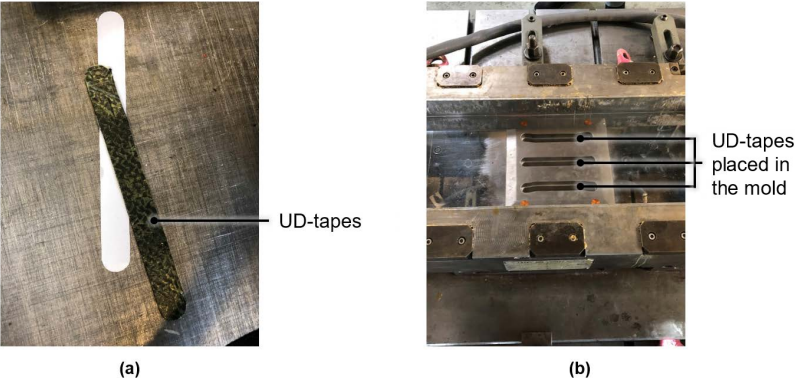
Figure 4.11: (a) Exemplary CF UD-tapes cut into shape (b) placement of the exemplary UD-tapes in the mold

Figure 4.12: Example of a recess for a UD-tape in the part geometry used for the mold filling simulation in Moldflow

In the next subsection the structural mechanical models are discussed, which are based on the results of the mold filling simulations.

4.2.1.2 Structural Mechanics

From the process simulations, for each finite element of the meshed geometry a specific fiber orientation tensor A (see Subsection 2.4.1) is calculated, which indicates the probability of the orientation of the fibers in the respective spatial direction. In addition, a homogenization (here for SMC: Tandon-Weng) of the material properties (see Subsection 2.4.2) can be performed in Moldflow, so that apart from the orientation information, the nine engineering constants (E_1, E_2, E_3, G_{12}, G_{13}, G_{23}, ν_{12}, ν_{13}, ν_{23}) are available per element. These engineering constants always refer to the local element coordinate systems, which is important to keep in mind when further processing the data. In the next step, this information resulting from the process simulation has to be transferred to a structural model using a mapping (see Section 2.6) in order to calculate the stiffness-optimized bead pattern and the stiffness-optimized bead cross section. By this procedure, the coupling of mold filling and structural simulation is realized, which was defined as a key requirement in Section 4.1 for the method to be developed. For the further procedure it has to be distinguished whether the stiffness-optimized bead pattern and, based on it, a bead cross section is to be calculated (→ *Beading Tool*) or whether an already beaded part is to be analyzed with regard to its stiffness and strength (→ *Structural Analysis*).

Beading Tool

To calculate the stiffness-optimized bead pattern, the trajectory-based bead optimization approach (see Subsection 2.7.2) is used, which has been implemented as a *beading tool* in Python at IPEK – Institute of Product Engineering and is thus part of the reference system of the present work. This beading tool requires a description of the structural problem as a shell model. However, the results of the mold filling simulations from Moldflow are available in solid elements. Therefore, a two-stage mapping was developed by the author (Revfi, Spadinger, & Albers, 2019), whose procedure is illustrated in Figure 4.13.

In the first stage, the fiber orientation tensors and engineering constants present in the tetrahedral mesh optimized by Moldflow for the flow simulation are mapped to a regular hexahedral mesh in Abaqus (see Figure 4.13). This target FE mesh in Abaqus is generated using the bottom-up technique based on the middle surface of the part. For this mapping, the MpCCI MapLib of Fraunhofer SCAI is employed (see Section 2.6). Here, it has to be taken into account that the engineering constants from Moldflow refer to the local element coordinate systems. Therefore, the material properties have to be translated into the same element-wise coordinate systems in Abaqus. (Revfi, Spadinger, & Albers, 2019) This is achieved by mapping the fiber orientation tensors, whose eigenvalues and associated eigenvectors define the local

element coordinate systems. Methodically, this means that subsequently each element has an individual material orientation with associated material properties.

In the second stage, the local coordinate systems and the corresponding material properties are translated into a shell layup (see Figure 4.13). For this purpose, a developed Python routine is used, which calculates the centroids (of the volume) of the regular 3D model to determine the closest centroid (of the area) of a 2D shell layup element and transfers the material properties and the local coordinate system to this element. (Revfi, Spadinger, & Albers, 2019) Important parameters for the two-stage mapping are the number of solid layers in the solid model (exemplary three layers in Figure 4.13) and the number of composite or shell layers in the shell model in Abaqus, as these influence the resulting stress state. More solid and shell layers provide a more accurate material description and affect the positions of the integration points. Since the resulting stress state is the basis for the subsequent trajectory calculation, it has a great influence on the result of the bead optimization.
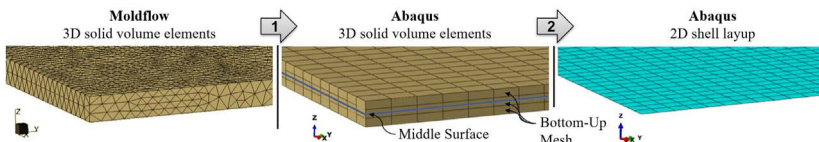
Figure 4.13: Two-stage mapping (exemplified for three layers in thickness direction) (Revfi, Spadinger, & Albers, 2019)

Subsequently, a structural mechanical modeling is necessary for the usually thin-walled, flat part that is to be stiffened by the beads. This means that the loads and boundary conditions must be translated from reality into the FE model. With the help of the shell model, the stresses occurring in the part are calculated.

The element-wise available stress tensors are then transferred to the beading tool. As a first step in the beading tool, the stress state is decomposed into bending and membrane stresses analogously to the procedure presented in Subsection 2.7.2. The solution of the resulting eigenvalue eigenvector problem leads to the principal bending stresses and the principal bending stress directions of each element. Based on this, the principal bending stress trajectories which determine the bead pattern are computed. For this purpose, the element-wise available principal bending stress values are sorted in a list by value. The elements with the highest principal bending

stress values are considered as starting points for the trajectories. Beginning with one of these starting points, the trajectories are formed along the highest principal bending stresses and their directions. The trajectories represent the centerline of the beads to be generated. Their course and position can be influenced by the product developer, for example by defining a design area (see Figure 4.14 (a)). Moreover, minimum trajectory radii and bead lengths or starting point distances can be specified. All potential trajectories are saved in another list. Then, starting from the highest principal bending stress, the beading tool runs through the trajectory list and adds those trajectories to the model that satisfy the position constraints (see Figure 4.14 (b)). Subsequently, a partition is generated along the trajectory, which has the width of the specified bead (see Figure 4.14 (b)).
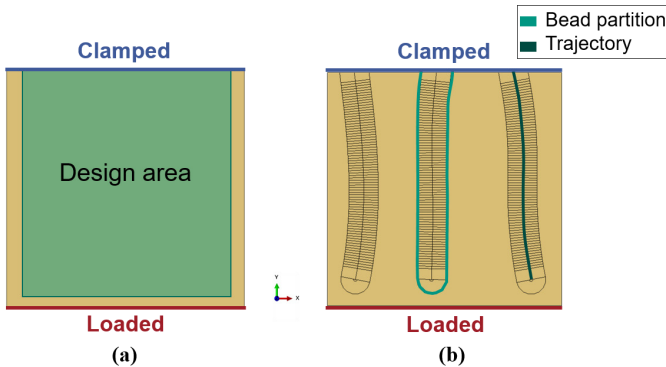
Figure 4.14: Beading tool: (a) design area (b) trajectories and bead partitions
adapted from Revfi, Spadinger, and Albers (2019)

Afterwards, the generated model is remeshed. In this remeshing, it is important to ensure that the element edge length in the partitioned area for the bead is small enough, as this allows a more accurate geometric description of the bead cross section. The global element edge length outside the partitioned areas can and should be chosen coarser in order to avoid an unnecessarily high number of elements. Finally, the bead cross section along the trajectory is generated by the nodal displacement perpendicular to the shell surface according to piecewise defined functions (see Figure 4.15 (a)). (Revfi, Mikus, et al., 2021) In this way, all bead parameters can be described geometrically and, as a result, a directly manufacturable bead

cross section is obtained. Accordingly, two key requirements for the method to be developed are fulfilled.
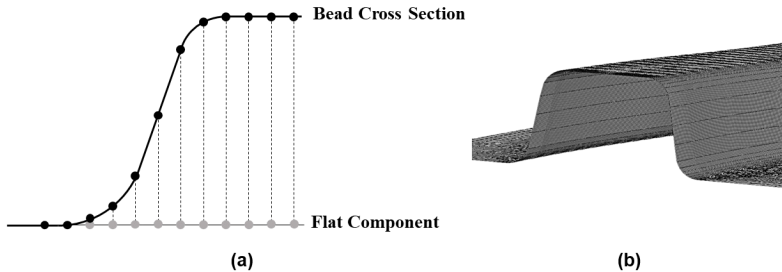
Figure 4.15: (a) Schematic bead generation through perpendicular nodal displacement (Revfi, Mikus, et al., 2021) (b) exemplary beaded shell model

The only bead parameter that influences the partition and thus the number of resulting elements of the model is the bead width. A variation of all other bead cross section parameters has no influence on the resulting number of elements. (Revfi, Mikus, et al., 2021) Due to the perpendicular nodal displacement, it is important to ensure that there is a sufficient number of nodes or elements in the radii and flanks of the bead cross section. Methodically, it is possible to create any bead cross section (except for the rectangular bead, since it has 90° flanks, which cannot be created by nodal displacement) by adapting the piecewise defined functions. However, in the context of the present work, only rounded trapezoidal beads are considered (see Figure 4.15 (b)).

On the basis of the beaded shell model generated with the previously described procedure, a solid mesh is generated using a both-sided offset (see Figure 4.16). For this purpose, the shell model is used as middle surface and a predefined number of solid element layers is generated in both directions. In these models, the specified bead parameters (see Figure 2.41) always refer to the middle surface.

This generated solid model serves as input for another mold filling simulation to calculate the fiber orientations occurring in the beaded part, and for structural analysis to evaluate the part stiffness.
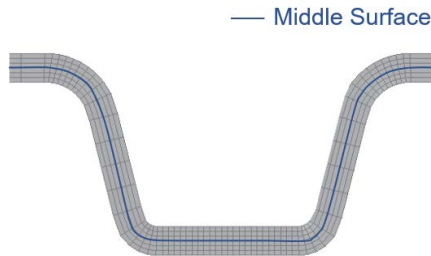
—— Middle Surface

Figure 4.16: Mesh generation based on both-sided offset using the shell model as middle surface

Structural Analysis

Also for the structural analysis of parts, a mapping is necessary, since the tetrahedral elements applied for the mold filling simulation in Moldflow, which are arranged in an optimized way to represent the flow characteristics, are only partially suitable for use in structural simulations. Tetrahedral elements with linear shape functions tend to cause an artificial increase in stiffness (Nasdala, 2012). Therefore, it is possible to either use quadratic shape functions in the tetrahedral elements, resulting in high computation times, or to switch to hexahedral elements (with linear shape functions and reduced integration). For the mapping of SMC parts, the same procedure is employed as for the first stage of the two-stage mapping (see Figure 4.13) and the fiber orientations and homogenized material properties computed in the process simulation are transferred to the solid model generated from the middle surface (see Figure 4.16). Accordingly, the fiber orientation tensors are mapped and the eigenvalues and eigenvectors are calculated to define the local coordinate systems. For this purpose, the product developer has to specify a number of solid element layers through the thickness in the Abaqus model. After mapping, the boundary conditions and loads on the part are modeled and the simulation is started. The SMC models as well as loads and boundary conditions studied in this work are explained in more detail in the context of the model design in Subsection 4.3.1.

Modeling the structural mechanics of parts reinforced with UD-tapes requires additional modeling assumptions, which are briefly presented in the following.

SMC in Combination with UD-Tapes

For the modeling of the UD-tapes in the structural simulation in Abaqus, a shell-layup modeling with a transversely isotropic material model (lamina) is applied. The number of tape layers used in the experiment and their stacking sequence (0°/90°/0°) are implemented equivalently in the simulation with the total thicknesses of 1.1-1.3 mm present in the respective experiment being evenly distributed among the plies. Due to the complexity of the geometry caused by the recess in the top chord of the bead (see Figure 4.12), tetrahedral elements are employed in the tape-reinforced models because they allow better meshing of the parts with respect to the mesh quality. At the same time, quadratic basis functions are chosen in the tetrahedral elements. The focus of the studies in this work is on the additional stiffening effect of the tapes in the linear elastic area. Accordingly, the failure mechanisms of the tapes as well as the interface region between SMC and tape are not modeled and the shell elements are firmly placed into the recess using a tie constraint. This means that no relative movements are possible between the tape and the SMC part, and an ideal interface is assumed.

In the context of this thesis, the UD-tapes are initially positioned in the top chord of the beads. This position is examined experimentally and simulatively (see Subsection 4.3.1.3). For the simulation, the workflow shown in Figure 4.18 is employed.

The presented models for compression molding, trajectory or bead calculation and structural mechanics can be used to calculate the structural behavior of a single part. For this purpose, the submethods have to be executed sequentially. Thanks to the modular applicability of the methods, if a mere structural analysis is to be performed, the trajectory or bead computation can be skipped. In the following, this sequential workflow is extended by an optimization scheme in order to automatically generate stiffness-optimized bead designs in FRP parts.

4.2.1.3   Optimization

To generate load-adapted bead patterns and cross sections in SMC parts, a method is developed to answer the third research question of the first research hypothesis (see Section 3.1), which couples the previously presented models in an automated optimization loop. The goal of this optimization method is to make the complexity of load-adapted bead design in FRP manageable for the product developer and to support him or her in the initial design process. To this end, the areas of design, manufacturing and material (see Subsection 2.3.3), which have to be considered in combination for product development with FRP structures due to their strong interactions, are taken into account. The optimization method should meet all the requirements defined in Section 4.1.

Most of the content of this subsection has been published previously in the publication Revfi, Mikus, et al. (2020) and Revfi, Mikus, et al. (2021).

For a concise representation of the interrelationships, the developed method is shown in Figure 4.17 in the IPEK coupling framework. As can be seen from the individual submethods, mainly commercial software is used. This was defined in the system of objectives in Section 4.1 as a requirement for the method. The advantage of commercial software has already been discussed previously.

Figure 4.17: Coupling framework for the optimization of process-based beads considering the SMC manufacturing and processing adapted from Revfi, Fünkner, Albers, and Behdinan (2021)

In the following, the developed method is described step by step. All models presented in Subsection 4.2.1.1 and Subsection 4.2.1.2 are executed automatically one after the other.

i)   CAD: Part geometry and initial Charge

The method starts with the geometric modeling of the initial charge and the flat, non-beaded part. For the initial charge, the real-world situation has to be respected as described in Subsection 4.2.1.1.

ii) FEM – Mold Fill: Fiber orientations and engineering constants

The mold filling simulation based on the modeled part and the initial charge geometry is set up. For this, all findings from Subsection 4.2.1.1 are included. The characterized material properties from experiments serve as an input.

iii) Mapping: Transfer of data

The fiber orientations and homogenized material properties are transferred to a structural mesh in Abaqus (see first stage of the two-stage mapping in Subsection 4.2.1.2).

iv) FEM – Structure: 2D stress calculation

The second stage of the two-stage mapping is conducted and the structural mechanic modeling is performed. On the basis of the shell layup model, the occurring stress state is calculated (see Subsection 4.2.1.2).

v) Mathematical Model: Principle bending stress calculation

Based on the calculated stress states in the non-beaded geometry, the principal bending stresses and principal bending stress directions are extracted as described in Subsection 4.2.1.2.

vi) Mathematical Model: Beading tool

Following this, the stiffness-optimized trajectories are computed (see Subsection 4.2.1.2). These trajectories are evaluated by the product developer with regard to the defined boundary conditions for the design and, if necessary, recalculated. Criteria for the evaluation can be, for example, the positions of the beads or their courses.

Afterwards, the beading tool creates a bead cross section as specified by the product developer and, based on that, generates a solid model which serves as an input for the subsequent mold filling simulation and whose structural behavior can be evaluated (see Subsection 4.2.1.2).

vii) FEM – Mold Fill: Fiber orientations and engineering constants

The generated solid model is used as an input for a further process simulation. All findings from Subsection 4.2.1.1 are included. Again, the characterized material properties from experiments are used.

viii) Mapping: Transfer of data

The results (fiber orientations and engineering constants) are mapped onto the solid model generated in step vi) according to the first stage of the two-stage mapping as described in in Subsection 4.2.1.2.

ix) FEM – Structure: 3D stiffness and stress calculation

For the solid model, the structural mechanic modeling (definition of loads and boundary conditions) is conducted. On the basis of this model, the resulting stiffness and stress are calculated. Accordingly, the resulting stiffness of *one* bead parameter combination is determined.

x) Bead Optimization: Genetic Algorithm

However, to identify a parameter set for a stiffness-optimized bead cross section, the bead parameters need to be varied. Due to the large number of possible combinations, it is not feasible to perform this variation "by hand". Therefore, a genetic algorithm (see gray method box in Figure 4.17) is employed in this thesis, whose optimization strategy is described in more detail in the following. As described in Subsection 2.5.1, genetic algorithms are suitable for the efficient exploration of the solution space if a large number of parameters are available. However, in principle, other optimization algorithms can also be implemented here, as was shown in the bachelor thesis by Sterr (2019)[30], which was co-supervised by the author of the present work, for a particle swarm optimization.

Based on the partitioned model (see Figure 4.14 (b)), the genetic algorithm generates different bead cross sections. In the context of the present work, only the bead cross sections are varied, whereas the bead pattern which is determined by the trajectories, remains unchanged. The variation of the bead cross section is achieved by varying the bead parameters height, width, flank angle, head radius and base radius (see Figure 2.41) in predefined ranges. The ranges can be selected more or less as desired by the product developer within the present geometric restrictions. This means that individual design space restrictions, such as the maximum possible bead height resulting from the integration of the part into the surrounding system structure, can also be taken into account during optimization. Due to the functionality of the beading tool, which only moves the nodes vertically in the partitioned area (see Figure 4.15), it is possible, depending on the element edge length, that only a few elements are located in the flank or in the radii, resulting in poor mesh quality

---

[30] Co-supervised thesis (unpublished)

due to distorted elements. (Revfi, Mikus, et al., 2020) Therefore, after a bead cross section is created by the genetic algorithm, the generated shell models are automatically checked if they satisfy the requirements for an adequate number of elements in all parts of the bead cross section. Bead cross sections that cannot be sufficiently modeled are automatically replaced by other parameter combinations. In order to adjust the limits resulting from the meshing, a finer mesh can be defined in the partitioned area.

Due to this functionality, any number of beaded parts are generated during optimization by the genetic algorithm. However, every change in the bead cross section also leads to a change in the part volume. As a result, the initial charge created at the beginning of the method cannot be carried over unchanged into the optimization process. Instead, it is necessary to maintain a constant relative additional volume for each compression molding process of a newly generated bead geometry in order to ensure complete filling of the mold despite the compressible material behavior. (Revfi, Mikus, et al., 2021) The additional volume can be estimated with the aid of the specified press compression force and the pv diagram shown in Figure 4.9. The adaptation of the initial charge volume per geometry is done automatically in the optimization loop by using the height of the initial charge as a variable and adjusting it according to an additional volume related to the final part volume during the initialization of the optimization. All other parameters of the initial charge (position and base) remain unchanged.

The evaluation of the different bead parameter sets is performed with a fitness function, which serves as objective function for the optimization. The fitness function f is defined in this thesis as described in Equation 43 by the quotient of the part volume V and the work of the external forces $ALLWK$ (Revfi, Mikus, et al., 2020).

$$f = \frac{V}{ALLWK}$$
$\qquad$ **43**

The goal of the optimization is to minimize the fitness function, thereby generating a design proposal with the maximum specific (i.e. volume-related) stiffness. The volume is used as an equivalent for the mass. Following the definition of the fitness function presented in Equation 43, the optimization results in a part with a lower mass if several geometries have the same stiffness. As discussed in Subsection 4.1.1, it is possible for anisotropic materials such as FRP to yield combinations where lower geometric stiffness is partially compensated by material stiffness depending on the fiber orientations resulting from the manufacturing process. As a result, two different bead cross sections can have similar stiffnesses. However, with

regard to a generalization of the developed method, it should be pointed out that the fitness function can easily be adapted so that the method can also be used for other optimization problems, such as for optimizing the mass with a given minimum stiffness. (Revfi, Mikus, et al., 2021)

In addition, a stress constraint is implemented to generate design proposals that satisfy the load capacity of the material (Revfi, Mikus, et al., 2020). Without this constraint, the optimization only tends towards the specific stiffest solution, which, in almost all cases, will be at the upper limit of the given range for the bead height. However, this can lead to stresses in the part caused by the loading, which can result in failure without, for example, achieving a required displacement. Since the developed method claims to support the initial design process, a conservative but simple maximum stress criterion is used. Nonetheless, due to the modular structure of the optimization method, more exact stress criteria can be implemented as well. Based on Equation 29, further simplifying assumptions are made and the stress criterion is formulated as shown in Equation 44. Instead of distinguishing between stresses that can be withstood parallel and transverse to the fiber direction, the smaller of the two values is chosen. Thus, only the material properties tensile strength R^t, compressive strength R^c and shear strength R_{shear} are required (Revfi, Mikus, et al., 2020). In addition, the principal stresses with the convention $\sigma_I < \sigma_{II} < \sigma_{III}$ are employed for the stress criterion. This stress criterion is checked element by element during the optimization (Revfi, Mikus, et al., 2020). If the stress of an element exceeds the limits defined by the maximum stress criterion, the corresponding geometry is discarded as a possible solution.

$$1 \geq max\left\{\frac{\sigma_I}{-R^c}, \frac{\sigma_{III}}{R^t}, \left|\frac{\sigma_{III} - \sigma_I}{2 \cdot R_{shear}}\right|\right\} \qquad \textbf{44}$$

For each optimization loop, the genetic algorithm, as described before, generates a new generation of individuals based on the nodal displacement of the middle surface. The number of individuals per generation has to be defined during the initialization of the optimization. In the context of the present work, each generation consists of eight individuals, which are initialized in the first generation. This relatively small number was chosen because eight workstations were available to perform the Moldflow simulations. Consequently, the mold filling simulations could be parallelized. This also means that more optimization loops have to be run in order to find an optimum. Each new generation is generated based on the previous generation by recombination and mutation according to a defined scheme (see Subsection 2.5.1). The best solution is carried over and recombined with other individuals that have passed the strength constraint. The probability of recombination of each

parameter is set to 60%. All individuals that do not meet the strength constraint are replaced by mutations of the current optimum, where two parameters are varied within a specified range (e.g., variation of the bead height in the range ± 2 mm). If all individuals of a generation have passed the strength constraint, the two worst solutions are replaced by mutations. This procedure allows an efficient investigation of the solution space. (Revfi, Mikus, et al., 2021)

To summarize, the optimization problem to be solved can be formulated according to Equation 45 (Revfi, Mikus, et al., 2021).

$$
\begin{array}{c}
\min f(\vec{x}) \\
\text{with} \\
\vec{x} = [bead\ height, bead\ width, flank\ angle, head\ radius, base\ radius]^T \\
\text{so that for each element} \\
\sigma_I(\vec{x}) \geq -R^c \\
\sigma_{III}(\vec{x}) \leq R^t \\
\sigma_{III}(\vec{x}) - \sigma_I(\vec{x}) \leq |2 \cdot R_{shear}|
\end{array}
\qquad \textbf{45}
$$

xi)   FEM – Structure: Optimized part

Finally, as the result of the optimization, the product developer is able to identify the stiffness-optimized bead cross section and bead pattern. With this result, he or she is able to proceed in the initial design.

For the SMC parts, which are additionally reinforced with UD-tapes, there is no automated optimization. Here, a manual, analysis-driven optimization of the tape geometry is carried out, which is explained subsequently.

SMC in Combination with UD-Tapes

The UD-tapes are studied in addition to the stiffening by beads. This means that they have to be integrated into existing beaded parts. Thereby, the beads can be used for the fixation of the tapes in the mold in order to prevent them from slipping out of position.

The optimization approach chosen for the UD-tapes results from the analysis of the experimental and simulative results and the conclusions derived from them. This results in a sequential workflow for the investigation of the stiffening effect of UD-tapes in the context of this work, which is shown in the IPEK coupling framework in Figure 4.18.

In the following, the developed method is described step by step.

i)   CAD: Adapted part geometry and initial charge

As described in Subsection 4.2.1.1, a new CAD model needs to be created for each UD-tape geometry and position, since a recess for the tapes is to be modeled.

ii)   FEM – Mold Fill: Fiber orientations and engineering constants

This adapted geometry is then imported in Moldflow to simulate the manufacturing process analogous to the parts without UD-tapes. For this, all findings from Subsection 4.2.1.1 are included.

iii)   Mapping: Transfer of data

Subsequently, the engineering constants and fiber orientation tensors are mapped to a mesh in Abaqus suitable for structural simulation according to the first stage of the two-stage mapping (see Subsection 4.2.1.2).

iv)   FEM – Structure: Tape modeling; 3D stiffness and stress calculation

Subsequently, the tapes are modeled in the tape recesses. For this, characterized UD-tape properties are used. Finally, the loads and boundary conditions are applied and the structural behavior is evaluated.
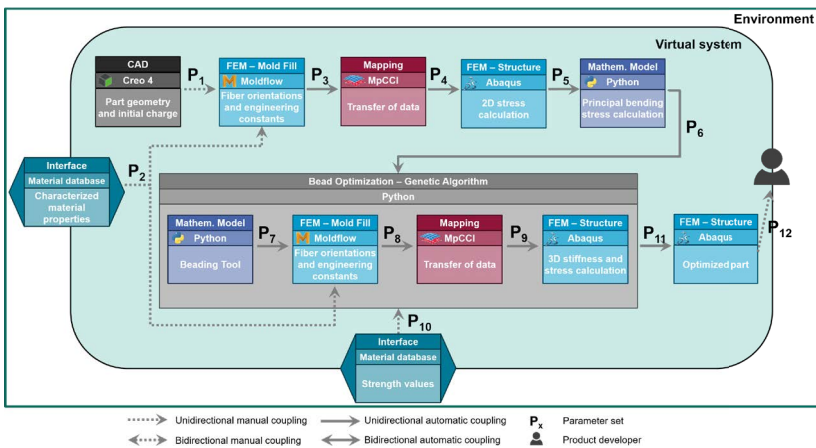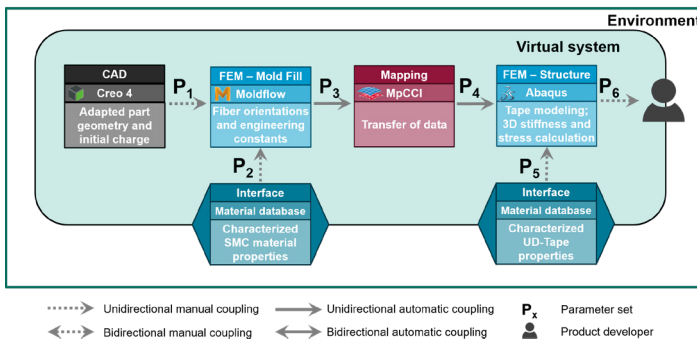

Figure 4.18: Coupling framework for the optimization of process-based beads considering the SMC manufacturing and processing as well as the influence of UD-tapes

Based on the knowledge generated with the UD-tapes positioned in the top chord (see Subsection 4.2.1.2), an optimized tape geometry is developed and subsequently evaluated again experimentally and simulatively. The studied tape geometries are presented in Subsection 4.3.1.4.

In the next subsection, LFT parts are discussed, which require a re-evaluation of the manufacturing and processing influences.

4.2.2   LFT

Due to the different processing (see Subsection 2.3.2) and the resulting different flow behavior (see Subsection 2.4.1), it is important to distinguish between SMC and LFT optimization. After introducing the SMC optimization that was developed on the basis of a characterized SMC material system in the previous subsection, this subsection is dedicated to the bead optimization of LFT parts. In addition to the different manufacturing and processing, the consideration of the LFT material system differs from the SMC material system in the context of this thesis primarily by taking into account the process-induced residual stresses. From a methodical point of view, the LFT optimization represents an extension of the optimization method presented for SMC parts, which is described in more detail in the following subsections. For this purpose, the same steps are followed as in the development of the SMC optimization method in Subsection 4.2.1, hence this serves as a reference system element for the development of the LFT optimization method. To avoid a duplication of content, only the differences to the assumptions in SMC are presented. As for SMC, the starting point also is the modeling of the manufacturing.

Most of the content of this subsection has been published previously in the publication Revfi, Mikus, et al. (2021).

4.2.2.1   Manufacturing and Processing

First, the manufacturing and processing of LFT is analyzed. Due to the reversed processing conditions compared to SMC (hot material into cold mold), a different flow behavior results (see Subsection 2.3.2 and Subsection 2.4.1), whose modeling in the context of this work will be discussed in the following.

The focus of the considerations is on parts that are produced in the LFT direct process. As discussed in Subsection 2.3.2, this means that the material is manufactured just before it is transferred to the press. Since no LFT material and process charac-

terizations were carried out in the DFG GRK 2078/2 research project, a character-ized long fiber reinforced polypropylene[31] (PP) from the Moldflow database is used. In contrast to SMC material systems, which are not available in the Moldflow 2019 database, there are at least a few LFT materials that can be selected. The chosen LFT contains glass fibers with a length l_F of 10 mm and a fiber weight fraction c_F of 0.3. For the simulations carried out in this thesis, the effective material properties for a perfectly aligned, unidirectional fiber orientation shown in Table 10 are used.

Table 10: Effective material properties: LFT composite (unidirectional fiber orienta-tion)[28]

Parameter	Symbol	Value	Unit
Density	ρ_C	0.97165	g/cm³
Young's modulus (1st prin-cipal direction)	E_{11}	7 378.04	MPa
Young's modulus (2nd prin-cipal direction)	E_{22}	3 444.88	MPa
Poisson's ratio	ν_{12}	0.4478	-
Poisson's ratio	ν_{23}	0.4748	-
Shear modulus	G_{12}	1 628.84	MPa
CTE	α_{11}	0.00001842	1/C
CTE	α_{22}	0.00005191	1/C

As in the processing of SMC, for LFT, the geometry and position of the polymer melt as well as the press profile need to be modeled according to the real-world process.

For the determination of the flow behavior, the balance equations are solved. For the modeling of viscosity and compressibility, the models provided in the database for the selected PP material are employed including the defined values. Therefore, they will not be discussed separately here. The assumption of isothermal pro-cessing, as in the case of SMC, is not appropriate for LFT. Accordingly, temperature dependencies have to be accounted for in the models. Here, again, the data pro-vided by Moldflow is used. As fiber orientation model, the ARD-RSC model is also

---

[31] Supran 1330 from Sambark LFT Co Ltd

applied for LFT (see Subsection 2.4.1), which was parameterized with values according to Table 11 computed by Moldflow.

Table 11:   Chosen values in the ARD-RSC model for LFT

Parameter	Symbol	Value	Unit
Reduced Strain Closure factor	κ	0.1	-
Parameters for long fiber ARD model	b_1	0.000192	-
	b_2	0.005839	-
	b_3	0.04	-
	b_4	0.000012	-
	b_5	0	-

The decisive process differences compared to SMC are in the modeling of the friction model and the residual stresses to be included for LFT. These two model assumptions are discussed in more detail next.

During compression molding of LFT, a fountain flow develops between the mold halves (see Subsection 2.4.1), since the hot material solidifies instantly when in contact with the cold mold surface and the polymer melt, which is in between the two solidification layers, is forced outward. This flow characteristic can be modeled by assuming an adhesion to the mold surface (v = 0 m/s). As a result, in comparison with SMC, there is no wall slip.

Another difference to SMC results from the process-induced residual stresses, shrinkage and warpage. The hot material cools during mold filling, solidifies in the mold and reaches room temperature after ejection (25°C is assumed for the studies in this work). To model this cooling, Moldflow computes the in-cavity stresses at room temperature with the part fully held constrained when the *uncorrected residual stress* model is chosen. In addition to the stresses due to solidification, these stresses include an additional stress which accounts for the thermal shrinkage that occurs after ejection during cooling down to room temperature. To predict this in-cavity stress distribution before ejection of the cooled part, a 3D thermo-viscous-elastic residual stress model is employed that assumes viscous behavior in the melt and linear elastic behavior in the solidified part (Fan et al., 2017). For this purpose, an orthotropic material model is applied in Moldflow for fiber reinforced materials,

which uses the results of the mold filling simulation (fiber orientations and mechanical properties) to describe the stress-strain relationship (see Equation 46 and Equation 47) (Fan et al., 2017).

$$
\begin{bmatrix} \sigma_{xx} \\ \sigma_{yy} \\ \sigma_{xx} \\ \tau_{xy} \\ \tau_{yz} \\ \tau_{zx} \end{bmatrix} = \begin{bmatrix} \dfrac{1 - \nu_{yz}\nu_{zy}}{E_y E_z \Delta} & \dfrac{\nu_{yx} + \nu_{zx}\nu_{yz}}{E_y E_z \Delta} & \dfrac{\nu_{zx} + \nu_{yx}\nu_{zy}}{E_y E_z \Delta} & 0 & 0 & 0 \\ \dfrac{\nu_{xy} + \nu_{xz}\nu_{zx}}{E_z E_x \Delta} & \dfrac{1 - \nu_{zx}\nu_{xz}}{E_z E_x \Delta} & \dfrac{\nu_{zy} + \nu_{zx}\nu_{xy}}{E_z E_x \Delta} & 0 & 0 & 0 \\ \dfrac{\nu_{xy} + \nu_{xy}\nu_{yz}}{E_x E_y \Delta} & \dfrac{\nu_{zy} + \nu_{xz}\nu_{yz}}{E_x E_y \Delta} & \dfrac{1 - \nu_{xy}\nu_{yz}}{E_x E_y \Delta} & 0 & 0 & 0 \\ 0 & 0 & 0 & G_{xy} & 0 & 0 \\ 0 & 0 & 0 & 0 & G_{yz} & 0 \\ 0 & 0 & 0 & 0 & 0 & G_{zx} \end{bmatrix} \begin{bmatrix} \varepsilon_{xx} \\ \varepsilon_{yy} \\ \varepsilon_{xx} \\ \gamma_{xy} \\ \gamma_{yz} \\ \gamma_{zx} \end{bmatrix}
$$

46

$$
\Delta = \frac{1 - \nu_{xy}\nu_{yx} - \nu_{yz}\nu_{zy} - \nu_{zx}\nu_{xz} - 2\nu_{xy}\nu_{yz}\nu_{zx}}{E_x E_y E_z}
$$

47

Finally, to calculate the initial stresses σ_g at each node, the pressure at freeze stresses σ_{g0} and the strains due to the thermal shrinkage ε_{g0} are combined according to Equation 48. D_g describes the stress-strain relationship matrix. (Fan et al., 2017)

$$
\{\sigma_g\} = -[D_g]\{\varepsilon_{g0}\} + \{\sigma_{g0}\}
$$

48

The initial stresses calculated with this model act on the part after ejection from the mold and cause warpage.

As with the SMC method, the requirements defined for the method in Section 4.1 are still fulfilled. However, the additional material and process properties required for LFT and the necessary consideration of temperature dependence result in a higher characterization effort.

Next, the structural mechanical models are considered, which build on the results of the mold filling simulations.

4.2.2.2 Structural Mechanics

The occurring warpage has to be accounted for in the initial design determination, which is why it is transferred to the structural simulations. The particularities arising from this, which relate to the calculation of the bead patterns (→ *Beading Tool*) or to the evaluation of the structural behavior (→ *Structural Analysis*), are discussed in the following. All other aspects of the modeling of the structural mechanics are done analogously to SMC. For homogenization, the model of Mori-Tanaka is used for the LFT studies in this work.

Beading Tool

The calculation of the load-adapted trajectories describing the bead pattern is performed analogously to the SMC approach using the two-stage mapping.

Since the beads are intended to stiffen against externally applied loads and should therefore explicitly not depend on part-specific warpage due to residual stresses, the residual stresses are not included in the two-stage mapping for the calculation of the trajectories in LFT parts (Revfi, Mikus, et al., 2021).

However, the situation is different for the structural analysis.

Structural Analysis

For the structural analysis of LFT parts, in addition to the engineering constants and the fiber orientation tensors, the in-cavity residual stresses are mapped from the process simulation. Thereby, the in-cavity residual stresses are applied as initial condition in the Abaqus model (Revfi, Mikus, et al., 2021). For this purpose, they are modeled as a local stress tensor for each element. The residual stresses cause part warpage and therefore affect stiffness and strength. If the residual stresses in the part are oriented in the direction of the stresses caused by the external forces, they constitute an additional load and have a negative effect on the part strength. If the residual stresses act in the opposite direction to the stresses applied by external forces, they reduce the locally occurring stresses. In contrast to the SMC method, the external forces are therefore only applied in a second step after calculating in the first step of the structural simulation the warpage resulting from the in-cavity residual stresses.

The distinction between the mapping for the beading tool and the mapping for the structural analysis also is to be taken into account in the automated optimization, which is presented in the following.

4.2.2.3 Optimization

The optimization process for LFT parts is similar to that for SMC (see Subsection 4.2.1.3). Therefore, not all steps will be discussed again in detail here, but rather only the main differences. Figure 4.19 shows the workflow of the developed method in the IPEK coupling framework.
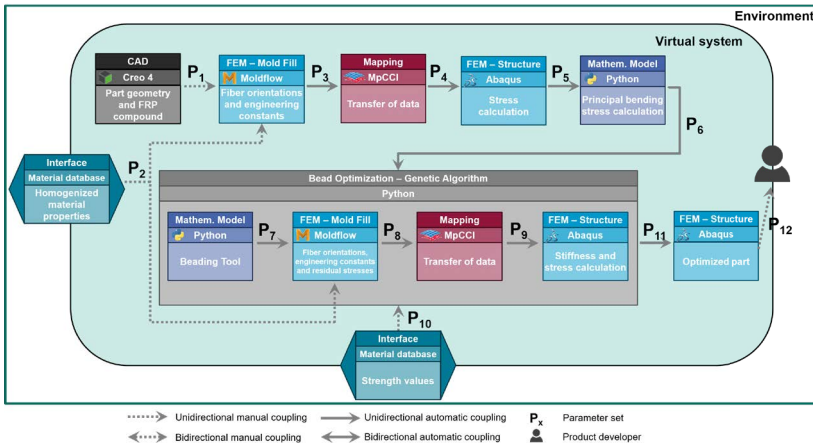
Figure 4.19: Coupling framework for the optimization of process-based beads considering residual stresses from the LFT manufacturing process adapted from Revfi, Mikus, et al. (2021)

After modeling the geometry of the part to be stiffened with beads and the geometry of the LFT compound, the processing needs to be simulated analogously to the SMC method. As described in Subsection 4.2.2.2, the resulting residual stresses are not mapped to the shell model in the two-stage mapping, because the beads to be calculated by the beading tool are not intended to stiffen against manufacturing and processing influences, but only against external loads. The subsequent steps and the optimization are structured analogously to the SMC method. After calculating the trajectories and partitioning the model, the genetic algorithm generates individuals with different bead cross sections, which are then forwarded to a process simulation. However, the biggest difference is in the structural simulation carried out in the optimization loop. Here, as described in Subsection 4.2.2.2, the residual stresses from compression molding are mapped for each individual. Therefore, the

structure simulation needs two steps as described before: First, the deformations of the part due to the process-induced residual stresses are calculated and, subsequently, the external load is applied (Revfi, Mikus, et al., 2021).

With regard to the fitness function, it is important to use the $ALLWK$ as an energy quantity, especially in LFT optimization. In contrast to the strain energy ($ALLSE$), which is often used as energy quantity in topology optimization, $ALLWK$ has the advantage that the initial stresses induced by the process and applied as initial condition in the structural simulation are not considered in the stiffness evaluation. (Revfi, Mikus, et al., 2021)

In summary, the methods presented in this section address the need for a bead optimization method for SMC (see Subsection 4.2.1.3) and LFT (see Subsection 4.2.2.3) parts that is tailored to the manufacturing process. For this purpose, they employ an automated, iterative coupling of manufacturing and structural simulations. Consequently, the developed methods represent the answer to the research question formulated at the beginning of this section.

In the following, in Section 4.3 the verification and validation of the models and the bead optimization method will be discussed.

4.3   Verification and Validation

This section is dedicated to the verification and validation of the models and methods for SMC and LFT presented in Section 4.2. In the context of product development, verification and validation are primarily understood as the comparison between the realization and the specification (verification) or the comparison of the developed product with the customer requirements (validation) according to VDI 2206 (2004). However, in the context of this work, the terms are defined specifically for simulation and according to the definitions of the American Society of Mechanical Engineers (ASME)[32,33].

---

[32] Verification: "The process of determining that a computational model accurately represents the underlying mathematical model and its solution." Schwer (2007, p. 248)

[33] Validation: "The process of determining the degree to which a model is an accurate representation of the real world from the perspective of the intended uses of the model." Schwer (2007, p. 248)

In the following, a distinction is made for SMC between the validation of the com-
pression molding simulation, the validation of the structural simulation and the veri-
fication of the model for trajectory calculation as well as the verification of the bead
optimization. The LFT optimization can only be verified because there was no pro-
duction of LFT parts in the DFG GRK 2078/2 project and therefore no experiments
on compression molding and structural behavior could be performed.

First, in each subsection, the research objects that are used for verification and val-
idation are presented in the model design. In terms of DRM, the models and meth-
ods presented in Section 4.2 represent the result, achieved through the present
work, of an iterative approach between method development and verification and
validation. Even though the development of the models and methods was iterative
and stepwise, not each development generation will be discussed in the following,
but only the final results will be presented.

With the help of this section, the fourth research question of the first research hy-
pothesis (see also Section 3.1) will be answered.

Research Question

iv. Which knowledge on the synthesis of bead designs is gained by applying
the developed optimization method to SMC/LFT parts compared to isotropic,
linear elastic material properties?

According to the two material systems addressed in the research question, this sec-
tion is divided into SMC (see Subsection 4.3.1) and LFT (see Subsection 4.3.2).

4.3.1 SMC

Due to the availability of data from manufacturing and processing as well as me-
chanical testing, the models for compression molding and structural simulation can
be validated. The validation is carried out with the help of the demonstrator part
designed in the project DFG GRK 2078/2 (see Figure 4.20). The production of the
demonstrator part was performed as part of project T1[34] of DFG GRK 2078/2 at the
Fraunhofer Institute for Chemical Technology (ICT) in Pfinztal (Germany).

---

[34] Sergej Illinzeer of the Institute of Vehicle System Technology (FAST, KIT)
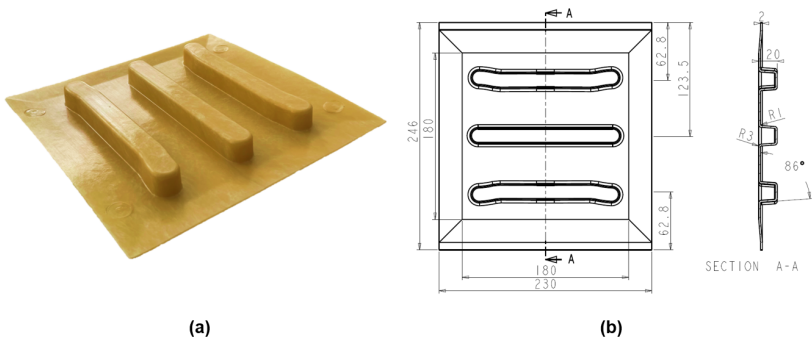
Figure 4.20: (a) Demonstrator part DFG GRK 2078/2 (b) technical drawing

The models are presented sequentially according to the bead optimization method presented in the IPEK coupling framework in Figure 4.17.

In the following, the models for compression molding are considered first.

4.3.1.1   Compression Molding

First, the models for compression molding are validated. For this purpose, the validation environment is initially described in terms of the model design. Based on this, the results of the validation are presented. Some of the content of these investigations has been published previously in the publication Revfi, Albers, et al. (2021).

(a)   Model Design

The mold used to manufacture the demonstrator part belongs to the inventory of the Fraunhofer ICT in Pfinztal. This mold can be modified by changing inserts, which means that the base mold can be used for several generations of different geometries. Therefore, for cost reasons, an insert was designed within the scope of the project that could be integrated into the existing mold. Figure 4.21 shows the installed insert in the mold. It can be seen that additional part volume is generated on both sides of the insert region (cf. Figure 4.20). However, this is very advantageous for the investigation and validation of the flow behavior during compression molding, since larger flow distances are covered in which the fibers are oriented.

(a)   (b)
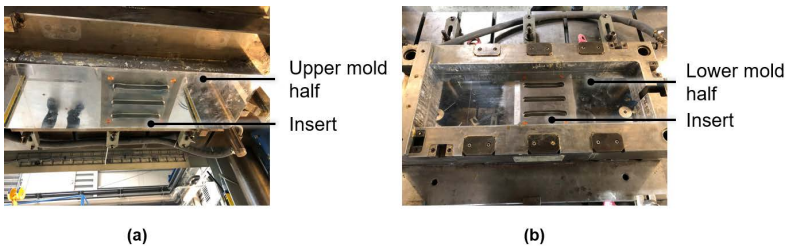
Figure 4.21: Mold of the Fraunhofer ICT in Pfinztal used in the DFG GRK 2078/2.
(a) Upper mold half with insert (b) lower mold half with insert

Based on these process conditions, CAD geometries are created, which serve as input for the mold filling simulation and are shown in Figure 4.22. The part thickness is 2 mm. The initial charge has a volume that is about 20% higher than the part to be manufactured.
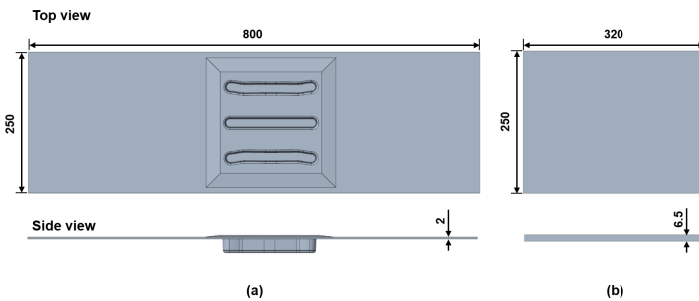
Figure 4.22: CAD geometry. (a) Part for the process simulation consisting of the demonstrator part and the additional part geometry[35] (b) initial charge

---

[35] For better readability, in the context of this subsection, the term *demonstrator part* refers to the geometry shown in Figure 4.22 (a) and not just the part shown in Figure 4.20 (a).

After importing in Moldflow, both geometries are meshed (see Figure 4.23).
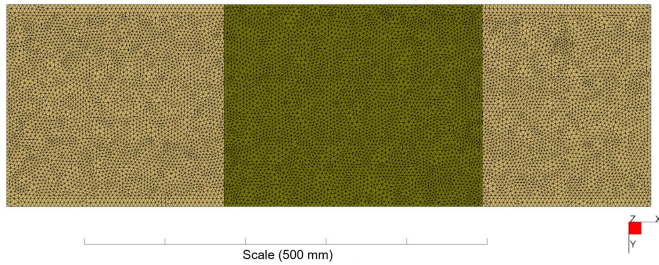
Figure 4.23: Mesh in Moldflow with the initial charge placed centrally over the beads of the demonstrator part

For this purpose, the auto-sizing option is activated for the definition of the element edge length. As mesh algorithm, Advancing Layers with ten elements through part thickness is selected. This results in approximately 1.1 million elements for the simulation model. Subsequently, the material properties are defined as derived in the method development in Subsection 4.2.1. In addition, the models for viscosity, friction on the mold wall and compressibility presented in Subsection 4.2.1 are employed. The position of the initial charge is initially chosen centrally over the beads of the demonstrator part (see Figure 4.23).

The press profile is specified according to Table 12 to match the profile applied in the real press. The initial press open distance is defined as 22.49 mm. The press compression force cap is set to 1400 kN, analogous to the specification in the real press.

Table 12:   Press profile

Step	Distance [mm]	Press compression speed [mm/s]
1	0	13.55
2	13.69	5
3	5	1
4	3.8	1

With this model design, compression molding is simulated and the fiber orientations relevant for the structural mechanical properties are validated afterwards.

(b) Validation

To validate the fiber orientation, computed tomography (CT) scans are often used to resolve the orientations of the fibers three-dimensionally over the thickness of the part. Since the demonstrator part dimensions are too large, it is not possible to analyze the entire part with the necessary resolution using the CT scanner available in the DFG GRK 2078/2 project. Therefore, in cooperation with project D1[36] of the DFG GRK 2078/2 a novel optical evaluation method was developed, which is presented in the following. The method has been published previously in the publication Revfi, Albers, et al. (2021).

In order to analyze the fiber orientations, in a first step, several individual images are taken, in which the demonstrator part is transilluminated (see Figure 4.24). The reason for several individual images is due to the size of the demonstrator part, which did not allow to take a single image at uniform transillumination with the available fluoroscopy possibilities. Since the demonstrator part is photographed, a distinction is to be made between the images of the top and the bottom side.
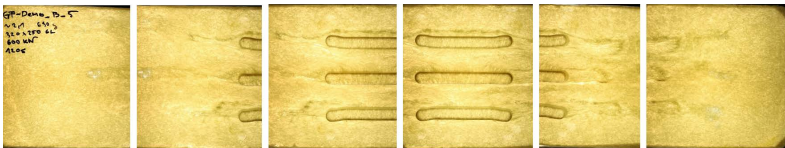
Figure 4.24: Individual images with uniform fluoroscopy of the bottom side of the demonstrator part[37]

The individual images are digitally processed in two steps in order to validate the fiber orientation. First, the individual images are merged in the correct order (see Figure 4.24). It can be seen that even though there are still overlapping areas, the fibers can be visually traced. In the second post-processing step, the overlapping

---

[36] Nils Meyer of the Institute of Vehicle System Technology (FAST, KIT)
[37] In cooperation with Nils Meyer (DFG GRK 2078/2, Project D1) of the Institute of Vehicle System Technology (FAST, KIT)

areas are removed, an overall image is created and the differences in light intensity between the fibers and the matrix are further elaborated. To this end, the color saturation of the image is reduced and the contrast is increased. The result of this second step can be seen in Figure 4.25 for the bottom side of the demonstrator part.
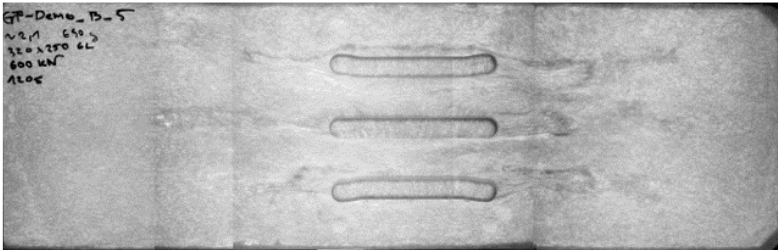
Figure 4.25: Post-processed image of the bottom side of the demonstrator part adapted from Revfi, Albers, et al. (2021)

This digitally processed image is subsequently available for fiber orientation analysis. For this, the method developed by Pinter et al. (2018) is adapted for 2D images. This adaption was made by project C2[38] of the DFG GRK 2078/2.

Figure 4.26 shows the results of the fiber orientation analysis for the bottom side of the demonstrator part. The left side of Figure 4.26 shows the fiber orientations in 1-direction, the right side shows the evaluation in 2-direction of the real demonstrator part (Figure 4.26 (top)), one bead in CT scan (Figure 4.26 (middle)) and the simulated demonstrator part (Figure 4.26 (bottom)). It should be noted that the evaluation of the images was only carried out in the area of the demonstrator part as shown Figure 4.26 (top). This means that the direct edge area and the end area of the right side were left out. The reason for this is that the edge area could not be captured properly during the image acquisition (cf. Figure 4.25) and the labeling on the right-hand side influences the evaluation algorithm. As a disadvantage of the developed optical method it has to be mentioned that only the fiber orientations close to the surface are evaluated. Due to the in-plane projecting method, no information on the fiber orientation distribution over the part thickness can be obtained from the image. However, this is not problematic for the study of the bending stiffness of parts. For

---

[38] Ludwig Schöttl of the Institute for Applied Materials – Materials Science and Engineering (IAM-WK, KIT)

bending loads it is mainly the orientation of the near-surface regions that is relevant, which can be captured by the method.
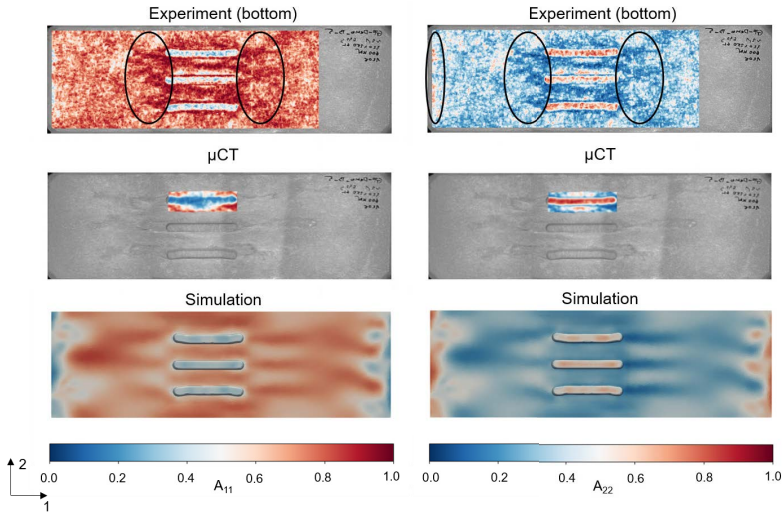
Figure 4.26: Comparison of the fiber orientation components A_{11} and A_{22} as a result of the fiber orientation analysis of the bottom side of the demonstrator part: orientation of the fibers in 1- (left) and 2-direction (right) – (top) real fiber orientations in the demonstrator part (middle) µCT scans (bottom) simulation results adapted from Revfi, Albers, et al. (2021). The red color shows a preferred orientation in the respective direction whereas the blue color implies that no fibers are oriented in the respective direction.

When comparing the experimentally determined fiber orientations with those calculated by the simulation, a high agreement can be found. However, it should also be mentioned at this point that this was not the case from the beginning on, as the boundary conditions for the wall slip model in Moldflow 2019 were not implemented in such a way that they could represent the real flow behavior. Only through direct cooperation with the Moldflow developers, this bug could be fixed and the results shown here could be generated.

Especially in the distinctive areas at the end of the beads, where there is a high fiber alignment in the flow direction, a high agreement of the simulation with the real part is evident. These flow marks can also be seen visually in Figure 4.25. The increased orientation in the 2-direction in the top chords of the beads can be seen both in the experiments and in the simulations. To further validate this finding, a CT scan of one bead was performed in addition to the developed optical evaluation method. The results of this evaluation are shown in Figure 4.26 (middle). The high agreement of the fiber orientations between the CT scan, the newly developed method and the simulation confirm the validity of the simulation results. It can also be concluded that the optical evaluation method provides a fast alternative to time-consuming CT scans, which are restricted to local regions.

One explanation for the orientation in the 2-direction in the top chords of the beads is that the material of the initial charge lying directly above the beads is stretched into the beads like in a forming process and is then displaced in the 1-direction. This causes the material to flow out of the beads, resulting in an increased orientation of the fibers in the top chord in the 2-direction (colored bluish in the A_{11} representation or reddish in the A_{22} representation). The fact that the immediate edge region is oriented even more clearly in the 2-direction in the simulation results is due to the insufficient depiction of the edge region in the evaluation of the real data. However, in principle, a reorientation of the fibers in the 2-direction forced by the edge is found both in the simulation and in the evaluation of the experimental data. This result is consistent with observed edge effects in SMC compression molding by Meyer et al. (2020).

Figure 4.27 shows the fiber orientations of the top side of the demonstrator part. The evaluation shows that the principally high agreement between the fiber orientations predicted by the simulation and the fiber orientations evaluated on the demonstrator part for the bottom side can be confirmed by the top side.

The previously mentioned areas in the top chord, the flow marks at the end of the beads and the edge areas show a high agreement between the experimentally determined data and the simulation results. The forming effect in the beads described for the bottom side is somewhat more pronounced in the evaluation of the top side of the real part than in the simulation, especially in the lower bead, but in principle still shows a high level of agreement in the prediction by the simulation. For the long flow distances to the edge areas, the A_{22} plot shows areas with an orientation in the 1-direction (reddish), which can be explained by local adhesion due to wall friction. Also these areas are predicted by the simulation.
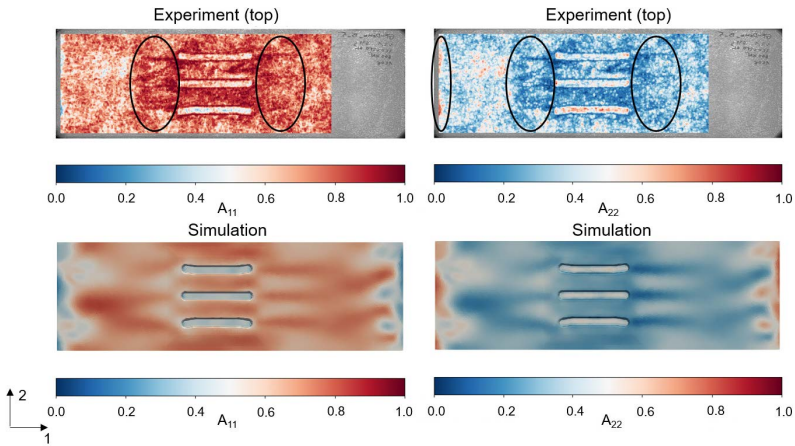
Figure 4.27: Comparison of the fiber orientation components A_{11} and A_{22} as a result of the fiber orientation analysis of the top side of the demonstrator part: orientations in the 1- (left) and 2-direction (right) – (top) real fiber orientations in the demonstrator part (bottom) simulation results[39]. The red color indicates a preferred orientation in the respective direction. The blue color indicates that no fibers are oriented in the respective direction.

In the context of the validation of the fiber orientations, the evaluation of the compression forces occurring during the processing is also of interest. Figure 4.28 in the upper half shows the tool opening over the compression time and in the lower half the compression force over the compression time. Here, the time $t = 0s$ indicates the switchover point from the displacement control into the force control of the press (Revfi, Albers, et al., 2021). The gray curves represent the median of five experimental results, and the orange curves are the results of the Moldflow simulation.

The gray shaded areas around the gray curves indicate the confidence interval between the upper and lower quartile. (Revfi, Albers, et al., 2021)
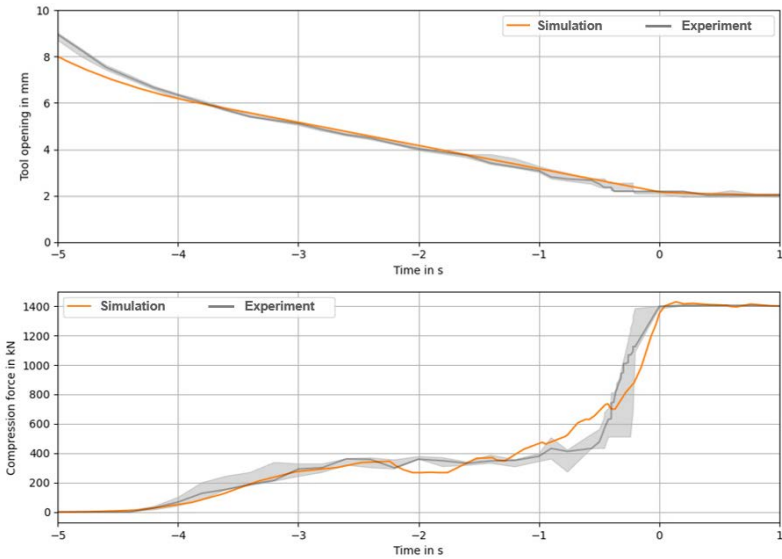
Figure 4.28: (top) Tool opening over compression time (bottom) compression force during the compression molding process over compression time adapted from Revfi, Albers, et al. (2021)

Looking at the tool opening, it is noticeable that the press closes slightly faster in the experiment than in the simulation (see Figure 4.28 at -5s). However, in the range from -4s, which is relevant for the mold filling process, the simulation reproduces the experiment with a very high agreement. Thus, it can be concluded that the converted press profile is accurately reproduced in Moldflow.

When evaluating the compression force, there also is a high agreement between the simulation result and the result averaged from five experimentally recorded data series. The force plateau that appears in the experiments is due to the sticking of the SMC to the mold wall until the lubrication layers have formed (Revfi, Albers, et al., 2021). Sticking occurs as long as the critical wall shear stress τ_C is not yet

reached, changing to slip as soon as this stress is exceeded. Therefore, for a realistic modeling of the force plateau in the simulation, the value of the critical shear stress τ_C has to be iteratively adapted to the material system. In the studies described in the present work, this is achieved with a value of $\tau_C = 0.2\ MPa$ (see Subsection 4.2.1). This value corresponds to real flow conditions, as shown by Meyer (2021), who determined a value of $\tau_C = 0.15\ MPa$ in experimental parameter studies. The wider confidence intervals in the experiment noticeable in the range of increasing force ($t > -0.5s$ in Figure 4.28) are due to oscillating data in this range, which, however, can be averaged out over the number of five experiments. After reaching 1400 kN, the press, like the simulation, switches to force control and holds this value until the mold is completely filled.

To further increase the validity of these findings, the initial charge position in the mold is changed both in the experiments and in the simulation and the evaluations are repeated. For this purpose, the initial charge is shifted by 60 mm in the negative x-direction from its position in Figure 4.23 (see Figure 4.29). All other simulation parameters remain identical to those previously described for the central position. The number of elements is also identical, since the meshed geometry is only repositioned in the model.
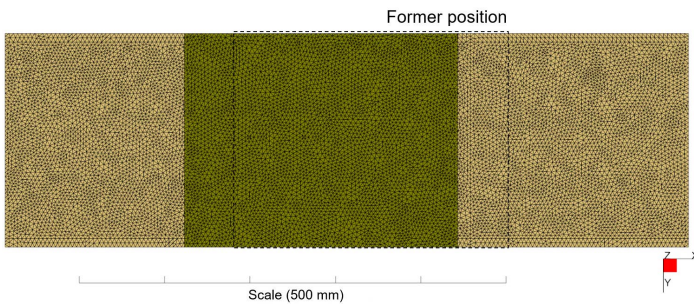
Figure 4.29: Mesh in Moldflow: initial charge shifted by 60 mm (compared to Figure 4.23) in negative x-direction

This results in a different flow behavior in the processing and thus different fiber orientations (see Figure 4.30). Whereas with the previously chosen position of the initial charge, distinct flow marks and thus highly oriented fibers can be seen on both sides of the end of the beads (see Figure 4.30 (a)), which are also reproduced by

the simulation (see Figure 4.26 and Figure 4.27), for the new position of the initial charge, such flow marks only appear on the left side (see Figure 4.30 (b)) and are also more extended.

(a)

(b)
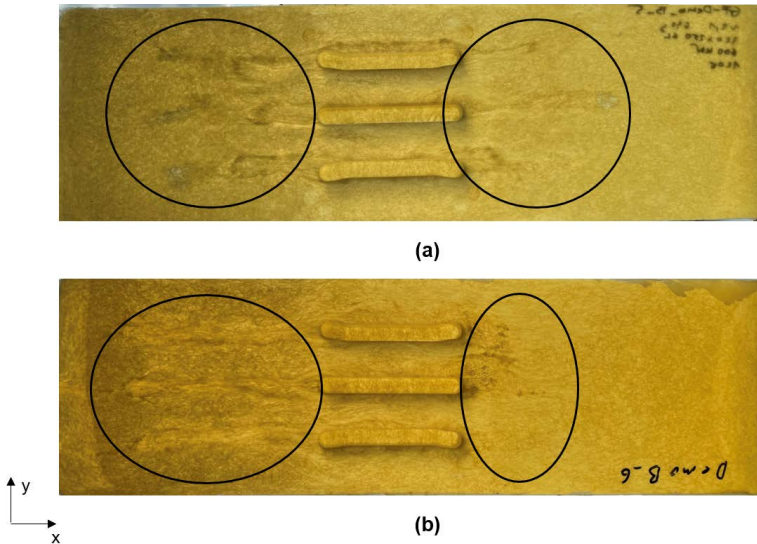
Figure 4.30: Fiber orientations in the demonstrator part after compression molding:
(a) initial charge positioned centrally over the beads (cf. Figure 4.23)
(b) shifted initial charge (cf. Figure 4.29)

The images are digitally processed in the same way as described previously (increase in contrast). The evaluation is repeated with two real demonstrator parts with shifted initial charge, whereby the results of the fiber orientation analysis are averaged. Figure 4.31 shows the fiber orientations of the bottom side averaged over the two real demonstrator parts as well as the corresponding simulation results.

The comparison of the results for the changed position of the initial charge also shows a high agreement between the experiments and the simulation. The flow marks, which now only occur on the left side of the part and also are significantly longer than before, are predicted by the simulation in this way. In the top chords of

the beads, there is again an orientation in the 2-direction. Here, the simulation results show a tendency towards an isotropic orientation on the right-hand upper chord half, which in the experiments rather indicate an orientation in the 2-direction. However, these deviations are still within acceptable ranges. At the right end of the beads, there is a high orientation in the 2-direction, which can be seen in the experiments as well as in the simulations. At both ends of the demonstrator part, an orientation of the fibers in the 2-direction is observed. This can also be seen in very similar form in the simulation results.
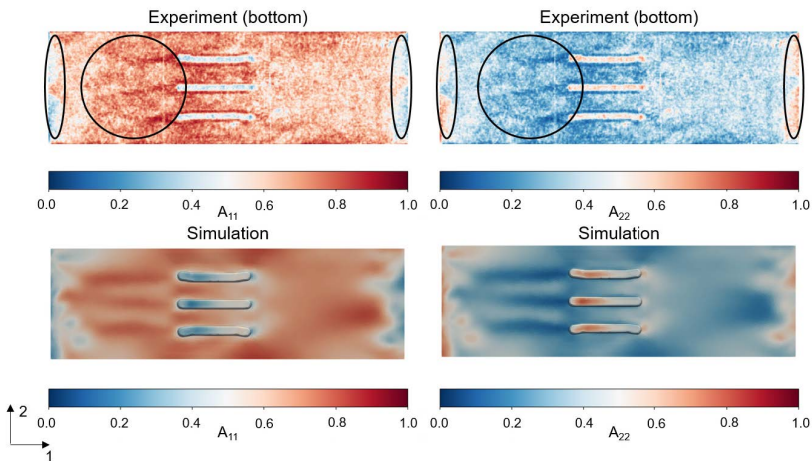
Figure 4.31: Comparison of the fiber orientation components A_{11} and A_{22} as a result of the fiber orientation analysis of the bottom side of the demonstrator part: orientations in 1- (left) and 2-direction (right) – (top) real fiber orientations averaged over two demonstrator parts (bottom) simulation results[39]. The red color indicates a preferred orientation in the respective direction. The blue color indicates that no fibers are oriented in the respective direction.

In summary, it can be stated that the simulation can predict the fiber orientations resulting from the mold filling process very well. As a result, the created models and the assumptions made (see Subsection 4.2.1.1) can also be evaluated as appropriate. Another important result of these studies is that the positioning of the initial

charge has a decisive influence on the resulting fiber orientations. For this reason, the positioning from the real process has to be modeled exactly in the simulation.

From a product developer's point of view, it is already confirmed here that the consideration of the manufacturing process of SMC in the design process is indispensable. The next step is to verify the model for trajectory calculation.

4.3.1.2 Model for Trajectory Calculation

Next, the model for trajectory calculation is evaluated (see Subsection 4.2.1.2). This study is carried out in two steps. First, the two-stage mapping (see Figure 4.13) is investigated in more detail ($\rightarrow$ *Two-stage Mapping*) and subsequently the developed approach is compared to an approach based on isotropic material modeling ($\rightarrow$ *Effect of Anisotropic Modeling*).

Most of the content of these investigations has been published previously in the publications Revfi, Fünkner, Albers, and Behdinan (2020) and Revfi, Spadinger, and Albers (2019).

Two-stage Mapping

In order to enable a process-based bead calculation, a two-stage mapping was developed, which transfers the results from Moldflow, available in 3D solid elements, to a 2D shell layup description in Abaqus (see Figure 4.13). The underlying method has already been presented in Subsection 4.2.1.2. The influence of the two-stage mapping on the calculated principal bending stresses and on the position of potential trajectory starting points is investigated and evaluated in the following.

(a) Model Design

A one-sided clamped, square plate (dimensions: 200 mm x 200 mm x 2 mm) under force-controlled bending load (see Figure 4.32) serves as the research object. This analysis problem is intentionally kept simple, since at this point the focus is on the evaluation of the developed method. For this purpose, a simple example allows the evaluation of the plausibility of the results. In the following, the results are all based on the same Moldflow simulation result, which was generated with a centrally positioned, square (dimensions: 130 mm x 130 mm) initial charge (see Figure 4.32). The Moldflow simulation model contains eight solid elements through the thickness in the interior of the part (Revfi, Fünkner, et al., 2020). The element edge length in Moldflow is 2 mm and the selected mesh algorithm is Advancing Layers. Simulations with 3D solid elements in Abaqus are performed with quadratic shape functions (C3D20R) and are used as a comparison to evaluate the influence of translating

these 3D models into 2D shell layup models with linear and quadratic shape functions (S4 and S8R). (Revfi, Fünkner, et al., 2020) As in Moldflow, the element edge lengths for all element types is 2 mm in Abaqus. The considerations are based on a linear elastic material model and consequently do not include plastic deformation or failure.
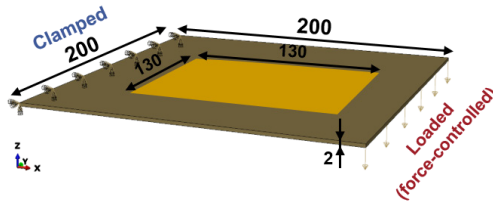
Figure 4.32: Model of the one-sided clamped plate under bending load with position of the initial charge adapted from Revfi, Fünkner, et al. (2020)

(b)   Verification

First, to verify the two-stage mapping, the calculated principal bending stresses along the clamped edge (see y-axis in Figure 4.32) are investigated. For this, on the one hand the influence of different element numbers through the thickness and on the other hand the dependence of the results on the choice of the element types (3D elements compared to 2D shell layers with linear and quadratic shape functions) are examined in more detail. Since eight solid elements are chosen through thickness in the Moldflow simulation, the element layers of the solid and shell models in Abaqus are varied between 1 and 11. The reason for the odd number of solid or shell layers is that the middle surface is added on top of the otherwise symmetrical models through the thickness.

The principal bending stress values, which are calculated based on 3D solid elements with quadratic shape functions, show higher values as the number of elements through the part thickness increases (see Figure 4.33 (a)). One reason for this is the position of the integration points inside the C3D20R elements where the stress is computed. The more elements are used through the part thickness, the closer the integration points get to the part surface. In a bending load case, the highest stresses occur at the top and bottom of the part, which consequently can never be accurately represented by the position of the integration points inside the

3D elements. However, the more solid elements are chosen through the thickness, the closer the principal bending stress value approximates the theoretical solution. This behavior can be seen in Figure 4.33 (a). In shell elements, the integration points are located directly on the part surface. Therefore, they have higher principal bending stress values (see Figure 4.33 (a)). A qualitative comparison of the curves of the principal bending stress values between 3D and shell modeling (each with quadratic shape functions) in Figure 4.33 (a) shows a very high agreement. There only is a constant offset of the values, which can be explained by the position of the integration points, as discussed before. From this, it can be concluded that the two-stage mapping applied has no influence on the curves of the calculated principal bending stresses, but only on their absolute value. In the overview plot in Figure 4.33 (a), the assumption arises that for the 2D shell modeling the number of elements through the thickness has no influence. Therefore, for this 2D shell modeling, the range with the highest principal bending stresses (between 50 mm and 150 mm on the y-axis) is plotted enlarged in Figure 4.33 (b). From this, it can be seen that the values of the principal bending stresses for all numbers of 2D layers through the part thickness are close together. However, a negligible change in PBS with further increase in the number of layers can only be seen from 9 layers or higher (difference between 9 and 11 layers <0,022%). Since eight solid tetrahedral layers were set through the thickness in the Moldflow simulation, this corresponds to one more shell layer in the structural simulation. In addition, Figure 4.33 (c) shows the dependence of the results on the choice of the shape functions in the shell layers. For the results already discussed, quadratic shape functions were used. From Figure 4.33 (c) it can be seen that linear shape functions can be applied to reduce the simulation time. The deviations in the values of the principal bending stresses between the linear (S4) and quadratic shape functions (S8R) are less than 0,19%. Figure 4.33 (d) summarizes the obtained results and once again shows the offset resulting from the choice of 3D solid elements as well as the influence of the chosen number of shell layers. (Revfi, Fünkner, et al., 2020)

Since the calculated principal bending stress values provide the basis for the calculation of the trajectory starting points, this is a very important finding with regard to the verification of the two-stage mapping.
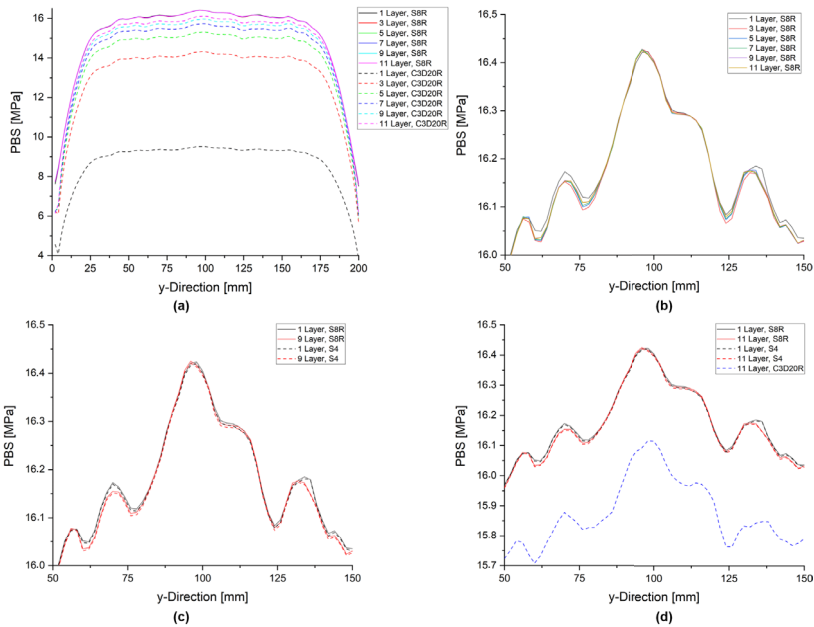
Figure 4.33: Calculated principal bending stresses along the clamped edge (y-axis) (a) comparison of different 3D and 2D thickness modeling (b) 2D shell layup: quadratic shape functions (c) 2D shell layup: linear vs. quadratic shape functions (d) comparison of the best 3D and selected 2D modeling (Revfi, Fünkner, et al., 2020, 2021)

However, in Figure 4.33 only the values along the clamped edge/y-axis are evaluated. Starting from these points, the course of the trajectory is developed over the part. Therefore, in a second step, the effect of different shell layer numbers through the thickness on the bead patterns will be analyzed. Based on the previously gained knowledge, only the shells with linear shape functions will be employed in the following.

Figure 4.34 (a) shows that the course of the central trajectory differs between the modeling with 5 layers and 7 layers. A further increase of the number of layers from 7 layers to 9 layers does not lead to any further difference (see Figure 4.34 (b)).

From this, it can be concluded that, in this simple example, the minimum number of solid and shell layers in Abaqus for calculating the trajectories can be chosen one element layer less than the number of solid element layers selected in Moldflow. At this point, however, the author of the present work points out that, due to the previously presented courses of the principal bending stresses, at least the same number of layers should be used in Abaqus as in Moldflow (preferably one layer more) in order to not lose any important information for the trajectory calculation due to the mapping, even in the case of more complex flow paths and load cases. (Revfi, Fünkner, et al., 2020) Furthermore, for the same reason and for the purpose of generalizability, it is recommended to apply quadratic shape functions in the shell layers if it is justifiable from the point of view of the required simulation time, even if linear approach functions were sufficient in this simple example.
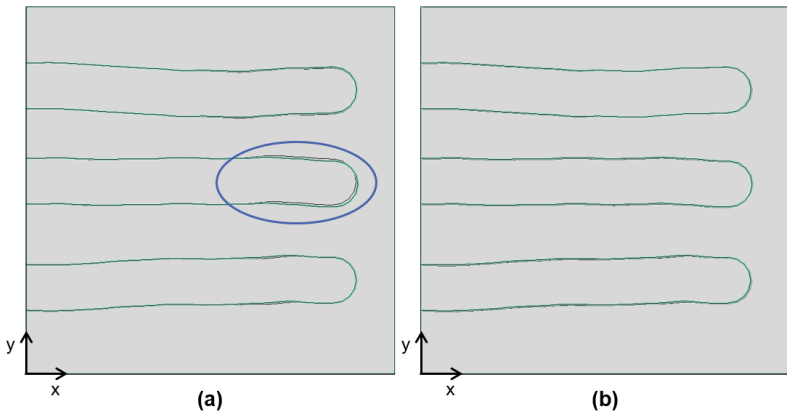
Figure 4.34: Bead pattern: (a) 5 layers (black) and 7 layers (green) (b) 7 layers (green) and 9 layers (black) adapted from Revfi, Fünkner, et al. (2020)

From the previous discussion, it can be concluded that the two-stage mapping is verified and that it can be applied in the optimization for the calculation of the trajectories. In this context, the sensitivity of the trajectory position and the trajectory course depending on the chosen thickness modeling of the part has to be considered. For this, concrete suggestions have been derived to assist in the modeling process. Even though the two-stage mapping in this subsection was developed for SMC, it can be considered independent of the material system. Next, the impact on

design of employing this two-stage mapping based on anisotropic material properties compared to an isotropic material modeling commonly used in practice is studied. In the state of the art, initial design proposals are still often generated on the basis of isotropic material models, which are afterwards evaluated by a single mold filling simulation and a subsequent structural simulation. If the resulting design does not meet the specified requirements, a manual optimization process is initiated. In the case of bead optimization, however, this procedure already results in a different bead pattern, as will be shown in the following subsection.

Effect of Anisotropic Modeling

Again, the model that serves as the research object is described first. Subsequently, the verification of the model is carried out.

(a) Model Design

The analysis problem for the investigations presented in the following again is the simple example of a one-sided clamped plate (dimensions: 200 mm x 200 mm x 2 mm) under bending load (see Figure 4.35). A force-controlled displacement of the nodes is applied to the edge opposite to the clamping. The advantage of this chosen example has been discussed before.
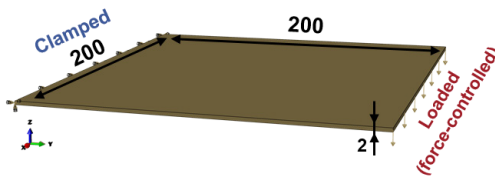
Figure 4.35: Model of the one-sided clamped plate under force-controlled load adapted from Revfi, Spadinger, and Albers (2019)

In order to investigate the influence of the manufacturing process on the bead pattern, the process simulations of these plates are performed with two different positions of the initial charge (see Figure 4.36). In this study, the dimension of the initial charge is 100 mm x 100 mm to cause longer flow distances. The element edge

length is chosen to be 1 mm and Advancing Front with six solid element layers through the thickness is specified as the mesh algorithm.
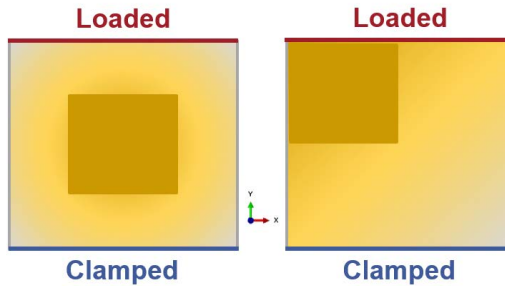
Figure 4.36: Investigated positions of the initial charge (Revfi, Spadinger, & Albers, 2019)

Following the mold filling simulations, the results are transferred to the shell layup models using the previously verified two-stage mapping and the trajectories are calculated. For this purpose, according to the knowledge generated in the previous subsection, one more element layer is used for the Abaqus models than in the Moldflow simulations. In these studies, this corresponds to an element layer number of 7 solid and 7 shell in each case. However, to further substantiate the findings, the results for 9 solid and 9 shell layers are also presented. Based on the trajectories calculated in this way, beads are generated by a nodal displacement in the shell model. For this, the bead parameters in Table 13 were chosen by the author based on his experience for bead parameters in steel sheets, since he, as a product developer, had no references for bead parameters in SMC structures, due to the research gap identified. The beaded shell model is then converted into a solid model by a both-sided offset (see Figure 4.16). This beaded 3D part is submitted to another mold filling simulation with the identical initial charge position and the same Moldflow parameters as used for the trajectory calculation. Its results are used for a simulation of the structural behavior (using C3D8R elements) after another mapping. Based on this structural behavior, the achieved part stiffness with the process-based method is evaluated.

Table 13: Defined bead parameters for the comparison of the influence of the manufacturing process on the calculated part stiffness (Revfi, Spadinger, & Albers, 2019)

Parameter	Value	Unit
Bead height	5	mm
Bead width	25	mm
Top chord width	10	mm
Base radius	3	mm
Head radius	3	mm
Bead distance	25	mm

The resulting initial bead design is compared to a design generated with isotropic material properties, which corresponds to the state of the art. For this purpose, isotropically homogenized SMC material parameters are used for the flat plate and, based on the resulting stresses, the trajectory calculation is performed analogously. Subsequently, the identical bead parameters are used for the bead generation (see Table 13). The beaded shell model is also converted into a solid model using a both-sided offset (see Figure 4.16). With the isotropic initial design proposal generated in this way, a mold filling simulation is performed for both initial charge positions and identical Moldflow parameters as for the anisotropic bead pattern, and after mapping, the part stiffness is evaluated. In this way, the state of the art can be compared to the process-based bead calculation approach.

The two described procedures are comparatively illustrated in Figure 4.37. Figure 4.37 (a) shows the workflow according to the state of the art based on isotropic material properties, while Figure 4.37 (b) presents the developed method based on the two-stage mapping.

The results generated using the two described workflows are discussed in the following.
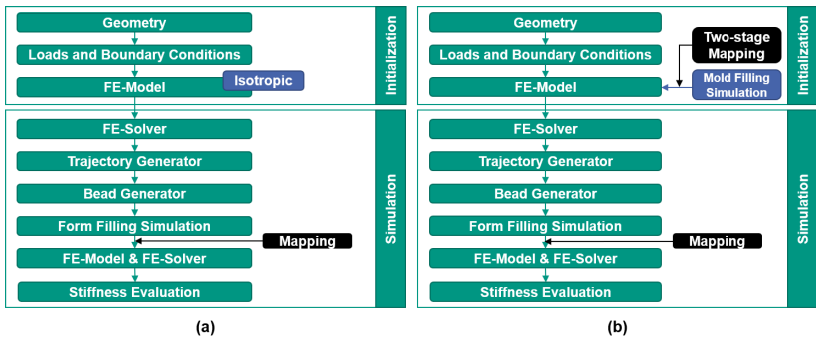
Figure 4.37: Stiffness evaluation. (a) Workflow according to the state of the art (b) process-based workflow with integrated mold filling simulation for trajectory calculation (adapted from Revfi, Spadinger, and Albers (2019))

(b)   Verification

To verify the process-based procedure, the bead patterns and the resulting stiffnesses of the parts are compared in the following. Figure 4.38 shows the trajectories generated by the models presented in the model design for 7 solid and 7 shell element layers. Figure 4.38 (a) displays the trajectories calculated based on the isotropic material properties. Figure 4.38 (b) and (c) show the trajectories generated on the basis of the mold filling simulation in Moldflow. They differ in the initial charge position. In Figure 4.38 (b) the initial charge was placed centrally, while in Figure 4.38 (c) a corner position was chosen. The exact position is shown in the small images in Figure 4.38. For 9 element layers in thickness direction, the trajectories are identical to those shown for 7 element layers, so they are not shown additionally. This confirms the findings from the subsection *Two-stage Mapping* that one more layer in Abaqus than in Moldflow is an expedient choice.
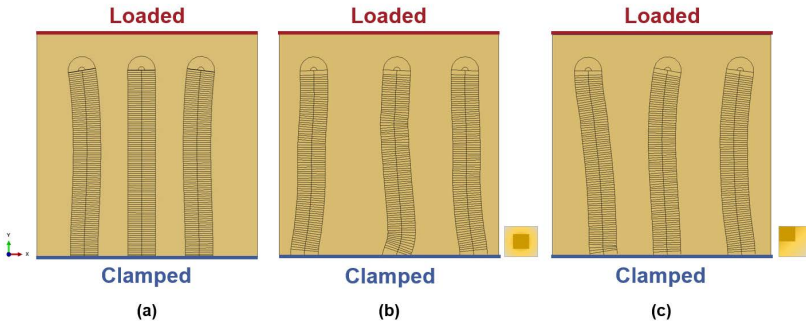
Figure 4.38: Trajectories: (a) isotropic (b) anisotropic – initial charge placed centrally (c) anisotropic – initial charge placed in the corner. All models consist of 7 solid and 7 shell layers in Abaqus.

From Figure 4.38 it is obvious at first glance that different bead patterns result depending on the modeling. The trajectories calculated based on isotropic material properties show a symmetrical pattern. This corresponds to the expected result, since the isotropic material model does not produce any directionality. For the trajectories generated on the basis of the mold filling simulation, the material properties resulting from the process are used in the principal bending stress calculation. This results in different stress states than in isotropic modeling, which means that different trajectory positions and courses are calculated. Although these bead patterns are still almost symmetrical, the difference to the isotropically generated bead pattern is instantly apparent. As a result, this observation already demonstrates that by taking into account the fiber orientations resulting from the manufacturing process and the material properties based on these orientations, a design is developed that deviates from the isotropic material modeling. This design is not intuitively predictable as in the case of design with isotropic materials, such as steel.

In the next step, the bead cross sections are generated in the partitioned areas according to the bead parameters from Table 13 and another mold filling simulation is performed in Moldflow. For the isotropically determined trajectories, a mold filling simulation is performed with the initial charge in the center and in the corner in order to be able to compare the results. The specific stiffnesses of the resulting parts, which are calculated for force-controlled displacements by multiplying the energy required for deformation by the part volume, are shown in Figure 4.39 and will be

compared in the following. Due to the definition of specific stiffness, smaller values indicate a higher specific stiffness.
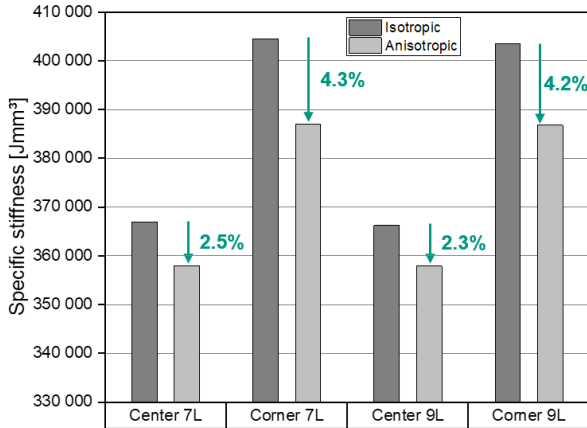
Figure 4.39: Specific stiffnesses of the different bead patterns. *Isotropic* refers to the trajectories generated on the basis of isotropic material properties, *Anisotropic* to the trajectories generated on the basis of a process simulation. Based on the respective trajectories (isotropic/anisotropic), a process simulation was subsequently performed in which the initial charge position was chosen according to the labeling on the x-axis.

Figure 4.39 indicates that the trajectories generated on the basis of the process simulation lead to stiffer parts for both initial charge positions. Moreover, the resulting difference is larger for the corner position of the initial charge than for the center position. This could be explained by the fact that the corner position results in more asymmetrical fiber orientations, the consideration of which already leads to advantages in the trajectory generation. The fact that slight deviations of 0.1% and 0.2% can be seen in the comparison of the respective results of 7 element layers and 9 element layers is due to the better resolution of the thickness direction with 9 element layers. For the selected C3D8R elements, a higher number of elements leads to a better resolution in the stiffness. Accordingly, these results can be used to verify the process-based approach.

In the present analysis problem, stiffer parts could be designed by taking into account the fiber orientations resulting from the manufacturing process in the trajectory calculation. At the same time, however, it should be noted that only a simple example of the one-sided clamped plate under bending load was studied here. Based on this one investigation, it is not possible to derive a generally valid statement. It might be that other procedures are better for other load cases or other initial charge positions. Nevertheless, this study shows that there can be configurations in which the process-based bead design has a clearly positive effect.

This result justifies the following research, which was carried out as part of this work. It is obviously possible to support the product developer in the stiffness optimized design of beads in SMC parts by offering appropriate simulation tools. Next, the structural mechanical models that can predict the real stiffnesses are validated.

4.3.1.3   Structural Mechanics

After the validation of the process simulation and the verification of the model for trajectory calculation, the structural mechanical models are considered subsequently. For this purpose, the demonstrator part (see Figure 4.20) is utilized again, which is exposed to a defined load case. In addition to the investigation of the beaded demonstrator part, UD-tape reinforced demonstrator parts are also examined. For the validation, the results of the simulations are compared to the experimentally measured results.

DiCo Demonstrator Part (Without UD-Tapes)

First, the validation environment is discussed in the context of the model design. Based on this, the results of the validation are presented. Some of the content of this subsection has been published previously in the publication Revfi, Albers, et al. (2021).

(a) Model Design

The demonstrator parts are tested in an experimental setup, which is shown in Figure 4.40. The experiments were carried out in cooperation with project C3[40] of the DFG GRK 2078/2. The demonstrator part developed in the project serves as a test specimen for all subprojects of the DFG GRK 2078/2. Each of the participating 14 subprojects should have the possibility to perform subproject-specific investigations

---

[40] Miriam Bartkowiak of the Institute for Applied Materials – Materials Science and Engineering (IAM-WK, KIT)

on this demonstrator part. Accordingly, the defined load case represents a compromise solution of the involved subprojects and does not correspond to any scenario derived from a real application. Nevertheless, it was aimed to keep the abstraction as close as possible to real bending tests, which are often performed in a three-point bending test. Therefore, the defined load case represents a modified three-point bending test. This modification is implemented by a two-sided clamped demonstrator part with two concentrated applied forces. The aim of this implementation is to reduce the frictional effects that occur in a conventional three-point bending test at the supports and the point of force application to a minimum.

(a)   (b)
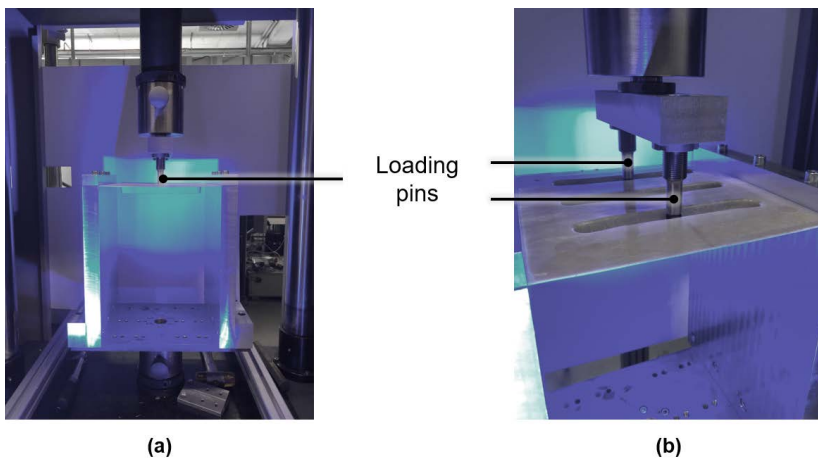
Figure 4.40: Experimental setup for measuring the force-displacement curves for the demonstrator part. (a) Front view (b) oblique top view adapted from Revfi, Albers, et al. (2021)

For this reason, the loading nose from a conventional three-point bending test, which initially applies the force in a line contact and later in a planar contact to the demonstrator part under investigation, is replaced by two loading pins. In addition, instead of the conventional supports used in a three-point bending test, a clamping is employed. For centering reasons and to apply the clamping force, a screwing is used (see Figure 4.41). The screwing is done at a sufficient distance from the demonstrator part so that it has no influence on the stress state in the part (Revfi, Albers, et al., 2021). This procedure for clamping specimens by screwing is also commonly used

in tensile tests and is specified in DIN EN ISO 527-4 for testing fiber reinforced polymers.
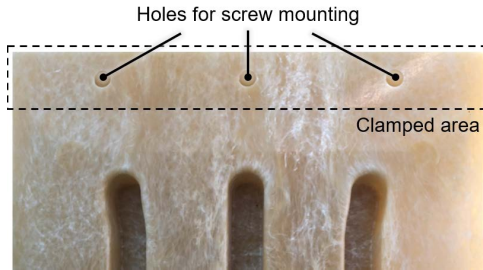
Figure 4.41: Realization of the clamping at the demonstrator part

The load is applied via two loading pins (see Figure 4.42). The cylinders that press on the demonstrator part are mounted in an articulated way in the loading pin so that they allow angular compensation on uneven surfaces and ensure uniform force application. There also is a radius at the edges of the cylinders to reduce the possibility of concentrated local load application when the cylinders are slightly inclined.

Figure 4.42: Loading pins with articulated mounting of the cylinders

The load is applied displacement-controlled to the demonstrator part via the loading pins (Revfi, Albers, et al., 2021). The forces that occur are recorded via a load cell and the associated displacements are recorded via an inductive sensor.

Based on this test setup, the corresponding simulation models are created. The cylinders of the loading pins are geometrically modeled in a simplified way, as shown in Figure 4.43. For the modeling, it is assumed that the loading pins are rigid bodies and therefore do not deform. So, they can be modeled either as analytical rigid or as discrete rigid. The articulated mounting of the loading pins is not modeled, since the demonstrator part has a plane surface in the simulation. The load is applied displacement-controlled analogously to the experiment.
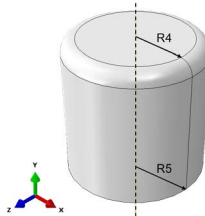
Figure 4.43: Model of a loading pin for use in the simulation

The part of the process simulation in Moldflow (here the validated model from Sub-section 4.3.1.1 is employed) which has the additional volume on both sides of the demonstrator part due to the mold at the Fraunhofer ICT is tailored to the demonstrator part geometry (see Figure 4.44). This can be realized by creating a model of the demonstrator part to be investigated (see Figure 4.44 (a) and (c)) and only mapping this region from the mold filling simulation. The clamping is not modeled with the screws, but rather by restricting the translational and rotational degrees of freedom of the surface nodes at the sides (see Figure 4.44 (a) – (c)) (Revfi, Albers, et al., 2021). The loading pins are placed analogous to the experiment (see Figure 4.44 (a) – (c)). The contact between the loading pins and the demonstrator part is modeled frictionless.
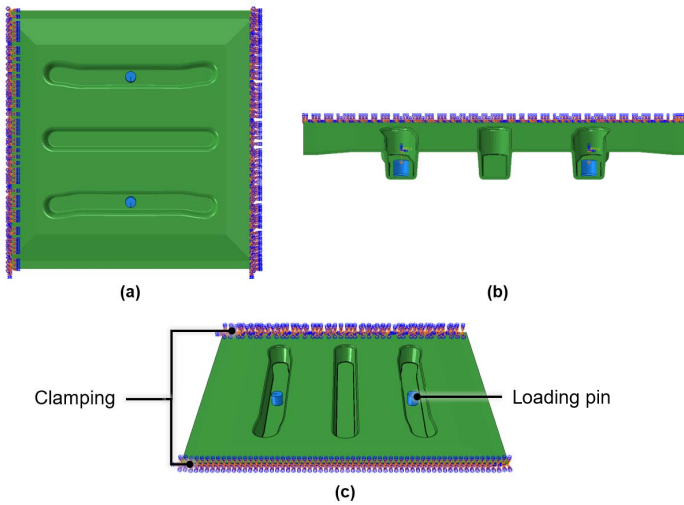
Figure 4.44: Model setup for simulating the force-displacement curves of the demonstrator part. (a) Top view (b) sectional view (c) oblique top view adapted from Revfi, Albers, et al. (2021)

In the context of the present work, for the structural simulation, hexahedral elements with linear shape function and reduced integration (C3D8R) are used to mesh the demonstrator part (Revfi, Albers, et al., 2021). They have been identified as the preferred element type for the beaded models in the studies by Mikus (2019)[41], as they provide sufficiently accurate results with significantly shorter runtime compared to C3D20 elements (with quadratic shape function). The element edge length is chosen to be 2 mm with nine element layers through the part thickness (see Figure 4.45). The nine element layers proved to be sufficient, since they can adequately represent the demonstrator part geometry also in the radii (see Figure 4.45). For the simulation in Abaqus, geometrical nonlinearities are taken into account.

---

[41] Co-supervised thesis (unpublished)
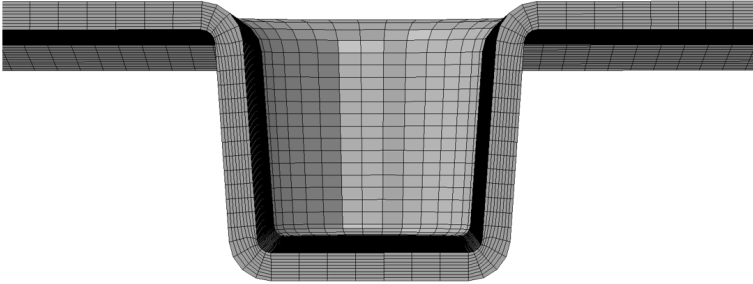
Figure 4.45: Mesh of the DiCo demonstrator part: nine hexahedral element layers (C3D8R) through the part thickness

Finally, the described models are compared to the experimentally recorded data and consequently the simulations are validated. Furthermore, a comparison of the process-based results to a structural simulation based on isotropic results is made. For the isotropic material properties, the material properties of the SMC on which this thesis is based (see Table 5) are homogenized appropriately. Table 14 shows the isotropic SMC material properties applied for the models.

Table 14: Isotropic SMC material properties[28]

Parameter	Symbol	Value	Unit
Young's modulus	E_{iso}^{SMC}	7 164.27	MPa
Poisson's ratio	ν_{iso}^{SMC}	0.34	-
Shear modulus	G_{iso}^{SMC}	2 676.40	MPa

Next, the validation of the simulation models is presented.

(b) Validation

The validation of the simulations of the DiCo demonstrator part (without UD-tapes) is first carried out on a part with a wall thickness of 2 mm and a centrally positioned initial charge (see Figure 4.46). Since the previously presented structural models

cannot describe damage, the validation only applies to the linear elastic region and not to the failure of the part. The linear elastic region was determined from the experimental results by identifying the region where a linear force-displacement relationship exists. The transition to the nonlinear region occurs at about 2.25 mm displacement (Revfi, Albers, et al., 2021). Even though the part thicknesses of 1.75 mm and 1.9 mm, which are also considered in the following, show different elastic deformations, the evaluation is subsequently presented up to a displacement of 2.25 mm in order to make the graphs comparable. Figure 4.46 illustrates the force-displacement curve of the experimentally recorded and the simulatively calculated data for the demonstrator part with a wall thickness of 2 mm. For the simulated results, both, the process-based result and the result based on the isotropic material model, are shown. In addition, the position of the initial charge in the mold is specified in the figure.
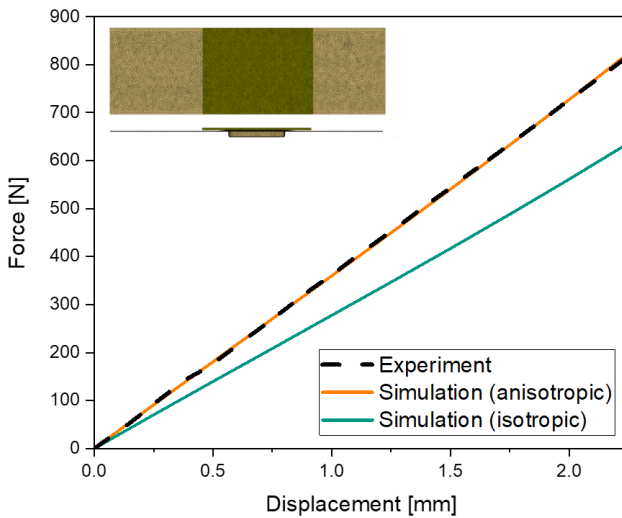
Figure 4.46: Force-displacement diagram: DiCo demonstrator part with 2 mm wall thickness adapted from Revfi, Albers, et al. (2021)

It can be seen from Figure 4.46 that the process-based structural simulation can reproduce the behavior of the real demonstrator part with a wall thickness of 2 mm very well. The force measured in the experiment at 2.25 mm displacement is

818.1 N, while the simulation predicts 824.1 N (Revfi, Albers, et al., 2021). This depicts a deviation of 6 N or 0.7%. In comparison, the data generated based on the isotropic material model differ significantly from the real measured force-displacement curves. At 2.25 mm displacement, the force predicted by the simulation is 636.4 N. This corresponds to a difference of 181.7 N or 22.2%. (Revfi, Albers, et al., 2021) Based on these results, the isotropic material modeling approach is not pursued in the further validation.

Due to the manual processing, which was present in the research project DFG GRK 2078 (see Subsection 4.2.1.1), it is difficult to produce the exact same part thickness several times. The part thickness of exactly 2 mm measured on the real demonstrator part could only be produced once. Validation on the basis of just one part is considered to be insufficient, which is why further investigations are carried out with different part thicknesses. In the scope of the validation, an investigation of different part thicknesses is to be regarded as positive, because it can be excluded that the models are only valid for a wall thickness of exactly 2 mm. In this way, the transferability of the method is simultaneously investigated.

Figure 4.47 shows the results for parts with a wall thickness of 1.75 mm. In this case, two demonstrator parts with identical wall thickness could be produced. The initial charge position remains unchanged.

The curve of the simulation shows a very high agreement with the curve of experiment 1. The force recorded in experiment 1 at 2.25 mm displacement is 599.5 N. The force as calculated by the simulation is 614.0 N. This depicts a deviation of 14.5 N or 2.4% even though the linear elastic region in this case of 1.75 mm wall thickness is already exceeded. Experiment 2 shows a deviation of the curve at the beginning of the measurement (see dashed ellipse in Figure 4.47), which leads to a steeper slope of the curve in the further course. The deviation of the curve is probably explained rather by setting effects of the loading pins than by irreparable damage to the part. Presumably, in the experimental setup, the two loading pins were not preloaded with the same force, resulting in a correction at the beginning of the measurement recording. Despite this effect, which occurred in the experiment and cannot be reproduced in the simulation, the simulation still shows an accuracy within a reasonable range with the curves determined from experiment 2. The force recorded in experiment 2 at 2.25 mm displacement is 646.5 N, which is 5.3% higher than predicted by the simulation. Compared to the results in Figure 4.46, it can be seen that the part thickness has a decisive effect on the force that can be applied to the demonstrator part. With a wall thickness of 2 mm, more than 800 N can be absorbed (linear) elastically at a displacement of 2.25 mm, while a reduction of the wall thickness by 0.25 mm results in a force of only about 600 N.
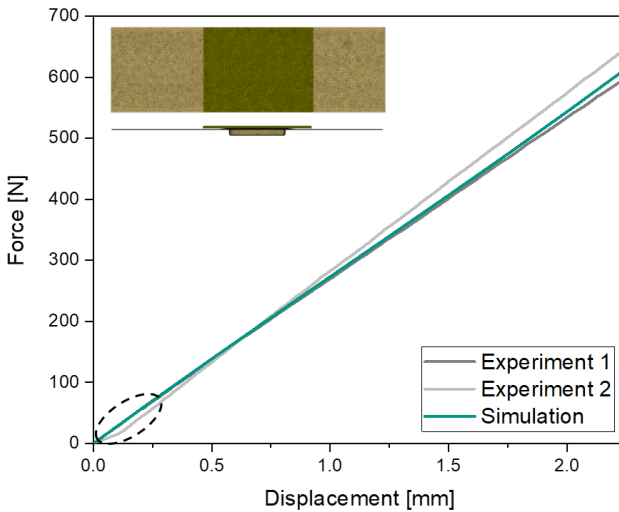
Figure 4.47: Force-displacement diagram: DiCo demonstrator part with 1.75 mm wall thickness[42]

As a further study, a part with a wall thickness of 1.9 mm is considered. Figure 4.48 shows the experimentally determined data and the corresponding simulation results. Also in this case, there is a basically high agreement between experiment and simulation. The experimental curve again shows a deviation at about 0.55 mm (see dashed ellipse in Figure 4.48), which results in an offset between the curve of the experiment and that of the simulation. Before this point, the curves are basically on top of each other. This leads to a force of 685.5 N in the experiment at 2.25 mm displacement, while the simulation predicts 733.5 N. As a result, there is a deviation of 48 N or 6.5%. Consequently, the largest delta between experiment and simulation is present in this study. However, this deviation can be explained and is therefore judged to be acceptable.
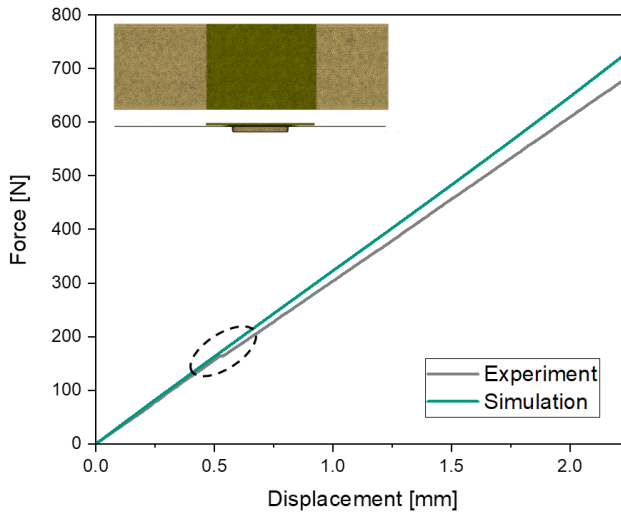
Figure 4.48: Force-displacement diagram: DiCo demonstrator part with 1.9 mm wall thickness[42]

In summary, it can be stated that the validation of the structural simulation based on the already validated flow simulation can be evaluated as successful. The maximum deviation between experiment and simulation, which can be explained by problems in the experimental measurement, is 6.5% and thus within an acceptable range. Likewise, it has been shown that isotropic material modeling does not lead to reliable results. Therefore, this approach will not be pursued subsequently.

As an extension to the long fiber reinforced, beaded SMC demonstrator parts, in the next subsection the demonstrator parts that are additionally reinforced with UD-tapes in the top chord of the bead are considered.

CoDiCo Demonstrator Part (with UD-Tapes)

In a further step, the model for structural simulation of the demonstrator parts rein-forced with UD-tapes in the top chords of the beads presented in Subsection 4.2.1.2 is validated. For this purpose, the validation environment is first presented in the model design. Based on the described model, the validation is carried out.

(a) Model Design

To further increase stiffness, the advantages of long and continuous fiber reinforced polymers are combined in a continuous-discontinuous design. For this purpose, the UD-tapes serve to further stiffen the parts in a specific direction. In the case, the beads not only provide stiffening but also help to position the UD-tapes in the pro-cessing, preventing them from slipping out of position due to the flowing material. Thus, costly tools for tape fixation can be dispensed with. In the first step, the UD-tapes were therefore placed in the mold in the top chord of the beads (see Fig-ure 4.11 (b)). This results in the CoDiCo demonstrator part as shown in Figure 4.49. For this design, the modeling is presented in the following.
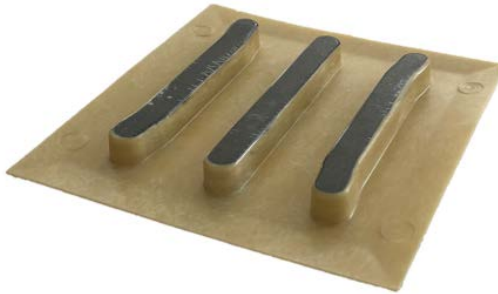
Figure 4.49: CoDiCo demonstrator part with UD-tapes in the top chord of the beads

The validation of the results is carried out using a demonstrator part with a wall thickness of 2 mm. The initial charge is positioned centrally over the insert, as before for the unreinforced demonstrator parts (see Figure 4.23). The test setup for the demonstrator parts reinforced with UD-tapes is identical to the previously presented unreinforced demonstrator parts. The parts are clamped on two sides, while the force is applied via the two loading pins. Therefore, the model design is analogous

to the beaded demonstrator part geometries without UD-tapes (see Figure 4.44). As described in the subsection on method development (see Subsection 4.2.1.2), three layers of tetrahedral elements in the thickness direction with a quadratic shape function (C3D10 elements) are applied due to the simpler meshing of the tape recesses (see Figure 4.50). In favor of the simpler meshing, the longer computation time in comparison to the hexahedral elements is accepted. That this meshing, which is only changed for the UD-tape models, does not lead to a negative effect on the quality of the results, was shown by the studies of Bayh (2020)[43].
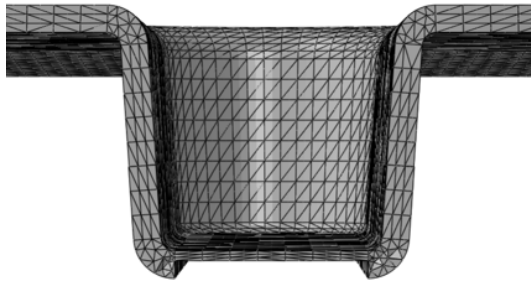
Figure 4.50: Mesh of the CoDiCo demonstrator part with three tetrahedral element layers with quadratic shape function (C3D10)

The quadrilateral shell elements for the modeling of the tapes in the defined recesses are also modeled with reduced integration (S4R) and an element edge length of 2 mm (see Figure 4.51). In the real-world manufacturing, three tape layers were stacked with a 0°/90°/0° orientation. In the simulation model, this is realized as introduced in Subsection 4.2.1.2 via shell-layup modeling, where each layer has a thickness of 0.43 mm. Therefore, the resulting UD-tape thickness (and correspondingly the depth of the recesses) is 1.3 mm. As a result, a SMC wall thickness of 0.7 mm remains in the top chords of the beads after deduction of the tapes. For the reasons described in the method development (see Subsection 4.2.1.2), the contact between the tapes and the part is modeled with a tie constraint at the bottom of the recess.

---

[43] Co-supervised thesis (unpublished)
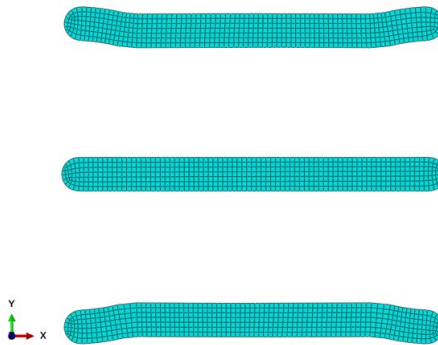
Figure 4.51: Mesh of the UD-tapes in Abaqus

In the following, the results generated by this modeling are presented and the simulations are validated.

(b) Validation

Figure 4.52 shows the force-displacement curve of the experimentally recorded and simulated data for the demonstrator part reinforced with UD-tapes in the top chord of the beads and the unreinforced demonstrator part with a wall thickness of 2 mm, which showed a very high agreement between experiment and simulation in the validation (see also Figure 4.46).

From Figure 4.52 it can be seen that the simulated structural behavior differs significantly from the one measured in the experiment. At a displacement of about 0.3 mm, the curves start to diverge. While the experiment indicates a force of 789.0 N at 2.25 mm, the simulation predicts a force of 922.8 N. This corresponds to a deviation of 133.8 N or 14.5%. These results are initially surprising, since the previously investigated demonstrator parts without UD-tapes showed a very high agreement between experiment and simulation. Therefore, the experimental data of the unreinforced demonstrator part are additionally shown in Figure 4.52. From this, it can be seen that the unreinforced demonstrator part is stiffer than the demonstrator part with tapes. The introduction of the tapes apparently has a negative effect on the stiffness, which is exactly opposite to their actual purpose. Therefore, the failure of the UD-tape reinforced demonstrator part is investigated in more detail. Figure 4.53 illustrates the damage pattern of the UD-tape reinforced demonstrator part.
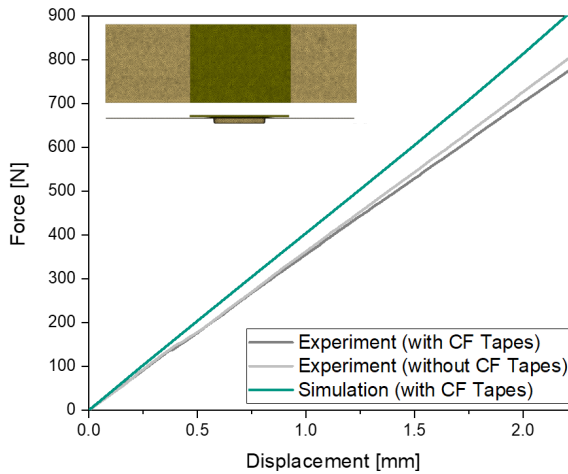
Figure 4.52: Force-displacement diagram: CoDiCo demonstrator part reinforced with UD-tapes with 2 mm wall thickness in the experiment and the simulation, and unreinforced demonstrator part with 2 mm wall thickness in the experiment[42]

Figure 4.53: Damage pattern of the CoDiCo demonstrator part reinforced with UD-tapes in the top chord. A speckle pattern was applied for optical measurement of the strain field with a Digital Image Correlation System (DIC).[40]

From this, it can be seen that the tapes in the two loaded beads are flaking off from the top chord. This indicates insufficient adhesion of the tapes to the SMC base part. As soon as failure occurs in the contact zone and the tapes no longer carry a load, the remaining stiffness only results from the DiCo part. As previously described, the DiCo part has a remaining thickness of only 0.7 mm in the top chord due to the tapes. Accordingly, it is significantly thinner at the points of force application compared to the unreinforced demonstrator part. On the one hand, this indicates that the demonstrator part reinforced with UD-tape starts to damage after a displacement of about 0.3 mm and, on the other hand, it explains the observation that the unreinforced demonstrator part is stiffer after a displacement of 2.25 mm than the demonstrator part reinforced with UD-tape.

This behavior cannot be reproduced by the developed simulation model. Due to the assumptions made in the modeling, the simulation is based on an ideal contact between the tape and the demonstrator part at all times. This also explains the higher stiffness predicted by the simulation compared to the unreinforced demonstrator part. At the same time, however, it is also evident that the tapes are able to provide a stiffening effect with a better adhesion.

The tape geometry obviously has to be optimized so that the tape length extends beyond the top chord of the bead. This will be addressed in the next subsection. In addition, the optimization method developed in the core of this thesis will be verified.

4.3.1.4 Optimization

Finally, the SMC optimization method presented in Subsection 4.2.1.3 is verified. A validation of the overall method is not possible, since each individual generated by the optimization would have to be produced and tested. Since each individual has different bead parameters, a separate insert would be required for the production of each individual (see Figure 4.21). This is not feasible due to time and cost constraints.

However, since the submethods for mold filling and structural simulation applied in the optimization method were successfully validated in the previous subsections, a conclusion can be drawn on the validity of the overall method, which is a coupling of these submethods. In addition, a verification of the optimization method by a comparison with an optimization based on an isotropic material modeling is performed in the following. In the subsection on the potential of beads, whose patterns are calculated based on the fiber orientations from the manufacturing process, it was already shown that there is a difference to the calculation with isotropic material parameters (see Subsection 4.3.1.2). Therefore, to ensure the comparability of the

results, the trajectories calculated on the basis of anisotropic material properties are used in the subsequent isotropic optimization

As described in Subsection 4.2.1.3, the bead parameters height, width, flank angle, head radius and base radius serve as design variables for the optimization. Consequently, the objective of the optimization is to identify the bead cross section within a given parameter range based on the calculated trajectories that leads to the volume-specific stiffest part.

In the following, the verification of the optimization method is performed in two steps. First, a one-sided clamped plate is investigated. Using this simple example, it is possible to study basic findings as it does not combine multiple phenomena. In the second step, the optimization method is applied to the DiCo demonstrator part (without UD-tapes).

One-sided clamped plate

First, the model design is discussed. Based on this, the results of the verification are presented. The general concept has been published previously in Revfi, Mikus, et al. (2020). Based on this publication, the models in the following investigations have been updated to the validated process simulations presented in Subsection 4.3.1.1.

(a)   Model Design

The analysis problem for the optimization is, for the reasons already mentioned, again the simple example of a one-sided clamped plate (dimensions: 200 mm x 200 mm x 2 mm) under bending load (see Figure 4.55).

The square plate is produced from an initial charge, that has a side length of 130 mm x 130 mm and is placed centrally in the mold. The height of the initial charge is iteratively adjusted in such a way that there is an additional volume of 21% for each geometry generated in the optimization. The chosen material is the SMC presented in the method development in Subsection 4.2.1.1 and whose manufacturing and processing was validated in the previous Subsection 4.3.1.1. Likewise, the other models and assumptions underlying the validated mold filling simulation are applied. The model is meshed in Moldflow with an edge length on surface of 2 mm, which is in accordance with Moldflow's recommendations for a part thickness of 2 mm (Autodesk Support, 2020). As mesh algorithm, Advancing Layers is employed. For the optimization, eight element layers are specified in the thickness direction in Moldflow, since depending on the investigated bead cross section, mesh warnings can occur with ten layers. As a different number of element layers should not be chosen for different geometries in the optimization and in order to ensure the comparability

of the results, the eight layers are specified globally. The resulting mesh in Moldflow and the position of the initial charge are illustrated in Figure 4.54.
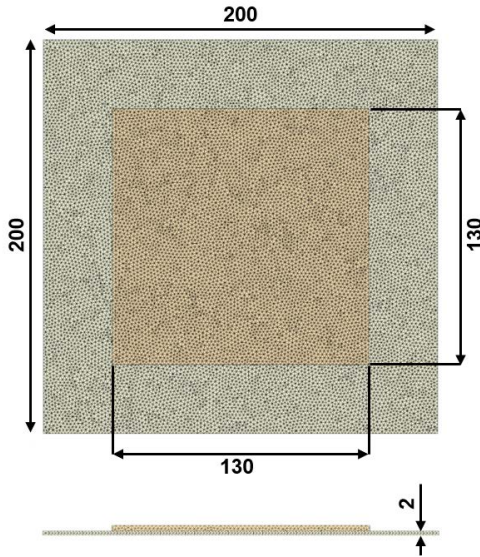
Figure 4.54: Meshed plate and initial charge in Moldflow adapted from Revfi, Mikus, et al. (2020)

The results of the mold filling simulations are transferred to the shell model in Abaqus using the two-stage mapping. For this purpose, the engineering constants are first mapped to a regular eight-layer hexahedral model and then transferred to a nine-layer shell layup model. Following the findings of Subsection 4.3.1.2, S8R elements with a quadratic approach function are applied due to the available computational capacities. Then, the shell model is loaded. During the optimization, the plate is subjected to a displacement-controlled load with a displacement of 10 mm in negative z-direction (see Figure 4.55).
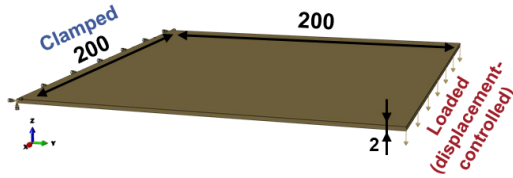
Figure 4.55: Model of the one-sided clamped plate under displacement-controlled load adapted from Revfi, Mikus, et al. (2020)

Based on the resulting stresses, the principal bending stresses and the trajectories in the specified design area (see Figure 4.56 (a)) are calculated. The calculated trajectories are illustrated in Figure 4.56 (b). Despite the same initial configuration in the process simulation as in the verification of the two-stage mapping in Subsection 4.3.1.2, different trajectory positions and courses result here, since a different edge is loaded (x-direction), a different design area is defined and the displacement-controlled loading causes a different stress state compared to the force-controlled loading.
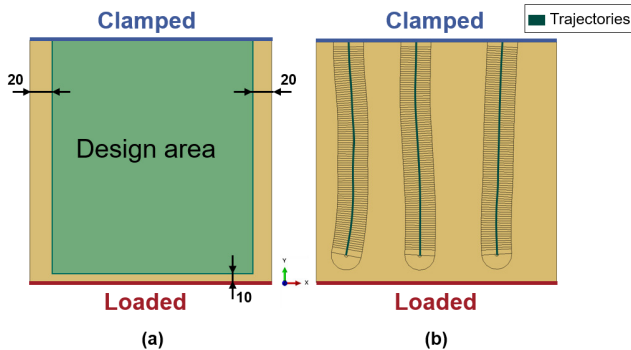
Figure 4.56: Bead optimization of the one-sided clamped plate: (a) design area (b) bead trajectories

In the partitioned area around the trajectories, an element edge length of 0.4 mm is specified so that the bead cross sections can be modeled accurately enough. Outside the partitioned areas, an element edge length of 1.6 mm is defined.

Based on the calculated trajectories, the genetic algorithm creates generations of eight individuals, which are assigned bead parameters in the specified ranges from Table 15. For the chosen local element edge length of 0.4 mm, which is a good tradeoff between simulation time and accuracy, these parameter ranges ensure a sufficiently precise modeling of the bead geometry and a high mesh quality.

Table 15:   Bead parameter range

Parameter	Range	Unit
Bead height	11-18	mm
Bead width	24-25	mm
Flank angle	70-86	°
Base radius	2-4	mm
Head radius	2-4	mm

The beaded shell models are then used as the middle surface for a both-sided offset mesh to again create an eight-layer solid model, whose manufacturing process in compression molding is simulated in Moldflow (also eight element layers through the thickness). This is followed by a mapping of the calculated engineering constants and fiber orientations onto the solid model generated by the two-sided offset, which allows the structural analysis to be performed.

For the load-adapted generation of beads, the stiffness has to be evaluated considering strength restrictions. For this purpose, it is necessary to specify the tensile strength R^t, the compressive strength R^c and the shear strength R_{shear} (see Subsection 4.2.1.3). For the tensile strength R^t and the compressive strength R^c, the values determined by Trauth (2018)[44] for the present SMC material are used. Since the developed optimization method is intended to support the product developer in generating an initial design draft, the most conservative values are applied in order to avoid eliminating too many solutions by the maximum stress criterion. The detailed dimensioning of the part with respect to its failure has to be done in later

---

[44]   Anna Trauth (DFG GRK 2078/1, Project C3) of the Institute for Applied Materials – Materials Science and Engineering (IAM-WK, KIT)

phases of the product engineering process. To determine the shear strength value R_{shear}, which is needed for the strength constraint, shear tests (see Figure 4.57) were performed in cooperation with Project C3[40] of the DFG GRK 2078/2.

(a)   **(b)**
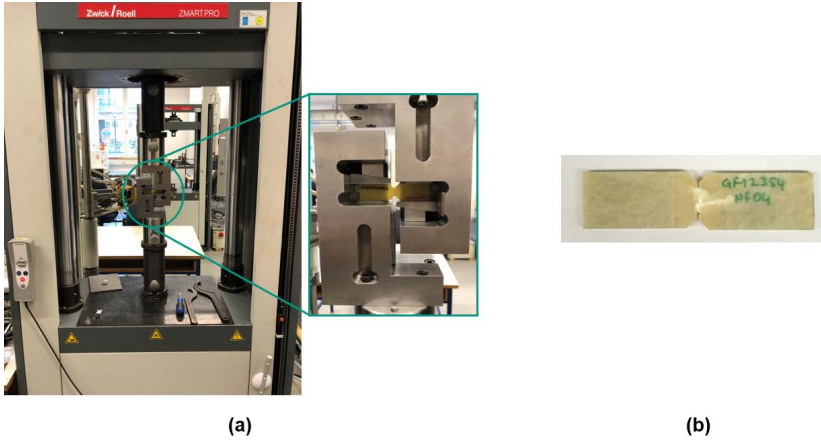
Figure 4.57: Shear test. (a) Experimental setup (b) shear-failed specimen

Table 16 summarizes the strength values applied for the maximum stress criterion in Equation 44. When evaluating the strength constraint during the optimization, another model assumption is made: Elements located directly at the clamped area are not taken into account in the evaluation because they are sensitive to numerical errors and can therefore overestimate the occurring stress.

Table 16:   Chosen strength values for the maximum stress criterion for SMC in the optimization of the one-sided clamped plate

Parameter	Symbol	Value	Unit
Tensile strength	R^t	55	MPa
Compressive strength	R^c	180	MPa
Shear strength	R_{shear}	116.3	MPa

To verify the optimization method, the process-based optimization approach is compared to optimization results generated based on isotropically modeled SMC. For this purpose, the isotropic material properties for the SMC are taken from Table 14.

(b) Verification

In the following, the results generated by the optimization method are presented and discussed in order to answer the fourth research question of the first research hypothesis (see Section 3.1). The SMC optimization method consists of the validated and verified submethods from the Subsections 4.3.1.1 to 4.3.1.3. To verify the optimization method, a stiffness optimization without strength constraint is performed first. Here, the results generated based on anisotropic material properties are compared to the results of an isotropic optimization run. Following this study, which does not result in load-adapted bead cross sections, the results with consideration of the strength constraint are presented in a second step.

(i) Stiffness optimization without strength constraint

First, the optimization method without strength constraint is discussed. Consequently, the optimization objective is to identify the volume-specific stiffest bead cross section based on the calculated trajectories (see Figure 4.56 (b)). For this purpose, the bead parameters are varied within the limits given in Table 15. Figure 4.58 shows the fitness values of the simulated anisotropic individuals in dependence on the different bead parameters.

Figure 4.58 clearly shows that the bead height is the parameter with the biggest influence on the achievable stiffness. This can be seen from the gradient of the individuals with the lowest fitness for the respective bead height (see dashed line in Figure 4.58 (a)). Also, the bead width is a stiffness influencing parameter, although the influence is not as big as for the bead height (see Figure 4.58 (b)). For the head and base radius, stiffer individuals are found with decreasing radii (see Figure 4.58 (c) and Figure 4.58 (d)). This can be explained by the fact that in the chosen modeling of the bead cross section by the piecewise defined function, smaller radii lead to a larger top chord. Since the material in the top chord is at a maximum distance from the centroidal axis, it significantly contributes to the increase of the second moment of area. But these findings for beads in SMC initially are not new compared to the experience with beads in steel sheets. However, a less clear tendency can be seen when looking at the fitness value versus the flank angle in Figure 4.58 (e).
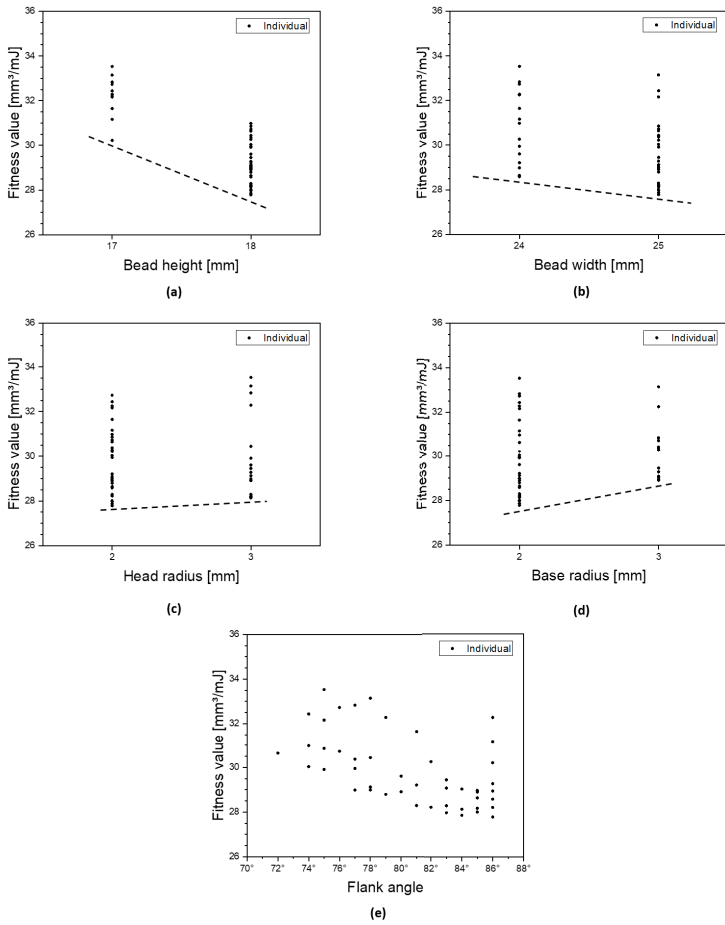
Figure 4.58: Anisotropic SMC optimization. Fitness values over different bead parameters: (a) bead height (b) bead width (c) head radius (d) base radius (e) flank angle

Although the stiffest bead cross section results from the extreme values of the bead parameters (see Table 17), the geometry with 85° flank angle (with extreme values for all other parameters) does not correspond to the expectation, since it yields a less specifically stiff result than the bead cross section with 84° flank angle (with extreme values for all other parameters).

Table 17: Optimum bead cross section (anisotropic SMC)

Parameter	Range	Unit
Bead height	18	mm
Bead width	25	mm
Flank angle	86	°
Base radius	2	mm
Head radius	2	mm

From the analytical consideration of the second moment of area, it can be derived that a steeper flank leads to a larger second moment of area. For the present optimization, the bead cross section with 85° flank angle is less stiff than the geometry with 86° flank angle, but at the same time less stiff than the geometry with 84° flank angle. This observation can also be confirmed with a further refinement of the mesh in Moldflow to an edge length of 1.4 mm (instead of the initial 2 mm).

In order to exclude an error in the optimization method that causes this result, a verification of the optimization workflow is carried out first. For this purpose, isotropic material parameters are used (see Table 14). Since the part stiffness, assuming isotropic, direction-independent material properties, only depends on the second moment of area achieved with the bead cross section, the optimization method also has to find the optimum in the geometry with the extreme values of the bead parameters (maximum height, maximum width and maximum flank angle as well as minimum head and base radius) if the workflow is correct. Moreover, it also has to show a clear tendency with regard to the flank angle. There is no further influence on the stiffness when assuming isotropic material properties (since no material thinning or similar is modeled within the scope of this work). Consequently, this means that steeper flanks must lead to a higher stiffness. Figure 4.59 illustrates the results of the isotropic optimization.
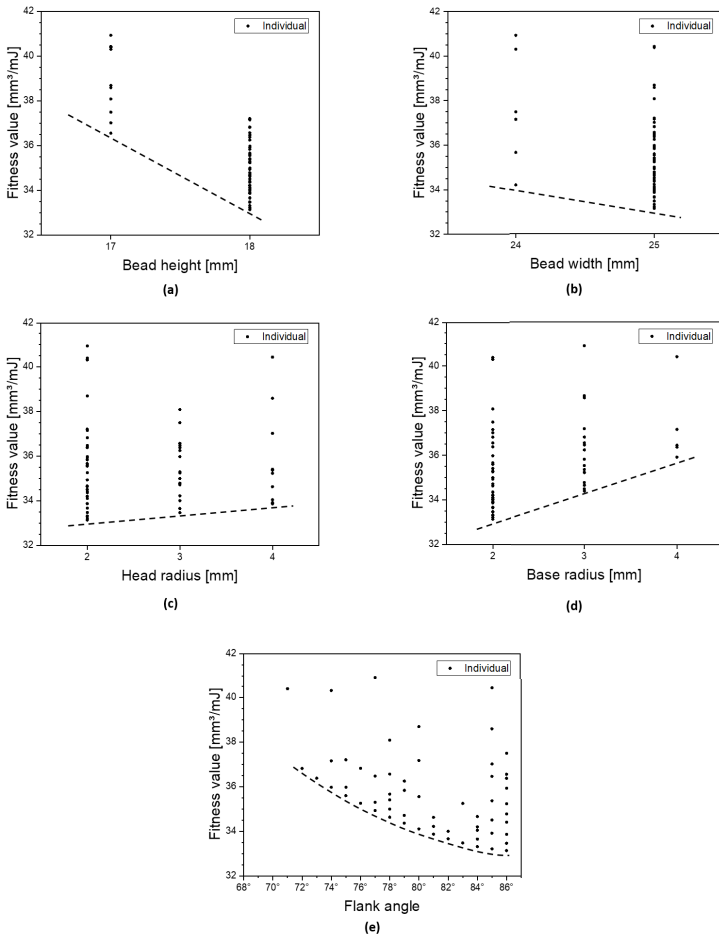
Figure 4.59: Isotropic SMC optimization. Fitness values over different bead parameters: (a) bead height (b) bead width (c) head radius (d) base radius (e) flank angle

It is instantly noticeable that the isotropically calculated fitness values are higher compared to the anisotropically calculated fitness values from Figure 4.58. This indicates a lower stiffness of the individuals. Considering the findings that the structural simulations performed on the basis of the compression molding results lead to sufficiently accurate agreements with real experiments (see Subsection 4.3.1.3), it can be concluded that the isotropically calculated stiffnesses provide the product developer with insufficient information.

As expected, the stiffest bead cross section is achieved in the extreme values of the bead parameters, analogous to the anisotropic optimization (see Table 17). In contrast to the anisotropic optimization, the isotropic optimization shows a clear tendency in the flank angle up to 86° (see Figure 4.59 (e)). From these results, it can be concluded that the optimization method is verified.

Obviously, the integration of the process-based fiber orientations and material properties leads to the deviating results observed in the anisotropic optimization. The hypothesis stated in Subsection 4.1.1 seems to be confirmed: Due to the fiber orientations resulting from the manufacturing process, the material stiffness partially compensates for the lower geometric stiffness. As discussed in Subsection 4.1.1, this effect can occur especially for large flank angles, since the gain in specific stiffness is smaller for larger flank angles. To verify this hypothesis, the angle φ between the fiber preferential direction (1-direction) and the isotropically determined direction of the maximum (magnitude) principal stress σ_P is analyzed in the following (see Figure 4.60).
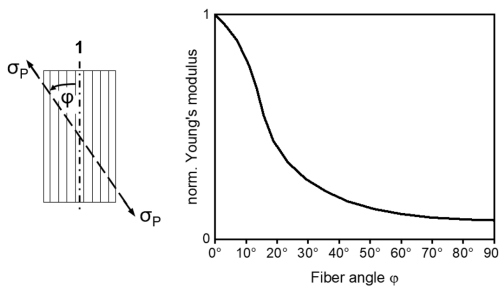
Figure 4.60: Fiber angle dependence of the Young's modulus adapted from Roos et al. (2017)

The isotropically determined direction of the maximum (magnitude) principal stress is chosen because the fibers should be oriented exactly in this direction in a load-adapted design.

The less the fibers deviate from the load direction, the more they contribute to the stiffness (see Figure 4.60). Therefore, the angular range $0° \leq \varphi \leq 45°$ is examined in the following. Figure 4.61 shows the number of elements in the respective angular range. When analyzing the diagram, it should be kept in mind that all three models have the exact same number of elements, so that the results are directly comparable with each other.
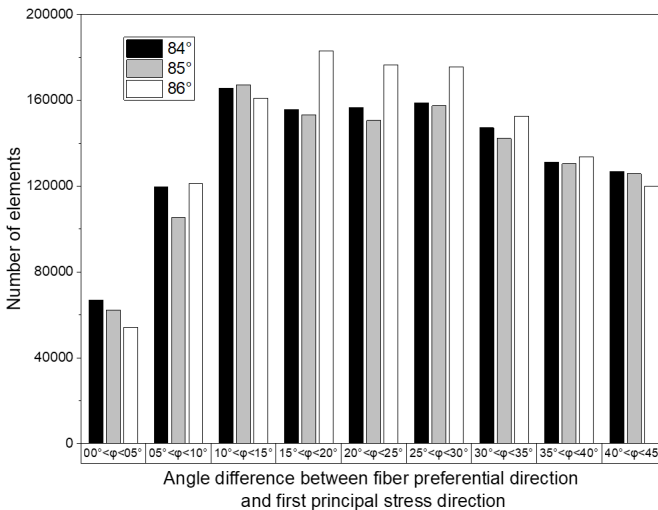
Figure 4.61: Number of elements with fiber orientations in the angle difference to the isotropically determined maximum (magnitude) principal stress

It is noticeable that the bead cross section with a flank angle of 84°, with the exception of the range of $10° \leq \varphi \leq 15°$, consistently has fiber orientations better suited to the present load case compared to the geometry with 85° flank angle. Especially in the highly stiffness-relevant range between $0° \leq \varphi \leq 10°$, there are significantly more elements in the geometry with the flank angle of 84°.

Figure 4.62 shows the cumulative number of elements in each range. Again, it should be noted that all three models have the exact same number of elements.
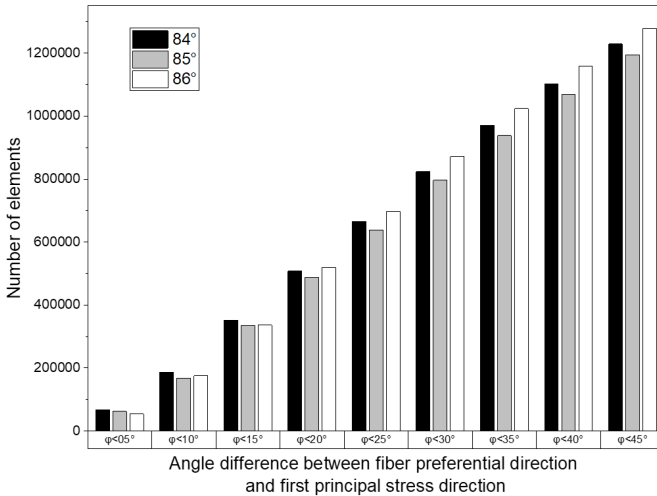
Figure 4.62: Cumulated number of elements in the specified angle difference

In addition to the previously described finding, it can be seen that the 85° and 86° flank angle geometries have similar numbers of elements in the range between $0° \leq \varphi \leq 10°$. However, the 86° geometry has a larger second moment of area, which makes it the absolute stiffest configuration in the combination of material stiffness and geometric stiffness. It also outperforms the 84° geometry, which has the most elements in this highly stiffness-relevant angular range between $0° \leq \varphi \leq 10°$. The larger number of elements advantageously oriented for the load case is also observed in the geometry with the flank angle of 84° compared to the geometry with a flank angle of 85° in the sum of elements up to an angular difference of $\varphi=45°$ between fiber orientation and load direction (see Figure 4.62). This analysis helps to explain the calculated fitness values.

In summary, the analysis of the angles between fiber preferential direction and the isotropically determined direction of the maximum (magnitude) principal stress supports the hypothesis that for certain parameter configurations the material stiffness

can compensate for the geometric stiffness. The presented result for the concrete values of the bead parameters is not generalizable and only applies to the described boundary conditions (initial charge geometry and position, load case, fiber orientation distribution, etc.). However, similar results were observed by the author for other bead patterns and slightly different process and material configurations (Revfi, Mikus, et al., 2020). In these studies, a bead cross section with 85° flank angle represented the specifically stiffest geometry. Thus, it can be concluded that the specific stiffest bead cross section depends on design, manufacturing and material, which proves the strong interdependency of the three subdisciplines for fiber-adapted design (see Subsection 2.3.3) also for the design of beads. Accordingly, the product developer is faced with application-specific challenges in the design of beads in SMC parts, to which there is no general solution. Rather, individual support is required in the initial design phase, which is offered by the presented method for bead optimization. However, the studies without strength constraint are of theoretical nature. More relevant for the practical application of the optimization method is the load-adapted bead design, which can only be achieved by taking the strength of the material into account. This will be discussed in the following.

(ii)   Stiffness optimization with strength constraint

In this subsection, the previously described bead optimization is repeated, but this time a strength constraint is additionally taken into account when evaluating the individuals. This means that, in addition to the fitness value, it is also checked whether the evaluated individual is only exposed to stresses within the specified limits (see Table 16).

Table 18 shows a comparison of the results of the optimization based on isotropic material properties and the process-based, anisotropic optimization under consideration of the strength constraint. In this context, it is important to mention that the meshes for the anisotropically and the isotropically simulated geometry are completely identical for each case. As a consequence, the results for the stresses are element- and mesh-independent and thus directly comparable with each other. This is an important requirement with regard to the evaluation of the strength constraint.

Since all adjacent parameter combinations around the respective optimum were simulated, a global optimum can be assumed with high likelihood.

Table 18: Optimization results (with strength constraint)

Parameter	Value	
	Isotropic optimization	Anisotropic optimization
Bead height	14 mm	13 mm
Bead width	25 mm	25 mm
Flank angle	71°	71°
Base radius	3 mm	4 mm
Head radius	2 mm	2 mm
Fitness value	56.13 mm³/mJ	54.25 mm³/mJ
Max. principal stress	54.59 MPa	54.24 MPa
Min. principal stress	98.70 MPa	91.59 MPa
Max. shear stress	46.67 MPa	44.24 MPa

In the optimizations, the calculated trajectory positions and courses allowed the individuals to achieve the maximum possible width of 25 mm (see Table 18) without exceeding the specified minimum distance between two beads. At the same time, the bead width is a stiffness-relevant parameter, which has, in the investigated example, only a minor influence on the resulting maximum stresses (in the critical region). Since, as seen in Figure 4.58, the bead width and the bead height are the two bead parameters that significantly influence the stiffness, in this case, a directed gradient is given in the search for the optimum. This means that, while maintaining the maximum bead width, the genetic algorithm only has to search in the direction of greater bead heights. If a certain bead height can be realized under consideration of the strength constraint, the algorithm does not need to analyze smaller bead heights anymore, since these would lead to smaller stiffness values due to the large influence of the bead height on the resulting stiffness (see Figure 4.58).

Furthermore, as shown in Table 18, the head radii have taken the minimum value of 2 mm. The reason for this is that the smallest possible head radius leads to an increase in the size of the top chord and thus to a larger second moment of area. Due to the load applied to the part, the head radii do not represent a strength-critical parameter (see Figure 4.63) and can be minimized by the optimizer.

This is different for the base radii. Due to the applied load, the base radius is responsible for exceeding the strength constraint (see Figure 4.63). The exceeding of the value defined in the strength constraint occurs at the base radius of the right bead. In addition, the influence of the anisotropic material modeling can be seen in Figure 4.63. Whereas in the case of isotropic material modeling (see Figure 4.63 (b)) a uniform stress distribution at the end of the beads can be seen, in the case of anisotropic material modeling (see Figure 4.63 (a)) an asymmetric stress distribution can be observed. This is particularly evident at the left bead.
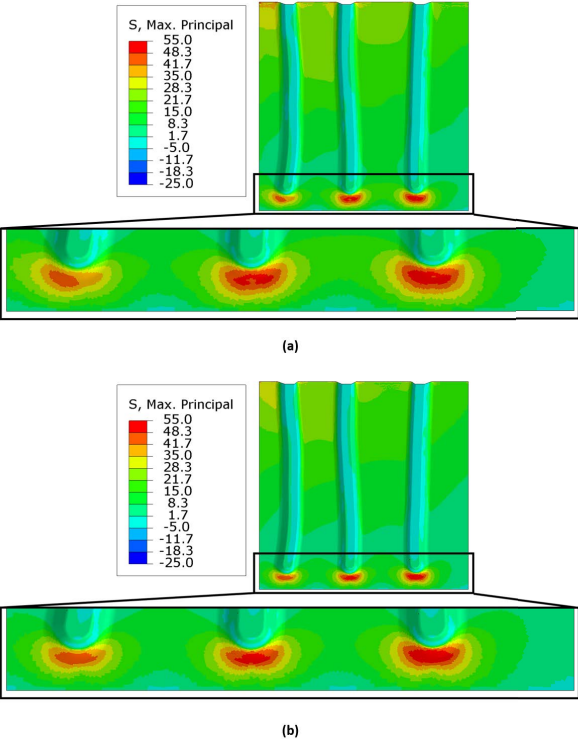
Figure 4.63: Maximum principal stress distribution for the (a) anisotropic and (b) isotropic optimization result

With the isotropic optimization, a bead height of 14 mm with a flank angle of 71° and a base radius of 3 mm can be realized (see Table 18). This results in higher geometric stiffness compared to the process-based optimum. In the process-based optimization, a cross section with a bead height of only 13 mm, also a flank angle of 71° and a larger base radius of 4 mm can be achieved as an optimum that passes the strength constraint (see Table 18). However, when considering the tensile stress versus the parameter bead height in Figure 4.64, it is noticeable that the optimum is the only individual with the height of 13 mm that just passes the strength constraint (54.24 MPa < 55 MPa (limit value for tensile strength)). In the case of a more conservative design, the product developer could therefore also decide to select the best individual with a bead height of 12 mm, which has a similar specific stiffness (54.76 mm³/mJ > 54.25 mm³/mJ (optimum)).
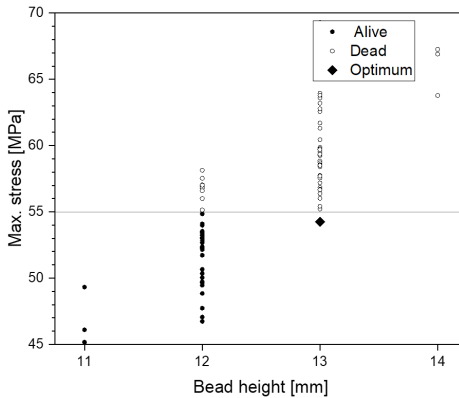
Figure 4.64: Influence of the strength constraint on the bead height

Regardless of whether it is continued conservatively or with the found optimum, it is to be noted that the isotropically identified bead cross section differs from the process-based bead cross section. This finding confirms the need of the process-based procedure, which can already be demonstrated by this simple application example. The difference in the stiffness-optimized bead cross sections resulting from the optimizations is illustrated graphically in Figure 4.65. Also for other bead patterns and other process and material configurations, the influence of the manufacturing process on the volume-specific stiffest bead cross section could already be confirmed (Revfi, Mikus, et al., 2020).
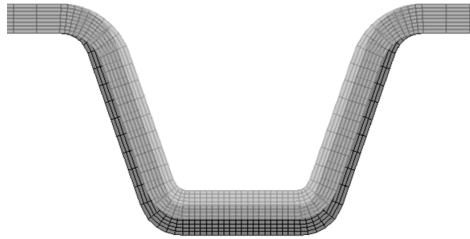
Figure 4.65: Bead cross section of the one-sided clamped plate for the bead pattern from Figure 4.56 (b): isotropic (dark gray) and anisotropic (light gray) optimum under consideration of the strength constraint

As a finding of the investigation of the one-sided clamped plate, it can be stated that the bead height in the process-based optimization is always smaller than with isotropic material modeling. In addition, it can be seen that the radii need to be considered together with the flank angle in order to evaluate the strength. Therefore, a general statement regarding the choice of these three beading parameters cannot be made. The evaluation has to be carried out individually in each case, taking into account all boundary conditions from the manufacturing process and structural mechanics. The bead width could always be set to the maximum possible width due to the bead parameters defined for this example. However, this only applies to this example and cannot be generalized, as the subsequent optimization of the demonstrator part will show.

In the next step, the developed optimization method discussed using the simple example of the one-sided clamped plate is applied to the demonstrator part without UD-tapes.

DiCo Demonstrator Part (Without UD-Tapes)

First, the model design is described, for which the results of the verification are then presented. Since the methodical procedure has already been discussed in detail before, this subsection is presented in a compact form.

(a) Model Design

For the bead optimization of the demonstrator part, the model shown in Figure 4.66 is employed. This corresponds to the model derived for the real experimental setup in Figure 4.40 except for the plateau shown in Figure 4.44, in which the beads are positioned. This plateau was only designed to allow a maximum bead height of 18 mm to be achieved with the molds used in the DFG GRK2078/2 project. This geometry adaptation, which was specially made for the mold at Fraunhofer ICT, was neglected in the optimization because the verification in the project is performed virtually and therefore no new insert is produced.
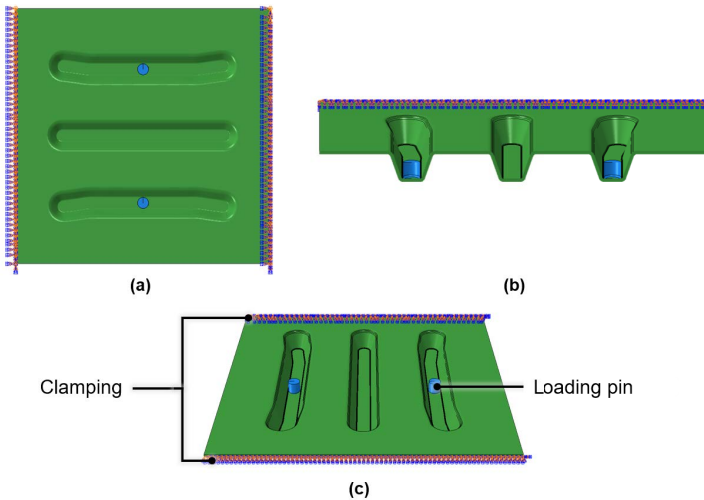
Figure 4.66: Model setup for the optimization of the demonstrator part. (a) Top view (b) sectional view (c) oblique top view adapted from Revfi, Fünkner, et al. (2021)

The demonstrator part has a thickness of 2 mm. The position and geometry of the initial charge can be seen in Figure 4.23. The height of the initial charge is iteratively adjusted so that there is an additional volume of 21% for each geometry generated in the optimization. The element edge length in Moldflow is defined as 4 mm. This choice was made as a trade-off between computation time and result accuracy and is consistent with Moldflow recommendations of an edge length of 1-2 times the part

thickness (Autodesk Support, 2020). Through the thickness of the demonstrator part, eight element layers are defined and the Advancing Layers mesh algorithm is used, analogous to the one-sided clamped plate.

The bead pattern corresponds to the one of the physical demonstrator part (see Figure 4.20). In the structural model, an element edge length of 0.4 mm is specified in the partitioned area around the trajectories, as for the one-sided clamped plate, so that the bead cross sections can be represented accurately enough. Outside the partitioned areas, an element edge length of 1.6 mm is defined. The structural model is created using eight hexahedral element layers (C3D8R) through the thickness, just like for the one-sided clamped plate.

The genetic algorithm creates generations of eight individuals which are assigned values for the bead parameters as design variables within the value ranges given in Table 19. For each of the individuals, a process simulation is performed in Moldflow using the model validated in Subsection 4.3.1.1, and the engineering constants and fiber orientations are mapped to the eight-layer structural model shown in Figure 4.66.

Table 19: Bead parameter range for the optimization of the demonstrator part (Revfi, Fünkner, et al., 2021)

Parameter	Range	Unit
Bead height	11-18	mm
Bead width	25-30	mm
Flank angle	70-86	°
Base radius	2-4	mm
Head radius	2-4	mm

When generating the individuals by the genetic algorithm, the parameter sets are checked for the resulting top chord width. Since the loading pin has a diameter of 10 mm (see Figure 4.43), a minimum top chord width of 12 mm was defined. In addition, the strength constraint was specified using the values from Table 20. Compared to the one-sided clamped plate, a larger tensile strength of 121.2 MPa is chosen. This is explained by the fact that the demonstrator parts tested in the experiment plastically deform at a displacement of 2.25 mm (see Subsection 4.3.1.3). With this information, the demonstrator part with 2 mm wall thickness from Subsection 4.3.1.3 was evaluated with respect to the stresses occurring at this

displacement and the value of 121.2 MPa was identified. This allowed the conservative value chosen for the one-sided clamped plate to be replaced. The values for compressive and shear strength are retained.

Table 20: Chosen strength values for the maximum stress criterion for SMC in the optimization of the demonstrator part

Parameter	Symbol	Value	Unit
Tensile strength	R^t	121.2	MPa
Compressive strength	R^c	180	MPa
Shear strength	R_{shear}	116.3	MPa

The optimization objective was defined as a linear elastic displacement of 3 mm taking into account the strength constraint (Revfi, Fünkner, et al., 2021). Accordingly, the demonstrator part geometry in the experiments would not be a valid solution, since the linear elastic region is exceeded after 2.25 mm.

In order to support the product developer in the initial design process, the developed bead optimization method shown in the IPEK coupling framework in Figure 4.17 is applied. The results obtained from the optimization are discussed in the following.

(b) Verification

For the verification of the optimization method, the process-based optimization approach is compared to optimization results generated on the basis of isotropically modeled SMC. For this purpose, the isotropic material properties for the underlying SMC from Table 14 are used. The results of the two optimizations are the bead parameter combinations shown in Table 21. Again, it should be mentioned that the meshes for the anisotropically and isotropically simulated geometry are completely identical in each case. Thus, as already mentioned for the one-sided clamped plate, the optimization results are directly comparable.

It can be seen from the results that the head radius is the only bead parameter that is identical in the comparison of the two optimization results. The stiffness-relevant parameter of the bead height differs by 3 mm (Revfi, Fünkner, et al., 2021). A detailed discussion of the results is not presented here due to the analyses already carried out for the one-sided clamped plate. These can be conducted analogously for the demonstrator part.

Table 21:   Optimization results for the load-adapted initial design of the demonstrator part (Revfi, Fünkner, et al., 2021)

Parameter	Value	
	Isotropic optimization	Anisotropic optimization
Bead height	17 mm	14 mm
Bead width	29 mm	28 mm
Flank angle	71°	72°
Base radius	3 mm	4 mm
Head radius	2 mm	2 mm

To visualize the differences between the two optimization results, the stiffness-optimized bead cross sections are again illustrated graphically in Figure 4.67. This also shows that the initial design based on isotropic material properties would have involved a costly and time-consuming trial-and-error process to achieve a load-adapted design (Revfi, Fünkner, et al., 2021).
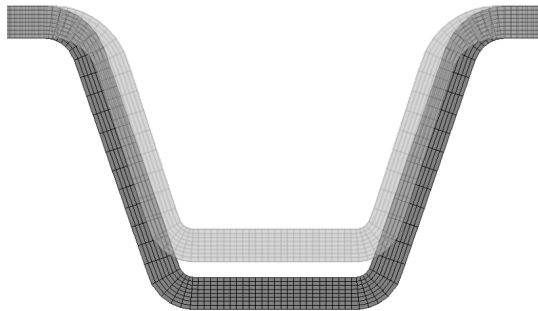
Figure 4.67: Bead cross section of the demonstrator part: isotropic (dark gray) and anisotropic (light gray) optimum under consideration of the strength constraint (Revfi, Fünkner, et al., 2021)

As a general finding that can be derived from the optimization results of the plate and the demonstrator part – and thus to answer the research question formulated at the beginning of the section – it can be stated that the bead height, as a parameter that significantly influences the stiffness, is always smaller in the SMC process-based optimization than with isotropic material modeling. This has to be taken into account in the initial design process. As a further finding, it can be concluded that it is not possible to make a general statement regarding the choice of the other bead parameters. They have to be chosen individually and with regard to the load case, the initial charge geometry, the initial charge position, the resulting fiber orientations, etc. This makes the developed method indispensable as a support tool for the product developer in the initial design of beaded SMC parts.

Finally, the optimization of the demonstrator parts reinforced with UD-tapes is presented. The integration of the optimization of the tape positions into the just discussed automated optimization was not part of the research work, since an automated optimization of the tape positions for stiffness increase has already been presented by Fengler et al. (2019).

CoDiCo Demonstrator Part (with UD-Tapes)

In the development of the CoDiCoFRP design, the problems of tape delamination described in Subsection 4.3.1.3 were found when only the top chords were reinforced. Therefore, this subsection addresses the optimization of the tape design taking into account the bead cross sections to support the tape positioning during mold filling.

(a) Model Design

In order to prevent the UD-tapes in the top chord from flaking off, a new tape geometry is developed that extends from the clamped area across the entire demonstrator part. Moreover, instead of reinforcing all three beads, only the two beads where the load is applied are reinforced (see Figure 4.68).

The validation of the results is conducted using a demonstrator part with a wall thickness of 1.8 mm. In the production of the real demonstrator parts, the initial charge position was chosen centrally in the mold (see Figure 4.29). This is modeled accordingly in the mold filling simulation in Moldflow. For the further modeling of the optimized demonstrator part, the procedure is analogous to the one for the first development generation in Subsection 4.3.1.3. The load case and the clamping remain the same, which is why the boundary conditions are modeled identically (see Figure 4.44). Also, three layers of tetrahedral elements with quadratic shape function

(C3D10 elements) are used again to model the SMC base part in the thickness direction (see Figure 4.50).

Figure 4.68: CoDiCo demonstrator part with optimized, I-shaped UD-tapes

One difference is the modeling of the tapes in the recesses. Here, the new I-shaped tape geometry has to be implemented. Again, shell elements with reduced integration and an element edge length of 2 mm are employed. However, due to the more complex geometry, not only quadrilateral shell elements, but also triangular elements in a quad-dominated mesh are applied (see Figure 4.69).
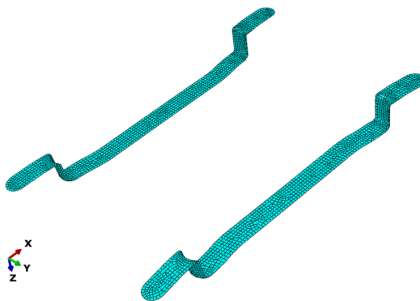
Figure 4.69: Mesh of the I-shaped UD-tapes in Abaqus

The composition of the used tapes, consisting of three individual UD-tapes in a 0°/90°/0° stacking, is again implemented via shell layups. For this, the 0° direction follows the centerline of the tape. The thickness of the tapes in the produced batch was 1.1 mm. Accordingly, a total thickness of 1.1 mm is modeled, which is equally subdivided among the three tape layers with 0.37 mm.

The results generated by this modeling are presented in the next subsection and the simulations are validated.

(b) *Validation*

Figure 4.70 (a) shows the force-displacement curves of two experimentally measured data sets of demonstrator parts with I-shaped UD-tapes, the simulation results generated for this case, and the force-displacement curve of an unreinforced demonstrator part with a thickness of 1.8 mm.

First, the experimental results are discussed. Within the scope of the scatter, the two investigated demonstrator parts show a very similar force-displacement behavior. When analyzing the data, it is noticeable that two different slopes of the curves can be identified in the considered range up to 2.25 mm displacement of the loading pins. At about 1.25 mm displacement, the slope of the curves decreases (see dashed line in Figure 4.70 (a) and (b)). Obviously, from this point on, the demonstrator part responds softer to the load. This significant difference in the slopes of the tangents is an indicator of the beginning failure of the tape adhesion to the demonstrator part. This failure has the effect that the desired increase in stiffness can no longer be achieved with the tapes. Accordingly, at 2.25 mm displacement, the result is that the geometry reinforced with the I-shaped tape requires a very similar force for further deformation as the unreinforced geometry (see Figure 4.70 (a)). The failure of the tapes at 1.25 mm displacement can be explained by the point of force application. By applying the load into the two beads, the tapes are immediately subjected to the force, which causes the interface between the SMC base part and the tape to fail more quickly. Since, as described before, no modifications could be made to the compromise solution of the load case within the scope of the research project, only the linear elastic region up to 1.25 mm with a properly functioning tape adhesion will be considered in the following.
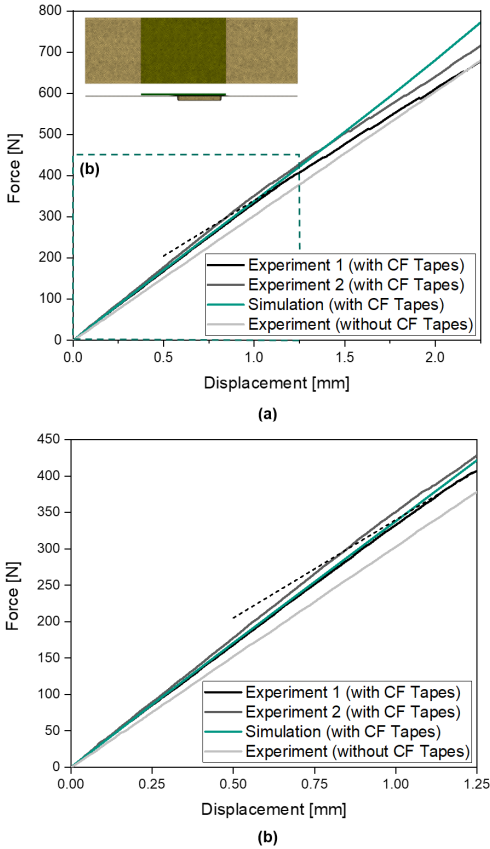
Figure 4.70: Force-displacement diagram: I-shaped UD-tape reinforced demonstrator part with 1.8 mm wall thickness (experiment and simulation) and unreinforced demonstrator part with 1.8 mm wall thickness (experiment)[42]. (a) Displacement up to 2.25 mm (b) detailed view: displacement up to 1.25 mm. The dashed line indicates the slope of the straight line determined on the basis of the experimental data, which decreases as the tapes begin to fail.

In this region up to 1.25 mm displacement, which is shown enlarged in Figure 4.70 (b), there is a very high agreement between the experimental and the simulated results. For the displacement of 1.25 mm, experiment 1 shows a force of 407.3 N, while experiment 2 indicates a force of 428.8 N. In comparison, the simulation predicts a force of 421.9 N. Thus, deviations of 3.5% and 1.6%, respectively, are obtained. This can be evaluated as a very high agreement of the results that can be achieved with the help of the simulation. Furthermore, it can be seen in this region that the tapes lead to an additional stiffening of the demonstrator part with an intact adhesion. The demonstrator part without tapes requires a force of 378.2 N to deform 1.25 mm. In relation to the demonstrator part reinforced with the I-shaped tape, this results in a stiffening effect of 7.1% and 11.8%, respectively. This shows the potential of the integration of the tape into the CoDiCo design of the demonstrator part. One of the reasons for the stiffening effect falling short of expectations is the concentrated force application on the tapes.

After verifying and validating the models and methods for the SMC material system in Subsection 4.3.1, in the next subsection the models for the LFT material system are verified.

4.3.2 LFT

As there was no production of LFT parts in the DFG GRK 2078/2 project, the mold filling simulation and structural behavior cannot be validated for this material system. However, a fully characterized LFT material system from the Moldflow database is used at this point (see Subsection 4.2.2). Based on the previously developed coupling for SMC, which now serves as a reference system element, an analogous approach is followed for LFT, adapting the flow simulation according to the model assumptions from Subsection 4.2.2.1. As an essential difference, the residual stresses occurring in the LFT process are mapped in the automated optimization to be taken into account in the evaluation of the specific stiffness.

The content of these investigations has been published previously in the publication Revfi, Mikus, et al. (2021).

(a) Model Design

For the investigations of the influence of residual stresses in LFT materials on the stiffness-optimized bead cross section, the square plate under bending load already employed in the SMC studies is used again. The reasons for this choice have been explained previously (see Subsection 4.3.1.2). The square plate again has a side length of 200 mm and a thickness of 2 mm (Revfi, Mikus, et al., 2021). The LFT

polymer melt is positioned centrally in the mold. The model is meshed with tetrahedral elements by the mesh algorithm Advancing Front. An element edge length of 2 mm is chosen. Six element layers are defined through the thickness. (Revfi, Mikus, et al., 2021) The mesh of the plate and the polymer melt are shown in Figure 4.71.
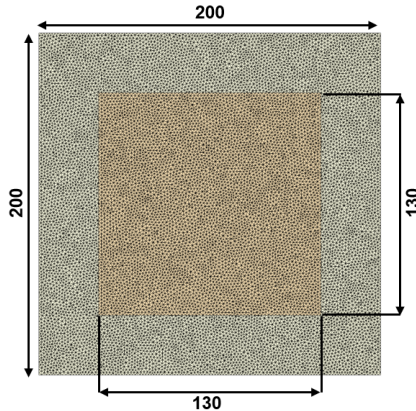
Figure 4.71: Meshed plate and polymer melt in Moldflow (Revfi, Mikus, et al., 2020)

In order to calculate the trajectories, the two-stage mapping is applied. Therefore, for the present LFT studies, the engineering constants are mapped according to the simulated fiber orientations to a six-layer hexahedral element model with an edge length of 2 mm in Abaqus. In a second step, the engineering constants are transferred to a seven-layer shell model (S4 elements) with an edge length of 2 mm. (Revfi, Mikus, et al., 2021) This procedure was developed in Subsection 4.3.1.2 for the simulations with SMC, but is to be considered independent of the chosen material system. Therefore, it can be resorted to at this point. The model generated in this way is assigned the load case and boundary conditions shown in Figure 4.55. The loaded edge is moved displacement-controlled 20 mm in negative z-direction (Revfi, Mikus, et al., 2021).

The stresses induced by the load in the part are used to calculate the principal bending stresses and principal bending stress trajectories (see Figure 4.72 (b)) in the specified design area (see Figure 4.72 (a)). As described in Subsection 4.2.2.2, residual stresses are not included for the calculation of the trajectories, since the

beads are intended to stiffen against external forces and not against residual stresses generated for a flat plate during processing.
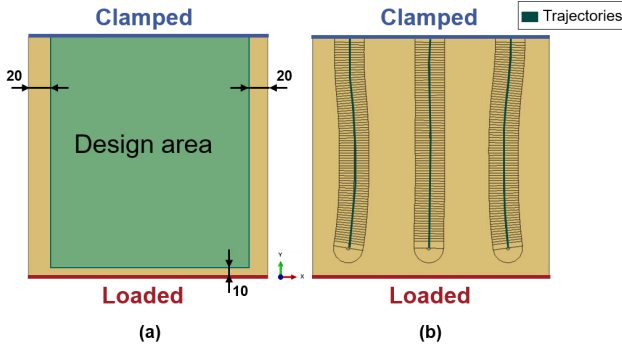
Figure 4.72: LFT optimization: (a) design area (b) bead trajectories

For the partitioned areas (see Figure 4.72 (b)), where the beads are generated by nodal displacement, a local element edge length of 0.4 mm is chosen. For the areas outside the partition, a global edge length of 1.6 mm is applied. Based on this model, the beaded shell part is generated, which subsequently serves as the middle surface for the both-sided offset. The solid models created by the offset are described with six hexahedral element layers through the thickness. (Revfi, Mikus, et al., 2021) Analogous to the SMC model, C3D8R elements are employed, which were found to be the preferred element type for the beaded models in the studies of Mikus (2019)[41]. As a result, there are about 1.3 million elements with about 1.5 million nodes per model. The exact element and node number depend on the specific bead width. Parts that have the same bead width contain exactly the same number of elements and nodes. (Revfi, Mikus, et al., 2021)

The solid models generated by the both-sided offset serve as an input for the mold filling simulation in Moldflow. The engineering constants calculated in Moldflow are subsequently mapped again to this both-sided offset solid model in Abaqus. However, in contrast to the SMC optimization method, the residual stresses are also mapped in this second mapping step and defined as initial stresses in the Abaqus model (see Subsection 4.2.2.2). Thus, the simulation in Abaqus for the LFT optimization method is divided into two steps. In the first step, the warpage caused by the

residual stresses is calculated. In the second step, the external loads are applied. As part of the modeling process, it is assumed for the present studies that the part to be optimized is mounted with other parts in an assembly. Consequently, two plane edges are present in the assembled state. This results in the following boundary and initial conditions. (Revfi, Mikus, et al., 2021)

First, the deformation of the clamped edge as well as the later loaded edge is restricted in the z-direction. However, a deformation in the xy-plane is possible. For the complete definition of the continuum problem, one node in the middle of the clamped edge is completely constrained in addition. Figure 4.73 shows an exemplary deformation state for the described boundary conditions before external loading. (Revfi, Mikus, et al., 2021)
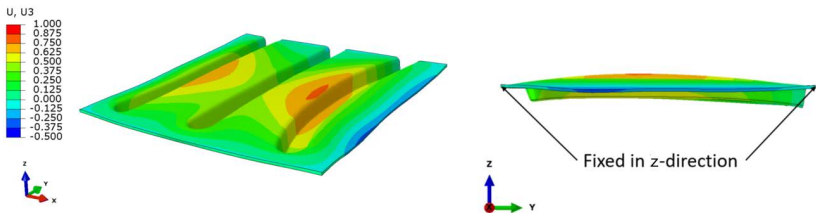
Figure 4.73: Deformation state induced by the residual stresses before the application of the external load. Displacement in z-direction (Scale factor: 10). (Revfi, Mikus, et al., 2021)

In the second simulation step, the external loads and boundary conditions are applied. At the clamped edge, all nodes are fixed and the nodes of the opposed edge are moved displacement-controlled by 20 mm in negative z-direction.

In the optimization, the bead parameters are varied by the genetic algorithm in the ranges given in Table 22. By applying an element edge length of 0.4 mm in the partitioned areas, radii of 2 mm can still be sufficiently represented, thus defining their lower limit.

Table 22:   Bead parameter range (Revfi, Mikus, et al., 2021)

Parameter	Range	Unit
Bead height	10-18	mm
Bead width	23-25	mm
Flank angle	70-86	°
Base radius	2-4	mm
Head radius	2-4	mm

For the tensile strength in the maximum stress criterion it is referred to the value stored in a plastics database (M-Base Engineering + Software GmbH, 2020). For the compressive strength it is assumed that it is as high as the tensile strength. This assumption is made here because the material could not be characterized in the DFG GRK 2078/2 project. The applied strength values are summarized in Table 23. However, these values can be substituted at any time.

Table 23:   Strength values for the maximum stress criterion for LFT adapted from
             Revfi, Mikus, et al. (2021)

Parameter	Symbol	Value	Unit
Tensile strength	R^t	113	MPa
Compressive strength	R^c	113	MPa
Shear strength	R_{shear}	90.4	MPa

Also, for LFT optimization, the elements in the clamped area are excluded from consideration in the strength constraint because they are sensitive to numerical errors, which can cause stresses to be overestimated (Revfi, Mikus, et al., 2021).

In the next subsection, the model built according to the previously described assumptions is verified.

(b) Verification

In the following, the influence of the process-induced residual stresses on the stiffness-optimized bead cross sections is investigated. Since there are complex superimposed effects for these geometries between geometric anisotropy, material anisotropy and the residual stresses, an estimation of the optimization results is not intuitive. Therefore, the verification is to be performed in three steps, with the strength constraint applied in each step. Also in these optimizations, the meshes for the anisotropically and isotropically simulated geometry are completely identical in each case. This means that the results for the stresses are element- or mesh-independent and thus directly comparable with each other.

In the first step, as a starting situation, an optimization based on isotropic material properties without consideration of residual stresses is performed. The necessary isotropic material properties were calculated for the selected LFT material[28] and are shown in Table 24.

Table 24:   Isotropic LFT material properties adapted from Revfi, Mikus, et al. (2021)

Parameter	Symbol	Value	Unit
Young's modulus	E_{iso}^{LFT}	3 299	MPa
Poisson's ratio	v_{iso}^{LFT}	0.338	-

The second step consists of an optimization based on linear elastic, locally anisotropic material properties from the manufacturing process but without considering residual stresses. Thus, this optimization corresponds to the method developed for SMC, except that the LFT material is selected in Moldflow and the model assumptions for the simulation of thermoplastics are implemented (see Subsection 4.2.2.1). The third step then corresponds to the most comprehensive optimization, which in addition to the procedure in the second step also takes into account the process-induced residual stresses.

(i)   Optimization based on isotropic LFT material properties

Table 25 shows selected results of the optimization based on the isotropic LFT material properties. The identified optimum is highlighted in gray. The other individuals are chosen because of their direct vicinity to the optimum. In the last column, the

minimum stress in the corresponding part is listed, as this minimum value leads to the strength constraint being exceeded in the present studies.

Table 25: Selected individuals of the isotropic optimization (optimum highlighted in gray) adapted from Revfi, Mikus, et al. (2021)

Width [mm]	Height [mm]	Flank angle	Head radius [mm]	Base radius [mm]	Fitness [mm³/mJ]	Min. stress [MPa]
25	16	83°	2	3	22.45	-123 (failure)
25	16	84°	2	4	23.34	-114 (failure)
25	16	83°	2	4	23.47	-113
25	16	82°	2	4	23.60	-112
25	16	81°	2	4	23.75	-111
25	15	85°	2	3	24.62	-112

The stiffness-optimized bead cross section has the maximum possible bead width of 25 mm, a height of 16 mm, a flank angle of 83°, a head radius of 2 mm and a base radius of 4 mm. With an occurring compressive stress of 113 MPa, the optimum just fulfills the strength constraint (cf. Table 23). All selected individuals in Table 25 have the maximum possible bead width of 25 mm, since a larger bead width increases the stiffness without (in the present example) affecting the strength. (Revfi, Mikus, et al., 2021)

Starting from the optimum, increasing the flank angle to 84° leads to a stiffer bead cross section because this results in a larger second moment of area. For an isotropic material modeling, a larger second moment of area can be directly seen from a smaller fitness value, since there is no individual contribution depending on the anisotropic material properties and the part stiffness is solely determined by the geometry. However, this increase in stiffness leads to a stress value of -114 MPa, which exceeds the limit for the compressive stress of 113 MPa (see Table 25). (Revfi, Mikus, et al., 2021)

A smaller base radius of 3 mm compared to the 4 mm of the optimum also results in a larger second moment of area and thus in a smaller fitness value, but also in exceeding the allowable compressive stresses (123 MPa > 113 MPa). The other individuals, which have a smaller flank angle or bead height, result in smaller fitness values due to their smaller second moment of area. (Revfi, Mikus, et al., 2021) This underlines that the optimization method can be considered verified.

Based on these results, the second verification step is carried out.

> (ii) Optimization based on anisotropic LFT material properties resulting from the manufacturing process, without consideration of residual stresses

In the next verification step of the optimization method, the anisotropic LFT material properties resulting from the manufacturing process are considered. For this, mold filling simulations are coupled into the optimization and their results are mapped onto the structural models. Residual stresses are not yet considered in this step.

Table 26 shows selected individuals of the optimization. The optimum is highlighted in light gray. The other individuals are bead parameter configurations that are in the direct vicinity of the optimum. The optimum has a bead width of 25 mm, a height of 13 mm, a head radius of 2 mm, a base radius of 4 mm and a flank angle of 81°. The first striking observation is that the optimum has a bead height that is 3 mm less compared to the isotropic optimization. This clearly shows the influence of the anisotropic material properties resulting from the manufacturing process on the optimization result. The consideration of the anisotropic material properties leads to a stress state that does not allow for a stiffer geometry. (Revfi, Mikus, et al., 2021)

Table 26: Selected individuals of the anisotropic optimization without residual stresses (optimum highlighted in light gray, further investigated individuals highlighted in dark gray) adapted from Revfi, Mikus, et al. (2021)

Width [mm]	Height [mm]	Flank angle	Head radius [mm]	Base radius [mm]	Fitness [mm³/mJ]	Min. stress [MPa]
25	13	81°	2	3	25.75	-119 (failure)
25	13	81°	2	4	26.83	-110
25	13	83°	3	4	26.90	-105
25	13	78°	2	4	27.00	-105
25	13	79°	2	4	27.07	-107
25	13	83°	2	4	27.07	-103
25	13	81°	3	4	27.10	-111

All individuals shown in Table 26 have the maximum bead width of 25 mm defined by the upper limit. The reason for that, analogous to the explanation in the isotropic optimization, is the relevance of the bead width for the stiffness, whereby the bead

width in the present example is not relevant for the strength (Revfi, Mikus, et al., 2021).

In order to check the plausibility of the optimization result, the individuals in the direct vicinity of the optimum are analyzed in more detail in the following. A reduction of the base radius from 4 mm to 3 mm leads to a larger second moment of area and thus to a smaller fitness value. At the same time, however, this change in the bead cross section causes the allowable stresses in the part to be exceeded by 6 MPa (see Table 26). The increase of the head radius to 3 mm leads to a smaller second moment of area, which cannot be compensated by the resulting fiber orientations. This results in a worse fitness value (27.10 mm³/J > 26.83 mm³/J). A larger flank angle of 83° in combination with a larger head radius of 3 mm results in the stresses occurring in the part still being allowable, but at the same time leads to a worse fitness value. Smaller flank angles (78° and 79°) also lead to worse fitness values while maintaining the other parameters of the optimum. (Revfi, Mikus, et al., 2021)

The two individuals marked in dark gray in Table 26 are conspicuous because they show an identical fitness value, although they differ in 4° in the flank angle. Therefore, these two individuals will be analyzed in more detail in the following. Obviously, the resulting fiber orientations in the 79° geometry here lead to a fiber orientation that is more suitable for the load case, which compensates for parts of the poorer geometric stiffness. To verify this hypothesis, analogous to the investigation of the resulting fiber orientations in the SMC optimization, the angle φ between the fiber preferential direction (1-direction) and the isotropically determined maximum (magnitude) principal stress direction σ_P can be evaluated (see Figure 4.60). The result of this evaluation is shown in Figure 4.74. For the analysis of Figure 4.74, it is important to note that all three presented geometries have the same total number of elements, so that the plotted results are directly comparable to each other. (Revfi, Mikus, et al., 2021)

The evaluation of the angles reveals why the geometry with 81° flank angle has a better fitness value than the geometry with 83° flank angle. In the stiffness-relevant angle range between 0° and 45°, there consistently are more elements with a fiber orientation more suitable for the load case in the geometry with 81° flank angle. As a result, a part of the worse geometric stiffness of the 81° geometry is obviously compensated by the material stiffness, so that the expected difference due to the different geometric stiffness is smaller. At the same time, the 81° geometry has a smaller volume. This combination results in a smaller fitness value and thus a higher specific stiffness. With a similar reasoning it can be explained why the bead cross section with a flank angle of 79° has a fitness value as good as the cross section with 83°, but a worse fitness value than the geometry with 81° flank angle. Compared

to the bead cross section with 81° flank angle, the geometry with 79° flank angle has a smaller number of elements in the range between 0°-15°, which is most relevant for stiffness, and is therefore not only geometrically less stiff, but the contribution of material stiffness is also lower. However, the comparison with the bead cross section with a flank angle of 83° shows that the fiber orientations in the 79° geometry are more consistent with the load direction and thus the material stiffness again compensates for parts of the geometric stiffness. To deform the part with the 83° flank angle, an energy of 3763.88 mJ is required, while only 3723.27 mJ have to be applied for the geometry with 79° flank angle. This indicates that the 83° geometry is still stiffer due to its greater geometric stiffness, but in relation to its volume not to a sufficient extent to achieve a better fitness value than the 79° geometry. (Revfi, Mikus, et al., 2021)
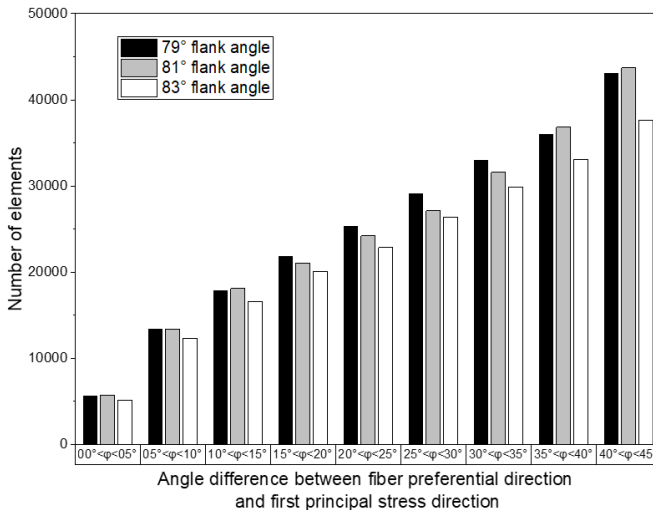
Figure 4.74: Number of elements with fiber orientations in the angle difference to the first principal stress for 79°, 81° and 83° flank angle adapted from Revfi, Mikus, et al. (2021)

Based on these investigations, it can be formulated analogously to the findings obtained at SMC that the consideration of the manufacturing process has a significant influence on the stiffness-optimized bead design.

The last step is the third verification step. With the first two steps have confirmed the findings from the SMC investigations also for LFT, the influence of the residual stresses resulting from the LFT manufacturing process on the stiffness-optimized bead cross sections is subsequently analyzed.

(iii)   Optimization based on anisotropic LFT material properties resulting from the manufacturing process, with consideration of residual stresses

For the studies, the optimization method for LFT presented in Subsection 4.2.2.3 and visualized in Figure 4.19 in the IPEK coupling framework is applied. The necessary changes in the structural simulation, to calculate in a first step the part warpage and in a second step the loading, have been explained in the model design and have to be kept in mind together with the chosen boundary conditions when interpreting the results.

Table 27 shows selected individuals from the optimization results. The stiffness-optimized bead cross section has a width of 25 mm, a height of 12 mm, a flank angle of 76°, a head radius of 2 mm and a base radius of 3 mm and is highlighted in gray in Table 27. It is instantly evident that, compared to the previous verification steps, only a bead cross section with a height of 12 mm can pass the strength constraint due to the consideration of residual stresses. At this point, the importance of considering residual stresses in the stiffness-optimized design of beads is already apparent. Compared to the isotropic optimization result, which proposes a bead cross section with a bead height of 16 mm, 83° flank angle, 2 mm head radius and 4 mm base radius, significant differences in bead height and flank angle can be seen. Having produced the mold based on an isotropic initial design, the deviations can only be corrected by a cost-intensive trial-and-error process. (Revfi, Mikus, et al., 2021)

Table 27:   Selected individuals of the anisotropic optimization with residual stresses (optimum highlighted in gray) adapted from Revfi, Mikus, et al. (2021)

Width [mm]	Height [mm]	Flank angle	Head radius [mm]	Base radius [mm]	Fitness [mm³/mJ]	Min. stress [MPa]
25	12	76°	2	3	29.49	-112
25	12	78°	2	3	29.64	-108
25	12	75°	2	3	29.74	-112
25	12	77°	2	3	29.82	-116 (failure)
25	12	83°	2	4	30.65	-107

As in the previous two optimizations, all individuals in the direct vicinity of the optimum have the maximum bead width. This can also be attributed to the previously mentioned reasons for this optimization.

With regard to the energy of the external forces (ALLWK) required for the deformation, the cross section with a flank angle of 78° shows a minimal advantage (ALLWK = 3352 mJ) compared to the optimum (ALLWK = 3351 mJ), but this does not lead to a specifically stiffer configuration due to the consideration of the volumes in the fitness value. Increasing the flank angle to 77° leads to the exceeding of the strength constraint (-116 MPa). This is initially surprising, since the bead cross sections in the direct vicinity at 75°, 76°, and 78° do not fail. In order to analyze this in more detail, Figure 4.75 shows the residual stresses that are present in the part after warpage. Only the end of the center bead on the bottom side of the plate is shown, since the geometries exceed the allowable stresses at this point. The elements marked in red are those elements that have the highest compressive stresses after the application of the external load in the next simulation step. In the case of the bead cross section with the flank angle of 77°, the element marked in red leads to the exceeding of the strength constraint. (Revfi, Mikus, et al., 2021)

For the bead cross section with the flank angle of 77° which exceeds the stress limit, it is noticeable that the element highlighted in red is located in an area with a local residual stress concentration. These residual stresses are superimposed by the applied external load in the next simulation step, resulting in stresses exceeding the limit. Consequently, the reason for the failure of the 77° geometry is a combination of the bead cross section and the resulting fiber orientations, which obviously causes an unfavorable warpage. (Revfi, Mikus, et al., 2021)
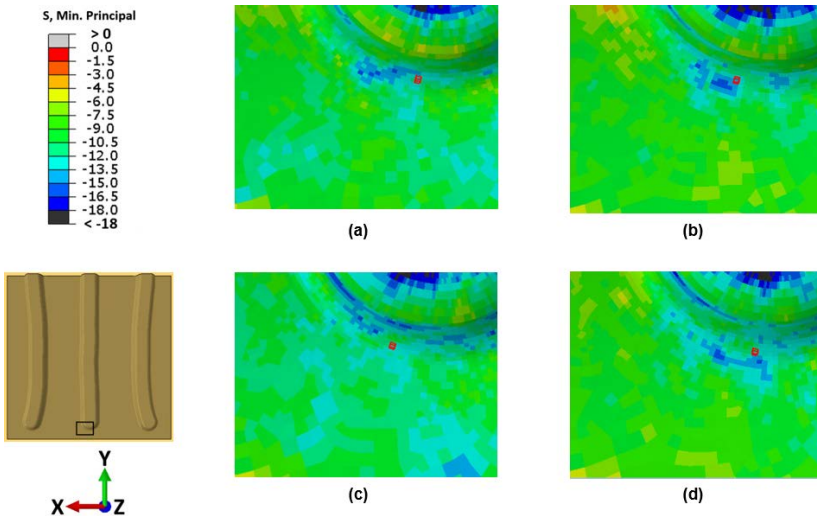
Figure 4.75: Residual stress state per flank angle: (a) 76° (optimum) (b) 77° (c) 78° (d) 75° and the element which has the highest stress in the loaded state (red marked elements) and leads to failure at the geometry with a flank angle of 77° (Revfi, Mikus, et al., 2021)

In summary – and as an answer to the second part of the fourth research question of the first research hypothesis (see Section 3.1) – it can be stated that an intuitive initial bead design taking into account the residual stresses from the manufacturing process is hardly possible. Due to the overlapping effects resulting from the fiber orientations and the residual stresses, it is inevitable to use a virtual product development as a support in the design process. Even though the achieved fitness values and stresses by the individuals are very close to each other and may not be fully predicted in detail by simulations, clear tendencies can be identified by comparing the isotropic modeling, the anisotropic modeling without residual stresses and the anisotropic modeling considering residual stresses. Figure 4.76 shows a comparison of the different bead cross sections resulting from the isotropic and the anisotropic optimization considering residual stresses.
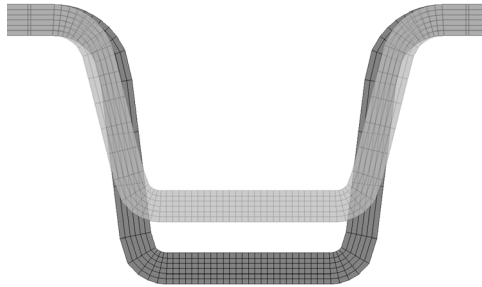
Figure 4.76: Isotropic optimum (dark gray) and anisotropic optimum under consideration of residual stresses from the manufacturing process (light gray)

As a finding, it can already be deduced from the studies with the simplified geometry of a plate – and thus supports the findings obtained from the SMC optimization – that, when taking into account the influences of the manufacturing process, the bead height has to be chosen smaller than it is predicted on the basis of an isotropic material modeling. The additional consideration of residual stresses required for LFT parts further corroborates this finding. The other bead parameters have to be chosen in accordance with each other and can only be evaluated in combination with the resulting fiber orientations and residual stresses. Therefore, it is not possible to make a generally valid statement on the choice of these bead parameters.

In conclusion, it can be stated that by taking the manufacturing process into account, fundamentally different stiffness-optimized SMC/LFT parts result compared to an optimization based on isotropic material properties. Consequently, the individual optimization results provide the answer to the research question formulated at the beginning of this section. With regard to the validity of the results, it is important to note that the presented bead designs determined by the optimization method only apply to the modeled system under investigation, as they depend on the boundary conditions (initial charge geometry and position, fiber orientation, residual stresses, etc.) as well as the defined loads.

4.4   Conclusion

The investigations in this chapter show the complexity in the design of parts made of long fiber reinforced SMC and LFT. In contrast to the construction with materials such as steel, where the material manufacturing process can usually be decoupled from the design, when using long fiber reinforced polymers, the final material properties result from the processing (May, 2020). Regardless of whether beaded SMC or LFT parts are considered, the bead catalogs known from the past, which are an established way of transferring knowledge, can no longer be used to find the design of FRP beads. This could be shown for both materials by opposing the process-based results to comparative isotropic optimizations. Therefore, the consideration of the manufacturing process in the synthesis is essential. The presented optimization methods (in Subsection 4.2.1.3 for SMC and in Subsection 4.2.2.3 for LFT) could show their potential to support the product developer in the initial design process of beaded FRP parts to further increase mass reduction. Thus, one of the central requirements for the optimization method to be developed can be considered fulfilled. Furthermore, a reasonable balance between effort and simulation depth could be created, so that the method can already be used in early phases for the initial design finding.

In order to develop this optimization method, four research questions were answered, verifying the formulated first research hypothesis:

i. Which demands exist with regard to methodical support for the product developer in the stiffness-optimized design of thin-walled, long fiber reinforced, beaded parts?
    ⇨   Section 4.1
ii. Which requirements for the method to be developed result from the identified demands?
    ⇨   Section 4.1
iii. Based on the SMC/LFT manufacturing process, how can an optimization method in the context of a product development process be structured to automatically provide a stiffness-optimized, load-adapted bead design for long fiber reinforced polymer structures?
    ⇨   SMC: Subsection 4.2.1
    ⇨   LFT: Subsection 4.2.2
iv. Which knowledge on the synthesis of bead designs is gained by applying the developed optimization method to SMC/LFT parts compared to isotropic, linear elastic material properties?
    ⇨   SMC: Subsection 4.3.1
    ⇨   LFT: Subsection 4.3.2

The central elements of the SMC optimization method could be validated in the research environment of the DFG GRK 2078/2. This included not only the mold filling simulations but also the structural simulations. The successful validation of the two submethods led to an increase in the quality of the model assumptions and thus to an increase in the maturity of the simulation results. The optimization method was verified in its functionality with the help of isotropic material models. The combination of the validated submethods for manufacturing and structural analysis and the verified optimization method allows conclusions to be drawn about the overall validity of the developed SMC optimization method. Thus, it can be classified as an important support tool in the initial synthesis of beaded parts. In the context of the present work, though, its validity only covers the SMC investigated within the DFG GRK 2078/2, since only for this material the material behavior was sufficiently characterized. However, due to the modular structure of the optimization method, it can be adapted to other objective functions or materials. For this purpose, the developed coupling framework (see Figure 4.17) serves as a basis for the strategic planning of changes in the sense of the PGE – Product Generation Engineering model and to assess the associated risk.

For use in other material systems, the models in Moldflow and the assumptions behind them need to be adapted, as each production process has to be modeled individually. Each model is only valid for its defined purpose. The importance of correct model assumptions for the success of the method could be shown. This applies not only to the mold filling simulation, but also to the structural simulation in order to be able to simulate realistic part behavior. The fact that this adaptation is possible was shown by the extension of the optimization method to include residual stresses that arise in the manufacturing process of LFT parts. As a result, the influence of residual stresses on the stiffness-optimized bead design could be demonstrated.

The relevance of this research work is given by the potential for cost savings in the design of the molds. By generating load-adapted, process-based initial designs, expensive mold modifications in later development phases can be reduced. Furthermore, more efficient parts can be identified using the developed method, which can only be found by chance in a trial-and-error process.

In the product engineering process, the developed optimization method provides additional support for the product developer in generating alternative solutions in the iPeM core activity *Model principle and embodiment*, which has to be performed iteratively with the iPeM basic activity *Validate and Verify* in order to obtain reliable results (see Figure 4.77).
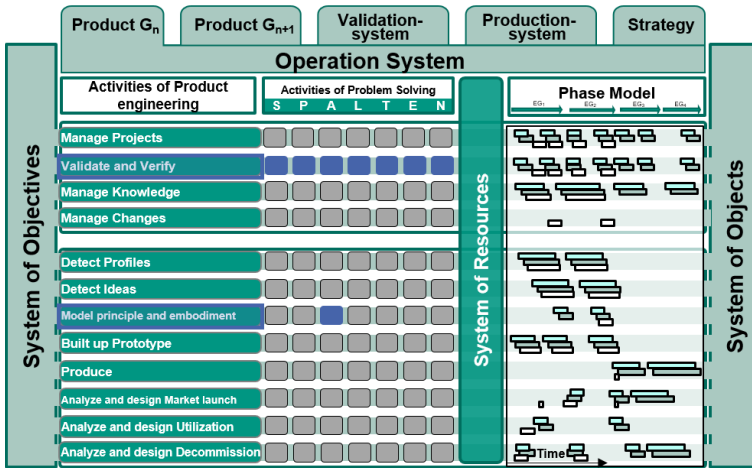
Figure 4.77: Support of the optimization method in the core activity *Model principle and embodiment* in iteration with the basic activity *Validate and Verify*

The required competence profile of the product developer to apply the developed optimization method poses a certain barrier. In order to be able to evaluate the simulation and optimization results of the individual submethods, an understanding of the phenomena occurring in the manufacturing process and in the structural simulation as well as a basic understanding of optimization is necessary. All three subdisciplines are already very complex independently of each other, so that a certain amount of experience is needed of the product developer in order to determine and abstract the relevant partial aspects. Accordingly, the necessary competence profile is that of an engineer with an affinity for simulation, who should have expertise in the areas of manufacturing and processing, structural analysis as well as optimization.

Finally, the question remains how potential components for the use of SMC and LFT can be identified during the design phase in order to meet the project goals despite higher costs and CO_2 emissions. As shown in Subsection 2.2.5, lightweight design is situated between the conflicting priorities of accepted additional costs per kilogram saved and generated CO_2 emissions during the product life cycle. As an approach to overcome these challenges, MMD, which aims for the right material in the right

places, was introduced in Subsection 2.2.4. Against this background, the question arises of how to identify "right places". These places go beyond the component and subsystem boundaries resulting from metal-based designs and require a fiber-adapted design (see Subsection 2.3.3) and an integration of newly developed sub-system solutions into an existing rest system. Accordingly, the iPeM core activity of *Detect Ideas* should already be considered in very early phases of the product en-gineering process in which the product concept is defined. For subsystems in which the use of SMC/LFT proves to be suitable, the automated bead optimization can be applied in order to raise further lightweight design potentials. One possibility of sup-porting the product developer in identifying and evaluating lightweight design poten-tial in the activity *Detect Ideas* is the Extended Target Weighing Approach (ETWA), whose development is presented in the next chapter.

5 An Approach to Multi-Material Design in System Lightweight Design – The Extended Target Weighing Approach (ETWA)

From the state of research, numerous lightweight design strategies and methods are known to support the product developer. Following the reasoning from Subsection 2.2.6, function-based lightweight design methods provide support in system lightweight design. Through this lightweight design strategy, it is possible to identify cross-subsystem lightweight design potential, which supports the development of multi-material designs relevant to this thesis. From the review of the state of research of function-based lightweight design methods in Subsection 2.2.6, the Target Weighing Approach (TWA) emerged as the most appropriate method for this thesis. Therefore, in this chapter, the TWA is used as a basis to extend it for the application between the conflicting priorities of mass, costs and CO_2 emissions important in lightweight design (see Subsection 2.2.5).

The development environment on the basis of which the author made the decisive experiences and observations in lightweight design developments and which allowed a rapid validation of initial development approaches was, in addition to the research environment of the IPEK – Institute of Product Engineering, the EU research and innovation project ALLIANCE[45]. This project was funded by the Horizon 2020 program for three years and was supported by EUCAR, the European Council for Automotive R&D[46]. In ALLIANCE, six European automotive OEM[47], four suppliers and eight knowledge partners (see Table 28) came together to develop affordable lightweight design solutions for automobiles that have a high potential for implementation in mass production and thus contribute to the decarbonization of road transport (ALLIANCE, 2019). The overall ALLIANCE project results can be found in an "Extended Publishable Executive Summary" (ALLIANCE, 2019). This thesis only focusses on the development of the Extended Target Weighing Approach (ETWA). Therefore, the results are to be evaluated mainly in the automotive context of moving

---

[45] http://lightweight-alliance.eu/ (accessed June 25, 2021)
[46] R&D = Research and Development
[47] OEM = Original Equipment Manufacturer

masses. However, in the evaluation of the results (see Section 5.3), the developed method will also be transferred to other industries, e.g. the packaging industry.

Table 28:   ALLIANCE project members

Members	Branch
Daimler	
Fiat-Chrysler Research Centre (FCA) represented by Centro Ricerche Fiat (CRF)	
Opel	Automotive OEM
Toyota	
Volkswagen	
Volvo	
Batz S. Coop.	
Benteler Automotive	Suppliers
Novelis Inc.	
ThyssenKrupp Steel Europe AG	
IPEK – Institute of Product Engineering, Karlsruhe Institute of Technology (KIT)	
Bax & Company	
Fraunhofer Institute for Structural Durability and System Reliability LBF	
Institute for Automotive Engineering (ika), RWTH Aachen University	Knowledge partners
inspire AG	
Ricardo UK Ltd.	
Swerea KIMAB AB	
Università degli Studi di Firenze	

First, in Section 5.1, empirical studies are presented which, on the one hand, investigate the potential of the TWA and thus support the decision to select it from the long list of function-based lightweight design methods and, on the other hand, identify potential for its improvement for use in system lightweight design. Based on the system of objectives that is derived with the help of the study results and the literature research, a modular enhancement of the TWA to the Extended Target Weighing

Approach (ETWA) is undertaken in Section 5.2. Finally, the developed method modules are evaluated in Section 5.3 through their application in the EU project ALLIANCE, in Live-Labs, in industrial case studies and further practical examples.

5.1 Assessment of Demand

In this section, the potentials of the Target Weighing Approach (TWA) as a basis for supporting the development of economic and ecological multi-material designs are investigated. The studies represent the Descriptive Study I for the investigation of the second research hypothesis. They have the two objectives of assessing the basic suitability of the TWA to support the development of new lightweight design concepts as well as identifying potential improvements in the existing method. Accordingly, the first and second research question of the second research hypothesis are to be answered with the help of this section.

Research Questions

---

    i.   Which potentials does the TWA offer in the support of the product developer when developing lightweight design solutions in system lightweight design?

   ii.   Which demands exist with regard to an extension of the individual process steps of the TWA?

The empirical study on the potentials of the TWA in Subsection 5.1.1 was conducted within the Live-Lab IP – Integrated Product Development (see Section 3.3) at IPEK – Institute of Product Engineering. For the identification of potentials for improvement of the method in Subsection 5.1.2, a survey with a questionnaire was performed in the EU project ALLIANCE.

5.1.1 Potential of the TWA as a Support Tool for the Development of Lightweight Constructions

The TWA has already demonstrated its potential to support the development of lightweight design solutions in two development projects – in the context of the development of a high-voltage battery and a climate control unit (Albers et al., 2013). However, in both cases there was no parallel comparative development process that proceeded without methodical support so that the generated results could have been compared to each other. This is generally not possible in product development processes in corporate practice, as the same product cannot be developed in par-

allel in two different development processes due to time and cost constraints. Therefore, the research environment of the Live-Lab IP – Integrated Product Development was employed, which allows to do research under realistic conditions of a development process. In addition, questionnaires were used to interview the participants in detail. The aim of the empirical study was to investigate the benefits of the TWA's support in the generation of lightweight design concepts in comparison with concepts developed according to a classic development process in companies.

The underlying study design and the study results are presented below. The results have been published previously in Revfi, Albers, and Stegmiller (2018).

5.1.1.1 Study Design

The Live-Lab IP was chosen as research environment. Thus, the number of study participants amounted to 37 master's students majoring in mechanical engineering. They were recruited through a selection process that included an interview. (Revfi, Albers, & Stegmiller, 2018) Hence, they are novices, but with an affinity for design and educated to become subject matter experts in their domain (Bromme, Jucks, & Rambow, 2004). Consequently, expert knowledge may not be assumed. However, there is the advantage of the simultaneous availability of 37 study participants as well as their openness to new methods. The participants were divided into two groups (TWA Group and Corporate Group) and these in turn into four teams consisting of four or five participants each (see Figure 5.1).
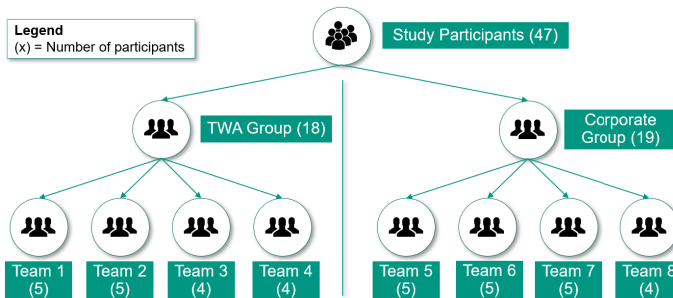
Figure 5.1: Division of the study participants into the TWA and the Corporate Group

Both groups got the task to identify lightweight design potentials on a given underbody of an automobile and to develop new concept ideas for these potentials. As a

constraint and in order to avoid unrealistic concepts, attention had to be paid to affordable lightweight design costs. This made the development task both challenging and application-oriented at the same time. Both groups were provided with identical basic information (objectives, documents, boundary conditions and a brief introduction to the system under consideration). At the end of the study, each team had to choose and present its preferred concept, so that eight concept ideas resulted. The TWA Group received a method training on the TWA at the beginning (and was instructed to use it), the Corporate Group only at the end of the study. The available time was 4.5 hours and was divided according to Figure 5.2. (Revfi, Albers, & Stegmiller, 2018)

Group 1 (4 TWA Groups)	Group 2 (4 Corporate Groups)	
Introduction and grouping (objectives, boundary conditions, presentation of system under investigation, available documents) (20 min)		Experts always available as contact persons for both groups
Presentation TWA (30 min)	Work Phase 1 (35 min)	
Function Analysis + Meeting with Experts (45 min)	Meeting (10 min)	
	Work Phase 2 (35 min)	
Creation of Function-Mass-Matrix + Paired Comparison + Meeting with Experts (45 min)	Meeting (10 min)	
	Work Phase 3 (35 min)	
	Meeting (10 min)	
Analysis of the Lightweight Design Potentials (20 min)	Work Phase 4 (35 min)	
	Meeting (10 min)	
Concept Design (70 min)	**Presentation TWA (30 min)**	
Presentation of the best concepts (One each Development Team) (20 min)		
Survey (20 min)		

Figure 5.2: Time schedule of the study adapted from Revfi, Albers, and Stegmiller (2018)

Since the performance of the individual phases of the TWA is very time-consuming and can last well beyond 4.5 hours, the individual work phases of the TWA Group were restricted in time. During the expert meetings, the results were reviewed and all groups were brought up to the same level. The Corporate Group was organized analogously to classic corporate structures, i.e. the four teams were responsible for different subsystems. Since in companies the responsibilities for individual subsystems usually lie in different departments, which also have separate locations, the exchange of information often only takes place in scheduled meetings. To reproduce this situation in the study, one person per team, i.e. per subsystem, was designated

as the team manager. The subsystem managers met in defined meetings (see Figure 5.2) to share their progress and discuss possible interfaces. In between the meetings, no communication was allowed between the team managers of the different subsystems. Communication was only allowed between team members of the same subsystem. Thus, an attempt was made to replicate the classic corporate development environment in the IP research environment. The organizers of the study were aware that the described setup was only a modeling approach to transfer the real environment in a university environment. Therefore, it should be noted that the investigations in a corporate environment may differ. (Revfi, Albers, & Stegmiller, 2018)

Following the study, a questionnaire comprising seven questions (see Figure 5.4) was distributed to the participants. The questionnaire inquired about the influencing factors important for the identification of lightweight design potential (distinct analysis phase, communication, subsystem interaction, cross-subsystem thinking and detachment from existing boundaries (interfaces) of the reference product), which were identified by the organizers prior to the study. (Revfi, Albers, & Stegmiller, 2018)

The concepts selected by the teams were evaluated by three experts from an automotive manufacturer in the lightweight design domain (Bromme et al., 2004) subsequent to the study. The concepts were evaluated in the categories of mass reduction (in relation to the reference underbody), costs (in relation to the reference underbody), degree of novelty/revolutionariness (in terms of design) and overall impression of the concept idea. (Revfi, Albers, & Stegmiller, 2018)

5.1.1.2   Study Results

In the following, the results of the study will be presented, analyzed and interpreted. This will be done against the background of the existing boundary conditions (such as the short time period available for such a complex system) and disturbing factors (such as the different expertise of the students). First, the experts' concept evaluations are presented before the results of the survey that was carried out with the help of a questionnaire among the study participants are evaluated.

Concept Evaluation by Three Experts from an Automobile Manufacturer

Due to the complexity of the task, the experience and knowledge of experts was needed to evaluate the concepts developed in the individual teams. These experts came from the lightweight design, underbody simulation and body concept development departments of a major car manufacturer. They knew the reference underbody very well because it was an underbody from their product portfolio.

The evaluation was made based on a relative, descending ranking (1 = best concept, 8 = worst concept) of the respective expert in the areas of mass reduction, costs, degree of novelty/revolutionariness and overall impression of the concept idea (see Figure 5.3). (Revfi, Albers, & Stegmiller, 2018)

	Teams	Experts			Results	Average
		Lightweight design	Vehicle body simulation	Vehicle body concepts		
Mass reduction	TWA-1	8	8	1	17	
	TWA-2	1	2	3	6	
	TWA-3	3	4	2	9	
	TWA-4	7	7	5	19	12,75
	Non-TWA-1	2	3	7	12	
	Non-TWA-2	6	5	4	15	
	Non-TWA-3	4	1	8	13	
	Non-TWA-4	5	6	6	17	14,25

	Teams	Experts			Results	Average
		Lightweight design	Vehicle body simulation	Vehicle body concepts		
Costs	TWA-1	7	7	5	19	
	TWA-2	1	2	3	6	
	TWA-3	3	4	4	11	
	TWA-4	8	8	7	23	14,75
	Non-TWA-1	2	3	6	11	
	Non-TWA-2	5	5	1	11	
	Non-TWA-3	4	1	2	7	
	Non-TWA-4	6	6	8	20	12,25

	Teams	Experts			Results	Average
		Lightweight design	Vehicle body simulation	Vehicle body concepts		
Degree of revolutionariness	TWA-1	1	2	1	4	
	TWA-2	4	5	3	12	
	TWA-3	2	4	5	11	
	TWA-4	3	1	4	8	8,75
	Non-TWA-1	5	6	6	17	
	Non-TWA-2	7	7	2	16	
	Non-TWA-3	6	3	8	17	
	Non-TWA-4	8	8	7	23	18,25

	Teams	Experts			Results	Average
		Lightweight design	Vehicle body simulation	Vehicle body concepts		
Overall impression	TWA-1	8	8	1	17	
	TWA-2	1	2	3	6	
	TWA-3	4	7	2	13	
	TWA-4	7	4	4	15	12,75
	Non-TWA-1	2	3	6	11	
	Non-TWA-2	5	5	5	15	
	Non-TWA-3	6	1	7	14	
	Non-TWA-4	3	6	8	17	14,25

Figure 5.3: Expert ranking of the developed eight concept ideas in the categories mass reduction, costs, degree of revolutionariness and overall impression (1=best, 8=worst). Results distinguished between TWA group and corporate group. In the average column the individual results of the respected group are summed up and divided by the number of groups. (Revfi, Albers, & Stegmiller, 2018)

This type of evaluation does not provide an equidistant scale, i.e. the qualitative distance between two concept ideas does not always have to be the same. Nevertheless, in order to make the evaluations comparable, the calculation of the mean value of the summed individual rankings is used below (see column *Average* in Figure 5.3, which shows the mean value for the TWA Groups and the Corporate Groups separately). To ensure a traceability of the individual rankings, these are also shown in Figure 5.3. (Revfi, Albers, & Stegmiller, 2018)

Although the evaluation was conducted by only three experts and thus there is no statistical significance, some interesting findings can be derived from it.

There are differences in the experts' assessment of the achievable mass reduction. This can be explained in particular by the low level of detail of the developed concepts. Especially for more disruptive concepts, the experts had difficulty assessing the achievable mass reduction. This usually leads to an evaluation in favor of concepts based on the reference product. But still, the TWA concepts were rated slightly better on average (12.75 (TWA Group) vs. 14.25 (Corporate Group)). In addition, the two best rated concepts came from teams that applied the TWA (TWA-2, TWA-3). This suggests that the TWA's cross-subsystem approach helps to identify greater lightweight design potential and to translate it into lighter concepts. (Revfi, Albers, & Stegmiller, 2018)

The next category of evaluation by the experts was the costs required to realize the concept ideas. Similar tendencies as in the evaluation of the mass reduction can be identified here. The evaluation of the costs incurred on the basis of the presented initial concept ideas posed a challenge to the experts. Usually, major changes to the reference underbody, such as those resulting from novel designs, lead to increased costs. This also explains why the teams from the Corporate Group performed better on average. However, it should be mentioned that the TWA approach does not necessarily lead to increased costs, as the best rated concept came from a TWA team. (Revfi, Albers, & Stegmiller, 2018)

The evaluation of the degree of novelty/revolutionariness shows a clear tendency. The cross-subsystem approach of the TWA leads to a significantly better evaluation here. Each of the concepts of the TWA teams was rated better in total than the concepts of the corporate teams. In the context of this study, it can therefore be concluded that the TWA led to more integrative and disruptive concepts. (Revfi, Albers, & Stegmiller, 2018)

The last category evaluated by the experts was the overall impression of the resulting concept ideas. This evaluation is similar to the evaluation of the concepts for costs and mass. Once again, the best rated concept comes from a TWA team

(TWA-2). Since the design of the corporate teams' concepts was very similar to the design of the reference underbody, they were all rated similarly. In contrast to that, the more revolutionary concept ideas from the TWA teams together with the low level of detail of the concepts led to deviating expert assessments. (Revfi, Albers, & Stegmiller, 2018)

Concluding, after the evaluation of the expert assessments, it can be stated that the use of the TWA in the context of this study supported the development of more revolutionary concept ideas. The evaluation of the mass reduction and the expected costs in some cases resulted in different expert evaluations. This was further reinforced due to the low level of detail of the concepts. (Revfi, Albers, & Stegmiller, 2018)

In the next subsection, the results of the survey of the study participants regarding the experiences they made in the study are presented.

Results of the Survey of the Study Participants

The aim of the survey of the study participants was to find out whether the TWA better addresses the influencing factors important for the identification of lightweight design potential (distinct analysis phase, communication, subsystem interaction, cross-subsystem thinking and detachment from existing boundaries (interfaces) of the reference product), which were identified prior to the study by the organizers based on literature (Albers, Reiß, Bursac, and Breitschuh (2016), Friedrich (2017)). The evaluation of the questionnaires is shown in Figure 5.4.

According to the problem solving method SPALTEN (see Subsection 2.1.1), a distinctive *Situation Analysis* and *Problem Containment* are important for a successful product development (Albers, Reiß, Bursac, & Breitschuh, 2016). Therefore, a reasonable amount of time (up to 70%) should be dedicated to these two steps in problem solving. This is the only way to find *Alternative Solutions* for the actual problem in the following. From the results to the first question (What percentage of the working time was used for S(ituation Analysis) and P(roblem containment)?) it is evident that the TWA Group spent more time on these two steps due to the method (see Figure 5.4). (Revfi, Albers, & Stegmiller, 2018)

The second question (In the course of the workshop, I was able to develop a comprehensive understanding of the overall system.) aimed at the cross-subsystem way of thinking that is necessary to raise the lightweight design potential of system lightweight design. The evaluation of the questionnaire shows that the TWA Group has developed a better overall understanding of the system, enabling them to work cross-subsystem. The result can be related to the first question. A more pronounced

situation analysis and problem containment in particular lead to a better understanding of the overall system. (Revfi, Albers, & Stegmiller, 2018)

This better overall understanding of the system also has an effect on the overview of the system interactions, as shown by the results of the third question (I always had an overview of the interactions of the subsystems in the overall system "underbody".). At this point, a larger difference between TWA Group and Corporate Group would actually have been expected. One possible explanation for this could be the high complexity of the system, which had to be mastered in a short time. (Revfi, Albers, & Stegmiller, 2018)

Regarding the question on the communication activities among the team members (The communication among the team members was sufficient.), the largest difference was found between the two groups. Even though this result should not be overestimated due to the study design, a tendency can be derived from it. The large difference can be explained by the necessary close, cross-subsystem collaboration in the performance of the TWA, while in the Corporate Group cross-subsystem meetings were only allowed at certain times. This explains the significantly poorer rating. However, communication often is a barrier in real companies due to subsystem responsibilities, so this study design is considered to be appropriate. (Revfi, Albers, & Stegmiller, 2018)

The answers to the fifth question (When optimising the subsystems, I had the interface to the surrounding components in mind at all times.) seem to be surprising at first. The TWA Group states that they focused less on the surrounding components, even though the TWA supports the overall understanding of the system (see second question). Therefore, an obvious explanation for this result is that the product is transferred to the solution-open level of functions by applying the TWA. Therefore, it is not necessary to consider the existing system boundaries. (Revfi, Albers, & Stegmiller, 2018)

Taking the deviation into account, the answers to the sixth question (For me the optimisation of individual subsystems was in the foreground.) show a balanced picture. Since the performance of the TWA also includes subsystem optimizations, this result is not contradictory to the previous results. (Revfi, Albers, & Stegmiller, 2018)

The last question (I give the workshop day the overall grad (1 = best, 6 = worst)) shows that the students rate the TWA positively, although it demanded a lot from them on the day the study was carried out. The fact that the students of the Corporate Group were partially overchallenged by the high complexity of the system is also reflected in their poorer evaluation. (Revfi, Albers, & Stegmiller, 2018)
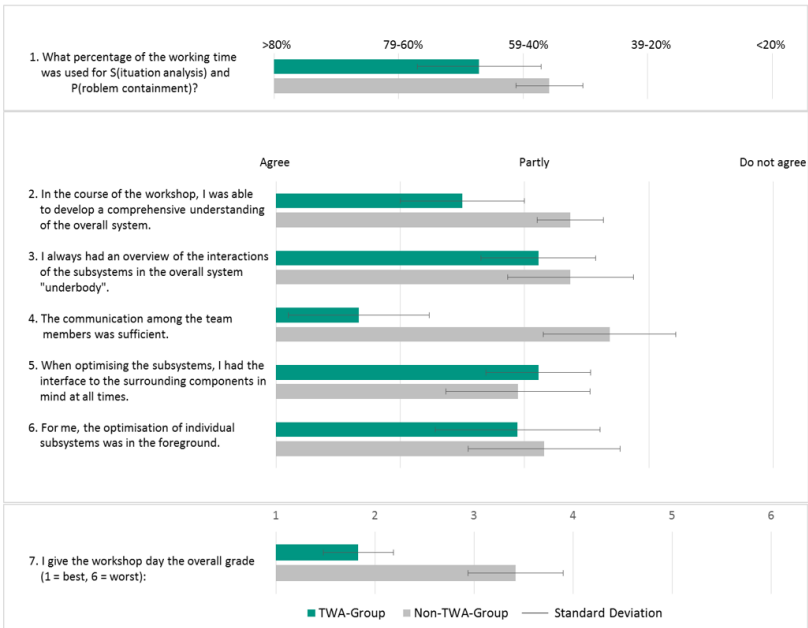
Figure 5.4:   Results of the survey of the study participants. Each question asks for an influencing factor for the identification of lightweight design potentials. (Revfi, Albers, & Stegmiller, 2018)

As a result of the study, it can thus be summarized that the students of the TWA Group built up an understanding of the system through a pronounced analysis phase and intensive communication, which enabled them to identify cross-subsystem lightweight design potential. Thereby, they detached themselves from existing interfaces, which allowed them to develop more revolutionary concept ideas in the eyes of the automotive experts. (Revfi, Albers, & Stegmiller, 2018)

Finally, it should be emphasized that the results cannot be seen as proof. In order to be able to prove the actual benefit of the TWA in the industrial environment, two parallel development processes would have to be run through – as mentioned at the beginning of this subsection – one with the support of the TWA, the other without.

However, as long as this is not possible, the results of the survey serve as a strong indication for the benefit of the TWA.

This study shows the potential of TWA as a support in the identification of lightweight design potentials and in the development of lightweight solutions. At the same time, this result supports the decision to select the TWA from the existing function-based lightweight design methods as a basis for its further development to apply it between the conflicting priorities of mass, costs and CO_2 emissions. The demands for further development of the TWA are investigated in the next subsection.

5.1.2 Assessment of Demand for the Further Development of the TWA

Having identified the potentials of the TWA in the Live-Lab, a questionnaire was developed asking the respondents to evaluate the individual methods in the work-flow of the TWA. The underlying study design and study results are discussed in the following. Since the workflow of the TWA can be divided according to the problem solving method SPALTEN (see Subsection 2.2.6), the results provide information about which problem solving step is sufficiently supported and where users would still like further support.

5.1.2.1 Study Design

The objective of this study was to identify demands for the extension of the TWA. For this purpose, a questionnaire was developed. Since the necessary precondition for answering the questionnaire was that the participants have already applied the TWA method, the number of requested participants was ten people. All of them were project members of the EU project ALLIANCE. Therefore, the questionnaire was designed as an online questionnaire, so that the participants spread across Europe all had the opportunity to complete it. Nine people participated in the survey and completely filled in the questionnaire. This represents a 90% response rate. The participants came from industry and research. The respondents from industry were engineers from two large European automotive manufacturers and can be classified as experts (according to Bromme et al. (2004)) in the domain of *lightweight design*. Consequently, this is a qualitative study in a panel of experts. Although nine participants do not represent a sample size from which statistical significance can be inferred, the responses do provide decisive indications of development potential from the perspective of industry and science. The questionnaire consisted of twelve questions and a comment field at the end of it. The questions were formulated in a closed response format. The answer options were given in the form of a six-point Likert scale. The choice of an even-point scale was motivated by the fact that respondents

were forced to choose a tendency. Both verbalized scales as well as scales with labeled end points were used. For two questions, yes-no questions were employed, followed by an open question depending on the answer. The complete questionnaire can be found in Appendix A.

5.1.2.2 Study Results

Figure 5.5 to Figure 5.10 show selected results of the survey, which are discussed in the following. Since neither the ceiling effect (> 80% full agreement) nor the floor effect (>80% full disagreement) occurs for any of these questions (Döring & Bortz, 2016), the questions asked can be used for evaluation.

First, the participants were asked about the benefits of the TWA for the identification and evaluation of lightweight design potential. The result is shown in Figure 5.5.
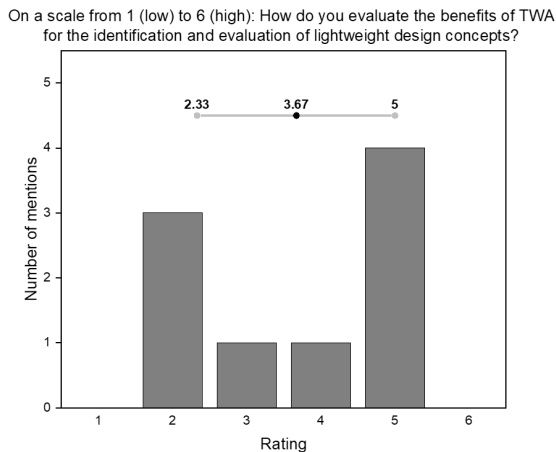
Figure 5.5: Evaluation of the survey – benefit of the TWA

The mean value of 3.67 indicates that the benefit of the TWA tends to be recognized, as it is on the side of an agreement with the statement. Five people rated the benefit positively, while four people were skeptical. That the result on this question would show answers on both sides was to be expected, since there are both proponents

of methods and skeptics of methods in almost every group. The methodical approach is based on a different way of working than it has been the case so far in the respondents' companies. However, the fact that the TWA is of benefit in identifying and evaluating lightweight design potential has already been demonstrated by the study carried out in the Live-Lab IP (see Subsection 5.1.1).

In order to better understand the very general assessment of the benefits, in the following, questions are asked about the individual method modules of the TWA, which can be divided according to SPALTEN. Therefore, first of all, the effort to fill in the Function-Mass-Matrix (see Subsection 2.2.6), which is used to support the *Situation Analysis*, is addressed. The result of the answers to this question is shown in Figure 5.6.
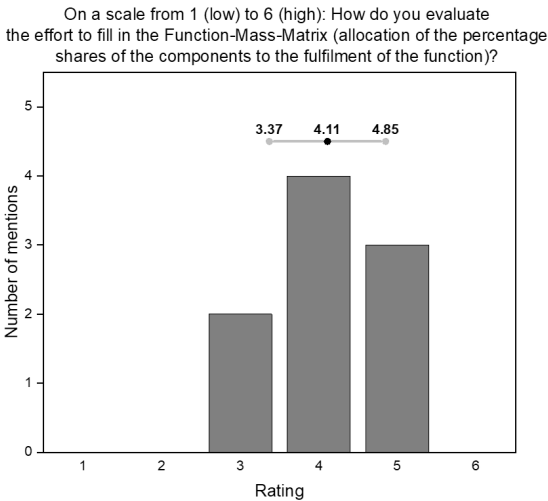
Figure 5.6:   Evaluation of the survey – effort to fill in the Function-Mass-Matrix

Seven respondents indicate the effort on the *high* side. However, besides the fact that filling in a $n \times m$-matrix is time-consuming, the result could also be caused, among other things, by the inexperience of the users. Also, this could be a first indicator of how the evaluation of the benefits of the TWA emerged. By an increased effort in conducting the situation analysis, the overall method might be rated as less

beneficial because it is not directly started with the development of solutions. Either way, it is a clear sign that a way to reduce the effort needs to be developed here.

After the percentage assignment of the components to the functions, search fields for lightweight design potentials can be derived by the TWA in the context of *Problem Containment* (see Subsection 2.2.6). The next question addresses the support for the identification of lightweight design potentials provided by these search fields. The result in the form of agreement or disagreement is shown in Figure 5.7.

The resulting lightweight design search fields support the identification of real lightweight design potentials. (1 - I agree; 6 - I disagree)
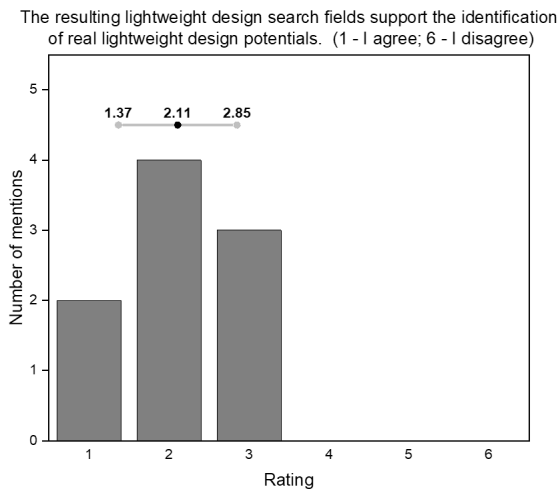
Figure 5.7: Evaluation of the survey – support for the identification of lightweight search fields

Even though the effort required to fill in the Function-Mass-Matrix was rated as high, the results that can be achieved with it in the form of the lightweight search fields are rated as consistently positive. All nine participants scored on the agreement side, two of them even with the highest agreement. Since the search fields are the result of the situation analysis and problem containment of the Target Weighing Approach, the support of the TWA in these problem solving activities can be evaluated as positive. In addition, for the further development of the method, the result also indicates

that the processing of the results of the problem containment by the search fields should be maintained.

Based on the identified search fields, new concept ideas are generated in the problem solving step *Alternative Solutions* (see Subsection 2.2.6). Therefore, the questionnaire asks for the methodical support of the TWA in synthesis. The answers to the question are shown in Figure 5.8.

On a scale from 1 (very good) to 6 (inadequate):
The methodological support by the TWA for the transfer of the identified
lightweight search fields in new concept ideas (= synthesis), I evaluate with:
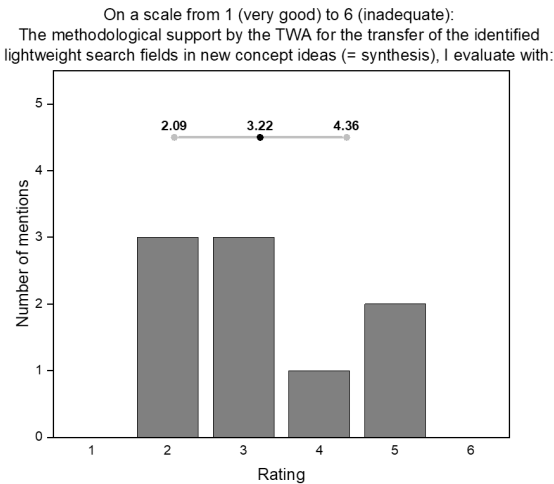
Figure 5.8: Evaluation of the survey – methodical support in the generation of new concept ideas

Here the participants differ in their opinions. While six respondents evaluate the support rather positively, three respondents see the support as rather insufficient. Ultimately, this leads to a mean value that tends to the negative side. When evaluating this question, it is important to note that the participants were already provided with selected creativity methods such as the 6-3-5 method by IPEK experts during the performance of the TWA. This may have been evaluated positively by the participants without being able to say whether an even more targeted synthesis based on the identified search fields would have been possible.

After the generation of concept ideas, the reduction of these ideas to a number, which is subsequently constructed, follows in the workflow of the TWA. This corresponds to the problem solving steps of *Selection of Solutions* and *Consequences Analysis*. The procedure of concept reduction was carried out with the project members following the three-step procedure according to the state of research of the TWA (see Subsection 2.2.6). The results of the evaluation are shown in Figure 5.9.

After generating new concept ideas based on the identified search fields, you must evaluate those concept ideas that are to be detailed later. On a scale from 1 (very good) to 6 (inadequate): How do you evaluate the methodical support of TWA in this selection process?
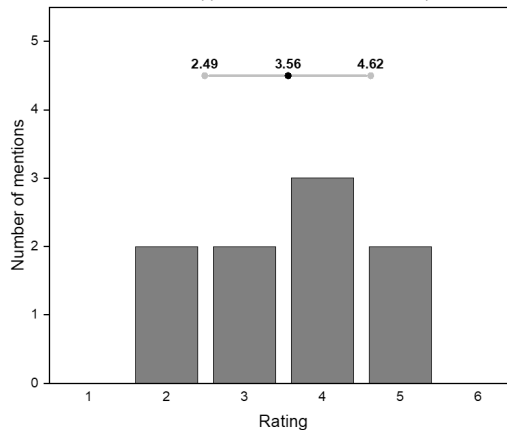
Figure 5.9: Evaluation of the survey – methodical support in concept reduction

Four participants rated the methodical support in the reduction of concept ideas on the positive side, while five participants considered the support to be rather insufficient. Therefore, the mean value tends towards "inadequate". From this, it can be concluded that the three-step procedure already provides support in concept reduction, but could be supplemented by further methods in the eyes of the study participants.

Last, the result of the survey on the participants' evaluation of the time required to perform the overall method is shown in Figure 5.10.

On a scale from 1 (low) to 6 (high): How do you evaluate the time required to perform the TWA (from functional analysis to the new product generation)?
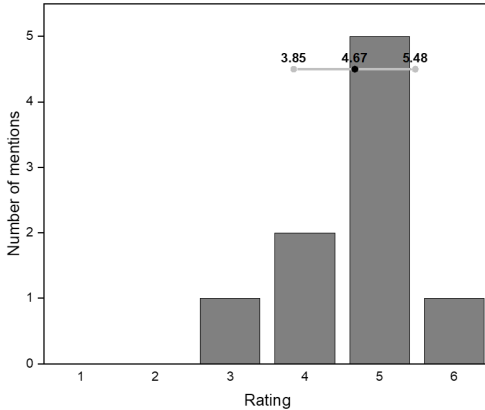
Figure 5.10: Evaluation of the survey – time required to perform the Target Weighing Approach

Here, eight responses are on the side that classify the time required as high, with five responses even rating this as the second highest. This clearly indicates that time optimization potentials need to be investigated and is in high agreement with the results on the time required to create the Function-Mass-Matrix.

This finding closes the circle to the evaluation of the benefit. A possible explanation for the evaluation of the benefit can lie in the increased expenditure of time, since in the subjective feeling of the user the benefit is often automatically evaluated in relation to the effort.

In summary, it can be stated that only the support of the lightweight search fields in the step of problem containment was rated as consistently positive. The expenditure of time was consistently rated as too high. Likewise, the evaluation of the support in the synthesis and consequences analysis turned out to be moderate with potential for improvement.

This finding is taken into account in the following definition of the system of objectives.

5.1.3 System of Objectives for the Extension of the TWA

Based on the potentials identified in Subsection 5.1.1 and the demands identified in Subsection 5.1.2, the system of objectives for the extension of the TWA is derived subsequently.

As shown with the empirical study in Subsection 5.1.1, the TWA in its current format according to the state of research generally provides support for the identification and evaluation of lightweight design potential. This demonstrated possibility of support induces the author of the present work to use the reference system element TWA which is an element of the KaSPro – Karlsruhe School of Product Engineering as a basis for the development of a lightweight design method for the integrated consideration of mass, costs and CO_2 emissions. For this, the strengths of the method, such as the systematic generation of lightweight search fields, are to be built upon and extended in a modular way.

According to the current state of research, in addition to mass, costs can also be considered in the TWA in a separate portfolio (Albers et al., 2013; Wagner, 2015). The existing format, though, does not include any consideration of ecological aspects. However, these conflicting priorities have to be taken into account in the development of lightweight design solutions, especially in the automotive sector (see Subsection 2.2.5). Consequently, there is a demand for an additional consideration of CO_2 emissions in the TWA in order to be able to jointly balance the dimensions of mass, costs and CO_2 emissions. Through the combined consideration of the dimensions, the development of lightweight design solutions, which meet the overall project goals, is to be supported. This is an essential requirement, especially for the development of multi-material designs, as different materials can be used according to their strengths. For example, FRPs are not automatically excluded from the material selection because of their costs or the CO_2 emissions associated with them. Instead, they are intentionally applied at those places in the product where they can realize their strengths.

From the surveys in the industrial environment of the EU project ALLIANCE in Subsection 5.1.2 further requirements for the method to be developed can be derived. The results show that additional methodical support is required for the synthesis of new embodiment concepts to be developed on the basis of the lightweight search fields and for the consequences analysis of individual concept ideas. Moreover, the expenditure of time for conducting the TWA is assessed as high and its reduction thus represents a further development objective and an element of the system of objectives.

With the results of the study in the Live-Lab IP, the survey in the EU project ALLI-ANCE and the definition of the system of objectives, the Descriptive Study I is considered to be completed. At the same time, the first and second research question of the second research hypothesis (see Section 3.1) were answered in Section 5.1. In the next section, the defined elements of the system of objectives will be addressed by newly developed methods.

5.2 Modular Extension of the Target Weighing Approach (TWA)

Based on the defined system of objectives in Subsection 5.1.3, the TWA is enhanced in this section to the Extended Target Weighing Approach (ETWA) (see Subsection 5.2.1). This ETWA includes the combined consideration of mass, costs and CO_2 emissions as well as a modular methodical extension to better support the product developer in synthesis (see Subsection 5.2.2) and consequences analysis (see Subsection 5.2.3). In addition, the potentials of the PGE – Product Generation Engineering model and the FAS4M approach as elements of the KaSPro – Karlsruhe School of Product Engineering to reduce the time needed to conduct the method are investigated (see Subsection 5.2.4).

5.2.1 Extended Target Weighing Approach (ETWA) – Balancing Mass, Costs and CO_2 Emissions

Since the basic suitability of the TWA for the identification and evaluation of lightweight design potentials was demonstrated in the study in the Live-Lab IP (see Subsection 5.1.1), the basic structure of the method is to be retained (see Subsection 2.2.6) and it is to be extended in a modular way to enable a combined consideration of mass, costs and CO_2 emissions. Accordingly, the third research question of the second research hypothesis (see also Section 3.1) will be answered with the help of this subsection.

Research Question

---

   iii.   How can the TWA be extended to systematically consider the conflicting priorities of mass, costs, and CO_2 emissions in the identification and evaluation of lightweight design potential?

The method was developed in close cooperation with the project members of the EU project ALLIANCE, who were available for evaluation purposes at any time. The

framework of the ETWA has been published previously in several publications, e.g., Albers, Revfi, and Spadinger (2017), Revfi, Albers, Holoch, and Spadinger (2018) as well as Albers, Revfi, and Spadinger (2020).

Figure 5.11 illustrates the workflow of the developed ETWA.
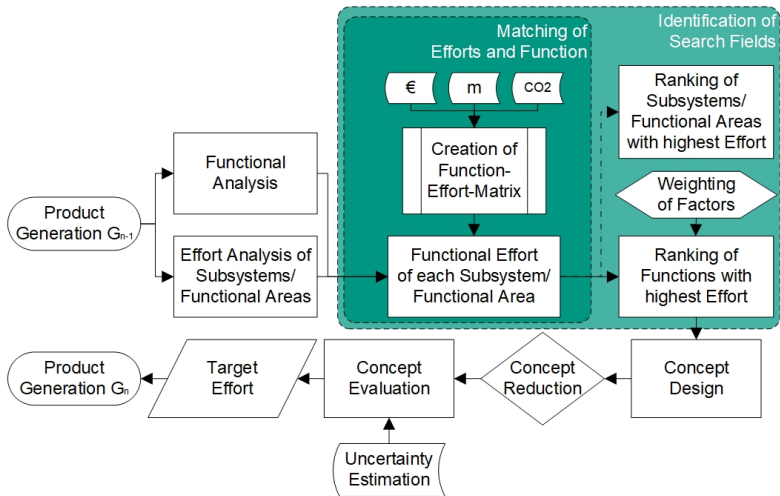
Figure 5.11: Workflow of the Extended Target Weighing Approach (ETWA) adapted from Albers, Revfi, and Spadinger (2020)

Starting with the definition of the reference system elements, it is determined which product (e.g., preceding product) is to be optimized in its mass. In this context, it is important to specify the right level of detail and to define the system boundary in order to achieve a common understanding of the system by the product developers. If there is a large number of components in the system boundary, it may make sense to group them into subsystems. (Albers, Matthiesen, et al., 2019) If there is only one component in the system boundary that needs to be optimized in its mass, the functional area-based approach can be applied. Here, the component is divided into different areas in which the functions are fulfilled. (Albers, Revfi, & Spadinger, 2017) In the following only the component-based approach is described, for which more

than one component is contained in the system boundary. However, the generated findings can be directly transferred to the functional area-based approach.

Following the definition of the system boundary, the functional analysis is conducted analogously to the TWA procedure, in which the technical functions of the previously defined system boundary are determined. This analysis activity can be performed with the help of expert knowledge and additionally systematically, methodically supported by the C&C²-Approach (see Subsection 2.1.3) (Albers, Revfi, & Spadinger, 2017).

In parallel, it has to be decided which factors from the conflicting priorities of mass, costs and CO_2 emissions should be considered in addition to mass. Depending on the system in development and the industry, it may make sense not to consider all factors. For example, the consideration of costs could play a minor role for companies from the aerospace industry (see Subsection 2.2.5).

Then the defined factors have to be determined for each subsystem in the system boundary. When optimizing an internal preceding product, this should be possible with little effort, since the data should be available within the company. If the data are not available, the costs can be determined, for example, using a (greenfield or brownfield) life-cycle cost (LCC) analysis and the CO_2 emissions with a life-cycle assessment (LCA) *from cradle to grave* (see Subsection 2.2.6). However, other approaches to determine costs and CO_2 emissions are also possible as long as they provide robust data sets as input to the ETWA and are available at the defined component or subsystem level. In the following, the term *effort* shall be understood as the triple of mass, costs and CO_2 emissions. (Albers, Revfi, & Spadinger, 2020)

Due to the methodical approach of mass- and cost-independent assignment of components/subsystems to functions, the TWA allows an extension by further factors (Wagner, 2015). This assumption is of central importance for the present work. Based on this assumption, the input to the Function-Mass-Matrix of the TWA is extended by costs and CO_2 emissions, so that with the ETWA the combined assessment of mass, costs and CO_2 emissions is made possible. This changes the structure of the matrix, which becomes the Function-Effort-Matrix (see Figure 5.12). Analogous to the TWA, in the Function-Effort-Matrix, the percentage contribution of each subsystem to the function fulfillment is assigned (Albers, Revfi, & Spadinger, 2017, 2020). For this, the question is posed how much component or subsystem x contributes to function y. This procedure indicates the cross-subsystem system lightweight design approach, as a function can be fulfilled by more than one component/subsystem (Albers, Revfi, & Spadinger, 2020). The assignment procedure is

crucial for the result of the method and at the same time very time consuming (see Subsection 5.1.2).
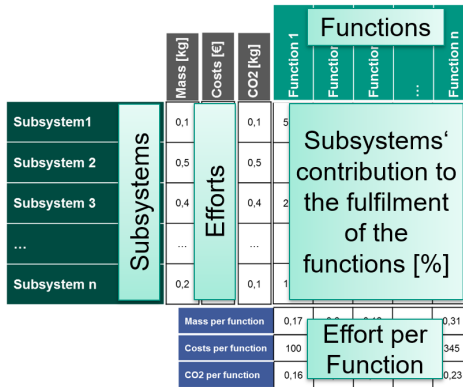
Figure 5.12: Function-Effort-Matrix adapted from Albers, Moeser, and Revfi (2018)

The assignment can be carried out in a purposeful way with the help of expert knowledge (Albers, Matthiesen, et al., 2019). In the absence of expert knowledge, the method should still be applicable. Therefore, Albers, Matthiesen, et al. (2019) developed a method that systematically supports the filling in of the matrix using the C&C²-Approach (see Figure 5.13).
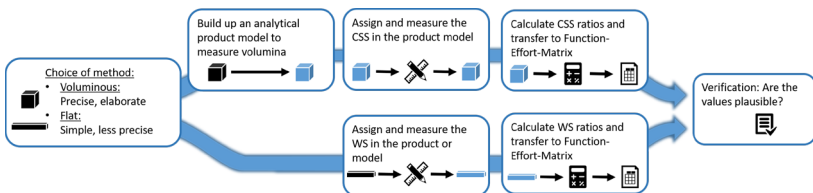
Figure 5.13: Modeling of embodiment function relation either based on WSP or CSS (Albers, Matthiesen, et al., 2019)

When applying the method, a distinction has to be made between the procedure for flat and voluminous subsystems. In the case of flat subsystems, the working surfaces involved in the respective function fulfillment are set in relation to the whole surface and the percentage share of the subsystem in the function fulfillment is determined in this way. In the case of the CSS-based approach, the volumes containing the CSS in the respective function fulfillment are set in relation to the total volume and the percentage values for the Function-Effort-Matrix are determined on this basis. (Albers, Matthiesen, et al., 2019) Figure 5.14 illustrates the different approaches on the example of the subsystem *piston crown*.
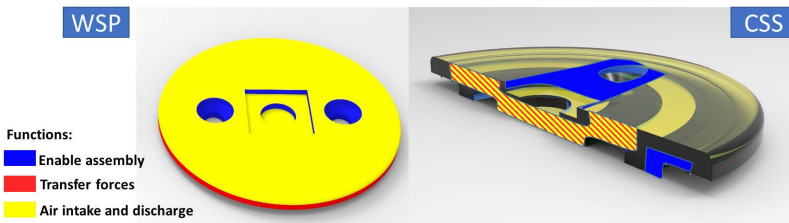
Figure 5.14: Comparison of WSP- and CSS-based approach (Albers, Matthiesen, et al., 2019) on the example of a piston crown

Based on the assigned contributions, mass, costs and CO_2 emissions can be determined for each function. As a result, the combined consideration of the three factors is already enabled in the iPeM core activity *Detect Ideas* in early phases of the product engineering process, in which a significant influence can be made on the subsequent efforts. Support in this activity is particularly important for the development of MMD solutions, since existing component structures often have to be dissolved for the combination of new materials. The functional mass, costs and CO_2 emissions are subsequently used to derive lightweight search fields taking into account costs and CO_2 emissions.

The identification of lightweight search fields in the ETWA that indicate lightweight design potential can be performed using various methods that follow the procedure of the TWA, since the derivation of the search fields was rated as good in the survey for the assessment of demands (see Subsection 5.1.2).

(a)

(b)

(c)
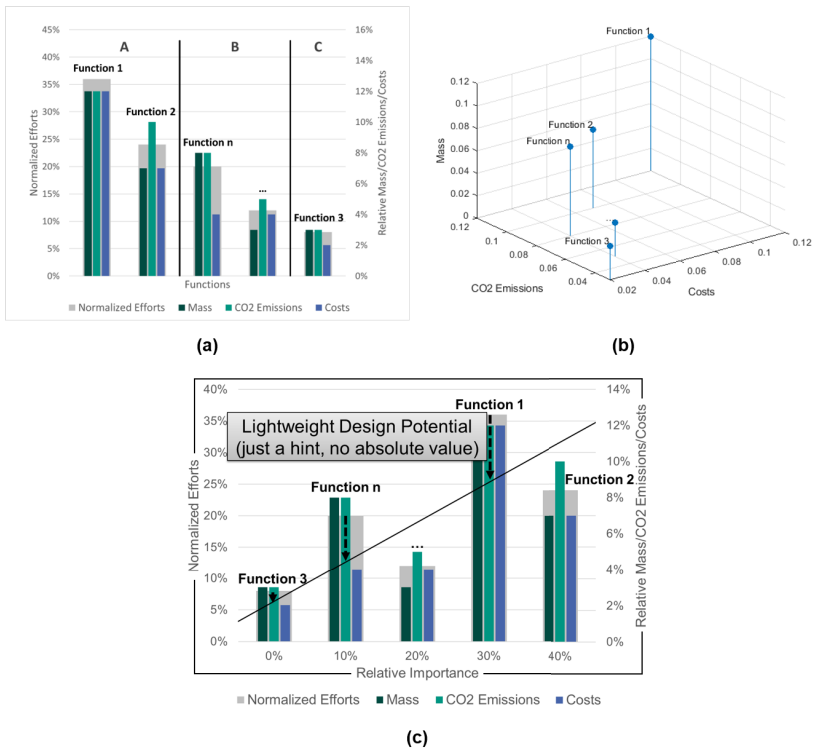
Figure 5.15: Identification of lightweight search fields. (a) ABC analysis (b) 3D portfolio with the efforts as axes (c) 2D function portfolio (adapted from Albers, Revfi, and Spadinger (2020))

Either the subsystems with the highest absolute effort can be considered or, for example, a function-based ABC analysis, in which the individual efforts remain transparent, can be performed (see Figure 5.15 (a)). Furthermore, the functional efforts can be visualized in a 3D graph, where mass, costs and CO_2 emissions represent the axes (see Figure 5.15 (b)). In addition, the evaluation can be done in a 2D function portfolio, where the functional effort is plotted over the relative importance of the individual functions for the overall system under consideration (see Figure 5.15 (c)). Here, the lightweight design potential is indicated by those functions whose effort is

above the regression line. The relative importance of the functions can be determined, for example, by a paired comparison performed by a team of experts. (Albers, Revfi, & Spadinger, 2020)

By weighting (indicated by the variables w_m, w_ϵ, w_{CO2}) the respective factors mass (m), costs (€) and CO_2 emissions ($CO2$), a company-specific focus or strategic positioning can be made in the evaluation (see Equation 49) (Revfi, Albers, Holoch, & Spadinger, 2018). For this purpose, different approaches are conceivable in principle. In the context of this work, a linear approach is used (see Equation 49) to enable intuitive applicability and simple traceability. Such an approach is also used, for example, by Ashby (2005) for material selection.

$$E = w_m \cdot m + w_\epsilon \cdot € + w_{CO2} \cdot CO2$$
$$\text{with } w_m + w_\epsilon + w_{CO2} = 1$$

49

Since the lightweight search fields provide the basis for all subsequent synthesizing activities, a combination of the evaluation methods should always be used in order to fully identify the potentials.

The subsequent steps of concept design, concept evaluation and concept consequences are carried out in a chronologically progressive, iterative process. Depending on the specific situation, different methods have to be used in the individual steps. The more detailed the concepts become, the more quantitative methods (such as CAE) can be employed. However, especially in early phases where, for example, hand sketches are available, the data basis is usually not yet sufficient to use reliable quantitative methods and therefore qualitative methods should be preferred. Thus, the selection of methods to support the process should be continuously reviewed. An exemplary selection of methods for the individual steps is presented in the following.

In order to generate new embodiment concepts based on the search fields in the TWA, Albers et al. (2013) and Wagner (2015) suggest, among others, the use of TRIZ. However, this very time-consuming method is not the only option. In the projects accompanied by the author, the Brainwriting Pool, the 6-3-5 method, or the World Café have also proven to be a good support for the ETWA. Further support for the situation-specific method selection can also be found in the *InnoFox* (see Subsection 2.1.1). Since the methods provided by the TWA were evaluated with

potential for optimization in the assessment of demands (see Subsection 5.1.2), another method to support synthesis in the context of the PGE will be developed for the ETWA (see Subsection 5.2.2).

For the selection of solutions, the TWA according to Albers et al. (2013) provides for a three-step evaluation procedure (see Subsection 2.2.6). After a rough preselection, for example, utility analyses based on hand sketches can be used. This is followed by the impact analysis (see Subsection 2.2.6), which, however, already requires concrete embodiment concepts. As the concepts are further detailed, they should later be supplemented by simulations or component and overall system tests. The ETWA enhances this proposed procedure for the selection of solutions by newly developed methods (see Subsection 5.2.3), which can be used after a utility analysis and before the impact analysis. In this way a broad, additional basis for decision-making is provided which is particularly important when implementing MMD concepts, since the concepts usually require several materials, manufacturing processes and joining technologies, which have to be evaluated in combination as a whole. This results in complex decision-making, which can hardly be made on the basis of empirical knowledge.

The steps of concept design, concept evaluation, and concept consequences analysis are performed iteratively until the target effort can be determined (Albers, Revfi, & Spadinger, 2020). The concept finally selected at the end of the process is ready for realization in a new product generation.

In summary, the ETWA represents a method that is built on the strengths of the TWA known from the KaSPro – Karlsruhe School of Product Engineering and extends it so that the conflict of objectives between mass, costs and CO_2 emissions becomes manageable for the product developer. Especially for the development of MMD, the manageability of the complexity arising from different material classes and manufacturing processes is crucial to enable a successful product development. Thus, the ETWA is the answer to the research question formulated at the beginning of this subsection (see also Section 3.1).

In the following, as previously described, a method for supporting the product developer in the synthesis of new concept ideas based on extended lightweight search fields is presented.

5.2.2   Synthesis

In order to further support the product developer in generating new concept ideas in the ETWA, a method for function-based benchmarking was developed, which is presented subsequently. Accordingly, the fourth research question of the second research hypothesis (see also Section 3.1) is to be answered within the scope of this subsection.

Research Question

    iv.   How can a method look like that supports the product developer in the Extended Target Weighing Approach (ETWA) within the function-based synthesis of new embodiment concepts based on a systematic analysis of the reference system?

The method has been published previously in the publication Albers, Revfi, Kraus, and Spadinger (2019).

In contrast to the established benchmarking based on components, the developed method utilizes the description of the products on the functional level available from the ETWA. With the aid of the solution-open product description based on its functions, the product developer can identify lightweight design potential in comparison with other products, which stimulates his or her creativity and supports the development of new concept ideas. The success of benchmarking crucially depends on the selection of the benchmark partner (cf. Subsection 2.1.5), which is the first step of the developed method. Figure 5.16 illustrates the workflow of the developed benchmark method.

A benchmark product is a product that is to be assessed and compared to the internal product which is to be optimized in its mass. The benchmark product is part of the reference system in terms of PGE – Product Generation Engineering. Benchmark products can be classified into different categories (see Subsection 2.1.5). Depending on the category, there is a different accessibility to the data needed for benchmarking. For internal benchmarking, the data is usually well accessible. For competition benchmarking, competitor products may need to be purchased and disassembled. However, in order to reduce this effort, in the meantime there are also

service providers who have specialized in collecting and selling benchmark information. In the automotive sector, for example, the benchmarking platform A2Mac1[48] offers data for vehicles from different manufacturers.
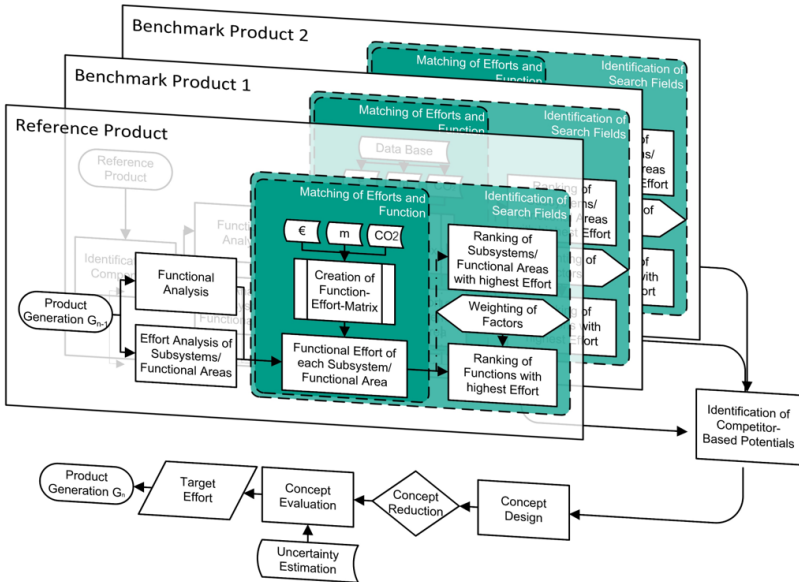
Figure 5.16: Workflow of the benchmark method within the ETWA (Albers, Revfi, et al., 2019)

The first layer of the method (Reference Product) in Figure 5.16 describes the workflow presented in Subsection 5.2.1 for conducting the ETWA on the internal product, which is to be optimized in terms of its mass while taking costs and CO_2 emissions into account. This procedure is completed up to the step of *Ranking of Functions with highest Effort*, in which the lightweight search fields are generated.

---

[48] https://portal.a2mac1.com/de/home-7/ (accessed March 17, 2021)

In parallel, the procedure is performed in a slightly modified version for the benchmark product (see second layer in Figure 5.16, which is illustrated separately in Figure 5.17).
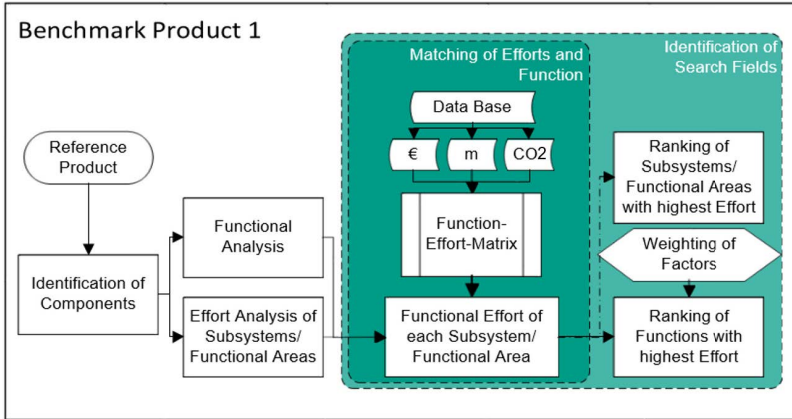
Figure 5.17: Workflow for a benchmark product (Albers, Revfi, et al., 2019)

For the analysis of the benchmark product, the first step is to determine the appropriate system boundary. This means that those components/subsystems have to be identified that comprise the identical system scope as in the internal reference product. For this, it can be helpful to ask the question in which area the benchmark product fulfills the same functions as the internal reference product. (Albers, Revfi, et al., 2019)

The next step is the functional analysis of the previously defined subsystems in the system boundary. Here, the functions of the internal reference product represent a good starting point, which can be adopted to a large extent via carryover variation. Supporting the analysis of the benchmark product, the C&C²-Approach (see Subsection 2.1.3) can be employed to infer the functions from the embodiment. The functional analysis has to be done very carefully, because if it is found that there is a function that the benchmark product does not fulfill which the internal reference product does, the choice of the system boundary has to be checked. The same check is necessary if it is found that the benchmark product fulfills additional functions. (Albers, Revfi, et al., 2019) If the analysis of the functions nevertheless leaves

a delta in the function scopes, this already marks a first approach for the identification of lightweight design potentials, as will be explained in the following.

In addition, mass, costs and CO_2 emissions of the benchmark product need to be determined. A2mac1 can be helpful for obtaining the mass. Alternatively, the corresponding subsystems can be weighed if the benchmark product is available in physical form. The determination of costs and CO_2 emissions is usually more difficult, as they depend on individual conditions in the companies. In this context, expert knowledge or internal company calculation models can be useful. (Albers, Revfi, et al., 2019) For the estimate of the CO_2 emissions, for example, the software GaBi[49] or the software Granta EduPack[50] can be used.

In the next step, the creation of the Function-Effort-Matrix for the benchmark product, expert knowledge is again helpful. Additionally, the C&C²-based method presented in Subsection 5.2.1 can provide support. Using the Function-Effort-Matrix, mass, costs and CO_2 emissions per function are also determined for the benchmark product. If multiple benchmark products are considered, the procedure is to be carried out analogously for all of them.

On the basis of the gathered efforts per function, the benchmarking can be performed. Assuming the same functions for the internal product as well as the benchmark product and the corresponding relative importance of these functions, the 2D benchmark function portfolio can be created. A generic 2D benchmark function portfolio is shown in Figure 5.18. The plotted regression line indicating lightweight design potential (see Subsection 5.2.1) refers to the internal reference product. (Albers, Revfi, et al., 2019)

The assumption of the same functions of the products to be compared as well as the corresponding same relative importance offers the product developer the possibility of a fast overview of possible lightweight design potentials, since the benchmark product does not need to be completely reassessed. (Albers, Revfi, et al., 2019) Kraus (2018)[51] shows in his thesis, which was co-supervised by the author, on the basis of a strut tower that this approach can be convenient. Nevertheless, it is a simplification whose applicability has to be verified in each individual case. Particularly in body construction for vehicles with internal combustion engines in the

---

[49] https://gabi.sphera.com/international/software/gabi-software/ (accessed March 18, 2021)

[50] https://www.ansys.com/products/materials/granta-edupack/ (accessed March 18, 2021)

[51] Co-supervised thesis (unpublished)

automotive industry, this assumption seems appropriate, since the functions of the body are largely identical for all manufacturers.
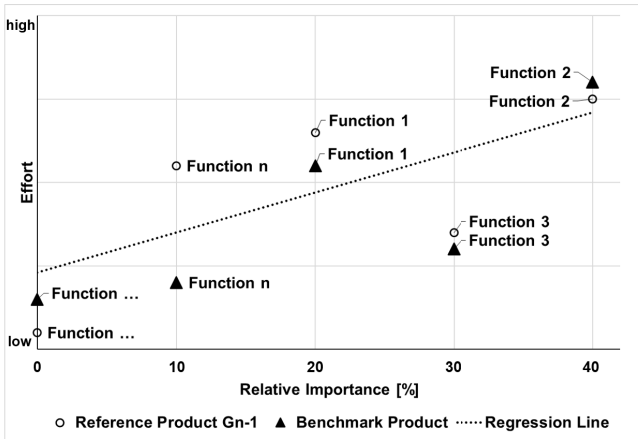
Figure 5.18: 2D benchmark function portfolio for the reference and the benchmark product assuming the same functions and relative importance adapted from Albers, Revfi, et al. (2019)

In the evaluation of the 2D benchmark function portfolio, the functions of the internal reference product (circles in Figure 5.18) that are above the regression line still indicate lightweight design potential. However, additional lightweight design potential is now also revealed if the functions of the benchmark product (triangles in Figure 5.18) are realized with less effort compared to the functions of the internal reference product (e.g., Function n in Figure 5.18). This gives a hint to the product developer that in the benchmark product the functions might be realized via a different conceptual design, which makes it possible to construct lighter, cheaper and/or more CO_2 efficient. (Albers, Revfi, et al., 2019)

If the functional analysis of the benchmark product results in other functions compared to the internal reference product, which are not the result of a different definition of the system boundary, the benchmark method can still be employed. In this case, it is important to consider in the evaluation that a different relative importance of the functions may occur. However, this can be eliminated, for example, by selecting only identical functions. In addition, it should be investigated why the functions

are different. If additional functions are found in the benchmark product, this provides a valuable indication for the product developer, because the benchmark product may be able to perform more functions with the same subsystems. This could indicate a different conceptual design. If the benchmark product performs less functions than the internal reference product, this also provides a valuable hint, because it is possible that certain functions are not needed or that they serve as a competitive differentiator against competitors on the market. (Albers, Revfi, et al., 2019)

Comparing products from different manufacturers or different segments can lead to another challenge. For example, if the underbodies of two different battery electric vehicles are compared, the benchmark product will in general have a different range than the internal reference product. The reason for this could be a different battery size. Accordingly, the vehicles have different battery weights, which in turn, for example, result in different requirements for the stiffness of the load-bearing subsystems. As a result, a direct comparison of the two products is difficult. In order to be able to still apply the synthesis support provided by function-based benchmarking in such situations, the function portfolio is enhanced by an additional axis. This axis specifies the requirements for the respective function, which means that different requirements for the same functions can be taken into account in the evaluation. Figure 5.19 illustrates the resulting 3D benchmark function portfolio. (Albers, Revfi, et al., 2019)
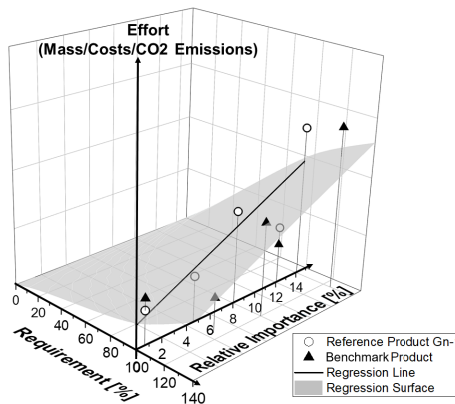
Figure 5.19: 3D function portfolio with requirements axis (Albers, Revfi, et al., 2019)

For the 3D function portfolio, the internal reference product is located at 100% on the requirement axis together with the regression line from the 2D function portfolio. Thus, the regression line is identical as described before. The identification of lightweight design potential based on all three dimensions is done using a new regression surface. This goes through the regression line and the intersection line at 0% requirement and zero effort. The underlying assumption is that a function that is fulfilled to 0% by its requirement is not allowed to cause any effort. With the help of this 3D function portfolio, benchmarking between products with different requirements becomes possible. (Albers, Revfi, et al., 2019)

In summary, the presented function-based benchmark method offers a way to support the product developer in the synthesis by extending the reference system and systematizing its analysis. Identified differences in the functional efforts between the internal reference product and one or more benchmark products help to stimulate the product developer's creativity in a focused way and at the same time expand the knowledge base. In this way, the developed method addresses the demand for the support of the product developer in the synthesis, as stated in the system of objectives for the extension of the TWA in Subsection 5.1.3, and answers the research question formulated at the beginning of this subsection (see also Section 3.1).

Further methods which support the material selection under consideration of the given project objectives regarding mass, costs and CO_2 emissions in the synthesis, were additionally developed by the author (Kaspar, Revfi, Albers, & Vielhaber, 2019; Revfi, Kaspar, Vielhaber, & Albers, 2019). These are mentioned here for completeness only and will not be further considered in the following.

In the next subsection, methods for supporting the product developer in the consequences analysis are presented, which are also defined as a requirement in the system of objectives of the method to be developed in Subsection 5.1.3.

5.2.3   Consequences Analysis

Having generated new embodiment concepts on the basis of the identified lightweight search fields, the product developer is confronted with the challenge of reducing them. In order to avoid hasty or gut decisions, an iterative consequences analysis is helpful. However, especially in early phases, there exists the problem that a decision has to be made despite a low level of detail. This subsection presents methods that go beyond the state of research of the TWA and which support the consequences analysis in the ETWA. Consequently, this subsection answers the fifth research question of the second research hypothesis (see also Section 3.1).

Research Question

v. For the concept ideas generated during the application of the ETWA, how can the consequences be assessed differentially in terms of technological uncertainties, maturity level and costs already in early phases?

In the following, three methods are presented as an answer to the research question. The method for the estimation of technological uncertainties (see Subsection 5.2.3.1) can already be applied in early phases of the product engineering process. The assessment of design maturity (see Subsection 5.2.3.2) is a method for quantifying the semi-quantitative factors Reference Product – Technology and Reference Product – Application Scenario introduced in Subsection 5.2.3.1. Finally, in Subsection 5.2.3.3, a method for the early, semi-quantitative evaluation of manufacturing costs is presented, which was developed in cooperation with BMW AG.

5.2.3.1   Technological Uncertainties

In the development of MMD, it is often necessary to dissolve existing subsystem boundaries and to think in new embodiment concepts and materials. The example of the design of SMC parts in Chapter 4 demonstrates the challenges faced by the product developer in finding a design and how these challenges can be made manageable. Opportunities such as large mass reductions can arise as a result, but these are countered by concept-specific risks and uncertainties. In order to be able to provide an objective metric with regard to the uncertainties of new concept ideas developed in the ETWA, a method is subsequently presented that was previously published in the publication by Albers, Revfi, and Spadinger (2018).

A distinction has to be made between risk and uncertainty. Risk is understood as the occurrence probability of an uncertainty. Uncertainty is defined as the difference between available information and the information that would be necessary to perform a certain activity (Galbraith, 1973). Thus, uncertainty is always associated with a lack of knowledge. Consequently, this means that uncertainty can be reduced by increasing knowledge. Furthermore, a distinction is to be made between market uncertainties and technological uncertainties (Reichwald, Engelmann, Meyer, & Walcher, 2007). Market uncertainty comprises concerns about meeting customer needs and the target market, while technological uncertainty covers concerns about technical requirements and feasibility.

For the success of a project it is decisive to what extent the uncertainties can be reduced during the early phase of product development (Moenaert, Meyer, Souder, & Deschoolmeester, 1995). The product developer's task is to develop products with the available knowledge and skills (Verworn, 2005). In the course of the product

engineering process, he or she generates knowledge, which reduces uncertainties. Accordingly, being aware of existing uncertainties in early phases makes a decisive contribution to a successful product development.

In the development of MMD, technological uncertainties arise, for example, due to the application of new materials, manufacturing processes or joining technologies, which should consequently be taken into account in the evaluation of the concepts. In order to determine these technological uncertainties and thus to introduce an additional module for the consequences analysis, a newly developed method is presented in the following. It is based on the KaSPro – Karlsruhe School of Product Engineering with the established description model of the PGE – Product Generation Engineering (see Subsection 2.1.2) and the Validation Prioritization Approach (VPA) (see Subsection 2.1.5).

The VPA supports the product developer in identifying those elements of a product that are associated with high uncertainty in order to reduce this uncertainty through validation (see Subsection 2.1.5). In this regard, the VPA is defined by the three factors *impact*, *technology* and *application scenario*. Based on the assumptions valid in the model of the PGE that new development shares in combination with their origin allow a conclusion about their uncertainty (see Subsection 2.1.2) and that carryover variations are associated with a comparatively smaller uncertainty, the four factors for the method to be developed are derived: *Impact*, *Carryover Variation Share*, *Reference Product – Technology*, *Reference Product – Application Scenario* (Albers, Revfi, & Spadinger, 2018). By adding up the values for the four factors, the technological uncertainty of an embodiment concept is obtained (Albers, Revfi, & Spadinger, 2018). The individual factors are specified in the following.

Impact

The *Impact* describes the cumulative relative importance of the functions affected by the new principle or embodiment concept. The idea behind impact is that designs which involve changes to important functions, such as the main functions, lead to a higher uncertainty. (Albers, Revfi, & Spadinger, 2018)

Having developed a new principle or embodiment concept, it can be directly determined which functions are affected by the design change with the help of a comparison to the reference product. To determine the Impact, the relative importance of these affected functions which are derived from the paired comparison are added up and the underlying uncertainty value is taken from the scale in Table 29. The scale is based on a scale for ABC analyses, since this method also uses a cumulative approach. However, it is to be pointed out that with each application it has to be

checked individually whether the choice of the value ranges is suitable for the present problem. (Albers, Revfi, & Spadinger, 2020) The value ranges shown in Table 29 were defined on the basis of the experiences gained in the EU project ALLIANCE.

Table 29:   Scale: Impact adapted from Albers, Revfi, and Spadinger (2018)

Cumulative importance of the affected functions [%]	Uncertainty Factor
>95	5
85.01-95	4
70.01-85	3
50.01-70	2
0-50	1

Carryover Variation Share

The factor *Carryover Variation Share* indicates how many subsystems from the reference product as part of the reference system are carried over as carryover variation into the newly developed embodiment concept. The underlying assumption is that a large number of subsystems that are carried over leads to a smaller uncertainty. In order to determine the Carryover Variation Share, the new embodiment concept is compared to the reference product. The number of subsystems that are carried over in relation to the total number of subsystems in the system boundary results in the Carryover Variation Share, which is associated with a corresponding uncertainty factor according to Table 30. (Albers, Revfi, & Spadinger, 2018) For this, a linear-distributed scale is proposed. However, this assumption can be adapted at any time depending on the specific application. (Albers, Revfi, & Spadinger, 2020)

Table 30:   Scale: Carryover Variation Share adapted from Albers, Revfi, and Spadinger (2018)

Carryover Variation Share [%]	Uncertainty Factor
<20	5
20.01-40	4
40.01-60	3
60.01-80	2
80.01-100	1

Reference Product – Technology

The factor *Reference Product – Technology* comprises the used materials, the occurring active principles as well as the involved production processes according to the definition in the VPA (Albers et al., 2014). An active principle is understood as the transfer of force, material, energy or information through a solid body, fluid, gas or field. To determine the value of this factor, the developed embodiment concept needs to be abstracted to the level of its principles. For the classification of the developed concept, the question can be asked in which context the used material, the used active principle and the required production process are/were already applied. For example, technologies that are only employed in research have a high technological uncertainty if they are intended to be used in industrial mass production. If the technology reference product comes from another branch, this also has to be assessed with an increased technological uncertainty, since the knowledge about the technology first has to be transferred to the right context (e.g., aerospace industry to automotive industry). The uncertainty factor to be selected depending on the context can be taken from Table 31. The scale is aligned with the risk portfolio of the PGE – Product Generation Engineering (see Subsection 2.1.2). (Albers, Revfi, & Spadinger, 2018)

Table 31: Scale: Reference Product – Technology adapted from Albers, Revfi, and Spadinger (2018)

Reference Product – Technology	Uncertainty Factor
Research	5
Other Branch	4
Same Branch	3
Company	2
Development Team	1

Reference Product – Application Scenario

The last factor is *Reference Product – Application Scenario*. This factor describes the fulfillment of functions of a subsystem, taking into account the associated boundary conditions and requirements as well as the use of the principle concept in the same context. In particular, this includes the occurring loads or load spectra. In order to be able to classify a developed concept in Table 32, the question can be asked where a similar subsystem is/was already used to fulfill the same function under the

same boundary conditions (= same context) and the same active principle. Ultimately, the factor Reference Product – Application Scenario describes the proximity of the developed concept idea to a possible reference product. (Albers, Revfi, & Spadinger, 2018) An example for this could be that the product developer decides to use a material that is new for his or her company, such as SMC, for load transfer. If there are competitors who are already implementing SMC under similar load collectives, then the technological uncertainty associated with the development should be evaluated smaller than if the implementation requires a scaling of a material that is currently being researched.

Table 32:   Scale: Reference Product – Application Scenario adapted from Albers, Revfi, and Spadinger (2018)

Reference Product – Application Scenario	Uncertainty Factor
Not yet applied in the same context	5
Research	4
Other Branch	3
Same Branch	2
Company	1

Based on the classification of the developed concept idea in the respective scale of the four factors, the technological uncertainty is determined by the addition of the individual values. This can also be represented as a surface in a radar chart (see Figure 5.20). In this way, a quick overview of the technological uncertainty associated with the developed concept idea is provided. (Albers, Revfi, & Spadinger, 2018)

By determining the technological uncertainty, further fields of action can be derived for the considered concept ideas. If, for example, there is a concept that shows high potential for mass reduction but at the same time indicates a high technological uncertainty, it might be better from the product developer's point of view to pursue a concept that offers less potential for mass reduction but can be implemented in his or her company with less uncertainty. Another case could be that a competitor uses the required technologies in similar application scenarios. In this situation, it could be promising to recruit an expert from the competitor. Thus, the method is also suitable for the support of management decisions. (Albers, Revfi, & Spadinger, 2018)
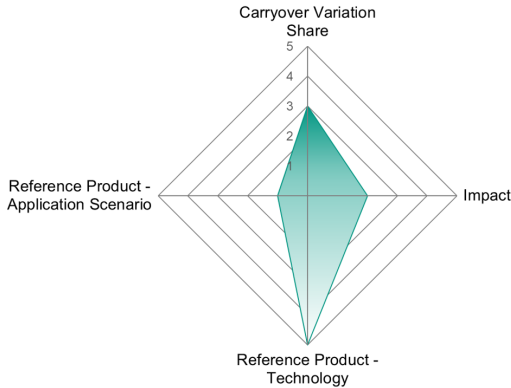
Figure 5.20: Visualization of the technological uncertainty adapted from Albers, Revfi, and Spadinger (2018)

The estimation of the technological uncertainty of concept ideas developed for subsystems is closely associated with the evaluation of their design readiness, which is presented in the next subsection. This design readiness represents a quantification of the two semiquantitative factors Reference Product – Technology and Reference Product – Application Scenario.

5.2.3.2 Design Readiness Level (DRL)

In the development of MMD concepts for lightweight design, it is not only the assessment of the manufacturability of the individual components that is relevant, but also the joinability of the components among each other and additionally their integration into the rest system that plays a decisive role. Particularly against the background of the PGE, the evaluation of the integration in the rest system is indispensable. Products are developed in generations by systematically combining PV, EV and AV of reference system elements. Thus, it is absolutely necessary to evaluate an integrability of newly developed subsystems into a rest structure that has been carried over. The Design Readiness Level developed as part of this thesis allows such an assessment for newly developed embodiment concepts by combining the assessment of the maturity level of the intended manufacturing technology with the

assessment of the maturity level of the required joining technology. Therefore, the DRL represents a further module in the consequences analysis of concept ideas developed in the ETWA. The method has been published previously in the publication Revfi, Wilwer, Behdinan, and Albers (2020).

The Design Readiness Level is inspired by the System Readiness Level, which multiplies the Technology Readiness Level by the Integration Readiness Level (see Subsection 2.1.5). In addition, the DRL is built on the work of Fahimian and Behdinan (2017), who converted the ordinal TRL into cardinal coefficients using the maturity time (see Subsection 2.1.5). As shown by Fahimian and Behdinan (2017), this calculation can be used with technologies that are considered retrospectively after their market entry. However, for technologies that are still in development and whose TRL and IRL are not identical, the cardinal coefficients do not provide a comparable measure (see Subsection 2.1.5). However, particularly in the development of new (MMD) concepts, it cannot be assumed that all manufacturing and joining technologies required have the same TRL and IRL.

This is the starting point for the DRL, which integrates the past temporal development of individual technologies for the extrapolation into the future until market maturity (TRL = 9 in the NASA scale) to enable a comparison of different design maturity levels based on the cardinal coefficients. (Revfi, Wilwer, et al., 2020)

The DRL vector is defined by multiplying the IRL cardinal coefficients (index c) and the TRL cardinal coefficients (see Equation 50). The central difference to the SRL is that the TRL and IRL values assigned are predicted into the future based on their development in the past to determine cardinal numbers instead of ordinal ones. For this purpose, e.g. in a very simple case, the forecast function in Microsoft Excel can be used, which applies an Exponential Smoothing (ETS) algorithm. The forecast quality is crucial for the success of the presented method. Additionally, expert knowledge can be of very great benefit for the forecast. The technology management in companies can also be a valuable support in forecasting. (Revfi, Wilwer, et al., 2020)

$$DRL_{m_K \times 1} = [\boldsymbol{IRL}]^c{}_{m_K \times m_K} * [TRL]^c{}_{m_K \times 1} \qquad \textbf{50}$$

The vector of the TRL cardinal coefficients is obtained for an MMD concept consisting of m_K components, for which different manufacturing technologies are used, according to Equation 51.

$$TRL^c_{m_K \times 1} = \begin{bmatrix} TRL^c_1 \\ TRL^c_2 \\ \vdots \\ TRL^c_{m_K} \end{bmatrix} \qquad \textbf{51}$$

The IRL matrix which contains the cardinal coefficients of the joining technologies between the m_K components is formulated according to Equation 52. IRL_{ij} (i, j ϵ 1, 2, ..., m_K) indicates the maturity of the joining technology for joining components *i* and *j*. Accordingly, it is equivalent to IRL_{ji}. The hypothetical joining IRL_{ii} is assumed to be 1. If there is no connection between two components, the value 0 is inserted. (Revfi, Wilwer, et al., 2020)

$$\textbf{IRL}^c_{m_K \times m_K} = \begin{bmatrix} IRL^c_{11} & \cdots & IRL^c_{1m_K} \\ \vdots & \ddots & \vdots \\ IRL^c_{m_K 1} & \cdots & IRL^c_{m_K m_K} \end{bmatrix} \qquad \textbf{52}$$

Consequently, the DRL of a newly developed embodiment concept depends on the maturity level of the applied joining and manufacturing technologies, but also on the system architecture (Revfi, Wilwer, et al., 2020). Following the findings of Sauser et al. (2009) on the SRL, the values for the DRL are normalized by dividing the DRL vector entry by the number of interactions. According to Equation 53, the overall system DRL is obtained by summing the normalized DRLs and dividing by the number of components (Revfi, Wilwer, et al., 2020).

$$DRL = \frac{\dfrac{DRL_1}{I_1} + \dfrac{DRL_2}{I_2} + \cdots + \dfrac{DRL_{m_K}}{I_{m_K}}}{m_K} \qquad \textbf{53}$$

with I_i = Number of interactions on subsystem i and with itself

In addition to the isolated DRL evaluation of the considered embodiment concepts which represents a quantification of the dimensions Reference Product – Technology and Reference Product – Application Scenario presented in Subsection 5.2.3.1, the evaluation of the integration of the concept into an existing rest structure is essential, as discussed at the beginning of this subsection. This is addressed in the following.

Figure 5.21 (a) shows an exemplary architecture model of a system consisting of 17 components. The components $m_K = 1..5$ are to be replaced by a new MMD concept. The surrounding twelve components represent the rest system. Since in the DRL evaluation, this system would now entail a 14x14 IRL matrix (S1-S3 do not interact directly with the subsystem to be developed and can therefore be neglected), there is a possibility to simplify the rest system. For this purpose, similar working principles according to the C&C²-Approach are aggregated. Similar working principles means that working surface pairs that are responsible for functional fulfillment only differ quantitatively and not conceptually. This applies, for example, to cylindrical press fits that only vary in their diameter and the transferred load. All these subsystems, which interact directly with the newly developed MMD concept and have similar working surface pairs, should be aggregated by a substitute system. In Figure 5.21 (b), subsystems A and B are simplified to K1, D1-D3 and E1-E3 to K2, and C to K3. Of course, this procedure is only possible if neither a component of the rest system nor the type of interaction is changed. If such a change is unavoidable, the system boundary of the newly designed subsystem should be extended. However, this is possible without any problems due to the fractal character of the C&C²-Approach. (Revfi, Wilwer, et al., 2020)
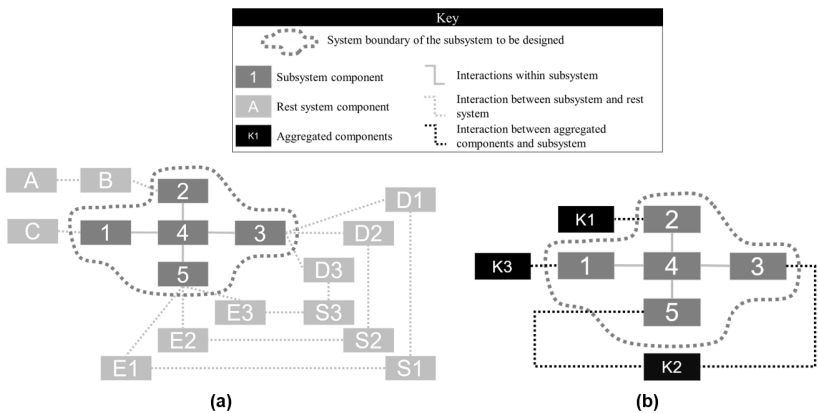
Figure 5.21: System diagram: (a) full representation (b) simplification adapted from Revfi, Wilwer, et al. (2020)

This procedure reduces the effort to calculate the DRL. For r substitute systems, the dimension of the TRL vector increases to $(m_K + r) \times 1$ and the dimension of the IRL matrix to $(m_K + r) \times (m_K + r)$. In the example from Figure 5.21, this corresponds to a reduction from 14 components to be considered to 8. (Revfi, Wilwer, et al., 2020)

Since all components belonging to the rest system are already in use in the preceding product, their sum of cardinal coefficients is assigned the value 1, which corresponds to series maturity. Due to the fact that only the integrability of the newly developed subsystem into the rest system is to be assessed, interactions between components or substitute systems in the rest system are not evaluated in the IRL matrix and thus set to 0. This has no influence on the calculation of the DRL of the subsystem to be developed. (Revfi, Wilwer, et al., 2020)

Accordingly, the presented method enables the product developer to quantify the dimensions Reference Product – Technology and Reference Product – Application Scenario defined in the uncertainty assessment. At the same time, however, this is associated with a higher effort than the semiquantitative procedure presented in Subsection 5.2.3.1. Therefore, it has to be decided on a situation-specific basis which benefit is to be expected in relation to the effort required. If the TRL and IRL values are already available in technology management, the effort required for implementation is reduced.

Both methods developed for uncertainty analysis and DRL evaluation focus on the technical feasibility of the developed embodiment concepts. However, since the ETWA also includes a combined consideration of costs, a method is presented subsequently that allows the evaluation of cost potentials of developed lightweight design solutions already in early phases.

5.2.3.3 Semiquantitative Evaluation Model for Manufacturing Costs of New Concept Ideas

In the performance of the ETWA according to Subsection 5.2.1, the concept ideas generated in the course of concept design need to be evaluated with regard to their costs. Due to the low maturity level of the concept ideas in early phases of product development, it is often not possible to perform detailed, quantitative cost assessments. In order to still be able to make a cost estimate, quantitative data can be generated based on an LCC (greenfield approach) as performed by the project partners in the EU project ALLIANCE (Revfi, Tamm, Thirunavukkarasu, & Timmer, 2020). Here, it is assumed that the production lines required for the developed concept are newly built on a greenfield site. Accordingly, the surrounding conditions of

existing production and logistics structures are not taken into account. In the following, a semiquantitative evaluation model for the manufacturing costs of newly developed design concepts with a low maturity level is presented, considering existing production and logistics structures (brownfield). Thus, the semiquantitative evaluation model represents another module for the consequences analysis in the ETWA and can also be employed for quick cost evaluations. Hence, the product developer can choose between the semiquantitative evaluation model and the LCC depending on the situation and application in order to perform a cost assessment of new concept ideas.

The developed semiquantitative model is the outcome of a collaboration between BMW AG and IPEK – Institute of Product Engineering. Thanks to the cooperation, the industrial applicability could be evaluated. The developed model has already been published previously in the publication Revfi, Gladysz, Spadinger, Albers, and Staeves (2020).

The method developed is not based on absolute numbers, but rather the potentials of the PGE – Product Generation Engineering are used by taking reference system elements that are already on the market and whose cost structures are known as a reference. The underlying evaluation model, which was developed on the basis of the VDI/VDE guideline VDI 2225 Part 1:1997-11 (1997), can be seen in Figure 5.22. (Revfi, Gladysz, et al., 2020)

Valuation metrics	Explanation (as per DIN 2225 Sheet 1)	Qualitative rating scale	
W_{EK} Direct material costs	Percentage changes in gross material costs (W_b)	+3 = { Direct costs > 200%} +2 = { 150% < Direct costs ≤ 200%} +1 = { 100% < Direct costs ≤ 150%} 0 = {Corresponding to reference} -1 = { 95% ≤ Direct costs < 100%} -2 = { 80% ≤ Direct costs < 95%} -3 = {Direct costs < 80%}	Evaluation of changes based on reference (neutral)
F_{EK} Direct manufacturing costs	Percentage change in direct manufacturing costs in relation to labor costs (L) and special direct costs (E_F)		
TL_{GK} Transport and storage overheads	Percentage changes in material overheads (G_W) in relation to transport and storage	+3 = { Overheads > 200%} +2 = { 150% < Overheads ≤ 200%} +1 = { 100% < Overheads ≤ 150%} 0 = {Corresponding to reference} -1 = { 95% ≤ Overheads < 100%} -2 = { 80% ≤ Overheads < 95%} -3 = {Overheads < 80%}	
F_{GK} Manufacturing overheads	Percentage changes in all relevant manufacturing overheads (G)		

Figure 5.22: Combined qualitative/quantitative evaluation of manufacturing and logistics costs related to the preceding product generation in terms of PGE adapted from Revfi, Gladysz, et al. (2020)

The evaluation model is based on the valuation metrics direct material costs, direct manufacturing costs, transport and storage overheads and manufacturing overheads. In the model, the direct costs and overheads relative to the costs of the reference product are determined for each concept alternative in a seven-point evaluation scale. The costs of the reference product represent the starting point, which is at 0 on the defined scale. To ensure reproducibility and traceability of the evaluations, threshold values are defined for each level of the scale. The threshold values shown in Figure 5.22 are chosen as examples and have to be adapted depending on the situation and the application. The sensitivities are chosen differently for cost increases than for cost decreases. The intention behind that is that lightweight design solutions that entail additional costs are not immediately excluded categorically on the basis of a poor rating. (Revfi, Gladysz, et al., 2020)

The evaluation made for each valuation metric can finally be plotted in a radar chart to provide the product developer with a quick overview of the changing cost structure (see Figure 5.23).
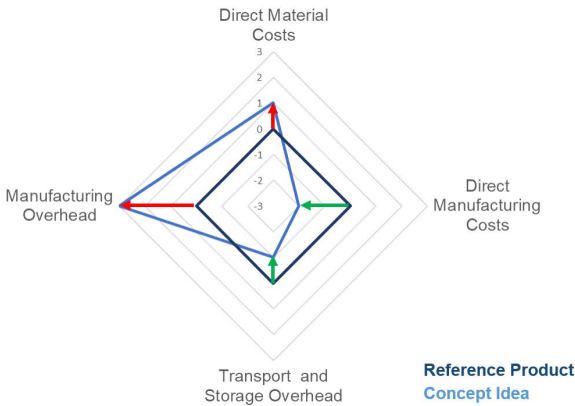
Figure 5.23: Exemplary radar chart of the semiquantitative manufacturing costs evaluation adapted from Revfi, Gladysz, et al. (2020)

By relating the estimated manufacturing costs of the concept idea to the manufacturing costs of a product generation currently on the market, the semi-quantitative approach offers advantages over qualitative evaluation methods frequently used in

practice, such as the traffic lights method, whose weaknesses are the objectivity and traceability of the performed evaluation. (Revfi, Gladysz, et al., 2020)

In summary, the methods presented in Subsection 5.2.3 address the demand for additional support of the product developer in the consequences analysis of new embodiment concepts as defined in the system of objectives for the method development in Subsection 5.1.3. Consequently, the developed methods represent the answer to the research question formulated at the beginning of this subsection (see also Section 3.1).

In the following, the last subsection focuses on potentials for the reduction of the time required to perform the ETWA, as defined in the system of objectives.

5.2.4 Synergy Effects with Further Methods of the KaSPro – Karlsruhe School of Product Engineering

Since the ETWA consists of different method modules that have to be carried out sequentially and iteratively, the time required for the performance of the method is increased. Due to the modular structure of the ETWA, it is not absolutely necessary to perform all method modules for each application. However, certain method modules cannot be dispensed with. These include the functional analysis and the filling in of the Function-Effort-Matrix in the situation analysis. But especially these two method modules require a high expenditure of time. Accordingly, based on the demand assessment in Subsection 5.1.2, the requirement for time reduction in the performance of the method was defined into the system of objectives in Subsection 5.1.3. The subsequently described synergy effects address this demand and answer the sixth research question of the second research hypothesis (see also Section 3.1).

Research Question

---

    vi.   How can the PGE – Product Generation Engineering model and the FAS4M approach as further elements of the KaSPro – Karlsruhe School of Product Engineering be employed in the application of the ETWA in order to reduce the necessary expenditure of time?

The approach has been published previously in the publication Albers, Moeser, and Revfi (2018).

For the functional analysis in the ETWA, usually expert workshops are held, in which the persons responsible for the subsystem identify the functions of the subsystems

in a moderated procedure. Since development based on functions is not yet very common in companies, especially in the automotive industry (Albers, Haug, Heitger, Fahl, & Hirschter, 2019), this results in a high expenditure of time for the people involved.

The KaSPro – Karlsruhe School of Product Engineering includes the SysML modeling approach FAS4M for the development of mechanical components. In this approach, the system is represented in four system views, two of them being the function and component view (see Subsection 2.1.5). In the component view, mass, costs and CO_2 emissions of the components can additionally be specified or retrieved from a CAD model via defined interfaces. For the generation of the FAS4M model, the technical functions of the product are also needed. This results in a synergy effect for model-based product developments, in which the ETWA is to be applied. Although there is still an increased initial effort for the definition of the functions within the scope of the modeling in terms of MBSE, however, through a consistent implementation of the model of the PGE, the functions defined in the model generated by the FAS4M approach can be transferred to the ETWA. This completely dispenses with the expenditure of time required for function definition during the performance of the ETWA. The implementation of the PGE also offers further potential. For example, by applying the PGE model across product generations, the next generation can also benefit from the functions in the reference system that originated from the preceding product, thus further reducing the expenditure of time. (Albers, Moeser, & Revfi, 2018) A function catalog created on the basis of the preceding product results in further potential for time reduction.

The identification of mass, costs and CO_2 emissions of the considered subsystems which takes place in parallel to the function definition, requires an additional expenditure of time. This time can be significantly reduced by using the model generated by the FAS4M approach, since the data are already connected in the model. Thus, they can be made available for the application in the ETWA. (Albers, Moeser, & Revfi, 2018)

In addition, in a model created using the FAS4M approach, the connections between subsystem and function are already implicitly available because the two system views are cross-linked. Thus, the Function-Effort-Matrix can be derived automatically from the MBSE model (see Subsection 5.3.4). (Albers, Moeser, & Revfi, 2018)

In summary, it can be stated that the consistent implementation of the PGE – Product Generation Engineering and the model-based development according to the FAS4M approach creates synergy effects in the application of the ETWA which re-

duce the expenditure of time. Consequently, the discussed synergy effects represent the answer to the research question formulated at the beginning of this subsection (see also Section 3.1).

After modularly enhancing the TWA to the ETWA to achieve the objectives defined in the system of objectives in Subsection 5.1.3, in the next subsection the evaluation of the developed methods is discussed.

5.3 Evaluation of the Modules

This section is dedicated to the evaluation of the methods developed in Section 5.2 and thus presents the results of Descriptive Study II. Due to the fact that every product engineering process is "unique and individual"[4] (Albers, 2010, p. 4), there was no possibility of a direct comparison between a development with the modularly enhanced ETWA and an identical development project without the support of the ETWA. Accordingly, the impact of the method on the development result is not directly quantifiable. Therefore, the developed methods were applied individually or in application specific combination in the industrial environment and the results obtained were assessed with regard to their benefit. In the following, the methods are presented in the same order as in Section 5.2.

5.3.1 Extended Target Weighing Approach (ETWA)

The ETWA is evaluated on the basis of the results achieved through its application in the EU project ALLIANCE. These are presented in Subsection 5.3.1.1. The method presented in Subsection 5.2.1 for supporting the product developer in filling in the Function-Effort-Matrix was investigated separately in the Live-Lab AIL – Agile Innovation Lab and is therefore also presented separately in Subsection 5.3.1.2.

5.3.1.1 Balancing Mass, Costs and CO₂ Emissions

First, the results obtained by the development and application of the ETWA in the R&D project ALLIANCE are considered. The results were developed in close cooperation with the project partners of the EU project ALLIANCE.

Subsequently, the study design and the study results are presented. In this regard, the EU project ALLIANCE is to be regarded as a case study.

Study Design

The demonstrator used to evaluate the ETWA consists of the strut tower and the rail (including attached parts) of the Opel Astra from model year 2016 (see Figure 5.24). The demonstrator was separated into two submodules according to the subsystem responsibility of the project partner Opel: the strut tower (SM1) and the rail (SM2) (see Figure 5.24).
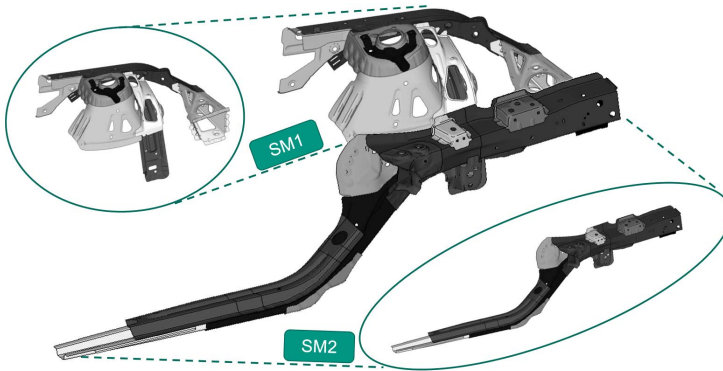
Figure 5.24: System in development: strut tower and rail of the Opel Astra adapted from Revfi, Tamm, et al. (2020) and Albers, Revfi, et al. (2019)

The ETWA was applied to both submodules separately. The generated subsystem solutions were finally reassembled to an overall demonstrator. From a methodical point of view, this division does limit the solutions that can be achieved, since from a solution-open function perspective it is best to consider the overall system. However, in product development processes in corporate practice it is not possible to develop the overall system in a single team, which is why the division is expedient from a practical point of view.

The demonstrator shown in Figure 5.24 defines the system boundary with the associated subsystems. The overall objective of the EU project ALLIANCE was to develop affordable lightweight solutions taking into account the associated CO_2 emissions. For the demonstrator, this meant a mass reduction of 22% with accepted additional costs of < 3 € per kilogram saved and a CO2 reduction of 6%. The development of the ETWA was mainly performed using the strut tower as an example, so

that the transferability of the method could be checked directly with the rail. However, due to the identical, parallel procedure for the strut tower and the rail, only the results for the strut tower are described in detail in the following. Finally, the overall result obtained from both subsystem solutions will be presented. These project results have already been published partially in Revfi, Tamm, et al. (2020) and Timmer et al. (2019). The overall ALLIANCE project results are published in an "Extended Publishable Executive Summary" (ALLIANCE, 2019).

In addition to the project results presented subsequently, a survey was conducted among eleven ALLIANCE project members who were asked about the potential of the ETWA to support systematic lightweight design activities. Thus, this is a qualitative study in a panel of experts. With eleven participants, statistical significance cannot be inferred, but the responses serve as an indicator for the evaluation.

Study Results

In two moderated workshop days with an interdisciplinary panel of experts (including design, simulation, optimization, material, costs), the functions of the two submodules were collaboratively identified. Figure 5.25 shows the functions analyzed for the strut tower, divided into main, sub and auxiliary functions. Main functions are essential for product functionality while sub functions support the main functions (Ibusuki & Kaminski, 2007). The auxiliary functions describe main and sub functions in detail.
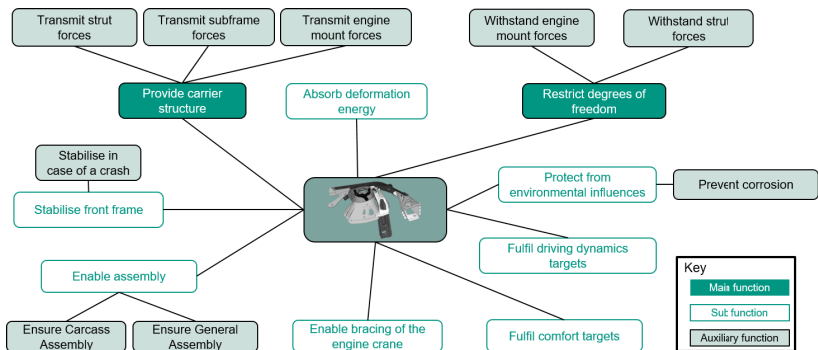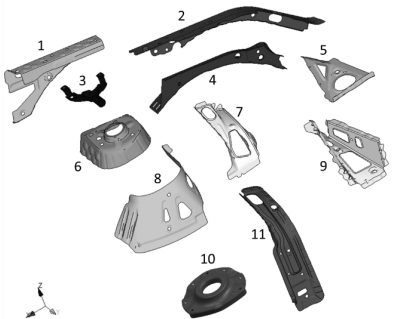
Figure 5.25: Results of the functional analysis adapted from Revfi, Tamm, et al. (2020)

During this functional analysis, several findings were obtained. First, both the component-based and the functional area-based approach were performed. It turned out that the functional area-based approach is not suitable for larger subsystem scopes, such as those present in this project. This strengthens the statement formulated in Subsection 5.2.1 that the functional area-based approach should be used when only one or at least very few components are to be optimized. Further it became evident that in industry the function-oriented development is not yet really present. Accordingly, no SysML models were available that could have significantly reduced the expenditure of time (cf. Subsection 5.2.4).

Parallel to the functional analyses for SM1 and SM2, the efforts of the subsystems were determined. For this purpose, LCC and LCA analyses *from cradle to grave* were performed by the project partners and served as an input for the ETWA. The results for the strut tower are shown in Table 33. Here, the costs and CO_2 emissions are given in relation to the overall strut tower.

Table 33: Reference product strut tower: results of the effort analysis adapted from Revfi, Tamm, et al. (2020)

Components of the strut tower	No.	Mass [kg]	Costs [%]	CO_2 [%]
	1	1.02	10.5	14.2
	2	0.57	9.2	8.4
	3	0.22	6.7	3.3
	4	0.69	9.2	9.5
	5	0.21	6.7	2.9
	6	1.59	13.1	21.6
	7	0.48	8.0	6.3
	8	0.86	10.1	12.2
	9	0.48	8.0	6.5
	10	0.38	7.6	5.8
	11	0.68	10.9	9.3
	Sum	7.18	100	100

Based on the identified functions and the defined components within the system boundary, together with the project partner Opel, the Function-Effort-Matrix was subsequently created and a paired comparison was carried out to determine the relative importance of the individual functions. When filling in the matrix and the paired comparison, comprehensive expert knowledge (according to Bromme et al. (2004)) was available in the project. Therefore, the method to support the filling in of the Function-Effort-Matrix (see Subsection 5.2.1) was not employed and is evaluated separately in Subsection 5.3.1.2. With the achieved results, the situation analysis could be completed successfully.

In the problem containment, a weighting of the factors mass, costs and CO_2 emissions in equal parts was defined (Revfi, Tamm, et al., 2020). On the basis of this weighting, the evaluations presented in Subsection 5.2.1 were undertaken. As an example, the 2D function portfolio is shown in Figure 5.26.
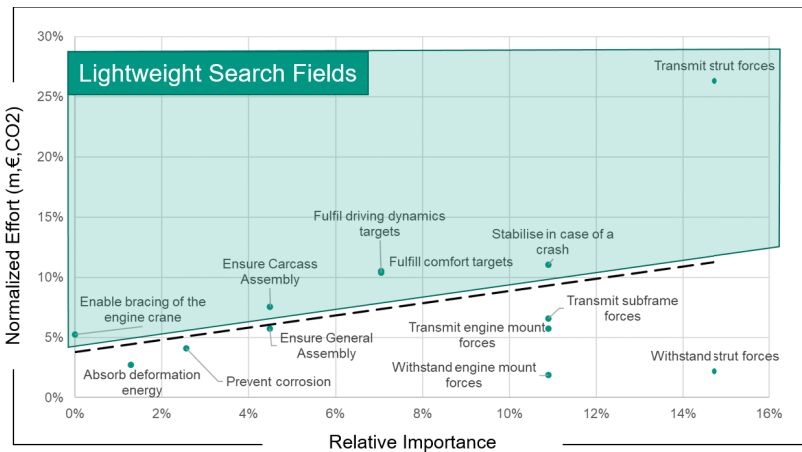
Figure 5.26: 2D function portfolio with highlighted lightweight search fields adapted from Revfi, Timmer, et al. (2019). The identified functions indicate lightweight design potential.

Based on Figure 5.26 and the combination of further evaluations (see Subsection 5.2.1), nine functions were identified as causing "too much effort" and therefore defined as lightweight search fields:

- Enable bracing of the engine crane
- Absorb deformation energy
- Prevent corrosion
- Ensure carcass assembly
- Ensure general assembly.

- Fulfill comfort targets
- Fulfill driving dynamics targets
- Stabilize in case of a crash
- Transmit strut forces

Supported by numerous creativity methods (e.g., brainwriting pool, brainstorming, 6-3-5 method, World Café), new embodiment concepts were developed subsequently. In a first step, a large number of solution ideas was collected on the basis of verbal descriptions and simple freehand sketches in order to design the nine functions named or the components involved in the functions with less effort (see Figure 5.27 (a)).

(a)   (b)
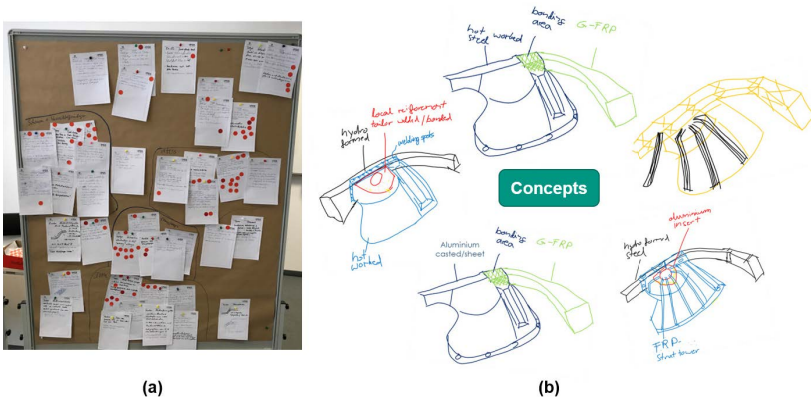
Figure 5.27: (a) Exemplary results of the brainwriting pool with clustering and scoring (b) selected initial freehand sketches derived from the ideas adapted from Revfi, Timmer, et al. (2019)

This was done in a workshop with an interdisciplinary panel of automotive experts, who also performed the functional analysis. In order not to limit the creativity in this phase, the solution space was initially kept open and the restrictions regarding mass, costs and CO_2 emissions were not defined quantitatively. In a subsequent step, the collected ideas were screened, clustered and evaluated by the workshop partici-

pants (see Figure 5.27 (a)). Afterwards, a preselection with respect to technical fea-
sibility was made by Opel. This procedure followed the suggestion for concept re-
duction proposed in the TWA. The best rated ideas were then combined in simplified
freehand sketches (see Figure 5.27 (b)) at IPEK. The other ideas that were not con-
sidered were stored in the KIS to be available for the development of further product
generations.

By combining the best rated partial solutions, 14 concepts each were developed for
SM1 and SM2, which were then presented to the expert panel. In accordance with
the procedure for concept reduction in the TWA, the concepts were then subjected
to a qualitative evaluation of the achievable mass, costs, CO_2 emissions and func-
tionalities, and the first concepts were excluded. Additionally, an initial conse-
quences analysis was conducted by Opel to identify opportunities and risks of each
concept so that new concept ideas could be derived by combining the strengths of
the individual concepts. This iterative procedure helped to improve the initial concept
ideas step by step and to reduce the number of concepts to five concepts that were
designed in CAD by the Institute for Automotive Engineering (ika) (RWTH Aachen
University). These concepts A to E for the strut tower are shown in Figure 5.28 and
the selected materials are annotated. Except for concept A, a multi-material design
is used for all concepts.
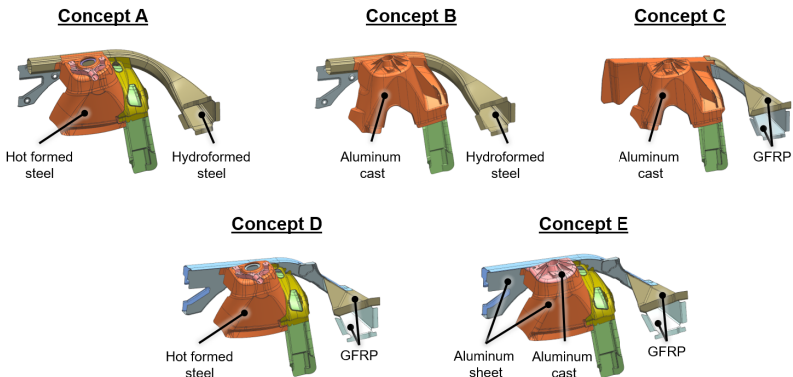
Figure 5.28: CAD models of the developed concept designs for the strut tower
adapted from Revfi, Tamm, et al. (2020)

Due to the selected materials, the question arose in the project of how to deal with uncertainties regarding individual materials. As an example, the use of glass fiber reinforced polymers can be named here, which have not yet been applied in the Opel Astra for the strut tower. This uncertainty in the implementation of the concept and the associated impact on the product success should be evaluated in the concept evaluation as an additional consequence to be contrasted with the quantitative mass, costs and CO_2 potentials. Therefore, the method for estimating technological uncertainties presented in Subsection 5.2.3.1 was developed and is evaluated separately in Subsection 5.3.3.1.

On the basis of the constructed concepts, a detailed, quantitative evaluation of the efforts generated by the concepts could be undertaken by Opel. These efforts are shown in Table 34 in relation to the reference product (see Table 33). Stiffness requirements were specified for the strut tower, while strength requirements were defined for the rail due to its function in the crash.

Table 34: Quantitative results of the developed concepts adapted from Revfi, Tamm, et al. (2020)

Concept	Mass saving [%]	Costs [€/kg]	CO_2 saving [%]	Stiffness analysis
A	18	4.27	19	Not tested
B	32	-0.30	27	Not tested
C	28	7.57	16	Not tested
D	10	27.31	11	Overfulfilled
E	53	3.54	43	Fulfilled

Based on these results, the requirements for the concepts (in addition to mass, costs and CO_2 emissions) in the system of objectives for the development were assessed in detail by Opel. In the case of Concept A, the mass reduction was too low and the costs generated by the lightweight design per kilogram saved were too high. Therefore, this concept was not followed. Concept B showed positive results in terms of mass, costs and CO_2 emissions, but was critically evaluated by the experts with regard to the stiffness requirement. For Concept C, the generated additional costs were too high, which is why this concept was also moved to the KIS. In Concept D, the mass reduction was too low and the additional costs required were far too high, even though the stiffness evaluation performed on the basis of a full vehicle simulation showed very good results. Due to the high effort involved, Concept D was also

transferred to the KIS. Therefore, in the end, the decision was made in favor of Concept E, which fulfills the stiffness requirement and shows significant potential savings in terms of mass and CO_2 emissions. Although the accepted additional costs of 3 €/kg were slightly exceeded with the isolated evaluation of the strut tower, this poses no problem as the assessment of the additional costs is to be carried out for the whole system in development, which means in combination with the rail.

Analogous to the procedure presented for the strut tower, the rail was also optimized. The only difference was that the stiffness simulations were replaced by crash simulations for the rail. As a result, a new MMD was developed that allows affordable and ecological lightweight design. The final design is presented in Figure 5.29.
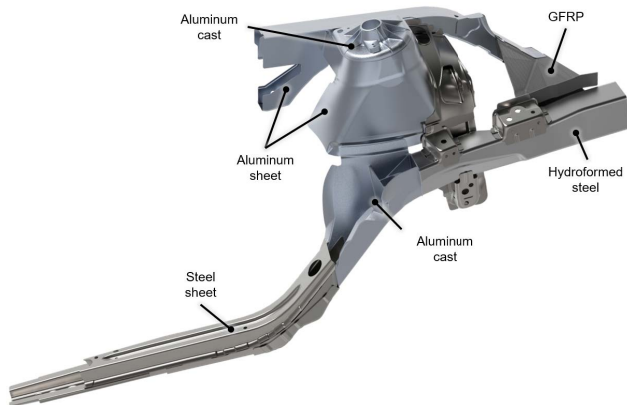
Figure 5.29: Final design of the system in development: strut tower and rail in MMD adapted from Timmer et al. (2019)

With the MMD, all project objectives were met (see Table 35). This confirms the assumption that the targeted use of the right material in the right place, while eliminating existing subsystem boundaries, helps to raise economic and ecological lightweight design potential. The achieved results are considered a success of the ETWA. The benefit of the method can also be derived from this. Indeed, it was not investigated to which results a parallel reference product engineering process without the support of the ETWA would lead, however, this is not possible in a real development environment. Nevertheless, the study on the TWA conducted in the Live-Lab provides indications of the results to be expected.

Table 35:   Evaluation of the final design adapted from Timmer et al. (2019)

Mass saving [%]	Costs [€/kg]	CO_2 saving [%]	Stiffness analysis	Crash analysis
35	1.53	28	Fulfilled	Fulfilled

In the MMD of the strut tower, GFRPs are used, which can be further optimized for fiber-adapted design, e.g. with the bead optimization presented in Chapter 4. This shows the potential of the combined application of the methods presented in the context of this thesis.

The potential of the ETWA in supporting the product developer in the systematic performance of lightweight design activities could also be confirmed by the result of a survey among eleven ALLIANCE project members. The results of the survey are shown in Figure 5.30. It can be seen that ten participants rated the potential of the ETWA to support systematic lightweight design activities with 4 or higher.
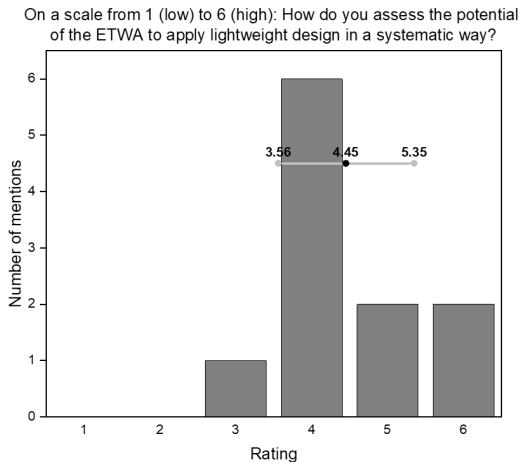
Figure 5.30: Evaluation of the survey – potential of the ETWA in supporting systematic lightweight design activities.

In the following, the evaluation of the method based on the C&C²-Approach to support the product developer in filling in the Function-Effort-Matrix is considered separately.

5.3.1.2   C&C²-Based Support for Filling in the Function-Effort-Matrix

In the EU project ALLIANCE, comprehensive expert knowledge could be used to fill in the Function-Effort-Matrix. However, the availability of expert knowledge should not be defined as a requirement for the application of the ETWA. Therefore, in Subsection 5.2.1, a method based on the C&C²-Approach was developed to support the product developer in filling in the matrix, which is evaluated in this subsection. In the following, the study design and the study results are presented. The results of the evaluation have already been published in Albers, Matthiesen, et al. (2019).

Study Design

The developed method was applied to a vacuum pump (see Figure 5.31 (a)) in the Live-Lab AIL as part of the student thesis by Schönhoff (2019)[52], which was co-supervised by the author of this work. AIL was designed to enhance the skills acquired in the Live-Lab IP (see Section 3.3). Thus, the AIL participants have a basic understanding of methods. The focus of the Live-Lab AIL is on the application and research of applied methods.

For the analysis of the reference vacuum pump, no subject matter experts were available. Accordingly, the filling in of the Function-Effort-Matrix had to be supported by the developed method. The reference vacuum pump was purchased, disassembled, analyzed, measured and weighed in the context of AIL.

Study Results

With the help of the developed, C&C²-based method, it was possible for the method-experienced student to fill in the Function-Effort-Matrix. Both approaches (WSP-based and CSS-based) were applied. With the support of the method, the student was able to analyze the pump in such a way that a lighter pump design could be developed based on the identified lightweight search fields. This new design is illustrated as a prototype in Figure 5.31 (b). In the course of the work it could be shown that the approach based on the CSS is universally applicable to determine the percentage share of any component design in function fulfillment, whereas the approach based on the WSP is suitable for a quick overview and is only recommended for the analysis of flat components. (Albers, Matthiesen, et al., 2019) Moreover, the

---

[52] Co-supervised thesis (unpublished)

methodical procedure based on the C&C²-Approach led to a distinct analysis phase, which enabled the student to generate a comprehensive overall system understanding.

(a)   (b)

Figure 5.31: (a) Reference product: vacuum pump[53] (b) derived prototype from the identified lightweight search fields adapted from Albers, Matthiesen, et al. (2019)

Whether the achieved mass reduction can be realized to the same extent in the practical implementation in the company could not be finally clarified due to the absence of an expert assessment. Nevertheless, the application of the method in a student project shows that the method supports novices with an affinity for design and methods (according to Bromme et al. (2004)) in analyzing the reference system in a targeted way and developing lightweight designs.

Having demonstrated the successes achieved through the application of the ETWA in this subsection, in the following, the modules to support the synthesis are evaluated.

---

[53] https://www.planet-air.de/en/pi-180c-compressor.html (accessed July 14, 2021)

5.3.2 Synthesis

The developed benchmark method (see Subsection 5.2.2) was applied in two case studies, which are described subsequently. With the help of these two case studies, the support of the developed method in the synthesis in the ETWA will be evaluated.

5.3.2.1 Case Study 1: Automotive Rail

In the context of the publication Albers, Revfi, et al. (2019), the developed method was used to create a 2D benchmark function portfolio. The underlying study design and the study results are presented in the following. In the student thesis by Kraus (2018)[51], which was co-supervised by the author, additional benchmarks were performed (e.g., internal reference products of a higher vehicle segment).

Study Design

The system under investigation was the rail of the Opel Astra model year 2016 from the EU project ALLIANCE (see Figure 5.24). This rail was compared to a competitor vehicle using the A2mac1 benchmarking platform. On A2mac1, the masses of the components within the system boundary "rail" could be retrieved for the competitor product.

In the application of the benchmark method, identical functions and their relative importance were assumed for the competitor product. The 2D benchmark function portfolio, which in this case is only considered in a reduced version for the mass due to the available database of the competitor product, is shown in Figure 5.32.

Study Results

An analysis of the function portfolio indicates a significant difference in mass for the functions *Absorb (crash) energy* and *Minimize front wall intrusion*. The components involved in fulfilling these two functions were therefore investigated in more detail. This revealed conceptual design differences as well as different material selections between the reference rail and the competitor product. These findings are then available to the product developer to stimulate the creativity in the generation of new concept ideas. (Albers, Revfi, et al., 2019) For more detailed discussions, at this point, it is referred to the student thesis of Kraus (2018)[51].

In the work, it is shown that the 2D function portfolio provides useful indications in the synthesis for the comparison in the same vehicle segment, while the comparability across segments is more difficult due to different system boundaries and requirements for the functions.
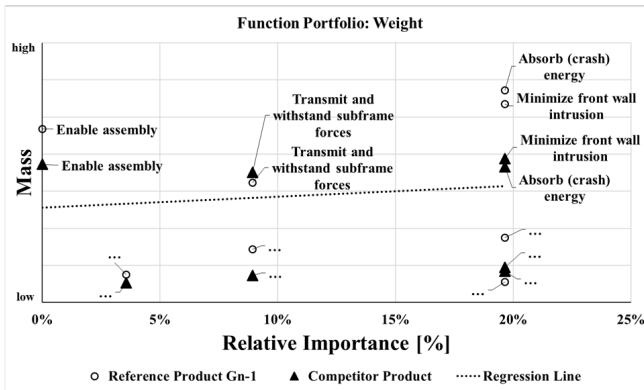
Figure 5.32: 2D benchmark function portfolio for the mass of the rail and the competitor product (Albers, Revfi, et al., 2019)

Therefore, the simplified 2D approach raises the question of whether different requirements may have existed for the compared products and whether these need to be taken into account in the evaluation (cf. Subsection 5.2.2). For this reason, the enhanced 3D function portfolio was evaluated in a further case study.

5.3.2.2 Case Study 2: Electric Handheld Device

In the following, the study design and the study results of the second case study on the evaluation of the 3D benchmark function portfolio are presented.

Study Design

The evaluation of the 3D function portfolio was carried out in cooperation with an industrial company as part of the student thesis by Maser (2019)[54], which was co-supervised by the author, for a handheld electrical device. The system under investigation was a strapping tool used in the packaging industry. An exemplary strapping tool is shown in Figure 5.33.

---

54 Co-supervised thesis (unpublished)
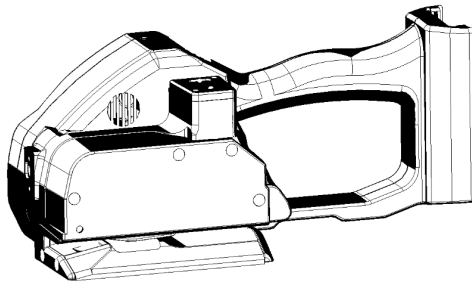
Figure 5.33: Exemplary strapping tool (Maser, 2019)[54]

This device served as reference product in the sense of the PGE. By applying the ETWA, lightweight design potentials were identified and lightweight design concepts with less effort were to be developed. For this purpose, the function-based benchmarking with the application of the 3D function portfolio was employed and the product was compared to a competitor product.

Study Results

The study shows that the function-based benchmarking helps to identify further competitor-based lightweight design potentials which go beyond the mere analysis of the internal reference product (see Figure 5.34). While the ABC analysis indicates lightweight design potential in four of 24 functions, the function portfolio already includes a total of ten functions. Thereby, the evaluation of the function portfolio includes the results of the ABC analysis. With the benchmark method four competitor-based lightweight design potentials are obtained additionally. Figure 5.34 provides an overview of the identified lightweight design potentials depending on the evaluation method.

At the same time, with regard to the electrical handheld device, it is found that for the mere identification of functions with lightweight design potential, it makes no difference whether the 2D or the 3D benchmark function portfolio is used. However, in the present case, this may be due to the fact that a competitor product from the same segment was chosen and therefore the requirements for the products are very similar. Nevertheless, for a more detailed analysis and determination of the optimization direction, the 3D benchmark portfolio offers decisive advantages (Maser, 2019)[54]. In the sense of PGE, an extension of the reference system with competitor

products for the generation of new concept ideas in ETWA is therefore recommended. Furthermore, it was revealed that the assumption of only one requirement specifying the function is not always sufficient (Maser, 2019)[54]. Therefore, an extension of the approach presented in Subsection 5.2.2 to include the consideration of multiple requirements for a function as well as a weighting of the individual requirements among each other is suggested.

	Lightweight design potential determined using...		
	...ABC-Analysis	...Function portfolio	...Benchmark-Analysis
Transmit forces	✔	✔	-
Absorb forces	✔	✔	-
Protect from environmental influences	-	✔	✔
Ensure assembly	✔	✔	-
Absorb torque	-	✔	✔
Lead strip	-	✔	✔
Transmit electrical information	-	✔	✔
Provide force (clamping)	-	✔	✔
Provide force (welding)	-	✔	✔
Provide force (pressing)	-	-	✔
Provide tension roller contact force	-	-	✔
Transfer speed and torque (welding)	-	-	✔
Convert rotary motion to linear motion (welding)	-	-	✔
Position components	✔	✔	-

Figure 5.34: Overview of the identified lightweight design potentials depending on the evaluation method adapted from Maser (2019)[54]

In addition to these findings, based on the results achieved with the ETWA in the work of Maser (2019)[54], it can be stated that the ETWA is transferable to problems outside the automotive industry. Also in this case study for handheld devices, the product developer is supported in the development of lightweight products through the application of the ETWA.

In order to reduce the concept ideas developed in the synthesis, methods were developed that are presented in Subsection 5.2.3. These will be evaluated in the next subsection.

5.3.3 Consequences Analysis

In the following, the developed methods, which are intended to provide additional support for the product developer in the consequences analysis, are evaluated. The method for the estimation of technological uncertainties is applied and evaluated in the context of the EU project ALLIANCE (see Subsection 5.3.3.1). The method for assessing the DRL is applied and evaluated in the context of a student thesis carried out in cooperation with industry (see Subsection 5.3.3.2). The developed semiquantitative method is applied within the Live-Lab IP to evaluate the costs resulting from new concept ideas (see Subsection 5.3.3.3).

5.3.3.1 Technological Uncertainties

In the following, the study design and the study results for the evaluation of the method for technological uncertainty estimation are presented.

Study Design

The presented method for estimating technological uncertainties was developed and applied in the EU project ALLIANCE. The development was carried out iteratively over the three-year project period. This means that the experiences in the application as well as the feedback of the expert panel were directly processed in the method in order to improve it. The method was applied on the basis of the CAD concepts for SM1 and SM2 and, within the context of the consequences analysis, represented a factor for evaluating the risks, which were contrasted with the opportunities resulting from the mass, costs and CO_2 reductions.

In addition to the results shown in the following, a survey was conducted among eleven ALLIANCE project members, who were asked about the benefits of the method for concept reduction after they had applied it. Consequently, this is a qualitative study in a panel of experts. Although eleven participants do not represent a sample size from which statistical significance can be inferred, the responses provide valuable information with regard to the added value of the developed method.

Study Results

For the strut tower, whose development with the help of the ETWA is described in Subsection 5.3.1.1, the values for the technological uncertainty shown in Table 36 were determined for the generated concepts in Figure 5.28.

Table 36: Technological uncertainties of the developed concepts for the strut tower in ALLIANCE based on Figure 5.28

Concept	Mass saving [%]	Costs [€/kg]	CO_2 saving [%]	Technological un-certainty
A	18	4.27	19	13
B	32	-0.30	27	14
C	28	7.57	16	16
D	10	27.31	11	14
E	53	3.54	43	16

With the help of the evaluations made by the expert panel for the two factors *Reference Product – Technology* and *Reference Product – Application Scenario*, which are related to the individual development environment of the automotive OEM, the technological uncertainties of Concepts A-E could be determined. The other two factors, *Carryover Variation Share* and *Impact*, could be derived with the help of the Function-Effort-Matrix. From the evaluations of the technological uncertainties, it can be seen that all concepts in which steel is used (Concepts A, B and D) are assessed with a lower risk. This testifies that the company has a large knowledge base in the development of products in which steel is used as a material and thus feels most confident. For the finally selected concept E, the individual evaluations of the four factors are presented in Figure 5.35. The detailed assessment of the concepts, in which all required components are evaluated in a company-specific context, is not shown here for reasons of confidentiality.

The result shows that the developed embodiment concept E carries over only very few components from the preceding product via carryover variation. This results in a value of 5 for the factor *Carryover Variation Share*. The *Impact* of concept E also gets the value of 5. This indicates that the implementation of the new concept affects many important functions. In case of problems during the implementation, this results in significant consequences for the functionality of the product. The *Reference Product – Technology* is rated 3 due to the use of GFRP. This evaluation shows that the experts are aware of the fact that the required materials, active principles and manufacturing technologies are already applied in the same branch. The *Reference Product – Application Scenario* is also assessed as 3. This indicates that, according to the experts' estimation regarding the proximity of other reference products, there only are comparable application scenarios in other branches.
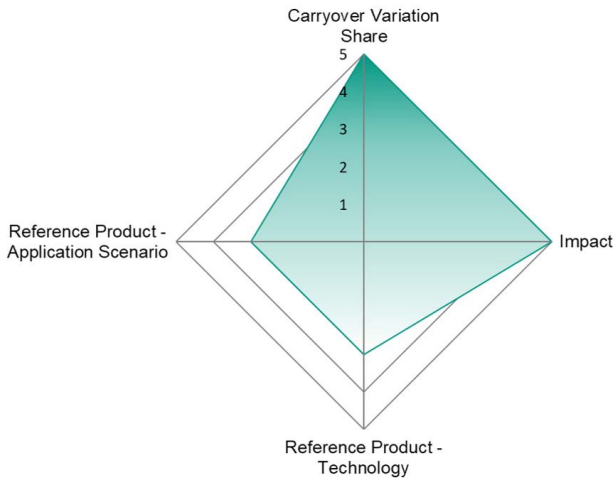
Figure 5.35: Technological uncertainty of Concept E. Total uncertainty: 16.

From a management point of view, an uncertainty of 16 out of a maximum of possible 20 points indicates an increased risk in the implementation of the concept idea. However, since the EU project ALLIANCE was a research and innovation project for an implementation horizon until 2025, it was decided to choose the increased risk in favor of the large potentials in mass, costs and CO_2 emissions. If the decision had concerned a short-term horizon, it is possible that the decision would have been different. It would then have been possible to perform further iterations in the ETWA or to adjust the project goals. This indicates the possibility of balancing different results at the management level.

In addition to the results discussed, a survey was conducted among eleven project members who applied the method. Figure 5.36 shows the evaluation of the survey. Eight of the eleven respondents agreed with the usefulness of the method as a supplement in the ETWA, six of them even indicating an increased agreement (2 on the scale).
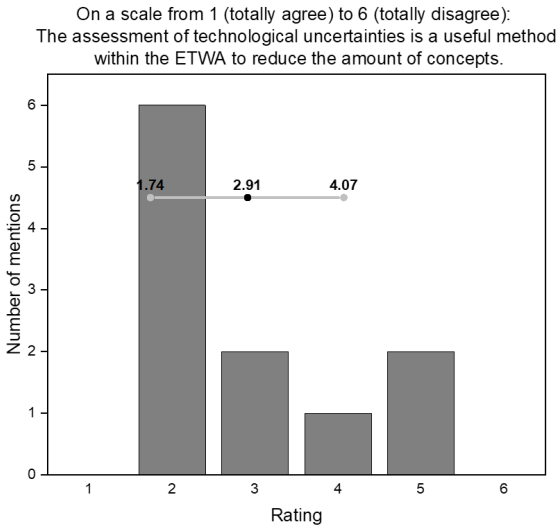
Figure 5.36: Evaluation of the survey – usefulness of the method for evaluating tech-
nological uncertainties in concept reduction

In summary, it can be stated that the estimation of the technological uncertainty represents a further support for the reduction of the generated embodiment concepts in the ETWA. This is achieved by making the involved technologies, application scenarios, impacts and carryover variation shares in the sense of the PGE required for the developed ideas objectively describable in a company-specific perspective. In this way, the method also demonstrates the potential of the KaSPro – Karlsruhe School of Product Engineering in supporting different phases in the product engineering process. The abstraction and transfer of the basic idea of the VPA developed by the research group led by Albers for the prioritization of validation activities into the context of concept evaluation was successfully achieved through the systematic application of the PGE.

In order to make the two factors Reference Product – Technology and Reference Product – Application Scenario quantitatively describable and to evaluate the integrability of the generated design concepts into the rest system, the DRL was developed, which will be evaluated in the following.

5.3.3.2 Design Readiness Level (DRL)

Subsequently, the study design and the study results for the evaluation of the DRL method are presented.

Study Design

The application and evaluation of the method in industry was carried out in the context of the student thesis by Wilwer (2019)[55], which was co-supervised by the author. Due to confidentiality, the development results cannot be discussed in detail. Therefore, only the evaluations of the method from the perspective of the subject matter experts from industry are presented from the thesis, while the substantial added value of the method is demonstrated subsequently using a fictitious application example of a scooter gearbox housing (see Figure 5.37). The application example has already been published in Revfi, Wilwer, et al. (2020).

The application example is intentionally chosen simple, even though the potential of the method lies in more complex, more interconnected systems in which there are many interactions between the individual components. However, the simple example clearly illustrates the functionality of the method and the indicators that can be derived from the results. (Revfi, Wilwer, et al., 2020)
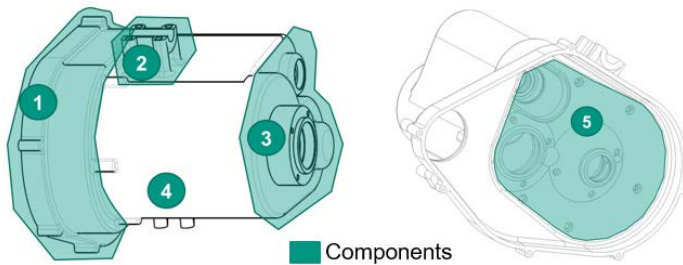
Figure 5.37: Application example: scooter gearbox housing adapted from Albers, Moeser, and Revfi (2018)

---

[55] Co-supervised thesis (unpublished)

Study Results

For three exemplarily developed MMD lightweight design embodiment concepts (see Table 37), the DRL is to be calculated, which depends on the one hand on the manufacturing technologies required for the production of the components (TRL) and on the other hand on the joining technologies required for the assembly and the integration into the existing rest system (IRL). K2 in Table 37 indicates the reduced rest system (cf. Subsection 5.2.3.2). (Revfi, Wilwer, et al., 2020) The corresponding system architecture is illustrated in Figure 5.21 (b).

The aim of this application example is to show the procedure of the method and does not claim to use universally reliable TRL and IRL values. Also the temporal forecast of the development of individual technologies, which is necessary for the calculation of the DRL, was exemplarily chosen here. The reference product as part of the reference system, for which the MMD design concepts were developed, is assumed to be made entirely of steel casting. In the MMD concepts, component 3 and 4 are produced using alternative manufacturing technologies. In Concept 1, an aluminum casting is employed, while in Concept 2, fiber reinforced injection molding is intended. In Concept 3, injection molding and aluminum casting are used in combination. The estimated TRLs in the fictitious example for the individual manufacturing processes are shown in Table 37, together with the joining technologies needed for assembling the components with each other and the housing in the existing rest system (scooter frame). (Revfi, Wilwer, et al., 2020)

If the concept selection was made only on the basis of achievable mass reduction, Concept 2 would be chosen here. However, the consequence of this decision is high because the DRL calculated based on the forecast of the development of the TRL and the IRL is significantly lower than for the other two concepts. According to the extrapolated data, the time frame required to reach series maturity is 24 months. The respective time-critical TRL and IRL are highlighted in gray in Table 37. (Revfi, Wilwer, et al., 2020)

Table 37: TRL, IRL and cardinal DRL of three exemplified gearbox housing concepts (Revfi, Wilwer, et al., 2020)

Component	Concept 1	TRL	Concept 2	TRL	Concept 3	TRL
1	steel casting	9	steel casting	9	steel casting	9
2	steel casting	9	steel casting	9	steel casting	9
3	aluminum casting	7	FRP injection moulding	7	FRP injection moulding	7
4	aluminum casting	7	FRP injection moulding	3	aluminum casting	7
5	steel casting	9	steel casting	9	steel casting	9
Joining technologies between components i, j	Concept 1	IRL	Concept 2	IRL	Concept 3	IRL
3, K2	cylindrical press fit steel - aluminum	7	inserts	5	inserts	5
1, 4	steel - aluminum	7	steel - FRP	3	steel - aluminum	7
...	...	...	...	...	...	...
3, 4	aluminum - aluminum	8	FRP - FRP	3	aluminum - FRP	3
Estimated weight reduction	low		high		medium	
Last technology to reach max. TRL / IRL	aluminum casting (in about 6 months)		FRP injection molding (in about 24 months)		aluminum - FRP (in about 12 Months)	
DRL [based on TRL & IRL forecast]	0.89		0.65		0.81	

An isolated consideration of the normalized DRL_i values (see Table 38) allows additional conclusions to be drawn about the maturity levels of individual components, which are an indication of the associated uncertainty. For the application example,

this shows that although the DRLs of Concepts 1 and 3 only slightly differ, component 3 in Concept 3 (highlighted in gray in Table 38) is significantly less mature in the combined assessment of TRL and IRL than in Concept 1. (Revfi, Wilwer, et al., 2020)

Table 38: Normalized DRL_i cardinal values for individual components adapted from Revfi, Wilwer, et al. (2020)

	DRL	DRL_1	DRL_2	DRL_3	DRL_4	DRL_5	DRL_{K1}	DRL_{K2}	DRL_{K3}
Con. 1	0.89	0.92	0.88	0.82	0.82	0.87	1	0.86	1
Con. 3	0.81	0.92	0.88	0.46	0.69	0.87	1	0.68	1

Following this procedure demonstrated on the example of the scooter gearbox housing, the method was applied by Wilwer (2019)[55] in a case study at a company in the aviation industry that focuses on the development of aircraft passenger seats. In this case, it was advantageous for the application that the company had a technology management department that documents the TRL and IRL of the manufacturing and joining technologies. Thus, for technologies that are already at an advanced stage, historical data on the temporal development is available, on the basis of which forecasts for future developments can be extrapolated. For companies that do not have documented technology developments, the application is more challenging, but not impossible. When assessing TRLs and IRLs for individual technologies, department-specific questionnaires have proven to be useful in the studies by Wilwer (2019)[55]. In a survey conducted as part of the thesis by Wilwer (2019)[55] among six corporate subject matter experts, they indicated that they saw potential use cases for the method in their company (mean value 4.7 out of possible 5). It was also commented that the developed method can not only provide support to inexperienced engineers, but can also help experienced engineers in the analysis of complex systems with a large number of interactions and interfaces (Wilwer, 2019)[55]. Thus, the developed method can be evaluated as positive not only on the basis of the results that can be achieved with it, but also with regard to its applicability.

The last method presented for an enhanced consequences analysis was the semi-quantitative cost evaluation, which is evaluated in the next subsection.

5.3.3.3 Semiquantitative Evaluation Model for Manufacturing Costs of New Concept Ideas

The study design and the study results for the evaluation of the semiquantitative cost evaluation method are presented in the following. The results have been previously published in Revfi, Gladysz, et al. (2020).

Study Design

In order to investigate the applicability of the semiquantitative evaluation model introduced in Subsection 5.2.3.3, the method was applied together with the project partner BMW AG in the Live-Lab IP.

The ETWA, including the methodical module for semi-quantitative cost evaluation, was presented to the IP students, which were organized in seven teams, in a workshop and they were taught how to apply the method. As part of the project, the teams applied the ETWA to develop lightweight design concepts for future vehicle bodies. Here, the ETWA provided support in the systematic identification and evaluation of lightweight design potential. In the course of the development project and prior to the milestone meetings, it was necessary to decide between three to seven concept alternatives within one week. For this purpose, the evaluation of the manufacturing costs per developed concept was carried out by the subject matter experts of BMW AG. The evaluation of the method was carried out by the student development teams. The feedback of the teams was collected in the form of interviews after the first application of the method as well as at the end of the project. (Revfi, Gladysz, et al., 2020)

Study Results

The explorative application within the Live-Lab IP has shown that the developed evaluation model is basically applicable and complements the already established ETWA. It was also found that the evaluation – especially of the manufacturing-related metrics – can be further improved by specific leading questions. In particular, the *direct material costs* and the *transport and storage overheads* could be estimated experientially on the basis of the material, mass and embodiment of the concepts and quantified in the form of the metrics. The experts had more difficulties in evaluating the manufacturing-related costs – in particular the overheads. However, an orientation on the basis of relative variation shares ("How many process steps are eliminated in production by this new concept?", "How fast can this concept be assembled compared to the reference system?") helped to determine the position on the scale. Further support could be given by providing an evaluation catalog that uses leading questions to guide the moderator as well as the subject matter experts

interviewed. However, such an evaluation catalog would have to be developed specifically for the company, since internal references are necessary for a better localization. (Revfi, Gladysz, et al., 2020)

With regard to the transferability of the developed method, it can be stated that the student teams were able to transfer the semiquantitative approach with relation to a reference system in the sense of PGE to other fields. For example, technology costs were also evaluated using this method in order to provide the project partner with a further decision support for concept selection. The evaluation in relation to a known element from the reference system turned out to be a positive attribute.

Finally, in the next subsection, the synergy effects with further methods of the KaSPro – Karlsruhe School of Product Engineering are evaluated.

5.3.4 Synergy Effects with Further Methods of the KaSPro – Karlsruhe School of Product Engineering

In this subsection, the synergy effects resulting from the combined application of the ETWA, the PGE – Product Generation Engineering and the FAS4M approach are evaluated. For this purpose, a case study was conducted, whose study design and study results are presented below. The results have already been published in Albers, Moeser, and Revfi (2018).

Study Design

In order to evaluate the synergy effects, no studies could be conducted in industry because the FAS4M approach, as a recently completed research work, has not yet been applied across several product generations. Therefore, an application example was defined in a case study on which the synergy effects were investigated.

As an application example, the system *scooter gearbox housing* (see Figure 5.37), is used again, which for this case study only consists of the components 1-4 (1 – Lid Side, 2 – Mounting, 3 – Bearing Seats, 4 – Centre Section). The gearbox housing performs the previously identified functions of (Albers, Moeser, & Revfi, 2018)

- Fix system
- Fix system components
- Absorb axial forces
- Absorb bending moments
- Seal against medium intrusion/leakage
- Dissipate heat
- Enable assembly.

In the following, the results of the case study are evaluated with regard to the emerging synergy effects.

Study Results

In model-based product development using the FAS4M approach, the four system views function, principle, concept and component are modeled. Figure 5.38 shows exemplarily how the MechML modeling of the function *Enable assembly* can be implemented in the software Cameo Systems Modeler.
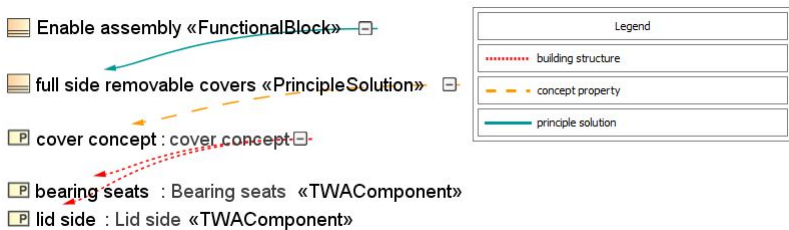
Figure 5.38: Exemplified modeling of the function *Enable assembly*: cross-linked MechML elements (Albers, Moeser, & Revfi, 2018)

From such a MechML model, the Function-Effort-Matrix for the ETWA can be derived automatically, in which even the fields of the matrix to be filled in with the percentage shares are already highlighted (see Figure 5.39). Based on these models, which are created in model-based development approaches anyway, the synergy effects for the ETWA are evaluated subsequently.

Due to the correlations between function and component contained in the MechML model, the need to conduct expert workshops for the function definition in the ETWA is completely obsolete. Based on the defined components in the design space, the functions are already implicitly included. Only a check of the completeness of the functions and components should then be performed, which can be done much faster. (Albers, Moeser, & Revfi, 2018)

Furthermore, a synergy effect arises from the automated generation of the Function-Effort-Matrix (see Figure 5.39), which can be realized by the consistent use of the PGE. This not only reduces the expenditure of time during the performance of the

ETWA, which is caused by the necessary identification of the correlation between subsystem and function, but also completely eliminates the error source of incorrect or forgotten function/subsystem assignments. (Albers, Moeser, & Revfi, 2018)

Figure 5.39: Correlation between functions and subsystems: (a) representation in the modeling tool (here: Cameo Systems Modeler) (b) representation after export to Microsoft Excel (Albers, Moeser, & Revfi, 2018)

Accordingly, the entire situation analysis in the ETWA can be supported in a model-based product engineering processes by consistently following the model of the PGE and thus be reduced in its expenditure of time. This also increases the return on investment (ROI) of the MechML models, which are also time-consuming in their generation. (Albers, Moeser, & Revfi, 2018)

In addition, SysML/MechML models offer the possibility of storing generated concept ideas that have not been implemented. Thus, the models simultaneously serve as KIS and allow reverting to existing ideas in the development of new product generations. (Albers, Moeser, & Revfi, 2018)

5.4   Conclusion

For the identification of lightweight design potentials and, based on them, the methodical development of MMD, the ETWA was developed in this chapter, which is based on the Target Weighing Approach of the KaSPro – Karlsruhe School of Product Engineering. The objective of the further development was to enable its applicability between the conflicting priorities of mass, costs and CO_2 emissions that are relevant for lightweight design. By this, the product developer is to be supported in the development of MMD concepts, which consider specified project objectives already in early phases during concept design. The function-based, solution-open approach, which questions existing subsystem structures, makes it possible to achieve a targeted application of different material classes in an economic and ecological MMD. This also makes GFRPs, for which a numerical design optimization was presented in Chapter 4, interesting for a wide range of applications despite their tendency to higher costs and CO_2 emissions.

In order to develop the ETWA, six research questions were answered, verifying the second research hypothesis:

i.   Which potentials does the TWA offer in the support of the product developer when developing lightweight design solutions in system lightweight design?
⇨   Subsection 5.1.1

ii.   Which demands exist with regard to an extension of the individual process steps of the TWA?
⇨   Subsection 5.1.2

iii.   How can the TWA be extended to systematically consider the conflicting priorities of mass, costs, and CO_2 emissions in the identification and evaluation of lightweight design potential?
⇨   Subsection 5.2.1 and Subsection 5.3.1

iv.   How can a method look like that supports the product developer in the Extended Target Weighing Approach (ETWA) within the function-based synthesis of new embodiment concepts based on a systematic analysis of the reference system?
⇨   Subsection 5.2.2 and Subsection 5.3.2

v.   For the concept ideas generated during the application of the ETWA, how can the consequences be assessed differentially in terms of technological uncertainties, maturity level and costs already in early phases?
⇨   Subsection 5.2.3 and Subsection 5.3.3

vi.   How can the PGE – Product Generation Engineering model and the FAS4M approach as further elements of the KaSPro – Karlsruhe School of Product

Engineering be employed in the application of the ETWA in order to reduce the necessary expenditure of time?

⇨ Subsection 5.2.4 and Subsection 5.3.4

On the basis of the TWA, which was used as a starting point due to its potential to support the product developer in the development of lightweight solutions, the identified demands for further development could be realized in the ETWA. The central elements of the ETWA were evaluated in the EU project ALLIANCE. Experiences gained in the project with regard to further support demands, e.g. in the synthesis, the consequences analysis or the methodical supported filling in of the Function-Effort-Matrix, were addressed by specifically developed method modules. These method modules were evaluated in separate case studies apart from the ALLIANCE project. By applying the ETWA in the aircraft and packaging industry, the transferability of the developed methods to industries outside the automotive industry could be demonstrated. Due to the modular structure of the ETWA, it is also possible to apply only certain method modules and thus to individualize it according to the specific application. All application cases have in common that they are accelerated and moving systems. Transferability to stationary systems has not yet been investigated.

The relevance of the research work is instantly evident from the results achieved in the EU project ALLIANCE. With the help of ETWA, it was possible to develop lightweight design solutions for load-bearing structures of the car body that were subject to strict economic and ecological project objectives. In this way, a contribution was made to the low-emission mobility of the future, which, due to the associated costs, should not be reserved only for the premium segments.

The potential of the method arises from the solution-open, function-based approach for the application in early phases of product development for the generation of the product concept to support the iPeM core activity *Detect Ideas* (see Figure 5.40). This enables methodical system lightweight design, which is continued in the subsequent phases via further lightweight design strategies. Based on the generated product concepts, the principle and embodiment are initially modeled, meaning that it is necessary to proceed iteratively between the two core activities (see Figure 5.40). Both core activities have to be accompanied by continuous validation and verification (see Figure 5.40), in order to not only verify the technical feasibility of the developed lightweight solutions, but also to perform a permanent comparison with the project objectives.

The PGE model and mindset are central to the ETWA, as the method does not propose developments starting from a white piece of paper, but is performed based on an existing reference system. This mindset is also central in the developed

method modules for synthesis and consequences analysis, as the generated concept ideas are compared to other elements of the reference system to either stimulate creativity or to be able to estimate technological feasibility.
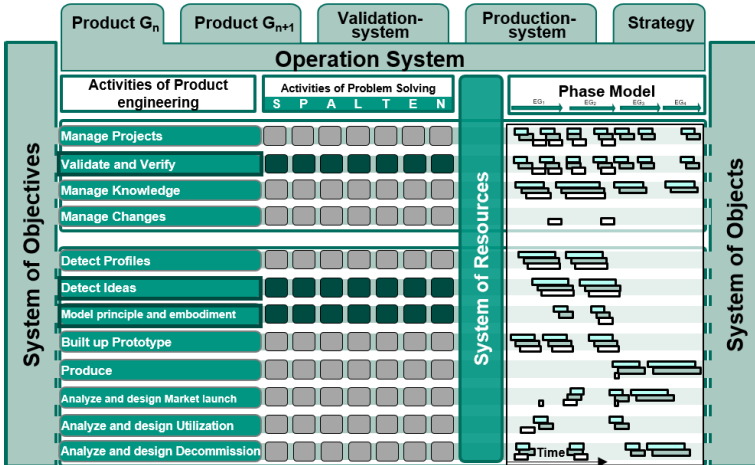
Figure 5.40: Support of the ETWA in the core activities *Detect Ideas* as well as *Model Principle and Embodiment* in iteration with the basic activity *Validate and Verify*

6 Summary and Outlook

In the following, the results and findings of the present work are summarized in Section 6.1. Finally, Section 6.2 provides an outlook on future research work.

6.1 Summary

The trend in product development is increasingly moving towards highly interconnected systems. In such systems, the product developer faces major challenges in performing lightweight design activities, as it is difficult to oversee all change propagations. A sequential application of lightweight design strategies is not sufficient in order to achieve the highest possible lightweight design potential. Rather, the individual integration of specific methods into each product engineering process is required. The present work provides a contribution for the support of the product developer in different development phases. On the one hand, the function-based Extended Target Weighing Approach (ETWA) was developed to support the identification and evaluation of lightweight design potentials, and thus to provide a possibility for the targeted development of MMD, while at the same time taking into account mass, costs and CO_2 emissions. Here, the ETWA offers support in early phases of product development, in which a major part of the later product mass is already specified. On the other hand, an optimization method for the design of beads in long fiber reinforced polymer parts was developed, taking the manufacturing process into account. Here, a coupling of validated process and structural simulations was developed in order to support the initial design process for a fiber-adapted design. Thus, the optimization method represents a possibility to optimize the design of the FRP parts in MMD concepts, which were developed e.g. with the help of the ETWA, in order to raise further lightweight design potentials.

In order to be able to develop the described methods, first of all the state of research was analyzed and based on that the need for research was identified, which is reflected in the overall research objective of the thesis.

Objective of the work

Development of an optimization method for the design of beads in long fiber reinforced polymer structures including the manufacturing process as an approach to realize methodically identified lightweight potentials.

This objective was converted into partial objectives through two research hypotheses to be investigated, which were operationalized through research questions (see Section 3.1). The research approach (see Section 3.2) to answer these research questions was based on the Design Research Methodology (DRM). In this context, first, the need for research was identified for both hypotheses within the scope of the Descriptive Study I. This need for research was then addressed by the developed methods within the context of the Prescriptive Study. Finally, the developed methods were evaluated and validated within the Descriptive Study II.

The developed optimization method for fiber-adapted bead design in long fiber reinforced parts (see Subsection 4.2.1.3 for SMC and Subsection 4.2.2.3 for LFT) is characterized by the integrated consideration of design, manufacturing and material. The three subdisciplines are inextricably connected for FRP. Only through an appropriate modeling (in terms of the main features according to Stachowiak) of all three subdisciplines, conclusions can be drawn about the investigated overall system. Therefore, the design method requires the validity of the individual models for the description of the manufacturing and processing as well as the structural mechanics. Figure 6.1 shows the method developed for the SMC material system summarized in the IPEK coupling framework.

The results obtained by applying the optimization method show the complexity of the design process for beaded SMC and LFT parts. The comparison of the anisotropic optimization results based on the developed approach with standard isotropic material modeling shows differences in the stiffness-optimized bead cross sections and a direct dependence of the results on the fiber orientations resulting from the manufacturing process. Thus, the necessity of supporting the product developer in the initial design process of beaded FRP parts by the developed method becomes obvious. The additional consideration of process-induced residual stresses in LFT parts results in further influences on the stiffness-optimized bead design, which is even more different from the isotropic results. The relevance of the results is given by the potential to reduce the number of prototypes as well as to save costs in the design of the molds necessary for the production of the parts.

316
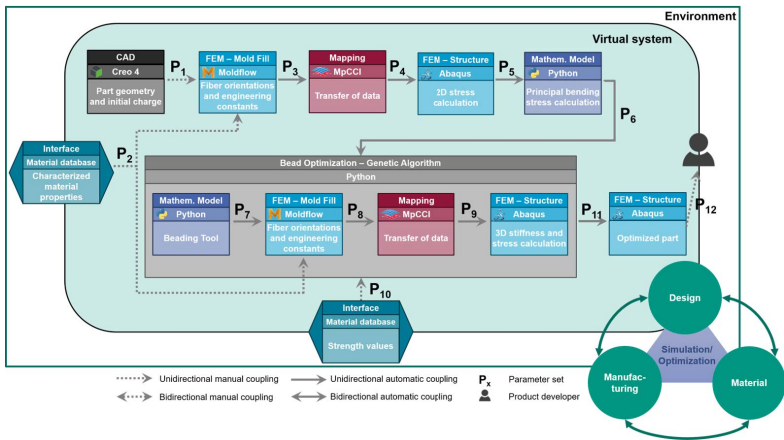
Figure 6.1: Coupling framework for the optimization of process-based beads in fiber reinforced polymer structures considering the SMC manufacturing and processing (cf. Figure 4.17)

After considering the question of "*how* beaded SMC/LFT parts can be designed in a fiber-adapted way", the question of "*where* fiber reinforced parts could be sensibly applied in terms of MMD" was then investigated. The Extended Target Weighing Approach (ETWA) was developed as a support to answer this question. The workflow of the ETWA including the application example from Subsection 5.3.1.1 is summarized in Figure 6.2.

The results achieved by applying the ETWA in the EU project ALLIANCE indicate the potential of the developed method. With the methodical support, it was possible to meet the defined project objectives in terms of mass, costs and CO_2 emissions. For this, a multi-material design was developed, which includes FRP. This demonstrated that through the systemic approach in early phases of product development, the individual strengths of the materials can be utilized purposefully and emissions can be reduced at the same time, while the necessary costs are less than €3 per kilogram saved. The transferability of the method to other areas outside the automotive industry was exemplarily demonstrated through case studies. The developed methods to support the synthesis and consequences analysis of new concept ideas helped to increase the creativity of the product developer and to enable an individual, systematic concept selection. Synergy effects with further methods of the

KaSPro – Karlsruhe School of Product Engineering can both support the filling in of the Function-Effort-Matrix and reduce the expenditure of time required to perform the ETWA.
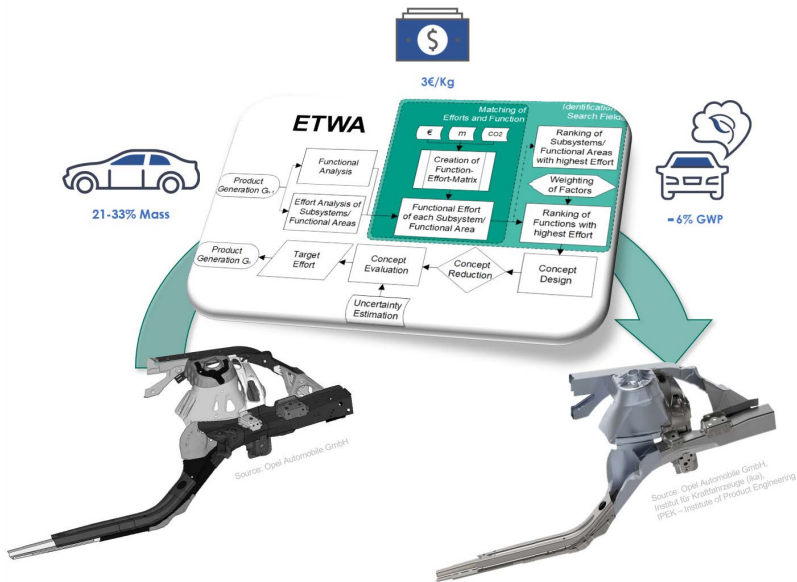
Figure 6.2: Extended Target Weighing Approach (ETWA) to balance mass, costs and CO_2 emissions in multi-material designs on the example of the developed strut tower and rail in the EU project ALLIANCE

In summary, it can be stated that the methods developed in the context of the present thesis represent further elements for the conceptual framework developed at IPEK – Institute of Product Engineering (Albers, Holoch, et al., 2021) for the continuous support of the product developer in lightweight design activities in the product engineering process.

The research results presented in the present work can be taken up by further research topics, which will be finally discussed in the following.

6.2 Outlook

The results and findings of the present work offer starting points for further research work. For this purpose, a distinction is made in the following between the process-based bead optimization and the function-based ETWA.

Process-Based Bead Optimization

Based on the developed method for the bead optimization of SMC/LFT parts, there are direct starting points for future research work. One possibility would be to include the trajectory position and the trajectory course in the parameter set for optimization. In the current state, the bead pattern is calculated once and the bead cross section is varied and optimized on this basis. By including the trajectory coordinates in the parameter set, the beads can be further optimized with regard to manufacturing and processing.

In addition, the SMC/LFT parts that are produced in compression molding allow variable bead cross sections to be realized along the trajectory. All that would be required is the manufacturing of the corresponding mold geometries. To implement this in the optimization, the beading tool would have to be extended to include variable bead cross section descriptions.

Another starting point for further research is a more detailed evaluation of the strength constraint. In the present work, a simple maximum stress criterion was applied, which leads to conservative estimates. Together with the research work at the Institute of Engineering Mechanics (ITM), which also conducts research in the DFG GRK 2078, macroscopic failure models can be developed that allow the material utilization to be increased even further.

Furthermore, the transferability of the optimization method to other objective functions is also conceivable, for example to optimize eigenfrequencies or NVH behavior.

In the DFG GRK 2078, the third generation of doctoral students is starting in direct succession. Thus, three more years of research work will follow based on the achieved results. The focus of the third generation will shift from the SMC material system to LFT. The residual stresses occurring during the production of LFT pose further challenges for the design process, as already demonstrated by the initial studies with regard to the stiffness-optimized bead design (see Subsection 4.3.2). For the continuing research work with the new material system, the characterization

of the manufacturing process together with the colleagues of the process optimization is a first important step. Furthermore, the objective function of the optimization could be extended to optimize designs with a low mass and reduced residual stress. As a further starting point in the overall context of the subproject D2 in the DFG GRK 2078, the combination of the topology optimization from the first generation of doctoral students with the bead optimization developed in this thesis could be considered. Here, the approach would be to use the bead profile defined by the bead optimization as design space for a topology optimization to create beaded-ribbed parts with additional stiffness. Also, the tape optimization developed in the first generation of doctoral students could be considered here in combination in order to generate additional part stiffness. Furthermore, it could also be a possibility to use the tapes for the reduction and targeted compensation of residual stresses.

The trajectory-based approach for bead optimization originating from the reference system of the KaSPro – Karlsruhe School of Product Engineering, which was further developed in the context of the present work, is already being used at IPEK – Institute of Product Engineering as a starting point for another basic research project[56]. In this project, the additional stiffening of beads by introducing UD-FRP into the top chord of the bead is being investigated. With the help of this research work, it should become possible to individualize a single basic sheet metal component for different use cases – up to batch size 1. For example, the battery housing of a vehicle can then be individually adapted to the battery capacity only through different fiber reinforcement. The continuation of research in the field of beads in a related context demonstrates the consistent planning with the help of PGE at IPEK. Based on this, the existing reference system elements are continuously developed and abstracted into other contexts. Building up on this, the application of bead optimization in multi-material systems would also be conceivable, where a large number of different material properties have to be taken into account simultaneously.

Also, the approach of process-based optimization is transferred in the sense of PGE to other material classes outside of long fiber reinforced polymers. Accordingly, there are already other basic research projects at the IPEK – Institute of Product Engineering for which the idea of process-based optimization has been carried over. In the DFG project SLM Topo[57], the material properties resulting from the Selective Laser Melting (SLM) process for the 3D printing of aluminum are iteratively taken

---

[56] Fiber Beads: Development of a numerical method for the synthesis of fiber-reinforced bead patterns; DFG project number 431606085

[57] SLM-Topo: Development of a process specific topology optimization method for additive manufacturing of lightweight structures exemplified by the SLM process; DFG project number 399233791

into account in a topology optimization method in order to obtain a design adapted to the printing process. The solution approach to address this research idea was systematically derived using the PGE – Product Generation Engineering model and the IPEK coupling framework of the present research work (Albers, Schulz, et al., 2021). The DFG project HyTop[58] deals with the coupled shape optimization of metal inserts in injection-molded, short fiber reinforced polymer parts in order to raise further lightweight design potential. In this way, the project thematically follows the coupling of structural optimization with process simulation and, with the optimization of steel inserts, considers a further class of materials.

Function-Based Extended Target Weighing Approach (ETWA)

The results of the present work on the ETWA also provide starting points for further research work. The ETWA is currently applied in the EU project RIGHTWEIGHT[59], which deals with the cross-sectorial transfer of lightweight design approaches between the automotive and aerospace industries. In this context, the ETWA is taught in companies and method modules such as the DRL are being evaluated in other practice-relevant applications.

As shown in the present work, the evaluation and the consequence of new lightweight design concepts are closely related to the consideration of the available production systems. This product-production system-co-design is taken into account in the current state of the ETWA via an evaluation of the concept consequences that is decoupled from the concept generation (see Section 5.2 on technological uncertainties, DRL and semi-quantitative cost evaluation). In the future, this consideration could already be considered when generating the lightweight search fields. First research approaches to this have already been published with the collaboration of the author in Albers, Stürmlinger, Revfi, and Behdinan (2021) and transferred into a draft for a research proposal. Due to the maturity of the ETWA, which has also been demonstrated in its application in the case studies in Section 5.3 in other branches than the automotive industry, it can also be applied in industry-oriented research projects or consulting projects. By introducing the method into an industrial development process, additional research ideas can potentially be derived.

---

[58] HyTop: Development of a coupled topology optimization method for injection-molded, short fiber-reinforced polymer-metal hybrid composites to support the product engineer in design synthesis; DFG project number 442072701

[59] https://www.nweurope.eu/projects/project-search/rightweight-novel-advanced-materials-solutions-for-affordable-lightweight-to-meet-auto-and-aero-makers-needs/#tab-1 (accessed July 15, 2021)

References

Advani, S. G., & Tucker, C. L. (1987). The Use of Tensors to Describe and Predict Fiber Orientation in Short Fiber Composites. *Journal of Rheology*, *31*(8), 751–784. https://doi.org/10.1122/1.549945

Albers, A. (2008). Vorwort zu Band 29. In A. Albers (Ed.), *Forschungsberichte des IPEK – Institut für Produktentwicklung am Karlsruher Institut für Technologie (KIT). Mentale und formale Modellbildung in der Produktentstehung – als Beitrag zum integrierten Produktentstehungs-Modell (iPeM). Dissertation M. Meboldt* (Vol. 29, pp. 7–8). Karlsruhe.

Albers, A. (2010). Five Hypotheses about Engineering Processes and their Consequences. In *Proceedings of the 8th International Symposium on Tools and Methods of Competitive Engineering, TMCE 2010* (Vol. 1, pp. 343–356). Ancona, Italy.

Albers, A., & Braun, A. (2011). A generalised framework to compass and to support complex product engineering processes. *International Journal of Product Development*, *15*(1/2/3), 6–25. https://doi.org/10.1504/IJPD.2011.043659

Albers, A., Braun, A., Heimicke, J., & Richter, T. (2020). Der Prozess der Produktentstehung. In F. Henning & E. Moeller (Eds.), *Handbuch Leichtbau: Methoden, Werkstoffe, Fertigung* (2nd ed., pp. 5–36). Munich: Hanser.

Albers, A., & Burkardt, N. (2011). Systemleichtbau – ganzheitliche Gewichtsreduzierung. In F. Henning & E. Moeller (Eds.), *Handbuch Leichtbau: Methoden, Werkstoffe, Fertigung* (1st ed., pp. 115–132). Munich: Hanser.

Albers, A., Burkardt, N., Meboldt, M., & Saak, M. (2005). SPALTEN Problem Solving Methodology in the Product Development. In *Proceedings of the 15th International Conference on Engineering Design (ICED 05)* (pp. 1–12). Melbourne, Australia.

Albers, A., Bursac, N., Heimicke, J., Walter, B., & Reiß, N. (2018). 20 years of cocreation using case based learning: An integrated approach for teaching innovation and research in product generation engineering. In *Proceedings of the 20th International Conference on Interactive Collaborative Learning* (pp. 636–647). Budapest, Hungary. https://doi.org/10.1007/978-3-319-73204-6_69

Albers, A., Bursac, N., & Rapp, S. (2017). PGE – Produktgenerationsentwicklung am Beispiel des Zweimassenschwungrads. *Forschung im Ingenieurwesen*, *81*(1), 13–31. https://doi.org/10.1007/s10010-016-0210-0

Albers, A., Bursac, N., & Wintergerst, E. (2015). Produktgenerationsentwicklung – Bedeutung und Herausforderungen aus einer entwicklungsmethodischen Perspektive. In *Beiträge zum 3. Stuttgarter Symposium für Produktentwicklung (SSP)* (pp. 1–10). Stuttgart, Germany.

Albers, A., Ebertz, J., Rapp, S., Heimicke, J., Kürten, C., Zimmermann, V., Bause, K., Blattner, R. (2020). *Produktgeneration 1 im Modell der PGE – Produktgenerationsentwicklung: Verständnis, Zusammenhänge und Auswirkungen in der Produktentwicklung* (KIT Scientific Working Papers No. 149). Karlsruhe: Karlsruher Institut für Technologie (KIT). https://doi.org/10.5445/IR/1000127971

Albers, A., Fahl, J., Hirschter, T., Endl, M., Ewert, R., & Rapp, S. (2020). Model of PGE – Product Generation Engineering by the Example of Autonomous Driving. In *Procedia CIRP* (Vol. 91, pp. 665–677). Kruger National Park, South Africa. https://doi.org/10.1016/j.procir.2020.03.113

Albers, A., Fahl, J., Hirschter, T., Haag, S., Hünemeyer, S., & Staiger, T. (2020). Defining, Formulating and Modeling Product Functions in the Early Phase in the Model of PGE – Product Generation Engineering. In *2020 IEEE International Symposium on Systems Engineering (ISSE)* (Vol. 6, n. p.). Vienna, Austria.

Albers, A., & Gausemeier, J. (2012). Von der fachdisziplinorientierten Produktentwicklung zur vorausschauenden und systemorientierten Produktentstehung. In R. Anderl, M. Eigner, U. Sendler, & R. Stark (Eds.), *acatech DISKUSSION. Smart Engineering: Interdisziplinäre Produktentstehung* (pp. 17–29). Berlin: Springer Vieweg. https://doi.org/10.1007/978-3-642-29372-6_3

Albers, A., Haug, F., Heitger, N., Fahl, J., & Hirschter, T. (2019). Entwicklungsgenerationen zur Steuerung der PGE – Produktgenerationsentwicklung: Von der Bauteil- zur Funktionsorientierung in der Automobilentwicklung. In *Beiträge zum 5. Stuttgarter Symposium für Produktentwicklung (SSP)* (pp. 253–262). Stuttgart, Germany.

Albers, A., Heitger, N., Haug, F., Fahl, J., Hirschter, T., & Bursac, N. (2018). Supporting Potential Innovation in the Early Phase of PGE – Product Generation Engineering: Structuring the Development of the Initial System of Objectives. In *Proceedings of the R&D Management Conference* (pp. 1–13). Milano, Italy.

Albers, A., Holoch, J., Dietrich, S., & Spadinger, M. (2018). SLM-Topo – A topology optimization method for additive manufacturing of lightweight design structures using the selective laser melting process. In *NAFEMS Nordic Seminar* (pp. 62–63). Helsinki, Finland.

Albers, A., Holoch, J., Revfi, S., & Spadinger, M. (2021). Lightweight design in product development: a conceptual framework for continuous support in the

development process. In *Procedia CIRP* (Vol. 100, pp. 494–499). Enschede, The Netherlands.

Albers, A., Klingler, S., & Wagner, D. (2014). Prioritization of Validation Activities in Product Development Processes. In *Proceedings of the DESIGN 2014 – 13th International Design Conference* (pp. 81–90). Dubrovnik, Croatia.

Albers, A., Majic, N., Ottnad, J., Spickenheuer, A., Uhlig, K., & Heinrich, G. (2009). 3-D topology optimisation in combination with fibre alignment for composite structures manufactured by tailored fibre placement. In *8th World Congress on Structural and Multidisciplinary Optimization. WCSMO 2009* (pp. 1–9). Lisbon, Portugal.

Albers, A., Majic, N., & Schmid, A. (2011). Virtuelle Produktentwicklung. In F. Henning & E. Moeller (Eds.), *Handbuch Leichtbau: Methoden, Werkstoffe, Fertigung* (1st ed., pp. 77–114). Munich: Hanser.

Albers, A., & Matthiesen, S. (2002). Konstruktionsmethodisches Grundmodell zum Zusammenhang von Funktion und Gestalt technischer Systeme. *Konstruktion*, *7/8*, 55–60.

Albers, A., Matthiesen, S., Revfi, S., Schönhoff, C., Grauberger, P., & Heimicke, J. (2019). Agile Lightweight Design – The Extended Target Weighing Approach in ASD – Agile Systems Design Using Functional Modelling with the C&C²-Approach. In *Proceedings of the 22nd International Conference on Engineering Design (ICED 19)* (Vol. 1, pp. 2667–2676). Delft, The Netherlands. https://doi.org/10.1017/dsi.2019.273

Albers, A., & Meboldt, M. (2007). IPEMM – Integrated Product Development Process Management Model, Based on Systems Engineering and Systematic Problem Solving. In *Proceedings of the 16th International Conference on Engineering Design (ICED 07)* (pp. 1–9). Paris, France.

Albers, A., Moeser, G., & Revfi, S. (2018). Synergy Effects by using SysML Models for the Lightweight Design Method "Extended Target Weighing Approach". In *Procedia CIRP* (Vol. 70, pp. 434–439). Nantes, France. https://doi.org/10.1016/j.procir.2018.02.025

Albers, A., Noel Rovira, L., Aguayo Tellez, H., & Maier, T. (2008). Optimization with Genetic Algorithms and Splines as a way for Computer Aided Innovation. In *Computer-Aided Innovation (CAI) – IFIP 20th World Computer Congress* (pp. 7–18). Milano, Italy.

Albers, A., & Nowicki, L. (2003). Integration der Simulation in die Produktentwicklung – Neue Möglichkeiten zur Steigerung der Qualität und Effizienz in der Produktentwicklung. In *Simulation in der Produkt- und Prozessentwicklung* (pp. 141–147). Bremen, Germany.

Albers, A., & Ottnad, J. (2010). Integrated Structural and Controller Optimization in Dynamic Mechatronic Systems. *Journal of Mechanical Design*, *132*(4), 1–8. https://doi.org/10.1115/1.4001380

Albers, A., Rapp, S., Birk, C., & Bursac, N. (2017). Die Frühe Phase der PGE – Produktgenerationsentwicklung. In *Beiträge zum 4. Stuttgarter Symposium für Produktentwicklung (SSP)* (pp. 1–10). Stuttgart, Germany.

Albers, A., Rapp, S., Fahl, J., Hirschter, T., Revfi, S., Schulz, M., Stürmlinger, T., Spadinger, M. (2020). Proposing A Generalized Description Of Variations In Different Types Of Systems By The Model Of PGE – Product Generation Engineering. In *Proceedings of the DESIGN 2020 – 16th International Design Conference* (Vol. 1, pp. 2235–2244). Dubrovnik, Croatia. https://doi.org/10.1017/dsd.2020.315

Albers, A., Rapp, S., Spadinger, M., Richter, T., Birk, C., Marthaler, F., Heimicke, J., Kurtz, V., Wessels, H. (2019). The Reference System in the Model of PGE: Proposing a Generalized Description of Reference Products and their Interrelations. In *Proceedings of the 22nd International Conference on Engineering Design (ICED 19)* (Vol. 1, pp. 1693–1702). Delft, The Netherlands. https://doi.org/10.1017/dsi.2019.175

Albers, A., Reichert, S., Serf, M., Thorén, S., & Bursac, N. (2017). Kopplung von CAE-Methoden zur Unterstützung des Produktentwicklers. *Konstruktion*, *69*(9), 76–82.

Albers, A., Reiß, N., Bursac, N., & Breitschuh, J. (2016). 15 Years of SPALTEN Problem Solving Methodology in Product Development. In *Proceedings of NordDesign 2016* (Vol. 1, pp. 411–420). Trondheim, Norway.

Albers, A., Reiß, N., Bursac, N., & Richter, T. (2016). iPeM – integrated Product engineering Model in context of Product Generation Engineering. In *Procedia CIRP* (Vol. 50, pp. 100–105). Stockholm, Sweden.

Albers, A., Reiß, N., Bursac, N., Walter, B., & Gladysz, B. (2015). InnoFox – Situationsspezifische Methodenempfehlung im Produktentstehungsprozess. In *Beiträge zum 3. Stuttgarter Symposium für Produktentwicklung (SSP)* (pp. 1–10). Stuttgart, Germany.

Albers, A., Revfi, S., Kraus, F., & Spadinger, M. (2019). Function-based benchmarking to identify competitor-based lightweight design potentials. In *Procedia CIRP* (Vol. 84, pp. 526–531). Póvoa de Varzim, Portugal. https://doi.org/10.1016/j.procir.2019.04.231

Albers, A., Revfi, S., & Spadinger, M. (2017). Extended Target Weighing Approach – Identification of Lightweight Design Potential for New Product Generations. In *Proceedings of the 21st International Conference on Engineering Design (ICED 17)* (Vol. 4, pp. 367–376). Vancouver, Canada.

Albers, A., Revfi, S., & Spadinger, M. (2018). Extended Target Weighing Approach – Estimation of Technological Uncertainties of Concept Ideas in Product Development Processes. In *SAE Technical Paper* (2018-37-0028, pp. 1–10). Turin, Italy. https://doi.org/10.4271/2018-37-0028

Albers, A., Revfi, S., & Spadinger, M. (2020). Funktionsbasierte Entwicklung leichter Produkte. In F. Henning & E. Moeller (Eds.), *Handbuch Leichtbau: Methoden, Werkstoffe, Fertigung* (2nd ed., pp. 133–152). Munich: Hanser.

Albers, A., Saak, M., Burkardt, N., & Schweinberger, D. (2002). Gezielte Problemlösung bei der Produktentwicklung mit Hilfe der SPALTEN-Methode. In *47. Internationales Wissenschaftliches Kolloquium der Technischen Universität Ilmenau IWK 2002* (pp. 83–84). Ilmenau, Germany.

Albers, A., Schulz, M., Haberkern, P., Holoch, J., Joerger, A., Knecht, S., Renz, R., Revfi, S., Spadinger, M. (2021). Strategische Planung des Entwicklungsrisikos gekoppelter CAE-Methoden. *Konstruktion*, [submitted].

Albers, A., Spadinger, M., Serf, M., Reichert, S., Heldmaier, S., Schulz, M., & Bursac, N. (2017). Coupling of Computer-Aided Methods: Supporting Product Developer During Embodiment Synthesis. In *12th World Congress on Structural and Multidisciplinary Optimization. WCSMO 2017* (pp. 536–548). Braunschweig, Germany. https://doi.org/10.1007/978-3-319-67988-4_41

Albers, A., Stürmlinger, T., Revfi, S., & Behdinan, K. (2021). Extended Target Weighing Approach (ETWA): Impact and risk analysis of lightweight concepts in the product-production system-co-design. In *Proceedings of the 23rd International Conference on Engineering Design (ICED 21)* (Vol. 1, pp. 1537–1546). Gothenburg, Sweden. https://doi.org/10.1017/pds.2021.415

Albers, A., Wagner, D., Ruckpaul, A., Hessenauer, B., Burkardt, N., & Matthiesen, S. (2013). Target Weighing – A New Approach for Conceptual Lightweight Design in Early Phases of Complex Systems Development. In *Proceedings of the 19th International Conference on Engineering Design (ICED 13)* (Vol. 5, pp. 301–310). Seoul, Korea.

Albers, A., Walter, B., Wilmsen, M., & Bursac, N. (2018). Live-Labs as real-world validation environments for design methods. In *Proceedings of the DESIGN 2018 – 15th International Design Conference* (pp. 13–24). Dubrovnik, Croatia.

Albers, A., Weiler, H., Emmrich, D., & Lauber, B. (2005). A new Approach for Optimization of Sheet Metal Components. *Advanced Materials Research*, *6*, 255–262.

Albers, A., & Wintergerst, E. (2014). The Contact and Channel Approach (C&C²-A): Relating a system's physical structure to its functionality. In A. Chakrabarti & L. T. M. Blessing (Eds.), *An Anthology of Theories and Models*

of Design: Philosophy, Approaches and Empirical Explorations (pp. 151–171). London, UK: Springer. https://doi.org/10.1007/978-1-4471-6338-1_8

Ali, N., Behdinan, K., & Fawaz, Z. (2003). Applicability and viability of a GA based finite element analysis architecture for structural design optimization. *Computers & Structures*, *81*(22-23), 2259–2271.

ALLIANCE (2019). Extended Publishable Executive Summary. Retrieved from http://lightweight-alliance.eu/wp-content/uploads/2019/12/alliance_extended-publishable-executive-summary.pdf (accessed on June 25, 2021)

Anand, G., & Kodali, R. (2008). Benchmarking the benchmarking models. *Benchmarking: An International Journal*, *15*(3), 257–291. https://doi.org/10.1108/14635770810876593

Ashby, M. F. (2005). *Materials Selection in Mechanical Design* (3rd ed.). Oxford, UK: Butterworth-Heinemann.

Autodesk Support (2020). Moldflow: Recommended mesh size for different mesh types. Retrieved from https://knowledge.autodesk.com/support/moldflow-insight/learn-explore/caas/sfdcarticles/sfdcarticles/Moldflow-Recommended-mesh-size-for-different-mesh-types.html?st=moldflow%20recommended%20mesh%20size (accessed on June 18, 2020)

Balaji Thattaiparthasarathy, K., Pillay, S., Ning, H., & Vaidya, U. K. (2008). Process simulation, design and manufacturing of a long fiber thermoplastic composite for mass transit application. *Composites Part A: Applied Science and Manufacturing*, *39*(9), 1512–1521. https://doi.org/10.1016/j.compositesa.2008.05.017

Barone, M. R., & Caulk, D. A. (1979). The effect of deformation and thermoset cure on heat conduction in a chopped-fiber reinforced polyester during compression molding. *International Journal of Heat and Mass Transfer*, *22*(7), 1021–1032. https://doi.org/10.1016/0017-9310(79)90175-3

Barone, M. R., & Caulk, D. A. (1986). A Model for the Flow of a Chopped Fiber Reinforced Polymer Compound in Compression Molding. *Journal of Applied Mechanics*, *53*(2), 361–371. https://doi.org/10.1115/1.3171765

Bathe, K.-J., & Zimmermann, P. (2002). *Finite-Elemente-Methoden* (2nd ed.). Berlin: Springer.

Behdinan, K., Fahimian, M., & Pop-Iliev, R. (2017). A Tool for Systematically Accessing the Level of Readiness of Engineering Design in Product Development. In *Proceedings of the Canadian Engineering Education Association (CEEA)* (Vol. 085, pp. 1–4). Toronto, Canada. https://doi.org/10.24908/pceea.v0i0.10128

Bender, B., & Gericke, K. (2016). Entwicklungsprozesse. In U. Lindemann (Ed.), *Handbuch Produktentwicklung* (pp. 401–424). Munich: Hanser.

Bendsøe, M. P. (1989). Optimal shape design as a material distribution problem. *Structural and Multidisciplinary Optimization*, *1*(4), 193–202. https://doi.org/10.1007/BF01650949

Bendsøe, M. P., & Sigmund, O. (2004). *Topology Optimization: Theory, Methods, and Applications*. Berlin, Heidelberg: Springer. https://doi.org/10.1007/978-3-662-05086-6

Bilik, C., Pahr, D. H., & Rammerstorfer, F. G. (2012). A bead laying algorithm for enhancing the stability and dynamic behavior of thin-walled structures. *Acta Mechanica*, *223*(8), 1621–1631. https://doi.org/10.1007/s00707-012-0645-9

Blessing, L. T. M., & Chakrabarti, A. (2009). *DRM, a Design Research Methodology*. London, UK: Springer. https://doi.org/10.1007/978-1-84882-587-1

Böhlke, T., Hrymak, A., Kärger, L., Pallicity, T. D., Weidenmann, K. A., & Wood, J. T. (2019). Introduction to Continuous-Discontinuous Fiber-Reinforced Polymer Composites: Fiber-Reinforced Composite Materials. In T. Böhlke, F. Henning, A. Hrymak, L. Kärger, K. A. Weidenmann, & J. T. Wood (Eds.), *Continuous–Discontinuous Fiber-Reinforced Polymers* (pp. 1–3). Munich: Carl Hanser Verlag GmbH & Co. KG.

Bromme, R., Jucks, R., & Rambow, R. (2004). Experten-Laien-Kommunikation im Wissensmanagement. In G. Reinmann & H. Mandl (Eds.), *Psychologie des Wissensmanagements: Perspektiven, Theorien und Methoden* (pp. 176–188). Göttingen: Hogrefe.

Bücheler, D. (2018). *Locally Continuous-fiber Reinforced Sheet Molding Compound* (Dissertation). Karlsruhe Institute of Technology (KIT), Karlsruhe. https://doi.org/10.5445/IR/1000079163

Butenko, V. (2020). Approach to support knowledge transfer and decision making in product development with fibre-reinforced plastics through situation-specific design guidelines. Dissertation. In A. Albers & S. Matthiesen (Eds.), *Forschungsberichte des IPEK – Institut für Produktentwicklung. ISSN: 1615-8113* (Vol. 121). Karlsruhe. https://doi.org/10.5445/IR/1000120717

Butenko, V., & Albers, A. (2019). CoDiCo-FiberFox – Decision-Support System in Early Phases of Product Development with Fiber-Reinforced Composites. In T. Böhlke, F. Henning, A. Hrymak, L. Kärger, K. A. Weidenmann, & J. T. Wood (Eds.), *Continuous–Discontinuous Fiber-Reinforced Polymers* (pp. 276–293). Munich: Carl Hanser Verlag GmbH & Co. KG.

Camp, R. C. (1989). *Benchmarking: The search for industry best practices that lead to superior performance*. Milwaukee: Quality Press.

Cha, W., Müller, S., Bursac, N., Albers, A., & Volk, W. (2017). Influence of process parameters on the formability of bead stamping part using advanced models.

Journal of Physics: Conference Series, *896*(1), 12005. https://doi.org/10.1088/1742-6596/896/1/012005

Chiang, H. H., Hieber, C. A., & Wang, K. K. (1991). A unified simulation of the filling and postfilling stages in injection molding. Part I: Formulation. *Polymer Engineering and Science*, *31*(2), 116–124. https://doi.org/10.1002/pen.760310210

Clark, K. B., & Fujimoto, T. (1991). *Product development performance: Strategy, organization, and management in the world auto industry*. Boston: Harvard Business School Press.

Cooper, R. G. (1990). Stage-Gate Systems: A New Tool for Managing New Products. *Business Horizons*, *33*(3), 44–54. https://doi.org/10.1016/0007-6813(90)90040-I

Davis, B., Gramann, P., Osswald, T. A., & Rios, A. (2003). *Compression molding*. Munich: Hanser.

Davis, B., Gramann, P., & Rios, A. (2002). Effect of Fiber Orientation Anisotropies on the Structural Performance of Molded FRP Composite Parts. Retrieved from https://www.madisongroup.com/publications/cfa2002.pdf (accessed on June 11, 2020)

Del Pero, F., Delogu, M., & Pierini, M. (2018). Life Cycle Assessment in the automotive sector: a comparative case study of Internal Combustion Engine (ICE) and electric car. In *Procedia Structural Integrity* (Vol. 12, pp. 521–537). Villa San Giovanni, Italy. https://doi.org/10.1016/j.prostr.2018.11.066

Delligatti, L. (2014). *SysML distilled: A Brief Guide to the Systems Modeling Language*. Upper Saddle River, NJ, Munich [i. a.]: Addison-Wesley.

Diestel, O., & Hausding, J. (2016). Pre-impregnated Textile Semi-finished Products (Prepregs). In C. Cherif (Ed.), *Textile materials for lightweight constructions: Technologies - methods - materials - properties* (pp. 361–379). Heidelberg: Springer.

DIN 8580 (2003). *DIN 8580:2003-09: Fertigungsverfahren - Begriffe, Einteilung*. Berlin: Beuth Verlag GmbH. https://doi.org/10.31030/9500683

DIN EN 1325 (2014). *DIN EN 1325:2014-07: Value Management - Wörterbuch - Begriffe*. Berlin: Beuth Verlag GmbH. https://doi.org/10.31030/9500683

DIN EN ISO 527-4 (1997). *DIN EN ISO 527-4:1997-07: Kunststoffe - Bestimmung der Zugeigenschaften - Teil 4: Prüfbedingungen für isotrop und anisotrop faserverstärkte Kunststoffverbundwerkstoffe (ISO 527-4:1997)*. Berlin: Beuth Verlag GmbH. https://doi.org/10.31030/7360910

Döring, N., & Bortz, J. (2016). *Forschungsmethoden und Evaluation in den Sozial- und Humanwissenschaften* (5th ed.). Berlin, Heidelberg: Springer. https://doi.org/10.1007/978-3-642-41089-5

Dörner, D. (1979). *Problemlösen als Informationsverarbeitung*. Stuttgart: Kohlhammer.

Dumont, P. J., Orgéas, L., Favier, D., Pizette, P., & Venet, C. (2007). Compression moulding of SMC: In situ experiments, modelling and simulation. *Composites Part A: Applied Science and Manufacturing*, *38*(2), 353–368. https://doi.org/10.1016/j.compositesa.2006.03.010

Ehrenstein, G. W. (2006). *Faserverbund-Kunststoffe: Werkstoffe - Verarbeitung - Eigenschaften* (2nd ed.). Munich, Vienna: Carl Hanser Verlag GmbH & Co. KG. https://doi.org/10.3139/9783446457546

Ehrlenspiel, K. (2009). *Integrierte Produktentwicklung: Denkabläufe, Methodeneinsatz, Zusammenarbeit* (4th ed.). Munich: Carl Hanser Verlag GmbH & Co. KG. https://doi.org/10.3139/9783446421578

Ehrlenspiel, K., & Meerkamm, H. (2017). *Integrierte Produktentwicklung: Denkabläufe, Methodeneinsatz, Zusammenarbeit* (6th ed.). Munich, Vienna: Carl Hanser Verlag GmbH & Co. KG.

Ellenrieder, G., Gänsicke, T., Goede, M., & Herrmann, H. G. (2013). Die Leichtbaustrategien. In H. E. Friedrich (Ed.), *Leichtbau in der Fahrzeugtechnik* (1st ed., pp. 43–118). Wiesbaden: Springer Fachmedien Wiesbaden.

Emmrich, D. (2004). Entwicklung einer FEM-basierten Methode zur Gestaltung von Sicken für biegebeanspruchte Leitstützstrukturen im Konstruktionsprozess. Dissertation. In A. Albers (Ed.), *Forschungsberichte des IPEK – Institut für Produktentwicklung. ISSN: 1615-8113* (Vol. 13). Karlsruhe.

Emmrich, D., & Albers, A. (2003). Neue Ansätze zur Optimierung von Schalenstrukturen. In *Simulation in der Produkt- und Prozessentwicklung* (pp. 179–187). Bremen, Germany.

Enkler, H.-G. (2010). Rechnergestützter Entwurf von Bauteilen mit stark streuenden Leitstützstrukturen am Beispiel hochbelastbarer urgeformter mikromechanischer Systeme. Dissertation. In A. Albers (Ed.), *Forschungsberichte des IPEK – Institut für Produktentwicklung. ISSN: 1615-8113* (Vol. 44). Karlsruhe.

Eshelby, J. D. (1957). The determination of the elastic field of an ellipsoidal inclusion, and related problems. *Proceedings of the Royal Society of London. Series A. Mathematical and Physical Sciences*, *241*(1226), 376–396.

European Alliance for SMC/BMC (2016). *Design for Success: A Design & Technology Manual for SMC BMC*. Brussels, Belgium.

European Commission (2018). Our Vision for A Clean Planet for All. Retrieved from https://ec.europa.eu/clima/sites/default/files/docs/pages/vision_1_emissions_en.pdf (accessed on April 14, 2021)

Eurostat (2021). Shedding light on energy in the EU: A guided tour of energy statistics. Retrieved from https://ec.europa.eu/eurostat/cache/infographs/energy/info.html?lang=en (accessed on July 21, 2021)

Fahimian, M., & Behdinan, K. (2017). On characterization of technology readiness level coefficients for design. In *Proceedings of the 21st International Conference on Engineering Design (ICED 17)* (Vol. 2, pp. 309–316). Vancouver, Canada.

Fahrni, F., Völker, R., & Bodmer, C. (2002). *Erfolgreiches Benchmarking in Forschung und Entwicklung, Beschaffung und Logistik*. Munich: Hanser.

Fan, Z., Yu, H., Zuo, Z., & Speight, R. (2017). Anisotropic Thermo-Viscous-Elastic Residual Stress Model for Warp Simulation of Injection Molded Parts. In *Proceedings of the SPE ANTEC 2017* (pp. 1401–1405). Anaheim, California, USA.

Feldhusen, J., Pahl, G., & Beitz, W. (2013). *Pahl/Beitz Konstruktionslehre: Methoden und Anwendung erfolgreicher Produktentwicklung* (8th ed.). Berlin, Heidelberg: Springer. https://doi.org/10.1007/978-3-642-29569-0

Fengler, B. (2019). *Manufacturing-constrained multi-objective optimization of local patch reinforcements for discontinuous fiber reinforced composite parts* (Dissertation). Karlsruhe Institute of Technology (KIT), Karlsruhe. https://doi.org/10.5445/IR/1000089502

Fengler, B., Hrymak, A., & Kärger, L. (2019). Multi-objective CoFRP patch optimization with consideration of manufacturing constraints and integrated warpage simulation. *Composite Structures*, *221*, 110861. https://doi.org/10.1016/j.compstruct.2019.04.033

Feyerabend, F. (1991). *Wertanalyse Gewicht: Methodische Gewichtsreduzierung – am Beispiel von Industrierobotern*. Düsseldorf: VDI-Verlag.

Fish, J., & Belytschko, T. (2007). *A first course in finite elements*. Chichester: John Wiley & Sons. https://doi.org/10.1002/9780470510858

Fitoussi, J., Bocquet, M., & Meraghni, F. (2013). Effect of the matrix behavior on the damage of ethylene–propylene glass fiber reinforced composite subjected to high strain rate tension. *Composites Part B: Engineering*, *45*(1), 1181–1191. https://doi.org/10.1016/j.compositesb.2012.06.011

Folgar, F., & Tucker III, C. L. (1984). Orientation Behavior of Fibers in Concentrated Suspensions. *Journal of Reinforced Plastics and Composites*, *3*(2), 98–119. https://doi.org/10.1177/073168448400300201

Foss, P. H. (2004). Coupling of flow simulation and structural analysis for glass-filled thermoplastics. *Polymer Composites*, *25*(4), 343–354. https://doi.org/10.1002/pc.20028

Friedrich, H. E. (Ed.) (2017). *Leichtbau in der Fahrzeugtechnik* (2nd ed.). Wiesbaden: Springer Fachmedien Wiesbaden. https://doi.org/10.1007/978-3-658-12295-9

Friedrich, H. E., & Krishnamoorthy, S. K. (2013). Leichtbau als Treiber von Innovationen. In H. E. Friedrich (Ed.), *Leichtbau in der Fahrzeugtechnik* (1st ed., pp. 1–30). Wiesbaden: Springer Fachmedien Wiesbaden.

Fusano, L., Priarone, P. C., Avalle, M., & Filippi, A. M. de (2011). Sheet metal plate design: a structured approach to product optimization in the presence of technological constraints. *The International Journal of Advanced Manufacturing Technology*, *56*(1-4), 31–45. https://doi.org/10.1007/s00170-011-3174-0

Galbraith, J. R. (1973). *Designing Complex Organizations* (1st ed.). Boston, USA: Addison-Wesley.

Gandhi, U. N., Goris, S., Osswald, T. A., & Song, Y.-Y. (2020). *Discontinuous fiber-reinforced composites: Fundamentals and applications*. Munich, Cincinnati: Hanser Publishers.

Gänsicke, T., & Goede, M. (2013). Die Technische Motivation. In H. E. Friedrich (Ed.), *Leichtbau in der Fahrzeugtechnik* (1st ed., pp. 31–42). Wiesbaden: Springer Fachmedien Wiesbaden.

Geiger, O., Henning, F., Eyerer, P., Brüssel, R., & Ernst, H. (2006). LFT-D: materials tailored for new applications. *Reinforced Plastics*, *50*(1), 30–35. https://doi.org/10.1016/S0034-3617(06)70870-0

German Federal Ministry for Economic Affairs and Energy (2019). Schlüsseltechnologie Leichtbau: Innovationstreiber und Garant für Ressourcen- und Energieeffizienz. Retrieved from https://www.bmwi.de/Redaktion/DE/Downloads/Monatsbericht/Monatsbericht-Themen/2019-05-schluesseltechnologie-leichtbau.pdf?__blob=publicationFile&v=6 (accessed on April 14, 2021)

German Federal Ministry for Economic Affairs and Energy (2021). Leichtbau: Schlüsseltechnologien. Retrieved from https://www.bmwi.de/Redaktion/DE/Dossier/leichtbau.html (accessed on April 15, 2021)

Görthofer, J., Meyer, N., Pallicity, T. D., Schöttl, L., Trauth, A., Schemmann, M., Hohberg, M., Pinter, P., Elsner, P., Henning, F., et al. (2019). Virtual process chain of sheet molding compound: Development, validation and perspectives. *Composites Part B: Engineering*, *169*, 133–147. https://doi.org/10.1016/j.compositesb.2019.04.001

Grauberger, P., Wessels, H., Gladysz, B., Bursac, N., Matthiesen, S., & Albers, A. (2019). The contact and channel approach – 20 years of application experience in product engineering. *Journal of Engineering Design*, *81*(1), 241–265. https://doi.org/10.1080/09544828.2019.1699035

Gries, T. (2013). Verstärkungsfasern. In *Handbuch Faserverbundkunststoffe/Composites: Grundlagen, Verarbeitung, Anwendungen* (4th ed., pp. 129–166). Wiesbaden: Springer Fachmedien Wiesbaden.

Gross, D., & Seelig, T. (2016). *Bruchmechanik: Mit einer Einführung in die Mikromechanik* (6th ed.). Berlin, Heidelberg: Springer Vieweg. https://doi.org/10.1007/978-3-662-46737-4

Guiraud, O., Dumont, P. J., Orgéas, L., & Favier, D. (2012). Rheometry of compression moulded fibre-reinforced polymer composites: Rheology, compressibility, and friction forces with mould surfaces. *Composites Part A: Applied Science and Manufacturing*, *43*(11), 2107–2119. https://doi.org/10.1016/j.compositesa.2012.06.006

Halpin, J. C., & Kardos, J. L. (1976). The Halpin-Tsai Equations: A Review. *Polymer Engineering and Science*, *16*(5), 344–352.

Harzheim, L. (2014). *Strukturoptimierung: Grundlagen und Anwendungen* (2nd ed.). Haan: Verlag Europa-Lehrmittel.

Heldmaier, S., Reichert, S., Li, S., & Albers, A. (2018). Integration of production restrictions into the sizing optimization of sheet metal components. In *NAFEMS DACH Konferenz* (n. p.). Bamberg, Germany.

Henderson, R., & Clark, K. B. (1990). Architectural Innovation: The Reconfiguration of Existing. *Administrative Science Quarterly*, *35*(1), 9–30.

Henning, F. (2011). Verarbeitung faserverstärkter Kunststoffe. In F. Henning & E. Moeller (Eds.), *Handbuch Leichtbau: Methoden, Werkstoffe, Fertigung* (1st ed., pp. 603–668). Munich: Hanser.

Henning, F. (2020). Fertigungstechnologien für faserverstärkte Kunststoffe. In F. Henning & E. Moeller (Eds.), *Handbuch Leichtbau: Methoden, Werkstoffe, Fertigung* (2nd ed., pp. 565–632). Munich: Hanser.

Henning, F., Drechsler, K., & Chatzigeorgiou, L. (2011). Faserverstärkte Kunststoffe. In F. Henning & E. Moeller (Eds.), *Handbuch Leichtbau: Methoden, Werkstoffe, Fertigung* (1st ed., pp. 337–392). Munich: Hanser.

Henning, F., Gauterin, F., Dollinger, A., & Burgert, T. (2019). Leichtbau für die Elektromobilität – Eine gewichtige Strategie? Auswirkung von Leichtbau auf den Energiebedarf eines Elektrofahrzeugs. Retrieved from https://lightweight.vdma.org/documents/266675/33646023/ICT_Prof.%20F.%20Henning_1557835775879.pdf/7316ebb8-bf24-535c-af8b-3a937186d762 (accessed on November 30, 2020)

Henning, F., Weidenmann, K. A., & Bader, B. (2020). Fertigungsrouten zur Herstellung von Hybridverbunden. In F. Henning & E. Moeller (Eds.), *Handbuch*

Leichtbau: Methoden, Werkstoffe, Fertigung (2nd ed., pp. 685–704). Munich: Hanser.

Herwig, H., & Schmandt, B. (2015). *Strömungsmechanik: Physik – mathematische Modelle – thermodynamische Aspekte* (3rd ed.). Berlin, Heidelberg: Springer Vieweg. https://doi.org/10.1007/978-3-662-45069-7

Heuss, R., Müller, N., van Sintern, W., Starke, A., & Tschiesner, A. (2012). *Lightweight, heavy impact*. Retrieved from https://www.mckinsey.com/~/media/mckinsey/dotcom/client_service/automotive%20and%20assembly/pdfs/lightweight_heavy_impact.ashx (accessed on July 18, 2021)

Hohberg, M. (2019). *Experimental investigation and process simulation of the compression molding process of Sheet Molding Compound (SMC) with local reinforcements* (Dissertation). Karlsruhe Institute of Technology (KIT), Karlsruhe. https://doi.org/10.5445/IR/1000089452

Hohberg, M., Kärger, L., Bücheler, D., & Henning, F. (2017). Rheological In-Mold Measurements and Characterizations of Sheet-Molding-Compound (SMC) Formulations with Different Constitution Properties by Using a Compressible Shell Model. *International Polymer Processing*, *32*(5), 659–668. https://doi.org/10.3139/217.3556

Hohberg, M., Kärger, L., Henning, F., & Hrymak, A. (2017). Rheological measurements and rheological shell model considering the compressible behavior of long fiber reinforced sheet molding compound (SMC). *Composites Part A: Applied Science and Manufacturing*, *95*, 110–117. https://doi.org/10.1016/j.compositesa.2017.01.006

Hohmann, M., Hillebrecht, M., & Schäfer, M. (2018). Leichtbaupotenzial in urbanen Elektrofahrzeugen. *Lightweight Design*, *11*(6), 48–51. https://doi.org/10.1007/s35725-018-0066-3

Holland, J. H. (1992). *Adaptation in natural and artificial systems. An introductory analysis with applications to biology, control, and artificial intelligence*. Cambridge, Massachusetts, USA: MIT Press.

Holoch, J., Czink, S., Spadinger, M., Dietrich, S., Schulze, V., & Albers, A. (2020). SLM-Topo – Prozessspezifische Topologieoptimierungsmethode für im Selektiven Laserschmelzen gefertigte Leichtbaustrukturen. *Industrie 4.0 Management*, *36*(4), 45–49.

Ibusuki, U., & Kaminski, P. C. (2007). Product development process with focus on value engineering and target-costing: A case study in an automotive company. *International Journal of Production Economics*, *105*(2), 459–474.

International Council on Systems Engineering (Ed.) (2007). *INCOSE Systems Engineering Vision 2020*. Retrieved from http://www.ccose.org/media/upload/SE-Vision2020_20071003_v2_03.pdf (accessed on November 11, 2020)

ISO 14040 (2006). *ISO 14040:2006-07: Environmental management — Life cycle assessment — Principles and framework*. Berlin: Beuth Verlag GmbH.

Jeffery, G. B. (1922). The motion of ellipsoidal particles immersed in a viscous fluid. *Proceedings of the Royal Society of London. Series A, Containing Papers of a Mathematical and Physical Character*, *102*(715), 161–179.

Joerger, A., Lin, T.-H., Bause, K., Spadinger, M., & Albers, A. (2020). Experimentelle und computergestützte Untersuchung des Reibungs- und Verschleißverhaltens graphitgeschmierter Axialwälzlager. In *61. Tribologie Fachtagung 2020* (Vol. 20, 1–10). Göttingen, Germany.

Kärger, L. (2019). Designing CoDiCoFRP Structures: Introduction. In T. Böhlke, F. Henning, A. Hrymak, L. Kärger, K. A. Weidenmann, & J. T. Wood (Eds.), *Continuous–Discontinuous Fiber-Reinforced Polymers* (pp. 249–252). Munich: Carl Hanser Verlag GmbH & Co. KG.

Kärger, L., Bernath, A., Fritz, F., Galkin, S., Magagnato, D., Oeckerath, A., Schön, A., Henning, F. (2015). Development and validation of a CAE chain for unidirectional fibre reinforced composite components. *Composite Structures*, *132*, 350–358. https://doi.org/10.1016/j.compstruct.2015.05.047

Kärger, L., Galkin, S., Zimmerling, C., Dörr, D., Linden, J., Oeckerath, A., & Wolf, K. (2018). Forming optimisation embedded in a CAE chain to assess and enhance the structural performance of composite components. *Composite Structures*, *192*, 143–152. https://doi.org/10.1016/j.compstruct.2018.02.041

Karger-Kocsis, J. (2014). Werkstoffe. In M. Neitzel, P. Mitschang, & U. Breuer (Eds.), *Handbuch Verbundwerkstoffe: Werkstoffe, Verarbeitung, Anwendung* (1st ed., pp. 31–71). s.l.: Carl Hanser Fachbuchverlag.

Kaspar, J., Revfi, S., Albers, A., & Vielhaber, M. (2019). Cross-Component Material and Joining Selection for Functional Lightweight Design based on the Extended Target Weighing Approach – A Detailed Application Example. In *Procedia CIRP* (Vol. 84, pp. 694–700). Póvoa de Varzim, Portugal. https://doi.org/10.1016/j.procir.2019.04.192

Kato, Y. (1993). Target costing support systems: Lessons from leading Japanese companies. *Management Accounting Research*, *4*(1), 33–47.

Kehrer, M. L. (2019). *Thermomechanical Mean-Field Modeling and Experimental Characterization of Long Fiber-Reinforced Sheet Molding Compound Composites*. Dissertation. *Schriftenreihe Kontinuumsmechanik im Maschinenbau:*

Vol. 15. Karlsruhe: KIT Scientific Publishing. https://doi.org/10.5445/KSP/1000093328

Kienzle, O. (1955). Die Versteifung ebener Böden und Wände aus Blech. In *Mitteilungen der Forschungsgesellschaft Blechverarbeitung* (Vol. 7, pp. 77–83). Düsseldorf, Germany.

Kirsch, U. (1993). *Structural Optimization: Fundamentals and Applications*. Berlin, Heidelberg: Springer. https://doi.org/10.1007/978-3-642-84845-2

Kleemann, S., Inkermann, D., Bader, B., Türck, E., & Vietor, T. (2017). A Semi-Formal Approach to Structure and Access Knowledge for Multi-Material-Design. In *Proceedings of the 21st International Conference on Engineering Design (ICED 17)* (pp. 289–298). Vancouver, Canada.

Klein, B. (2013). *Leichtbau-Konstruktion* (10th ed.). Wiesbaden: Springer Fachmedien Wiesbaden. https://doi.org/10.1007/978-3-658-02272-3

Klein, B. (2015). *FEM: Grundlagen und Anwendungen der Finite-Element-Methode im Maschinen- und Fahrzeugbau* (10th ed.). Wiesbaden: Springer Vieweg. https://doi.org/10.1007/978-3-658-06054-1

Klein, B., & Freitag, D. (1995). Praxisfähiges Werkzeug zur Konturoptimierung. *Technica*, *44*(22), 27–34.

Klein, B., & Gänsicke, T. (2019). *Leichtbau-Konstruktion: Dimensionierung, Strukturen, Werkstoffe und Gestaltung* (11th ed.). Wiesbaden: Springer Fachmedien Wiesbaden. https://doi.org/10.1007/978-3-658-26846-6

Kopp, G., Burkardt, N., & Majic, N. (2011). Leichtbaustrategien und Bauweisen. In F. Henning & E. Moeller (Eds.), *Handbuch Leichtbau: Methoden, Werkstoffe, Fertigung* (1st ed., pp. 57–76). Munich: Hanser.

Kornas, P. (2013). Ungesättigte Polyesterharze. In *Handbuch Faserverbundkunststoffe/Composites: Grundlagen, Verarbeitung, Anwendungen* (4th ed., pp. 38–50). Wiesbaden: Springer Fachmedien Wiesbaden.

Krause, D., Schwenke, J., Gumpinger, T., & Plaumann, B. (2018). Leichtbau. In F. Rieg & R. Steinhilper (Eds.), *Handbuch Konstruktion* (2nd ed., pp. 485–507). Munich: Hanser. https://doi.org/10.3139/9783446456198.017

Kugler, S. K., Kech, A., Cruz, C., & Osswald, T. (2020). Fiber Orientation Predictions – A Review of Existing Models. *Journal of Composites Science*, *4*(2), 69. https://doi.org/10.3390/jcs4020069

Kuhn, C., Walter, I., Täger, O., & Osswald, T. (2018). Simulative Prediction of Fiber-Matrix Separation in Rib Filling During Compression Molding Using a Direct Fiber Simulation. *Journal of Composites Science*, *2*(1), 2. https://doi.org/10.3390/jcs2010002

Kunc, V., Frame, B., Nguyen, B. N., Tucker, C. L., & Velez-Garcia, G. (2007). Fiber length distribution measurement for long glass and carbon fiber reinforced injection molded thermoplastics. In *SPE Automotive and Composites Divisions – 7th Annual Automotive Composites Conference and Exhibition, ACCE 2007 – Driving Performance and Productivity* (Vol. 2, pp. 866–876). Troy, USA.

Larbi, A. B. C., Sai, K., Sidhom, H., & Baptiste, D. (2006). Constitutive Model of Micromechanical Damage to Predict Reduction in Stiffness of a Fatigued SMC Composite. *Journal of Materials Engineering and Performance*, *15*(5), 575–580. https://doi.org/10.1361/105994906X124569

Laufer, F., Roth, D., & Binz, H. (2018). Supporting Engineers In Lightweight Design: The Energy Distribution Analysis (EDA). In *Proceedings of the DESIGN 2018 – 15th International Design Conference* (pp. 829–840). Dubrovnik, Croatia. https://doi.org/10.21278/idc.2018.0122

Laufer, F., Roth, D., & Binz, H. (2019). Derivation of Criteria for Identifying Lightweight Potential – A Literature Review. In *Proceedings of the 22nd International Conference on Engineering Design (ICED 19)* (Vol. 1, pp. 2677–2686). Delft, The Netherlands. https://doi.org/10.1017/dsi.2019.274

Laufer, F., Roth, D., & Binz, H. (2020). An Approach For The Multi-Criteria Derivation Of Lightweight Potential. In *Proceedings of the DESIGN 2020 – 16th International Design Conference* (Vol. 1, pp. 977–986). Dubrovnik, Croatia. https://doi.org/10.1017/dsd.2020.21

Leichtbau BW GmbH (2015). *Systemeffizienter Hybrider Leichtbau in Baden-Württemberg – Positionspapier*. Stuttgart, Germany.

Leiva, J. P. (2003). Methods for generating perturbation vectors for topography optimization of structures. In *5th World Congress on Structural and Multidisciplinary Optimization. WCSMO 2003* (n. p.). Venice, Italy.

Li, Y., Chen, Z., Xu, H., Dahl, J., Zeng, D., Mirdamadi, M., & Su, X. (2017). Modeling and Simulation of Compression Molding Process for Sheet Molding Compound (SMC) of Chopped Carbon Fiber Composites. *SAE International Journal of Materials and Manufacturing*, *10*(2), 130–137. https://doi.org/10.4271/2017-01-0228

Lin, B., Jin, X., Zheng, R., Costa, F., & Fan, Z. (2004). 3D Fiber Orientation Simulation for Plastic Injection Molding. In *AIP Conference Proceedings* (Vol. 712, pp. 282–287). Columbus, USA. https://doi.org/10.1063/1.1766537

Lüdeke, T. F. (2016). *Beitrag zur gewichtsoptimierten Entwicklung mechatronischer Produkte* (Dissertation). Saarland University, Saarbrücken. https://doi.org/10.22028/D291-23161

Luo, J. H., & Gea, H. C. (1998). Optimal bead orientation of 3D shell/plate structures. *Finite Elements in Analysis and Design*, *31*(1), 55–71. https://doi.org/10.1016/S0168-874X(98)00048-1

Maiwald, J. (1992). *Auslegungskriterien für Sicken in dünnen Karosserieblechen* (Dissertation). Technical University Aachen, Aachen.

Majic, N. (2014). Entwicklung einer FEM-basierten Methode zur fertigungsorientierten Sickenmustergestaltung für biegebeanspruchte Tragstrukturen. Dissertation. In A. Albers (Ed.), *Forschungsberichte des IPEK – Institut für Produktentwicklung. ISSN: 1615-8113* (Vol. 80). Karlsruhe.

Majic, N., Albers, A., Kalmbach, M., & Clausen, P. (2013). Development and statistical evaluation of manufacturing-oriented bead patterns. *Advances in Engineering Software*, *57*, 40–47.

Mankins, J. C. (1995). *Technology Readiness Levels: A White Paper*. Washington, DC, USA: NASA.

Marxen, L. (2014). A Framework for Design Support Development based on the integrated Product Engineering Model iPeM. Dissertation. In A. Albers (Ed.), *Forschungsberichte des IPEK – Institut für Produktentwicklung. ISSN: 1615-8113* (Vol. 74). Karlsruhe.

Mattheck, C., & Moldenhauer, H. (1990). An Intelligent CAD-Method Based On Biological Growth. *Fatigue & Fracture of Engineering Materials and Structures*, *13*(1), 41–51. https://doi.org/10.1111/j.1460-2695.1990.tb00575.x

Matthiesen, S. (2002). Ein Beitrag zur Basisdefinition des Elementmodells Wirkflächenpaare & Leitstützstrukturen zum Zusammenhang von Funktion und Gestalt technischer Systeme. Dissertation. In A. Albers (Ed.), *Forschungsberichte des Instituts für Maschinenkonstruktionslehre und Kraftfahrzeugbau. ISSN: 1615-8113* (Vol. 6). Karlsruhe.

Matthiesen, S. (2011). Seven years of product development in industry – experiences and requirements for supporting engineering design with 'thinking tools'. In *Proceedings of the 18th International Conference on Engineering Design (ICED 11)* (pp. 236–245). Copenhagen, Denmark.

Matthiesen, S. (2021). Gestaltung – Prozess und Methoden. In B. Bender & K. Gericke (Eds.), *Pahl/Beitz Konstruktionslehre: Methoden und Anwendung erfolgreicher Produktentwicklung* (9th ed., pp. 397–465). Berlin: Springer.

Matthiesen, S., Grauberger, P., Hölz, K., Nelius, T., Bremer, F., Wettstein, A., Gessinger, A., Pflegler, B., Nowoseltschenko, K., Voß, K. (2018). *Modellbildung mit dem C&C²-Ansatz in der Gestaltung – Techniken zur Analyse und Synthese* (KIT Scientific Working Papers No. 58). Karlsruhe. https://doi.org/10.5445/IR/1000080744

May, D. (2020). *Integrierte Produktentwicklung mit Faser-Kunststoff-Verbunden* (1st ed.). Berlin: Springer. https://doi.org/10.1007/978-3-662-60286-7

M-Base Engineering + Software GmbH (2020, February 20). Material Data Center | Datasheet SUPRAN® PP1330. Retrieved from https://www.materialdatacenter.com/ms/en/Supran/Lotte+Chemical+Corporation/SUPRAN%C2%AE+PP1330/1276e7a5/6952 (accessed on February 20, 2020)

Medina, L., Mack, J., & Christmann, M. (2014). Imprägnierte Halbzeuge. In M. Neitzel, P. Mitschang, & U. Breuer (Eds.), *Handbuch Verbundwerkstoffe: Werkstoffe, Verarbeitung, Anwendung* (1st ed., pp. 135–199). s.l.: Carl Hanser Fachbuchverlag.

Metehri, A., Serier, B., Bachir bouiadjra, B., Belhouari, M., & Mecirdi, M. A. (2009). Numerical analysis of the residual stresses in polymer matrix composites. *Materials & Design*, *30*(7), 2332–2338. https://doi.org/10.1016/j.matdes.2008.11.009

Meyer, N. (2021). *Mesoscale simulation of the mold filling process of Sheet Molding Compound* (Dissertation). Karlsruhe Institute of Technology (KIT), Karlsruhe.

Meyer, N., Schöttl, L., Bretz, L., Hrymak, A. N., & Kärger, L. (2020). Direct Bundle Simulation approach for the compression molding process of Sheet Molding Compound. *Composites Part A: Applied Science and Manufacturing*, *132*, 105809. https://doi.org/10.1016/j.compositesa.2020.105809

Michell, A. G. M. (1904). LVIII. The limits of economy of material in frame-structures. *The London, Edinburgh, and Dublin Philosophical Magazine and Journal of Science*, *8*(47), 589–597. https://doi.org/10.1080/14786440409463229

Moenaert, R. K., Meyer, A. de, Souder, W. E., & Deschoolmeester, D. (1995). R&D/marketing communication during the fuzzy front-end. *IEEE Transactions on Engineering Management*, *42*(3), 243–258. https://doi.org/10.1109/17.403743

Moeser, G., Grundel, M., Weilkiens, T., Kümpel, S., Kramer, C., & Albers, A. (2016). Modellbasierter mechanischer Konzeptentwurf: Ergebnisse des FAS4M-Projektes. In *Tag des Systems Engineering* (pp. 417–428). Herzogenaurach, Germany. https://doi.org/10.3139/9783446451414.040

Mori, T., & Tanaka, K. (1973). Average stress in matrix and average elastic energy of materials with misfitting inclusions. *Acta Metallurgica*, *21*(5), 571–574.

Nasdala, L. (2012). *FEM-Formelsammlung Statik und Dynamik: Hintergrundinformationen, Tipps und Tricks* (2nd ed.). Wiesbaden: Vieweg+Teubner Verlag. https://doi.org/10.1007/978-3-8348-2260-4

Nestler, D. J. (2014). *Beitrag zum Thema Verbundwerkstoffe – Werkstoffverbunde: Status quo und Forschungsansätze* (Habilitationsschrift). Chemnitz: Universitätsverlag Chemnitz.

Ntv (2018, February 15). Das Ende der Diät: Macht Leichtbau bei E-Autos keinen Sinn? Retrieved from https://www.n-tv.de/auto/Macht-Leichtbau-bei-E-Autos-keinen-Sinn-article20284912.html (accessed on September 30, 2020)

Oehler, G. (1951). *Gestaltung gezogener Blechteile. Konstruktionsbücher: Vol. 11*. Berlin, Heidelberg: Springer. https://doi.org/10.1007/978-3-662-01240-6

Oehler, G., & Draeger, E. (1971). *Versteifen von Stahlblechteilen* (1st ed.). *Merkblatt Stahl: Vol. 350*. Düsseldorf: Beratungsstelle für Stahlverwendung.

Oehler, G., & Weber, A. (1972). *Steife Blech- und Kunststoffkonstruktionen. Konstruktionsbücher: Vol. 30*. Berlin, Heidelberg: Springer. https://doi.org/10.1007/978-3-642-99997-0

Osswald, T. A., & Menges, G. (2012). *Materials Science of Polymers for Engineers* (3rd ed.). Munich, Cincinnati: Carl Hanser Verlag. https://doi.org/10.3139/9781569905241

Pedersen, C. B. W., Hessenauer, B., Sigmund, O., & Albers, A. (2009). Topology Optimization of Dynamically Loaded Structures with Respect to Issues of Noise, Vibration and Harshness (NVH). In *NAFEMS World Congress* (n. p.). Kreta, Greece.

Perez, R., Chung, J., & Behdinan, K. (2000). Aircraft conceptual design using genetic algorithms. In *8th Symposium on Multidisciplinary Analysis and Optimization* (pp. 1–11). Long Beach, CA, USA. https://doi.org/10.2514/6.2000-4938

Perez, R., Liu, H., & Behdinan, K. (2004). Evaluation of Multidisciplinary Optimization Approaches for Aircraft Conceptual Design. In *10th AIAA/ISSMO Multidisciplinary Analysis and Optimization Conference* (pp. 1–11). Albany, NY, USA. https://doi.org/10.2514/6.2004-4537

Phelps, J. H., & Tucker, C. L. (2009). An anisotropic rotary diffusion model for fiber orientation in short- and long-fiber thermoplastics. *Journal of Non-Newtonian Fluid Mechanics*, *156*(3), 165–176. https://doi.org/10.1016/j.jnnfm.2008.08.002

Pinter, P., Dietrich, S., Bertram, B., Kehrer, L., Elsner, P., & Weidenmann, K. A. (2018). Comparison and error estimation of 3D fibre orientation analysis of computed tomography image data for fibre reinforced composites. *NDT & E International*, *95*, 26–35. https://doi.org/10.1016/j.ndteint.2018.01.001

Ponn, J., & Lindemann, U. (2008). *Konzeptentwicklung und Gestaltung technischer Produkte*. Berlin, Heidelberg: Springer-Verlag.

Ponn, J., & Lindemann, U. (2011). *Konzeptentwicklung und Gestaltung technischer Produkte: Systematisch von Anforderungen zu Konzepten und Gestaltlösungen* (2nd ed.). Berlin, Heidelberg: Springer-Verlag. https://doi.org/10.1007/978-3-642-20580-4

Posner, B., Binz, H., & Roth, D. (2013). Operationalisation of the Value Analysis for Design for Lightweight: The Function Mass Analysis. In *Proceedings of the 19th International Conference on Engineering Design (ICED 13)* (pp. 271–280). Seoul, Korea.

Posner, B., Binz, H., & Roth, D. (2014). Supporting Lightweight Design Potential Assessment in the Conceptual Phase. In *Proceedings of the DESIGN 2014 – 13th International Design Conference* (pp. 353–362). Dubrovnik, Croatia.

Posner, B., Keller, A., Binz, H., & Roth, D. (2012). Holistic Lightweight Design For Function And Mass: A Framework For The Function Mass Analysis. In *Proceedings of the DESIGN 2012 – 12th International Design Conference* (pp. 1071–1080). Dubrovnik, Croatia.

Prager, W., & Shield, R. T. (1968). Optimal Design of Multi-Purpose Structures. *International Journal of Solids and Structures*, *4*, 469–475.

Puck, A. (1996). *Festigkeitsanalyse von Faser-Matrix-Laminaten: Modelle für die Praxis*. Munich: Hanser.

Rao, R. V., & Savsani, V. J. (2012). *Mechanical Design Optimization Using Advanced Optimization Techniques*. London, UK: Springer. https://doi.org/10.1007/978-1-4471-2748-2

Reichert, S. (2019). An approach to investigate surface roughness influence on the running-in behaviour of mixed-lubricated sliding contacts using the finite element method. Dissertation. In A. Albers & S. Matthiesen (Eds.), *Forschungsberichte des IPEK – Institut für Produktentwicklung. ISSN: 1615-8113* (Vol. 124). Karlsruhe. https://doi.org/10.5445/IR/1000105142

Reichert, S., Lorentz, B., & Albers, A. (2016). Influence of flattening of rough surface profiles on the friction behaviour of mixed lubricated contacts. *Tribology International*, *93*, 614–619. https://doi.org/10.1016/j.triboint.2015.01.003

Reichwald, R., Engelmann, M., Meyer, A., & Walcher, D. (2007). *Der Kunde als Innovationspartner* (1st ed.). Wiesbaden: Gabler Verlag.

Reinhart, G., Lindemann, U., & Heinzl, J. (1996). *Qualitätsmanagement: Ein Kurs für Studium und Praxis*. Berlin: Springer-Verlag.

Reiß, N. (2018). Ansätze zur Steigerung der Methodenakzeptanz in agilen Prozessen der PGE – Produktgenerationsentwicklung. Dissertation. In A. Albers & S.

Matthiesen (Eds.), *Forschungsberichte des IPEK – Institut für Produktentwicklung. ISSN: 1615-8113* (Vol. 112). Karlsruhe. https://doi.org/10.5445/IR/1000084762

Revfi, S., Albers, A., Holoch, J., & Spadinger, M. (2018). Extended Target Weighing Approach – A system lightweight design approach for new product generations. In *Symposium Lightweight Design in Product Development (LWD-PD18)* (pp. 29–31). Zurich, Switzerland. https://doi.org/10.3929/ethz-b-000283432

Revfi, S., Albers, A., Meyer, N., Kärger, L., Schöttl, L., Bartkowiak, M., & Behdinan, K. (2021). Manufacturing Simulation of Sheet Molding Compound (SMC). In *NAFEMS World Congress* (n. p.). Online-Conference.

Revfi, S., Albers, A., & Stegmiller, M. (2018). Target Weighing Approach: Study to evaluate the benefits of a methodical approach in comparison to classical company processes for the identification of lightweight design potentials. In *Proceedings of NordDesign 2018* (n. p.). Linköping, Sweden.

Revfi, S., Fünkner, M., Albers, A., & Behdinan, K. (2020). Einfluss der Volumen- und Shell-Dickenmodellierung auf die hauptspannungsbasierte Trajektorienberechnung zur Bestimmung von Sickenverläufen. In *NAFEMS DACH Konferenz* (pp. 98–101). Online-Conference.

Revfi, S., Fünkner, M., Albers, A., & Behdinan, K. (2021). Prozessbasierte Sickenoptimierung langfaserverstärkter Kunststoffbauteile. *NAFEMS Online-Magazin, 60*, 41–49.

Revfi, S., Gladysz, B., Spadinger, M., Albers, A., & Staeves, J. (2020). Erweiterter Target Weighing Ansatz (ETWA): Semiquantitatives Bewertungsmodell für Herstellkosten neuer Konzeptideen. *Konstruktion*, *72*(01-02), 72–77.

Revfi, S., Kaspar, J., Vielhaber, M., & Albers, A. (2019). Function-Based Material Selection for Cross-Component Lightweight Design Within the Extended Target Weighing Approach. In *Proceedings of the 22nd International Conference on Engineering Design (ICED 19)* (Vol. 1, pp. 2715–2724). Delft, The Netherlands. https://doi.org/10.1017/dsi.2019.278

Revfi, S., Mikus, M., Behdinan, K., & Albers, A. (2020). Bead optimization in long fiber reinforced polymer structures: Consideration of anisotropic material properties resulting from the manufacturing process. *Advances in Engineering Software*, *149*, 102891. https://doi.org/10.1016/j.advengsoft.2020.102891

Revfi, S., Mikus, M., Behdinan, K., & Albers, A. (2021). On the bead design in LFT structures: the influence of manufacturing-induced residual stresses. *Design Science*, *7*, e5. https://doi.org/10.1017/dsj.2021.4

Revfi, S., Spadinger, M., & Albers, A. (2019). Manufacturing-oriented Bead Patterns for Long Fiber-Reinforced Polymer Structures. In *NAFEMS World Congress* (n. p.). Québec, Canada.

Revfi, S., Tamm, C., Thirunavukkarasu, D., & Timmer, A. (2020). Methodology for the Identification of Lightweight Solutions in Vehicle Applications. *ATZ Worldwide*, *122*(6), 60–63. https://doi.org/10.1007/s38311-020-0248-3

Revfi, S., Timmer, A., Michler, T., Seidel, K., Thirunavukkarasu, D., Atzrodt, H., & Tamm, C. (2019, May 20). *Erweiterter Target Weighing Ansatz: Ein Ansatz zum Systemleichtbau für neue Produktgenerationen*. [Presentation]. 6. Technologietag Hybrider Leichtbau, Stuttgart, Germany.

Revfi, S., Wilwer, J., Behdinan, K., & Albers, A. (2020). Design Readiness of Multi-Material Concepts: Manufacturing and Joining Technology Integrated Evaluation of Concept Maturity Levels Using Cardinal Coefficients. In *Proceedings of the DESIGN 2020 – 16th International Design Conference* (Vol. 1, pp. 1067–1076). Dubrovnik, Croatia. https://doi.org/10.1017/dsd.2020.274

Richter, T., Felber, A., Troester, P. M., Albers, A., & Behdinan, K. (2020). Visualization of requirements engineering data to analyse the current product maturity in the early phase of product development. In *Procedia CIRP* (Vol. 91, pp. 271–277). Kruger National Park, South Africa. https://doi.org/10.1016/j.procir.2020.02.176

Richter, T., Schmidt, D., Hahlweg, H., Behdinan, K., & Albers, A. (2020). Objective based process model for enhancing the product maturity level in the early phase of a development process. In *Procedia CIRP* (Vol. 91, pp. 207–213). Kruger National Park, South Africa. https://doi.org/10.1016/j.procir.2020.02.169

Richter, T., Troester, P., Felber, A., Albers, A., & Behdinan, K. (2020). Measuring the concretization level of Systems of Objectives in the early phase of product development to derive the product maturity. In *14th Annual IEEE International Systems Conference (SysCon)* (n. p.). Montreal, QC, Canada / Virtual Conference. https://doi.org/10.1109/SysCon47679.2020.9275666

Richter, T., Wong, W., & Albers, A. (2020). LDA Models for Objective Validation in the Early Phase of Product Development. In *Digital Proceedings of TMCE 2020* (pp. 499–514). Dublin, Ireland.

Rios, A., Davis, B., & Gramann, P. (2001). Computer Aided Engineering in Compression Molding. In *Proceedings of the Composites Fabricators Association* (n. p.). Tampa, FL, USA.

Roos, E., Maile, K., & Seidenfuß, M. (2017). *Werkstoffkunde für Ingenieure: Grundlagen, Anwendung, Prüfung* (6th ed.). Berlin: Springer Vieweg. https://doi.org/10.1007/978-3-662-49532-2

Ropohl, G. (1975). Einleitung in die Systemtechnik. In G. Ropohl (Ed.), *System-technik – Grundlagen und Anwendung* (pp. 1–77). Munich Vienna: Carl Hanser Verlag.

Rosenbaum, E. E., & Hatzikiriakos, S. G. (1997). Wall slip in the capillary flow of molten polymers subject to viscous heating. *AIChE Journal*, *43*(3), 598–608. https://doi.org/10.1002/aic.690430305

Rösler, J., Harders, H., & Bäker, M. (2019). *Mechanisches Verhalten der Werk-stoffe* (6th ed.). Wiesbaden: Springer Vieweg. https://doi.org/10.1007/978-3-658-26802-2

Saaty, T. L. (1990). How to make a decision: The analytic hierarchy process. *Euro-pean Journal of Operational Research*, *48*(1), 9–26. https://doi.org/10.1016/0377-2217(90)90057-I

Sabisch, H., & Tintelnot, C. (1997). *Integriertes Benchmarking*. Berlin, Heidelberg: Springer. https://doi.org/10.1007/978-3-642-59148-8

Sander, C., Petrich, D., & Albers, A. (2012). Erweiterte Topologieoptimierung zur Steigerung der Energieeffizienz bei dynamisch bewegten Systemen. In *NAF-EMS DACH Konferenz* (pp. 1–4). Bamberg, Germany.

Sanwald, S., Henning, F., Bertram, B., Weidenmann, K. A., Brylka, B., Müller, V., & Böhlke, T. (2013). Geschlossene Simulation und experimenteller Vergleich der effektiven Bauteilsteifigkeit unter Berücksichtigung der lokalen Materialeigen-schaften einer im Fließpressprozess hergestellten SMC-Sickenstruktur. In *19. DGM-Symposium Verbundwerkstoffe* (pp. 574–580). Karlsruhe, Germany.

Sauser, B., Gove, R., Forbes, E., & Ramirez-Marquez, J. E. (2010). Integration maturity metrics: Development of an integration readiness level. *Information Knowledge Systems Management*, *9*(1), 17–46. https://doi.org/10.3233/IKS-2010-0133

Sauser, B., Ramirez-Marquez, J. E., Magnaye, R., & Weiping, T. (2009). *A sys-tems approach to expanding the technology readiness level within Defense Ac-quisition*. Retrieved from https://calhoun.nps.edu/bitstream/han-dle/10945/446/NPS-AM-09-002.pdf?sequence=1&isAllowed=y (accessed on June 17, 2021)

Sauter, J., Mulfinger, F., & Müller, O. (1992). Neue Entwicklungen im Bereich der Gestalt- und Topologieoptimierung. In *ANSYS Users' Meeting* (n. p.). Arolsen, Germany.

Schemmann, M. (2018). *Biaxial Characterization and Mean-field Based Damage Modeling of Sheet Molding Compound Composites*. Dissertation. *Schriften-reihe Kontinuumsmechanik im Maschinenbau: Vol. 13*. Karlsruhe: KIT Scien-tific Publishing. https://doi.org/10.5445/KSP/1000084270

Schemmann, M., Görthofer, J., Seelig, T., Hrymak, A., & Böhlke, T. (2018). Anisotropic meanfield modeling of debonding and matrix damage in SMC composites. *Composites Science and Technology*, *161*, 143–158. https://doi.org/10.1016/j.compscitech.2018.03.041

Schmidt, W., & Puri, W. (2000). Systematische Entwicklung gewichtsoptimierter Bauteile. In *DFX 2000: Proceedings of the 11th Symposium on Design for X* (pp. 37–40). Schnaittach/Erlangen, Germany.

Schmidt, W., & Puri, W. (2001). Betrachtungen zur Konzeptphase im Konstruktionsprozess von Leichtbauteilen. In *DFX 2001: Proceedings of the 12th Symposium on Design for X* (pp. 21–28). Neukirchen, Germany.

Schöll, R., Friedrich, H. E., Kopp, G., & Kopp, G. (2009). Innovative Fahrzeugstruktur in Spant- und Space-Frame-Bauweise. *ATZ – Automobiltechnische Zeitschrift*, *111*(1), 52–58. https://doi.org/10.1007/BF03222047

Schumacher, A. (2020). *Optimierung mechanischer Strukturen: Grundlagen und industrielle Anwendungen* (3rd ed.). Berlin: Springer Vieweg. https://doi.org/10.1007/978-3-662-60328-4

Schumpeter, J. A. (1912). *Theorie der wirtschaftlichen Entwicklung*. Berlin: Duncker und Humblot.

Schürmann, H. (2007). *Konstruieren mit Faser-Kunststoff-Verbunden* (2nd ed.). Berlin, Heidelberg: Springer. https://doi.org/10.1007/978-3-540-72190-1

Schwarz, D. (2002). *Auslegung von Blechen mit Sicken (Sickenatlas): FAT-Schriftenreihe*. Frankfurt/Main: Forschungsvereinigung Automobiltechnik e. V.

Schwer, L. E. (2007). An overview of the PTC 60/V&V 10: guide for verification and validation in computational solid mechanics. *Engineering with Computers*, *23*(4), 245–252. https://doi.org/10.1007/s00366-007-0072-z

Siebel, T. (2021, April 15). „Ein ideales Momentum für den Leichtbau". *Springerprofessional.de*. Retrieved from https://www.springerprofessional.de/leichtbau/hannover-messe/-ein-ideales-momentum-fuer-den-leichtbau-/19067038 (accessed on May 20, 2021)

Silva-Nieto, R. J., Fisher, B. C., & Birley, A. W. (1980). Predicting mold flow for unsaturated polyester resin sheet molding compounds. *Polymer Composites*, *1*(1), 14–23. https://doi.org/10.1002/pc.750010105

Sommer, M., Edelmann, K., Lahr, R., Hildebrandt, K., Grebel, K., & Medina, L. (2014). Pressverfahren. In M. Neitzel, P. Mitschang, & U. Breuer (Eds.), *Handbuch Verbundwerkstoffe: Werkstoffe, Verarbeitung, Anwendung* (1st ed., pp. 383–432). s.l.: Carl Hanser Fachbuchverlag.

Spadinger, M., & Albers, A. (2019). Designing CoDiCoFRP Structures: A Process-Related Topology Optimization Method to Design DiCoFRP Structures. In T.

Böhlke, F. Henning, A. Hrymak, L. Kärger, K. A. Weidenmann, & J. T. Wood (Eds.), *Continuous–Discontinuous Fiber-Reinforced Polymers* (pp. 265–276). Munich: Carl Hanser Verlag GmbH & Co. KG.

Specker, O., Osswald, T. A., & Michaeli, W. (1990). *Methoden zur Vorausberechnung der Faserorientierung beim Pressen von SMC mit geschnittenen Glasfasern: FAT-Schriftenreihe*. Frankfurt/Main: Forschungsvereinigung Automobiltechnik e. V.

Spiess, H., Oeckerath, A., & Landvogt, B. (2018). *MapLib Manual: Version 2013.0*. Sankt Augustin, Germany.

Stachel, P. (2013). SMC/BMC. In *Handbuch Faserverbundkunststoffe/Composites: Grundlagen, Verarbeitung, Anwendungen* (4th ed., pp. 243–277). Wiesbaden: Springer Fachmedien Wiesbaden.

Stachowiak, H. (1973). *Allgemeine Modelltheorie*. Vienna: Springer-Verlag.

Steinbuch, R. (1998). *Finite Elemente – Ein Einstieg*. Berlin, Heidelberg: Springer. https://doi.org/10.1007/978-3-642-58750-4

Sunderland, P., Yu, W., & Månson, J.-A. (2001). A thermoviscoelastic analysis of process-induced internal stresses in thermoplastic matrix composites. *Polymer Composites*, *22*(5), 579–592.

Talbi, E.-G. (2009). *Metaheuristics: From design to implementation* (1st ed.). Hoboken, New Jersey: John Wiley & Sons. https://doi.org/10.1002/9780470496916

Tamil, J., Ore, S. H., Gan, K. Y., Koh, D., In, M. G. T., Liew, B. P., Park, T. W., Ng, G., Yang, Y. B., The, D., et al. (2012). Molding Flow Modeling and Experimental Study on Void Control for Flip Chip Package Panel Molding with Molded Underfill Technology. *Journal of Microelectronics and Electronic Packaging*, *9*(1), 19–30. https://doi.org/10.4071/imaps.319

Tandon, G. P., & Weng, G. J. (1984). The Effect of Aspect Ratio of Inclusions on the Elastic Properties of Unidirectionally Aligned Composites. *Polymer Composites*, *5*(4), 327–333.

Teschner, M., & Mattheck, C. (1997). Struktur- und Formoptimierung mechanischer Bauteile durch Simulation biologischer Designfindung. *ATZ – Automobiltechnische Zeitschrift*, *58*, 68–74.

Thomas, H., Zhou, M., & Schramm, U. (2002). Issues of commercial optimization software development. *Structural and Multidisciplinary Optimization*, *23*(2), 97–110. https://doi.org/10.1007/s00158-002-0170-x

Timmer, A., Michler, T., Spadinger, M., Revfi, S., Seidel, K., Thirunavukkarasu, D., Atzrodt, H., Tamm, C. (2019). Opel demonstrator (virtual): Strut tower, wheel house and integrated rail: ALLIANCE final event. Retrieved from

http://lightweight-alliance.eu/results/#1570617351582-a34afa58-dad9 (accessed on March 31, 2021)

Trauth, A. (2018). *Characterisation and Modelling of Continuous-Discontinuous Sheet Moulding Compound Composites for Structural Applications* (Dissertation). Karlsruhe Institute of Technology (KIT), Karlsruhe.

Troll, D. (2015). Optimierung langfaserverstärkter Strukturen unter Berücksichtigung der streuenden Materialeigenschaften und der Robustheit. Dissertation. In A. Albers (Ed.), *Forschungsberichte des IPEK – Institut für Produktentwicklung. ISSN: 1615-8113* (Vol. 90). Karlsruhe.

Troll, D., Marston, M. P., & Albers, A. (2013). Macroscale modeling of long-fiber-reinforced composite parts with varying material properties for robust rib optimization. In *NAFEMS World Congress* (n. p.). Salzburg, Austria.

Troll, D., Marston, M. P., & Albers, A. (2014). Makroskopische Modellierung von langfaserverstärkten Bauteilen mit streuenden Materialeigenschaften – Berücksichtigung der Robustheit in der Strukturoptimierung. *NAFEMS Online-Magazin*, *29*, 63–74.

Tsai, S. W., & Wu, E. M. (1971). A General Theory of Strength for Anisotropic Materials. *Journal of Composite Materials*, *5*, 58–80.

Tucker III, C. L., & Liang, E. (1999). Stiffness predictions for unidirectional short-fiber composites: Review and evaluation. *Composites Science and Technology*, *59*, 655–671.

Vanderplaats, G. N. (1999). *Numerical optimization techniques for engineering design* (3rd ed.). New York: Vanderplaats Research & Development, Inc.

VDI 2206 (2004). *Design methodology for mechatronic systems*. VDI guideline. Düsseldorf: Verein Deutscher Ingenieure e.V.

VDI 2221 Part 1 (2018). *Entwicklung technischer Produkte und Systeme: Modell der Produktentwicklung*. VDI guideline. Düsseldorf: Verein Deutscher Ingenieure e.V.

VDI 2225 Part 1:1997-11 (1997). *Konstruktionsmethodik – Technisch-wirtschaftliches Konstruieren – Vereinfachte Kostenermittlung*. VDI guideline. Düsseldorf: Verein Deutscher Ingenieure e.V.

Venkayya, V. B., Khot, N. S., & Reddy, V. S. (1968). Optimization of structures based on the study of energy distribution. In *Proceedings of the Second Conference on Matrix Methods in Structural Mechanics* (pp. 111–153). Ohio, USA.

Verworn, B. (2005). *Die frühen Phasen der Produktentwicklung: Eine empirische Analyse in der Mess-, Steuer- und Regelungstechnik*. Wiesbaden: Deutscher Universitätsverlag. https://doi.org/10.1007/978-3-663-09708-2

Wagner, D. (2015). Methodengestützte Entwicklung eines elektrischen Energie-speichers zur Erschließung von Leichtbaupotenzialen als Beitrag zur Produkt-generationsentwicklung. Dissertation. In A. Albers (Ed.), *Forschungsberichte des IPEK – Institut für Produktentwicklung. ISSN: 1615-8113* (Vol. 89). Karlsruhe.

Wah Fong, S., Cheng, E. W., & Ho, D. C. (1998). Benchmarking: a general reading for management practitioners. *Management Decision*, *36*(6), 407–418. https://doi.org/10.1108/00251749810223646

Walden, D. D., Roedler, G. J., Forsberg, K., Hamelin, R. D., & Shortell, T. M. (Eds.) (2015). *Systems engineering handbook: a guide for system life cycle processes and activities* (4th ed.). Hoboken, New Jersey: John Wiley & Sons.

Wang, J., O'Gara, J. F., & Tucker, C. L. (2008). An objective model for slow orientation kinetics in concentrated fiber suspensions: Theory and rheological evidence. *Journal of Rheology*, *52*(5), 1179–1200. https://doi.org/10.1122/1.2946437

Weber, J. (2009). *Automotive Development Processes: Processes for Successful Customer Oriented Vehicle Development*. Berlin, Heidelberg: Springer.

Whitney, D. E. (1990). Designing the design process. *Research in Engineering Design*, *2*(1), 3–13. https://doi.org/10.1007/BF02029818

Widmann, M. (1983). *Herstellung und Versteifungswirkung von geschlossenen Halbrundsicken* (Dissertation). University of Stuttgart, Stuttgart.

Wilhelm, H. (2013a). Heißpressen von SMC/BMC. In *Handbuch Faserverbundkunststoffe/Composites: Grundlagen, Verarbeitung, Anwendungen* (4th ed., pp. 407–428). Wiesbaden: Springer Fachmedien Wiesbaden.

Wilhelm, H. (2013b). Spritzgießen langfaserverstärkter Thermoplaste (LFT). In *Handbuch Faserverbundkunststoffe/Composites: Grundlagen, Verarbeitung, Anwendungen* (4th ed., pp. 447–461). Wiesbaden: Springer Fachmedien Wiesbaden.

Willems, F., Reitinger, P., & Bonten, C. (2020). Calibration of Fiber Orientation Simulations for LFT – A New Approach. *Journal of Composites Science*, *4*(4), 163. https://doi.org/10.3390/jcs4040163

Wynn, D. C., & Clarkson, P. J. (2018). Process models in design and development. *Research in Engineering Design*, *29*(2), 161–202. https://doi.org/10.1007/s00163-017-0262-7

Student theses co-supervised by the author in the context of this dissertation at IPEK – Institute of Product Engineering at Karlsruhe Institute of Technology (KIT):

Bayh, J. (2020). *Untersuchung der Versteifungswirkung von Sicken, Rippen und Tapes in aus langfaserverstärktem Kunststoff hergestellten Demonstrator-Bauteilen.* Unpublished bachelor thesis. IPEK – Institute of Product Engineering, Karlsruhe Institute of Technology (KIT), Karlsruhe.

Kraus, F. (2018). *Benchmarking im Kontext des Erweiterten Target Weighing Ansatzes – Erschließung wettbewerbsorientierter Leichtbaupotentiale am Beispiel der Automobilindustrie.* Unpublished bachelor thesis. IPEK – Institute of Product Engineering, Karlsruhe Institute of Technology (KIT), Karlsruhe.

Maser, J. (2019). *Untersuchung der Leichtbaupotenziale eines elektrischen Handgerätes mit dem funktionsbasierten Erweiterten Target Weighing Ansatz.* Unpublished master thesis. IPEK – Institute of Product Engineering, Karlsruhe Institute of Technology (KIT), Karlsruhe.

Mikus, M. (2019). *Numerische Optimierung der Sickengeometrie in langfaserverstärkten Kunststoffbauteilen unter Berücksichtigung von Herstellungseinflüssen aus dem Formpressen.* Unpublished master thesis. IPEK – Institute of Product Engineering, Karlsruhe Institute of Technology (KIT), Karlsruhe.

Reichmann, B. (2019). *Trajektorienbasierter, numerischer Vergleich der Biegesteifigkeiten in langfaserverstärkten, polymeren Leitstützstrukturen bei Einsatz von Sicken, Rippen und unidirektionalen Tapes.* Unpublished bachelor thesis. IPEK – Institute of Product Engineering, Karlsruhe Institute of Technology (KIT), Karlsruhe.

Schönhoff, C. (2019). *Agiler Leichtbau – Integration des ETWA in einen agilen Ansatz zur Mechatroniksystementwicklung unter Nutzung von Gestalt-Funktion-Zusammenhängen.* Unpublished master thesis. IPEK – Institute of Product Engineering, Karlsruhe Institute of Technology (KIT), Karlsruhe.

Sterr, B. (2019). *Numerische Steifigkeitsoptimierung langfaserverstärkter Polymerbauteile durch deren Versickung mittels naturanaloger Optimierungsalgorithmen.* Unpublished bachelor thesis. IPEK – Institute of Product Engineering, Karlsruhe Institute of Technology (KIT), Karlsruhe.

Wilwer, J. (2019). *Systematische Evaluation von Leichtbaukonzepten auf Grundlage der Unsicherheitsbewertung des Erweiterten Target Weighing Ansatz.* Unpublished master thesis. IPEK – Institute of Product Engineering, Karlsruhe Institute of Technology (KIT), Karlsruhe.

Appendix A

Questionnaire: Assessment of Demand

5) On a scale from 1 (easy) to 6 (difficult): How do you evaluate the formulation of the functions in the step of functional analysis?

1	2	3	4	5	6
☐	☐	☐	☐	☐	☐

6) On a scale from 1 (low) to 6 (high): How do you evaluate the effort required to perform the paired comparison?

1	2	3	4	5	6
☐	☐	☐	☐	☐	☐

7) The resulting lightweight design search fields support the identification of real lightweight design potentials.

I agree					I disagree
☐	☐	☐	☐	☐	☐

8) On a scale from 1 (very good) to 6 (inadequate): The methodological support by the TWA for the transfer of the identified lightweight search fields in new concept ideas (= synthesis), I evaluate with:

1	2	3	4	5	6
☐	☐	☐	☐	☐	☐

9) After generating new concept ideas based on the identified search fields, you must evaluate those concept ideas that are to be detailed later. On a scale from 1 (very good) to 6 (inadequate): How do you evaluate the methodical support of TWA in this selection process?

1	2	3	4	5	6
☐	☐	☐	☐	☐	☐

10) You understood the TWA in its entirety right from the first moment on.

I agree					I disagree
☐	☐	☐	☐	☐	☐

11) Do you see any potential for improvement in the application in a step of TWA?

☐ Yes

Which potential for improvement do you see in which step?

....

☐ No

12) Would it have made sense to use other methods in the execution of the TWA?

☐ Yes

Which one? ....

☐ No

Comments field